



# THE UNIVERSITY *of* EDINBURGH

This thesis has been submitted in fulfilment of the requirements for a postgraduate degree (e. g. PhD, MPhil, DClinPsychol) at the University of Edinburgh. Please note the following terms and conditions of use:

- This work is protected by copyright and other intellectual property rights, which are retained by the thesis author, unless otherwise stated.
- A copy can be downloaded for personal non-commercial research or study, without prior permission or charge.
- This thesis cannot be reproduced or quoted extensively from without first obtaining permission in writing from the author.
- The content must not be changed in any way or sold commercially in any format or medium without the formal permission of the author.
- When referring to this work, full bibliographic details including the author, title, awarding institution and date of the thesis must be given.

**Modulation of host intestinal epithelium by**  
**gastrointestinal nematode secreted**  
**extracellular vesicles**



Ruby Florence White

*Thesis submitted for the degree of Doctor of Philosophy*

*The University of Edinburgh*

2022

## **Declaration**

I, the undersigned, declare the contents of this thesis has been comprised by myself solely and has not been submitted elsewhere for any other degree or professional qualification. Except where explicitly stated or acknowledged in this thesis or below, all work was carried out by me.

In Chapter 1, parts of Section 1.5.3 are previously published as part of a review in *Frontiers of Cellular Infection Microbiology* which was co-authored with Maria A. Duque-Correa, Amy Buck and Frances Blow (Appendix III). The sections of text from this review were primarily written by me but with input and editing by the co-authors. In Chapter 1, the first paragraph of Section 1.4.2 text was used from a perspective piece that has been accepted for publication in the *Journal of Extracellular Vesicles*, text used was written by me with editing from co-authors (Appendix IV).

Ruby Florence White

Date: 27/12/22

## **Contributions**

cryoEM in Chapter 3 was performed by Martin Tuijtel and Martin Singleton by the Central Optical Instrument Laboratory (COIL) at the Wellcome centre for cell biology, Edinburgh.

Chapter 5, Section 5.2.2 contains some experiments performed in the Berriman lab at the Wellcome Sanger Institute in Cambridge, U.K in collaboration with Maria Duque-Correa. Chapter 5 also included microscopy of mice injected intralumenally with *H. bakeri* EVs, training surgeries were performed by Dr. David Donaldson at the Roslin Institute with approval from Professor Neil Mabbot.

The raw processing and edgeR differential gene expression analysis of RNA seq data presented in Chapter 6 of this thesis was analysed by Jose Roberto Bermudez Barrientos. All CAMERA analysis of RNA seq data was also performed by Jose Roberto Bermudez Barrientos with discussion with the author. RNA seq was performed by the Wellcome Trust Clinical Research Facility in Edinburgh.

In Chapter 6, flow cytometry assisted sorting of 2-D organoid cells for scRNA seq was performed by Martin Waterfall in the FACs facility at the Institute of Infection and Immunology Research (IIIR). scRNA seq libraries were prepared by Elisabeth Freyer and Susan Campbell at the FACs facility in the Institute of Genetics and Cancer (IGC) at the University of Edinburgh. Sequencing was performed by the Wellcome Trust Clinical Research Facility in Edinburgh. All scRNA seq analysis was performed by Yenetzi Villagrana Pacheco with supervision from Cei Abreu-Goodger.

## **Acknowledgements**

The scientific community - as scientists we stand on the shoulders of those that came before us, and as such there are many excellent scientists (too many to name individually) that have contributed indispensable knowledge required for this project, even before its conception. However, in particular, Professor Amy Buck, Dr. Gillian Coakley, and Dr. Maria Duque-Correa who laid the groundwork for my project. I am grateful to the helminth field as a whole for their unmatched generosity, warmth and enthusiasm about all things worms! Finally, to my PhD committee members for seeing me through the last four years Chris Ponting, Jenny Regan and Dietmar Zaiss (special thanks to Dietmar for the 8.30 am immunology discussions/pop quizzes).

Amy, I have learnt so much from you and I couldn't have asked for a more supportive supervisor, thank you for the freedom you always granted me and words of encouragement when needed! As well as facilitating many opportunities for me throughout the last four years that have provided me with a depth of experience not every student gets – for that I am very grateful.

Maria, it has been a pleasure to work together, and I am immensely grateful for your continued input on this project, which was invaluable, and for teaching me all things organoids! You have been so generous with your time and knowledge and always gave perfectly timed sage advice academic or otherwise.

I have a big thank you for Cei, Yenetzi, Beto, and Sujai who turned the mumbo jumbo of FASTA files into something that I could make sense of with their magical bioinformatic powers!

Over the last 4 years I have worked fantastic Buck lab mates both past and present who all contributed in their own way to my scientific progression namely Kyriaki, Sarah, Kat, Elaine (an extra special thanks to you for making that worm life cycle go round!!), Xiaochen, Frances, Yvonne, Sujai, Beto, Tom F and Tom Y. To Roo, my student turned friend, it was a pleasure to supervise your project and teach you to pipette! To all the people on Ash 2 level 1 past and present for provided many laughs, coffees and advice throughout - especially my original office mate Alex for all the office and TC chats, and for keeping the boys in the office in check.

It's safe to say I would have struggled without the support and commandry of my PhD cohort. I will treasure all the memories from Panto days to viva celebrations, and all the pub nights, camping trips, and zoom quizzes in between! Mary-Kate – from that first PhD seminar I knew I wanted to be your friend, you have been the person I go to first for every high and low over the last 4 years. I could not even imagine having done this without you by my side. You made me die laughing on a daily basis, without which my serotonin levels would have severely suffered. Rory, even though we wind each other up no end I wouldn't have it any other way, thanks for always being there for reliable advice and a pint. Row, you've been the embodiment of a fairy godmother over the last few years. And you are always the first person to offer a helping hand when I needed it. Thanks for all the worm-y enthusiasm, dreaming up experiments with me (even if we never find time to actually do them) and being my Hydra 2.0 buddy.

To my “non-wormy” friends, those who became my Edinburgh family, Steven, Liv and Martha you three are truly some of my favourite people in the world. Thank you for the respite from PhD life, the Christmas's, and for always keeping me in check.

Jack. Thank you for listening patiently to my seemingly endless blathering's, picking me from work on teary nights post experimental failures, and really being there in the true low points. Equally, you bring me so much happiness every single day, and I am so grateful this PhD led me here, and to you.

To my best friends that have been with me since 14, Ava, Bei, Brenna, Clare, and Sarah – school was always a happy place for me because of you, who knows if I would have made it this far if you hadn't made it so much fun. Brenna, I can't think of another person in my life who has shaped me more than you. I have endless gratitude for who you are, your authenticity, and how deeply you love everyone around you. I wish I could have been with you more over the last few years, but no matter where we are you will always be my soul mate <3.

It is an impossible task to write a succinct paragraph expressing the extent of my gratitude to my family especially my parents, but I will try. Dad - Thank you for always making us all believe we could do anything we put our minds to. I have yet to meet someone who lives life in the way that you do, your endless enthusiasm for a new hobby, skill, religion, or philosophy at any age, and your constant curiosity for the world around you have made a massive impact on my career choice. Thank you for always being equally up for a frivolous chat as you are a philosophical one. Mum - I don't think I will ever be half as hardworking or as kind as you, but I will try. Watching you go back to university after four kids was something I only truly appreciated as an adult, but you set such an amazing (and probably unattainable) example of someone that can truly do it all and always with grace. Thank you for everything. To my siblings Sophie, Grace and Thomas thank you for all the support throughout my life, having three wonderful older siblings to look up (and sometimes just straight up copy) is no doubt a large reason why I am where I am today... specifically in Scotland.

To my whole family - without a doubt the hardest part of my PhD has been not being able to be there during the hard moments. I was not able to be there with you in the most difficult time and I am sorry for that. Finally, I know that without the hard work of my grandparents Donald Riley and Norma Riley, our family would not be what it is, and I would not have been afforded the opportunities I have. So, I would like to dedicate this thesis to them.

*Aroha nui.*

## **Lay Summary**

Parasites are organisms that live off or on another organism, called the host. Parasites require host resources such as food for their survival and thereby negatively impact the host. Parasitic worms, also known as helminths, are an ancient problem for human civilisations. Evidence of helminth infection has been found in human fossils from 6200 years ago, although it is thought that this relationship is likely much older. Today, despite some available drug treatments for helminth infection, over 1 billion people are still infected by helminths particularly in sub-tropical countries and areas with poor sanitation. Gastrointestinal (GI) helminths (helminths which live in the gastrointestinal tract of their host) take resources from the host and cause symptoms of malnutrition, diarrhoea, iron deficiency and impaired growth and development.

The large number of people worldwide infected with GI helminths is reflective of these parasites' ability to survive in the host environment. Over the millions of years that helminths have lived alongside their hosts they have developed the ability to manipulate the host in order to survive. It is well understood that one way helminths achieve successful infection is by suppressing of the host immune system by releasing a plethora of products referred to as excreted and/or secreted (ES). Although it is known that ES can interfere with the host immune system, currently only a small fraction of the individual molecules within ES have been well characterised. ES products contain several of the basic molecules used by cells including proteins, nucleic acids, and more recently it was discovered to contain extracellular vesicles (EVs). EVs are small membrane enclosed particles that contain material such as proteins and small RNAs (a type of nucleic acid) from the parasite. Conceptually EVs can be thought of as parcels that are released by the parasite, much like a trojan horse, that can enter host cells inconspicuously and alter them from within. It is hypothesised that in this way helminth EVs play a role in communication between the helminth and the host and may prolong the parasites' survival. However, this is a new field and we still do not understand exactly how they affect host cells, which host cells they target, and how they do so.

Our lab studies a helminth species that infects mice called *Heligmosomoides polygyrus bakeri* (*H. bakeri*) as a model of human helminth infection. In the adult stage of *H. bakeri* infection the parasite resides in the GI tract at the top of the small intestine. The small intestines are lined with a tissue called the epithelium, which is comprised of a self-renewing, almost impenetrable layer of cells containing 7 specialised cell types. The function of the epithelium is to absorb nutrients and prevent food or unwanted foreign organisms in the lumen of the intestine (the inner tube of the intestine that food passes through) from entering the body. In addition, the epithelium plays important dual roles in both detecting helminths and alerting the immune system to respond. In order to help clear the infection. Recently, it has also been shown that ES products from *H. bakeri* can modify the epithelium.

My hypothesis was that *H. bakeri* worms modulate the intestinal epithelium through the secretion of EVs, which I propose enter these epithelial cells and modify their ability to respond to infection. To address this hypothesis my first aim was to establish a model of the intestinal epithelium. The intestinal epithelium can be cultured in the laboratory and grown into enclosed balloon-like structures termed 3-D organoids. 3-D organoids grown in this way have the intestinal lumen, that part of the intestine that normally contains the food moving through the gut as well as bacteria, on the inside. However, delivering substances into this internal lumen in 3-D organoids is very difficult. My next aim was to develop a method for growing organoids in a 2-D 'open' structure that results in a layer of cells representing the intestinal epithelium with an accessible lumen. This model has an upper compartment of a cell culture plate, and lower compartment that is physically separated by this layer of epithelial cells. These cultures successfully represented 6 of the 7 of the cell types of the intestinal epithelium and serve as a model for following experimentation.

We then tested our hypothesis that *H. bakeri* EVs enter cells within the intestinal epithelium and found that they are capable of entering a proportion of the cells in 2-D organoids. I also saw a lower percentage of cells took up EVs than in cell line cultures which are comprised of a single cell type. I then hypothesised this could be due to *H. bakeri* EVs entering a specific subtype(s)



of cell within the intestinal epithelium. I don't yet have conclusive results as to which cells *H. bakeri* EVs enter, and this remains an area of current investigation.

Once EVs enter cells it is still unknown how the molecules they carry will act on the host cell. Therefore, to further our understanding of how *H. bakeri* EVs impact the host I wanted to characterise the changes that occur in the host upon *H. bakeri* EV treatment. To do so I measured which genes are turned on or off, referred to as gene expression, in cells that were treated with *H. bakeri* EV compared to control cells. As a comparison I also characterised the changes that occur when treated with EV depleted ES. Upon EV treatment I found subtle changes to genes. Many of the genes suppressed by *H. bakeri* EVs have known roles in maintenance of the intestinal epithelium or related to host antimicrobial responses which could impact the success of infection either directly or indirectly.

One ongoing question is whether *H. bakeri* EVs target a specific cell type. Our data shows suppression of genes that are only expressed by a certain cell subtypes namely intestinal stem cells, Paneth cells and trans-amplifying cells. These findings suggest that either i) *H. bakeri* EVs specifically enter these cells, or ii) *H. bakeri* EVs enter cells in a non-specific manner but affect cell type specific processes within these cell subtypes.

We also aimed to address the question of cell type specificity using single cell RNA sequencing (scRNA seq), this is a technique that looks at gene expression at the individual cell level. scRNA seq is powerful for teasing out changes occurring in a tissue that is composed of multiple cells types. I performed this on 2-D organoids treated with either EVs, EV-depleted ES or control samples and aimed to compare each cell subtype upon treatment to identify if specific cell types are targeted. Unfortunately, I discovered variable quality between samples, and this made interpreting whether changes were driven by treatment or by cell quality difficult. However, I did detect subtle changes after EV treatment in a number of cell type specific genes including those identified by previous studies of ES treated organoids. This data further

suggests that *H. bakeri* EVs may modify this tissue during infection. Optimisation of the protocol for generating this data has been done and repeating this experiment with an improved design could be a future direction of the project.

Finally, I highlighted the future applications of this 2-D organoid model by co-culturing live *H. bakeri* parasites in these cultures for 24 hours and then assessed gene expression. I found strong gene expression changes in the intestinal epithelium after co-culture, including both previously identified and novel changes. This represents the first co-culture of the intestinal epithelium with live *H. bakeri* parasites.

In summary, this thesis demonstrates the development of 2-D organoid models that are suitable for the study of large multicellular organisms such as helminths and studies of their ES products. I utilised our 2-D organoid model to progress our knowledge of how *H. bakeri* EVs may act to modulate the intestinal epithelium during infection. However, the 2-D organoid model presented in this thesis could also have far reaching implications for helminth research beyond this project.

## **Scientific Abstract**

Helminths have co-evolved alongside their hosts for millions of years and have adapted eloquent mechanisms that allow them to reside in the host without causing significant pathology, or elimination. The ability of these parasites to manipulate their specialised host is reflected by their continued persistence as a global health concern, with ~1 billion people infected with soil transmitted helminths (STHs). Helminth infections have long been associated with reduced allergic and autoimmune diseases leading to the hypothesis that helminth suppress the host immune system, and this has been confirmed in both animal models and controlled human infection studies. Many studies have shown that many suppressive effects of infection on the host immune system can be attributed to helminth excreted/secreted products (ES). A small but growing list of individual molecules from helminth ES have been characterised, and the mechanism of action elucidated. For example, multiple helminth species have been identified to secrete TGF $\beta$  mimic proteins that can bind host TGF $\beta$  receptor and induce T-regulatory (Treg) immunosuppressive cells. However, the full repertoire of helminth secreted molecules that modulate the host is hypothesised to be far from complete.

Our lab discovered the presence of extracellular vesicles (EVs) within ES from the mouse infective helminth *Heligmosomoides polygyrus bakeri* (*H. bakeri*). EVs are lipid bilayer enclosed nanoparticles that carry proteins, lipids and nucleic acids and are released ubiquitously by all cells and organisms studied to date. In mammalian systems EVs provide a mechanism of communication between near or distal cells. In the context of host-pathogen dynamics it is proposed that EVs could play a role in enabling parasites to condition their environment during infection. There is mounting evidence of host-parasite EV mediated modulation occurrence between plants and colonising fungal cells, bacteria and mammalian host cells, and several parasites and their mammalian hosts including several helminth species.

During *H. bakeri* infection host immune suppression is thought to primarily occur during the adult stage of infection when the parasite resides in the lumen of the duodenum in close proximity to the intestinal epithelium. The intestinal epithelium plays an integral role both in helminth detection, and in mediating parasite clearance. Therefore, I hypothesised that adult *H. bakeri* EVs target the intestinal epithelium and directly modulate this tissue. The goal of this thesis was to determine the role of helminth EVs in infection dynamics and host modulation in the intestinal epithelium. I aimed to address whether *H. bakeri* EVs enter the intestinal epithelium, whether uptake is targeted to a specific cell type and how these effects the function of this tissue using intestinal organoid models.

To address these aims development and refinement of methods for high purity EV preparations and EV labelling was required in order to directly implicate *H. bakeri* EVs as the causative agent in host responses. In Chapter 3, I compared various combinational approaches to EV isolation and improved the purity of our EV and EV depleted HES preparations. I then assessed EV preparations using cryoEM which furthered our understanding of the morphology and diversity of *H. bakeri* secreted EVs. I trialled multiple labelling methodologies and found a low-background labelling method that allowed high confidence identification of uptake for subsequent chapters. However, I later discovered that the majority of labelling techniques trialled had variable labelling efficiency with low proportions of EVs labelled; this is a caveat to consider when interpreting results using labelled EVs.

To understand how *H. bakeri* EVs interact with the intestinal epithelium I developed methods to grow small intestinal 2-D organoids (enteroids) which are *in vitro* cultures that reconstitute the intestinal epithelium (Chapter 4). 2-D enteroids have greater cellular complexity as compared to a homogenous cell line and allow us to address the question of cell type specificity for uptake. 2-

D enteroid cultures maintained cellular polarisation and differentiated into 6-7 major cell types of the intestinal epithelium.

In Chapter 5, I demonstrated by using fluorescently labelled EVs that *H. bakeri* EVs enter organoid cells, however at a lower proportion than I see side-by-side for our cell line cultures. This led to the hypothesis that *H. bakeri* EVs could target specific cellular populations within the intestinal epithelium. To identify whether uptake of *H. bakeri* EVs occurs in a targeted fashion by specific cell types I performed microscopy experiments aiming to co-localise EVs with certain cell types. Microscopy approaches did not provide a definitive answer to the question of whether uptake is cell type specific. Next, I modified the cellular proportion of our 2-D enteroids to identify whether this altered the proportion of EV uptake. Goblet and tuft cells are specialised cells of the epithelium that are strongly induced during helminth infection and mediate helminth clearance; I reasoned that *H. bakeri* EVs may specifically enter and modulate these cell types. Organoid cultures that were enriched in goblet and tuft cells showed no enhanced ability to take up EVs, suggesting that neither goblet nor tuft cells are specifically targeted over other cell types; however, this data does not rule out that *H. bakeri* EVs can enter these cell types and modulate them. Whether cell type specificity exists for the uptake of *H. bakeri* EVs within the intestinal epithelium remains unclear and is still an active area of investigation.

To understand how EV treatment of 2-D enteroids altered host gene expression in Chapter 6, I performed RNA sequencing (RNA seq) and characterised the transcriptional changes within 2-D enteroids to *H. bakeri* EVs or EV depleted ES after 24 h. Genes critical for maintenance of stem cells, cell cycle and antimicrobial defence were downregulated by *H. bakeri* EVs. Within the intestinal epithelium only a proportion of the cells are mitotic, therefore changes in cell cycle suggest a modulation of either stem cells or Transit-amplifying (TA) cells. I also identified several changes in cell type restricted

genes expressed specifically by stem cells, Paneth cells, TA cells or Enteroendocrine cells (EECs). I now hypothesise EVs specifically modify these cell types. To define the cell type specific responses after EV or EV depleted ES treatment I performed single cell RNA seq, unfortunately the quality of our control sample made interpreting these results difficult. However, these data serve as conformation of the cellular composition of our 2-D enteroids model.

In addition, I also utilised our 2-D organoid model to perform novel co-cultured experiments with live adult or larval stage 4 (L4) *H. bakeri* and performed transcriptional analysis of the host epithelium under these conditions. These data allow us to uncouple the impact of infection with whole parasites on the intestinal epithelium from any immune driven changes in the epithelium that occur *in vivo*. These data also serve as a comparison between host effects attributed specifically to *H. bakeri* EVs, and changes induced by the whole parasite.

In summary, this thesis contributes new knowledge to our understanding of *H. bakeri* interactions with the intestinal epithelium in the absence of host immune driven responses and distinguishes the role of secreted *H. bakeri* EVs in modulating this tissue. I determined that *H. bakeri* EVs enter host epithelial cells in 2-D enteroids, but whether this is specifically targeted to certain subpopulations remains elusive. I characterised the host gene expression changes upon *H. bakeri* EV treatment in 2-D enteroids, these findings further our understanding as a field of which host genes and pathways are targeted by *H. bakeri*. In the future, this thesis along with continued research, could have important implications for helminth eradication. Conversely, where *H. bakeri* EVs suppress specific genes or pathways involved in diseases of the intestinal epithelium such as ulcerative colitis, Crohn's disease, or adenocarcinoma, they could provide novel strategies for therapeutics.

## **Table of contents**

<b>Declaration</b> .....	<b>ii</b>
<b>Contributions</b> .....	<b>iii</b>
<b>Acknowledgements</b> .....	<b>iv</b>
<b>Lay Summary</b> .....	<b>vi</b>
<b>Scientific Abstract</b> .....	<b>x</b>
<b>Table of contents</b> .....	<b>xiv</b>
<b>Chapter 1: General Introduction</b> .....	<b>1</b>
1.1 Soil transmitted helminths .....	2
1.1.1 Introduction and distribution of STHs .....	2
1.1.2 STH attributed morbidity .....	4
1.1.3 Current therapeutics and interventions .....	6
1.1.4 Non-human animal models of human helminth infection .....	7
1.2 Host-helminth dynamics .....	10
1.2.1 Host immune response to helminth infection .....	11
1.2.2 Recognition of helminths at the barrier site and associated immune responses .....	12
1.2.3 Key components of anthelmintic responses .....	13
1.2.4 Regulatory responses .....	16
1.2.5 Contribution by innate immune cells .....	17
1.2.6 Humoral immune responses .....	20
1.2.7 Effector mechanisms of helminth destruction and clearance in the intestinal epithelium .....	23
1.3 Immunomodulation by helminths .....	24
1.3.1 Hygiene hypothesis .....	24
1.3.2 Helminth immunomodulatory effector molecules .....	26
1.4 Extracellular vesicles .....	29

1.4.1	Definition, biogenesis and cargo of extracellular vesicles.....	29
1.4.2	Helminth EV mediated immunomodulation.....	34
1.5	Intestinal epithelium and organoids .....	37
1.5.1	The intestinal epithelium .....	37
1.5.2	Intestinal organoids.....	54
1.5.3	Intestinal organoid use in helminth infection.....	55
1.6	Thesis aims .....	62
<b>Chapter 2: Materials &amp; Methods.....</b>		<b>63</b>
2.1	Cell culture medias .....	64
2.2	Buffer solutions.....	67
2.3	Cell culture.....	69
2.3.1	R-spondin conditioned media .....	69
2.3.2	L-Wnt3a conditioned media .....	70
2.4	Organoid culture .....	70
2.4.1	3-D Organoid Isolation .....	70
2.4.2	3-D Organoid maintenance.....	71
2.4.3	2-D Transwell organoid cultures .....	72
2.5	<i>H. bakeri</i> lifecycle and HES production .....	74
2.6	EV separation, concentration & quality control.....	75
2.6.1	EV separation & concentration by ultracentrifugation.....	75
2.6.2	EV separation & concentration by Sepharose size exclusion column	76
2.6.3	Qubit .....	77
2.6.4	Zetaview® size quantification and concentration.....	77
2.6.5	Silver stain .....	78
2.6.6	Cryogenic Electron Microscopy (cryoEM).....	78



2.7	Fluorescent labelling of <i>H. bakeri</i> EVs.....	79
2.7.1	TFP ester labelling (AF488) & NHS ester labelling (AF647).....	79
2.7.2	Memglow™ labelling .....	79
2.8	EV uptake assays .....	79
2.8.1	MODE-K.....	80
2.8.2	2-D Enteroids .....	80
2.9	Microscopy .....	80
2.10	Harvesting 2-D transwell organoids for flow cytometry .....	83
2.11	Fluorescence-activated cell sorting (FACS).....	84
2.12	RNA methods.....	84
2.12.1	RNA extraction.....	84
2.12.2	Reverse transcription and quantitative PCR.....	84
2.13	Sequencing methods.....	87
2.13.1	10x Chromium scRNA-seq .....	87
2.13.2	Whole transcriptome sequencing .....	88
2.14	Bioinformatic analysis.....	89
2.14.1	Whole transcriptome sequencing analysis .....	89
2.14.2	scRNA-seq analysis.....	91
2.15	<i>In vivo</i> experiments .....	92
2.15.1	Vaccination experiments.....	92
2.15.2	Intraluminal injections under anaesthetic.....	92
<b>Chapter 3: Optimisation of EV isolation &amp; methods for EV labelling</b>		<b>94</b>
	Abstract .....	95
3.1	Introduction.....	96
3.2	Results.....	99
3.2.1	EV preparation methods .....	99

3.2.2	Sequential isolations of <i>H. bakeri</i> EVs .....	106
3.2.3	CryoEM of EVs in native HES.....	111
3.2.4	Methods of fluorescent EV labelling for <i>in vitro</i> & <i>in vivo</i> use .	112
3.3	Discussion .....	117
3.3.1	Considerations and limitations of EV isolation .....	118
3.3.2	Morphology of <i>H. bakeri</i> EVs .....	120
3.3.3	Fluorescent labelling of <i>H. bakeri</i> EVs .....	121
<b>Chapter 4:</b>	<b>Development of 2-D enteroid cultures.....</b>	<b>123</b>
	Abstract .....	124
4.1	Introduction.....	125
4.2	Results.....	127
4.2.1	Defining the conditions for 2-D enteroid growth.....	127
4.2.2	2-D enteroid cultures recapitulate the host intestinal epithelium 145	
4.2.3	Modulating the cellular composition of 2-D enteroids .....	149
4.3	Discussion .....	152
<b>Chapter 5:</b>	<b><i>H. bakeri</i> EV uptake by intestinal epithelial cells.....</b>	<b>157</b>
	Abstract .....	158
5.1	Introduction.....	159
5.2	Results.....	162
5.2.1	<i>H. bakeri</i> EV-647 uptake properties in the MODE-K cell line..	162
5.2.2	Caecaloid cells take up <i>H. bakeri</i> EVs .....	165
5.2.3	<i>H. bakeri</i> EVs enter 2-D enteroid cells.....	170
5.2.4	Searching for evidence of <i>in vivo</i> <i>H. bakeri</i> EV uptake .....	172
5.3	Discussion .....	176
5.3.1	Limitations.....	179

5.3.2	Future directions .....	180
<b>Chapter 6:</b>	<b>Functional effects of <i>H. bakeri</i> on 2-D enteroids .....</b>	<b>181</b>
	Abstract .....	182
6.1	Introduction .....	183
6.2	Results.....	188
6.2.1	Gene expression changes in 2-D enteroids in response to <i>H. bakeri</i> ES products.....	188
6.2.2	EV and EVdepHES induce concordant changes as well as unique changes 2-D organoids .....	194
6.2.3	<i>H. bakeri</i> EVs & EVdepHES modifies expression of genes integral to the intestinal epithelium and immune response .....	197
6.2.4	2-D organoids co-culture with live worms drastically modifies the epithelium.....	208
6.2.5	scRNA-sequencing of treated 2-D enteroids .....	222
6.2.6	Bifurcation of UMAP data is driven by cell quality which may or may not be related to treatment .....	232
6.2.7	Summary of Chapter 6 results .....	235
6.3	Discussion .....	236
6.3.1	Limitations for RNA-seq .....	237
6.3.2	Impact of <i>H. bakeri</i> and its secreted products of the stem cell niche 240	
6.3.3	Impact of <i>H. bakeri</i> and its secreted products on sub-populations within 2-D enteroids .....	242
6.3.4	Synergistic effects of vesicular and non-vesicular components of HES 244	
6.3.5	scRNA-seq analysis of EV and EVdepHES 2-D organoids ....	245
6.3.6	Limitations of scRNA-seq.....	246
<b>Chapter 7:</b>	<b>General discussion.....</b>	<b>248</b>

7.1	EV uptake and cell type specificity in the intestinal epithelium.....	249
7.2	<i>H. bakeri</i> EVs functional response in the host intestinal epithelium 252	
7.3	Organoid models advance the study of host-helminth interactions at the epithelium. ....	255
7.4	Future directions.....	257
7.5	Concluding remarks.....	258
	<b>Supplement tables and figures .....</b>	<b>260</b>
	<b>References .....</b>	<b>265</b>
	<b>Appendices .....</b>	<b>294</b>

**Chapter 1: General Introduction**

## 1.1 Soil transmitted helminths

### 1.1.1 Introduction and distribution of STHs

Helminth is a non-taxonomic term referring to a diverse group of Macroparasites that include species from the phyla Nematoda and Platyhelminthes (Trematoda and Cestoda) (Coghlan et al., 2019). Soil-transmitted helminths (STH) infect over one billion people globally, making them the most widespread of the neglected tropical diseases (NTD), and therefore a major focus of WHO intervention since 2010 (Jourdan et al., 2018). STH infection causes significant morbidity to those infected and symptoms include anaemia, malnutrition, diarrhoea, malaise, impaired growth or mental development in children, and in high worm burden cases, intestinal obstruction (Jourdan et al., 2018). A number of helminth species contribute to the global number of human STH infections, namely the roundworm *Ascaris lumbricoides*, *Trichuris trichuria* also known as whipworm, and the hookworm species *Necator americanus* and *Ancylostoma duodenale* (Montresor et al., 2020). The umbrella term soil-transmitted helminths refer to these four species due to their similarities in transmission, morbidity, interventions and therapies used for eradication. The faecal-oral route of transmission is utilised by all STH species, either through ingestion of eggs, in the case of *A. lumbricoides* & *T. trichuria*, or by ingestion of free-living L3 larvae for *N. americanus* and *A. duodenale* (Loukas et al., 2016). In addition to ingestion of larvae, *N. americanus* and *A. duodenale* can also infect individuals through transcutaneous penetration of the skin barrier (Loukas et al., 2016). Upon entering the host, eggs hatch releasing larvae, which undergo subsequent larval stages before maturing to adult worms where they reside mostly in the gastrointestinal tract (Else et al., 2020; Jourdan et al., 2018; Loukas et al., 2016). *A. lumbricoides*, *N. americanus* and *A. duodenale* all migrate through the lung of the host before arriving as L4 larvae in the intestine and moulting

to adult worms. *T. trichuria* however bypasses invasion of the lung and migrates directly to the caecum of the large intestine (Else et al., 2020). Once adult worms are in the GI tract they will reproduce and release eggs in the host faeces – beginning the cycle of infection once more.

Considering the transmission route of STH's it is not surprising that risk factors for STH include inaccessibility of safe clean water, poor sanitation systems, lack of footwear, and poor hygiene practices (Strunz et al., 2014). This is reflected in the global distribution of STH infection, which predominantly impact low- and middle-income regions, although it should be noted that infection also affects vulnerable populations within high-income countries (Figure 1.1) (Bartsch et al., 2016; Montresor et al., 2020). Additionally, external factors like temperature, moisture and soil pH are an important components in the survival of helminth eggs once outside of the host and thus impact STH prevalence (Booth, 2018). Tolerance of eggs to environmental conditions varies between species, but generally temperatures of 20-40°C combined with adequately moist soil is advantageous for egg embryonation and larval survival and helminth transmission (Booth, 2018). This underpins the seasonal shifts in transmission of STHs identified in various regions (Mabaso et al., 2003; Udonsi et al., 1980; Wardell et al., 2017). Many global regions that fulfil the optimal climate conditions for STH survival unfortunately overlap with regions with substantial poverty, poor sanitation, limited access to clean water and inaccessible healthcare, culminating in ideal conditions for STH transmission and leading to a high prevalence of infection and persistence of disease (Figure 1.1).

STH's display aggregated distribution within affected communities, where individuals show susceptibility for either high or low intensity infections. Aggregated distribution results in most individuals carrying low burden chronic infections, while a few individuals will carry a disproportionately high number of worms (Hotez et al., 2006). Within highly prevalent regions some groups are at higher risk of STH infection, these being i) pre-school aged children, ii) school aged children and iii) women of reproductive age (Montresor et al.,

2020). In 2018, the numbers of at-risk individuals for these groups were 310 million, 762 million, and 688 million respectively (Montresor et al., 2020; WHO, 2020). This impact of STH infection for these vulnerable groups is troubling, as STH associated malnutrition and anaemia can have detrimental long-term impacts either on the individual's growth and development, or on the developing foetus in the case of pregnant women (Blackwell et al., 2015). Additionally, STH infections often occurs in the context of pre-existing health conditions such as, anaemia, malnutrition, iron deficiency, and other co-infections, exacerbating the negative impact of STH infection (Loukas et al., 2016). The impact of STHs on the growth and development of children has detrimental effects on both the educational advancement, and economic stability of highly prevalent regions. Furthermore, the impact of STH helps to propagate a continuation of the cycle of poverty which in turn keeps conditions prime for STH infection.

### 1.1.2 STH attributed morbidity

Although STH resulting in death is very rare, STH infection has negative impacts on the lives of those infected (referred to as morbidity). Morbidity can be measured by disability-adjusted life years (DALYs), a measure defined by the World Health Organisation (WHO). DALYs account for the impact of disease throughout an individual's lifespan and is calculated by combining three measurements, i) the burden of disease by combining life years lost living in less than full health ii) life years lost to premature mortality and iii) healthy life years lost due to disability (Murray & Acharya, 1997). However, DALYs are an estimate and may be underestimated due to unreliable data in some regions, or because the impact of some symptoms e.g., malnutrition, iron deficiency and anaemia are difficult to attribute to a specific causative agent. Irregardless, 2010 estimates suggested 1 million, 500,000, and 4 million DALYs can be associated to *Ascaris* infection, *T. trichuria* infection and



hookworms (*A. duodenale* and *N. americanus*) respectively (Bartsch et al., 2016; de Vlas et al., 2016; Jourdan et al., 2018).

A major implication and contributor of DALYs associated with STH infection is blood loss caused by worms feeding on host blood supply in the case of human hookworm, or due to intestinal tearing and inflammation in the case of non-hematophagous helminths (Loukas et al., 2016). In hookworm infections, although the amount of blood consumed per worm per day is low (0.001 ml), substantial amounts (>1 ml) are lost through the site of attachment due to parasite derived anti-coagulant factors (Layrresse et al., 1965; Stassens et al., 1996). High worm burden infections therefore can lead to significant blood loss, as well as iron deficiency anaemia (IDA) and protein deprivation (Figure 1.1) (Loukas et al., 2016). IDA is pronounced during pregnancy as maternal iron supplies are diverted to the growing foetus, and iron deficiency during pregnancy can result in premature birth, impaired lactation and lowered birth weight (Blackwell et al., 2015). While in adults heavy worm burden is required for the development of IDA, in children it can result even with relatively low worm burden infections and can lead to developmental delays (Loukas et al., 2016). Furthermore, co-infection with multiple species of STHs, schistosomes, or malaria (it is not uncommon for individuals to suffer co-infection with all three) exacerbates the risk and severity of IDA (Loukas et al., 2016).

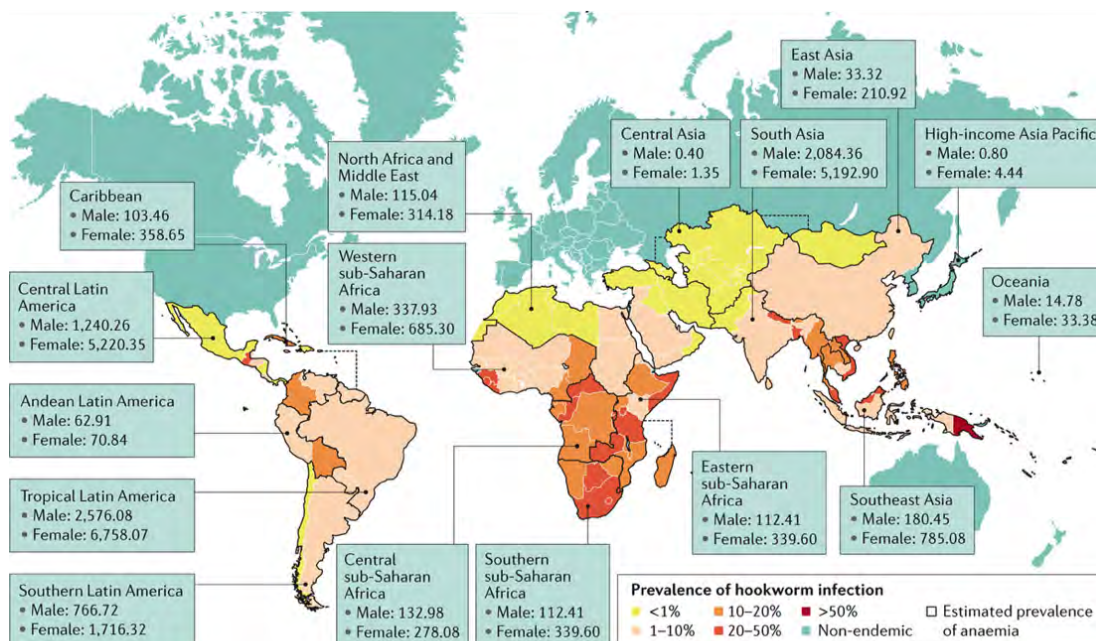


**Figure 1.1 | Distribution of hookworm worldwide and estimated prevalence of hookworm associated anaemia.** Countries for which data is available are coloured according to hookworm (*A. duodenale* and/or *N. americanus*) prevalence. Countries indicated with black borders have boxes that denote the estimated prevalence of hookworm associated anaemia in prevalence rate per 100,000 people, stratified by sex. Figure from Loukas *et al.*, 2016.

### 1.1.3 Current therapeutics and interventions

The most preventative intervention for STH infection is implementation of improvements to water, sanitation, and hygiene (WASH) which is associated with reduced odds of STH infection (Strunz *et al.*, 2014). WASH practices are a part of the proposed plans for STH eradication detailed by the WHO in their roadmap for NTD 2021-2030 (WHO, 2020). Although WASH programmes are outside the scope of this thesis and will not be discussed further, it is imperative to mention them as without the implementation of these practices it is unlikely that currently available interventions alone will eradicate STH infection (Loukas *et al.*, 2016).

In 2012, the World Health Organisation (WHO) presented the Neglected Tropical Disease (NTD) roadmap which detailed plans for the control or eradication of 10 NTDs globally including STHs (WHO, 2012). The mostly widely used and available anti-helminthic drugs are ivermectin, which is only

effective against *Trichuria* and *Strongyloides spp*, or the superior benzimidazoles drugs Albendazole and Mebendazole (Speich et al., 2016). In order to implement its roadmap, the WHO, utilised preventative chemotherapy (PC) which refers to the delivery of single-use safe medicines (mostly benzimidazoles) at a large-scale (WHO, 2012). Despite a decrease in disease prevalence globally, WHO have fallen short of their goal of 75% coverage of PC in 100% of countries with only 16/63 countries meeting this for pre-school aged children and 28/96 for school aged children. The WHO have expanded their roadmap for 2020-2030 to address the ongoing problem of STH infection (WHO, 2020).

Treatment with benzimidazoles does not always lead to parasite clearance, and importantly, it does not protect against subsequent infection (De Clercq et al., 1997; Soukhathammavong et al., 2012). Concerningly, there is also evidence initially in livestock of emerging helminth resistance against benzimidazoles, and in human populations repeated treatment with mebendazole resulted in lowered efficacy over time (Demeler et al., 2013; Doyle & Cotton, 2019; Sihite et al., 2014). Therefore, new targets for anthelmintic drugs or effective vaccines continue to be sought after.

#### 1.1.4 Non-human animal models of human helminth infection

Human hookworms require passage through human hosts for completion of their lifecycle, providing a significant challenge for primary research in human hookworm infection and immunity. In recent years there has been an increase in controlled human hookworm studies proving that helminth infection can be well tolerated and safe in experimental settings. This has also yielded valuable understanding into human helminth infection processes (Chapman et al., 2021). However, research requiring human participants has many limitations with regard to experimental read outs, ethical constraints and practicalities (Chapman et al., 2021). Therefore, alternative animal infective helminth parasites that are either closely related to human infective species, or have

similar infection dynamics, can be used as a model of human helminth infection (Loukas et al., 2016).

Human hookworm is most closely replicated in the laboratory by two species, *Nippostrongylus brasiliensis* (*N. brasiliensis*) and *Heligmosomoides polygyrus bakeri* (*H. bakeri*) (Camberis et al., 2003). *N. brasiliensis* naturally infects rats, although it can also infect mice, and enters the host through penetration of the skin barrier similarly to human hookworm (Camberis et al., 2003). *N. brasiliensis*, like human hookworm, migrates to the lung where it undergoes a moulting stage to develop into larval stage 4 (L4) larvae (Camberis et al., 2003). *N. brasiliensis* then migrates to the intestine where it carries out the remainder of its lifecycle. The second species that is commonly used as a model of human hookworm is *Heligmosomoides polygyrus bakeri* (*H. Bakeri*). *H. bakeri* has a contentious nomenclature, initially called *Nematospiroides dubious*, and then incorrectly identified as the wood mouse (*Apodemus sylvaticus*) infective species *Heligmosomoides polygyrus polygyrus* for decades before it was re-named *Heligmosomoides polygyrus bakeri* (Behnke & Harris, 2010; Cable et al., 2006). Here I will use the nomenclature used by the International Helminth Genome Consortium where *H. bakeri* refers to the parasite species that infects the house mouse (*Mus musculus*) which is used in laboratory settings (Camberis et al., 2003; Coghlan et al., 2019).

*H. bakeri*, like human hookworm spp. *A. duodenale* and *N. americanus*, is also a clade five nematode (Coghlan et al., 2019). Unlike human hookworm, *H. bakeri* infects via the ingestion of infection larval stage 3 (L3) larvae, rather than by burrowing through the skin (Camberis et al., 2003) (Figure 1.2). *H. bakeri* does not transit through the skin, blood vessels, or lung during infection (Camberis et al., 2003). Instead, *H. bakeri* L3 larvae go first to the fundic region of the stomach between 4 h and 36 h post infection (p.i.) which may provide important signals for exsheathment or larval development. *H. bakeri* L3 larvae then migrate directly to the most proximal end of the small intestine, the duodenum. In the duodenum L3s burrow through the intestinal epithelium, and into the underlying submucosa (Camberis et al., 2003). Once in the submucosa the larvae undergo two moults to become, first L4 larvae, and then

adult parasites (Camberis et al., 2003). Once worms mature into adults, they will make their way out of the submucosa into the intestinal lumen of the duodenum, and by day 8-10 post infection the majority of infective larvae are now adult worms that reside in the lumen of the intestine. Adult *H. bakeri* worms reproduce and eggs are released in the host faeces, which are detectable from ~day 10 onwards (Camberis et al., 2003; Reynolds et al., 2012). *H. bakeri* worms are cleared naturally by the host as early as 4-6 weeks after infection in some mouse strains, while in other mouse strains *H. bakeri* can persist for more than 20 weeks. At least some of the strain to strain variation in parasite clearance is underpinned by genetic differences in loci of key immune genes e.g., major histocompatibility complex (MHC) (Reynolds et al., 2012).

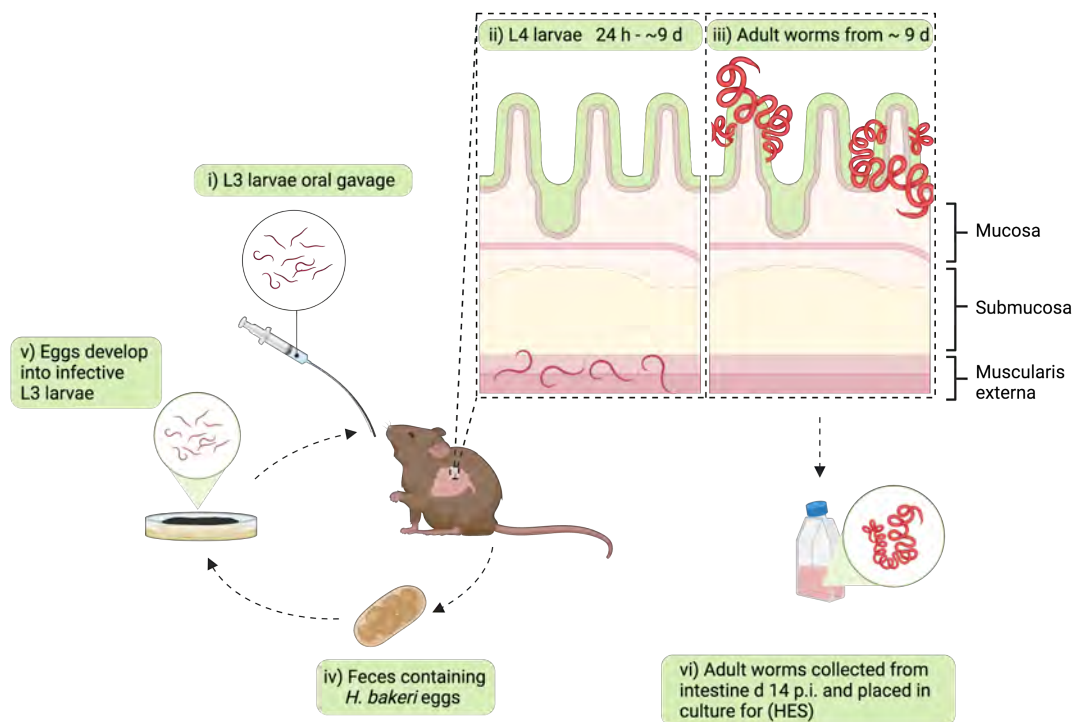


**Figure 1.2 | Laboratory lifecycle of *H. bakeri*.** i) Larval stage 3 (L3) larvae are delivered to *Mus musculus* via oral gavage. ii) L3 larvae burrow into the submucosa where they undergo two moulting stages to develop first into larval stage 4 (L4) larvae, and then adult worms. iii) Between approximately day 9-14 adult worms exit the submucosa and make their way back to the intestinal lumen where they reside, reproduce and lay eggs. iv) *H. bakeri* eggs are expelled in mouse faeces, or in the laboratory animals are sacrificed and colonic contents collected. v) *H. bakeri* eggs are cultured in charcoal patties as described by Camberis *et al*, 2003 until infective L3 larvae develop, and the lifecycle can be continued. vi) For collection of *H. bakeri* excretory/secretory products (HES) worms are collected from small intestinal contents, washed as described in Johnston *et al*, 2005, and cultured for 1-2 weeks for HES generation. p.i. = post infection, d = days, HES = *H. bakeri* excretory/secretory products (HES).

## 1.2 Host-helminth dynamics

Helminths are ancient parasites, thought to have arisen during the Mesozoic period (~66-252 million years ago) (De Baets et al., 2021). The oldest direct evidence of human helminth infection comes from helminth eggs found in mummies dated to 1250 – 1000 B.C. demonstrating their ancient relationship with humans (De Baets et al., 2021; Hoespli, 1956). Over long periods of evolutionary time, helminths have become eloquently adapted to the environment of their obligate hosts, and as such have evolved mechanisms of host manipulation that researchers are still uncovering today (Rick M. Maizels et al., 2018; Henry J. McSorley & Maizels, 2012). Hosts are not passive carriers of these parasites either, and entire arms of the immune system (Type 2 responses) are proposed to have evolved in order to respond to this type of parasitic infection (Allen & Wynn, 2011). Proinflammatory Type 1 immune responses are effective against bacterial and viral infections, because they induce direct killing of bacterially- or virally infected host cells, or bacteria themselves (Allen & Wynn, 2011). While in the context of infection with large metazoan parasites like helminths, type 1 immune responses are unlikely to efficiently kill these worms, and even if successful they would cause substantial immune associated pathology (Allen & Wynn, 2011). Effective host responses to helminth infection in general are driven by type 2, and regulatory immune responses, which act to limit host pathology whilst also driving effector mechanisms that promote pathogen clearance and/or reduce parasite fitness (Henry J. McSorley & Maizels, 2012). The balance between type 2 immune responses and regulatory responses in a given individual seemingly determines the outcome of infection, and ranges from complete tolerance resulting in a chronic high burden infections, to effective clearance coinciding with collateral damage to the host (Henry J. McSorley & Maizels, 2012). Most human infections result in the middle ground scenario of low burden chronic infections that cause minimal pathology based on epidemiological data (Hotez et al., 2006). Finally, hosts are particularly poor at inducing immune memory

and resistance to subsequent helminth infections, resulting in persistent re-infection in endemic areas after drug assisted clearance (Loukas et al., 2016). Despite natural infection resulting in poor memory immune responses, vaccination with irradiated parasite antigen is effective at inducing memory immune responses (Hotez et al., 2010). The fact that natural helminth infections do not induce protective immunity, but vaccination with attenuated worms does, suggests that live parasites actively interfere with the development of effective host immune responses during natural infection (Henry J. McSorley & Maizels, 2012).

### 1.2.1 Host immune response to helminth infection

#### *Generalised response*

The immune response to different helminth species shares many overlapping features, although differences in the routes of transmission and the host organs that are infected may result in immune response dynamics that are context specific. However, in general helminth infection is more commonly associated with a strong type 2 immune responses, dominated by the Th2 cytokines interleukin (IL) -4, -13, -5 & -9 which together suppress Th1 responses, coordinate anthelminthic effector cells and initiate tissue repair (Anthony et al., 2007; Ben-Smith et al., 2003). Th2 cytokines have multiple cellular sources during helminth infection including Mast cells (Hepworth et al., 2012); ILC2s (Herbert et al., 2019); and adaptive Th2 cells (Urban, Katona, & Finkelman, 1991; Urban, Katona, Paul, et al., 1991). Together, the Th2 cytokines function to recruit myeloid cells, polarise macrophages in the tissue to a M2 reparative phenotype, activate ILC2s and Th2 cells, and induce antibody responses particularly for the isotypes IgE, IgG1 and IgG4 (Anthony et al., 2007; Figueiredo et al., 2010; Henry J. McSorley & Maizels, 2012; Wahid & Behnke, 1993). Despite the fact that helminths are large multicellular parasites that cause significant tissue damage in their hosts, these infections generally result in surprisingly minimal host pathology (Allen & Wynn, 2011).

This is due to Th2 responses not only inducing effector functions that mediate the clearance of helminths, but also playing a critical role in tissue repair (Allen & Wynn, 2011). In addition to Th2 responses, many murine and human infective helminths also induce significant numbers of T regulatory (Treg) cells, which act to constrain immune responses and subsequent pathology during infection (Finney et al., 2007; Metenou et al., 2010; Nausch et al., 2011; Ricci et al., 2011; Wammes et al., 2010, 2012). Finally, host immune responses during infection are also countered by helminth modulation of the hosts immune system, that in general result in higher immune tolerance and allows for persistent infection (Alabi et al., 2021; R. Maizels et al., 2018; Rick M. Maizels & McSorley, 2016).

### **1.2.2 Recognition of helminths at the barrier site and associated immune responses**

The first fundamental barrier that all infecting helminths interface with, and must overcome, is the epithelial barrier. The epithelium protects host tissues, whether this be the epithelium of the skin in the case of cutaneous invading helminths (e.g., *N. brasiliensis*, *A. duodenale*, *N. americanus*), the intestinal epithelium for gastrointestinal parasites (e.g., *H. bakeri*, *T. muris*, *T. trichuria*), or in the lung (e.g., *N. brasiliensis*, *A. duodenale*, *N. americanus*) (Loukas et al., 2016). Upon early infection, epithelial cells respond to helminth infection by rapidly secreting alarmin cytokines (IL-33, IL-25, TSLP), damage associated molecular patterns (DAMPs) and adenosine 5' triphosphates (ATP) (Coakley & Harris, 2020; Patel et al., 2014; Shimokawa et al., 2017). However, the exact mechanisms by which these epithelial first responders sense helminths are not entirely delineated. Although there is evidence of responses associated with generalised tissue damage, for example by mast cells and epithelial cells (Patel et al., 2014; Shimokawa et al., 2017), as well as evidence of sensing specific helminth associated molecules. For example, tuft cells which are specialised cells of the intestinal epithelium (discussed further



Section 1.5) have recently been shown to sense helminths through taste *Tas2r* family receptors (Luo et al., 2019), these same cells can also sense helminth derived cysteinyl leukotrienes through an unknown receptor (McGinty et al., 2020), and the metabolite succinate via the receptor *Sucnr1* (Lei et al., 2018; Nadjombati et al., 2018; Schneider et al., 2018). Recent work showed that *N. brasiliensis* secretes succinate metabolites that can be directly detected by intestinal tuft cells, and infection with *N. brasiliensis* induces hyperproliferation of tuft cells (Lei et al., 2018; Saz et al., 1971). However, *Sucnr1*<sup>-/-</sup> mice infected with *N. brasiliensis* showed no deficiency in tuft cell hyperplasia, suggesting tuft cells possess redundancy in their mechanisms for helminth detection (Lei et al., 2018). Whether tuft cells also sense helminths via these mechanisms in other tissues, such as the lung and skin epithelium, has not been investigated. However, single cell analysis has demonstrated tuft cells in the lung (also termed brush cells) (Krasteva & Kummer, 2012), while in the skin sensory cells of similar characteristics to tuft cells have also been described (Cernuda-Cernuda & García-Fernández, 1996). The sensing and subsequent production of alarmin cytokines by epithelial cells then sets off a cascade of responses involving several cell types, that culminates in an anthelmintic defence (Figure 1.3).

### 1.2.3 Key components of anthelmintic responses

The immune response to helminths is comprised of a complex network of cellular responses that have variable importance for overall parasite clearance. In this following section I will break down the components of anthelmintic responses that have been implicated characterised as critical for effective immunity.

#### *T helper cells & cytokines*

Th2 cells are primed by helminth antigen loaded dendritic cells, in the Peyer's patches or mesenteric lymph nodes (mLN), whereafter they undergo clonal expansion and migrate to the site of infection (Ronchese et al., 1994) .

Activated Th2 cells produce the Th2 cytokines IL-4, IL-5, IL-13 and IL-9 (Svetić et al., 1993). The importance of Th2 cells in various helminth infections has been delineated by several lines of evidence, below I describe in detail a major role for the cytokines IL-4 and IL-13. IL-5, which is also produced by Th2 cells, is dispensable at least in *H. bakeri* clearance (Urban, Katona, Paul, et al., 1991). Conversely, IL-5 may be important in human hookworm infections, as in *N. americanus* infections levels of IL-5 correlate with protection against subsequent infections (Quinnell et al., 2004).

Data from human populations in hyperendemic regions has found increased levels of Th2 associated cytokines production is seen in T cells isolated from individuals infected with *Ascaris lumbricoides* and/or *Trichuris trichuria*, both when unstimulated, or upon re-stimulation with antigen from the infective species (Figueiredo et al., 2010). Use of animal models has allowed us to better understand the relationship between Th2 cells, their cytokines and helminth infection. Infection of *Mus musculus* with *H. bakeri* results in a dominant Th2 cytokine response that is initiated by an early wave of IL-5, -9 and -13 in a T-cell independent manner, which then subsequently activates Th2 cell to produce IL-4 (Svetić et al., 1993). The critical dependence on T- and B-cells for the clearance of helminth parasites has been well demonstrated in athymic mice (which lack T-cells); and in severe combined immunodeficient (SCID) mice (which lack T- and B- cells). Additionally,  $\alpha$ -CD4 blocking antibodies (which block T helper cells) results in increased parasite success in *H. bakeri* infection (Hashimoto et al., 2009; Urban, Katona, Paul, et al., 1991; Urban et al., 1995). These data, from both human and mice, taken together implicate Th2 cells, and B-cells (discussed further below) in effective protection against helminths. The direct assessment of the extent to which CD4+ T cells contribute to protective immunity against *H. bakeri* was shown later through adoptive transfer of these cells from chronically infected mice. Naïve mice that received CD4+ T cells from infected mice showed significantly reduced worm burdens upon a primary *H. bakeri* infection (Rausch et al., 2008). Yet in SCID mice (lacking T- and B- cells) recombinant IL-4 enhances helminth responses,

demonstrating that the cytokine IL-4 itself partially accounts for the requirement of T- and B- cells (Urban et al., 1995).

### *IL-4 signalling in helminth infection*

Evidence in the 1990's clearly demonstrated an important role for Th2 cells and their cytokines, particularly IL-4, in helminth immune responses (Urban, Katona, Paul, et al., 1991; Urban et al., 1995). While blocking IL-4 during infection does reduce helminth clearance, blocking the IL4 receptor alpha (IL4R $\alpha$ ) completely ameliorates parasite clearance (Urban, Katona, Paul, et al., 1991). The IL4R $\alpha$  is a component of not only the IL-4 receptor but can also dimerise with the IL13 receptor  $\alpha$ 1 (IL13R $\alpha$ 1) to form the IL-13 receptor complex (Junttila, 2018; Zurawski et al., 1993). The critical importance of the IL4R $\alpha$ , indicates that together IL-4 and IL-13 co-ordinate all of the indispensable immune responses that comprise effective anthelminthic responses (Urban, Katona, Paul, et al., 1991). Since these findings, it has been elucidated that IL-4 and IL-13 signalling is required for many processes important in the response to helminth infection including: i) the polarisation of M2 macrophages (Anthony et al., 2006; Bouchery et al., 2015; Minutti, Jackson-Jones, et al., 2017), ii) ILC2 signalling to Th2 cells, and with the intestinal epithelia to drive hyperplasia of goblet and tuft cells (Gerbe et al., 2012; Hashimoto et al., 2009; Howitt et al., 2016; Pelly et al., 2016; Von Moltke et al., 2016), iii) antibody switching in B-cells to IgE, IgG2 and IgG4 isotypes (Gascan et al., 1991; Lebman & Coffman, 1988; Punnonen et al., 1993) and finally, iv) in wound repair processes that occur after invasion by large multicellular pathogens such as helminths, by signalling to fibroblasts and through the induction of M2 macrophages (Allen & Wynn, 2011; Minutti, Jackson-Jones, et al., 2017; Minutti et al., 2019).

### *ILC2s*

Innate lymphoid cells (ILCs) are tissue-resident innate lymphoid cells that lack antigen specific T- or B- cell receptors (Herbert et al., 2019). ILCs mirror helper T cell subtypes, with ILC2's producing similar cytokines to Th2 cells, and both cell types requiring Gata3 expression for secretion of cytokines (Herbert et al., 2019). During helminth infection, ILC2 rapidly respond to IL-25, -33 and TSLP produced by epithelial cells during *N. brasiliensis* and *H. bakeri* infection (Moro et al., 2010; Neill et al., 2010; Price et al., 2010). In response to exposure to these aforementioned alarmin cytokines, ILC2s produce the early wave of Th2 associated cytokines IL-5, -13, -9, amphiregulin (AREG) and small amounts of IL-4 prior to the activation of Th2 cells (Herbert et al., 2019). The rapid production of this set of cytokines by ILC2s helps to repair tissue damage at the site of infection, and amplify anthelmintic responses by contributing to CD4+ Th2 effector T cell response (Allen & Wynn, 2011; Oliphant et al., 2014). For example, depletion of ILC2s during *N. brasiliensis* infection resulted in perturbed Th2 cell cytokine secretion and worm clearance (Oliphant et al., 2014). ILC2s enhance Th2 cells by acting as antigen presenting cells interacting with Th2 cells at tissue sites via antigen loaded MHC-II, and amplifying Th2 cell cytokine secretion (Oliphant et al., 2014). In turn, Th2 produces IL-2 which enhances the production of IL-13 by ILC2s thus amplifying cytokine levels in the tissue (Oliphant et al., 2014). Fascinatingly, Rag2<sup>-/-</sup> mice (which lack functional T cells), but maintain their ILC2 compartment, are unable to clear *N. brasiliensis* infection; however in the same settings when animals were given IL-2, animals showed complete worm clearance (Oliphant et al., 2014). In summary, ILC2s are essential for the response to helminth infection, but their ability to fully respond is dependent on IL-2 signalling provided Th2 cells (Figure 1.3).

#### 1.2.4 Regulatory responses

Regulatory T cells are a subset of Fox3p expressing CD4+ T cells, that can be induced by exposure to transforming growth factor beta (TGFβ) (Belkaid &

Tarbell, 2009; Williams & Rudensky, 2007). Once differentiated, Tregs produce ample amounts of the regulatory cytokines IL-10 and TGF $\beta$  (von Boehmer, 2005). Treg cells, via cytokine secretion, have the ability to suppress both Th1 and Th2 cells thereby constraining the amplitude of immune responses, and minimising immune associated pathology (Belkaid & Tarbell, 2009). While Treg cells play an important role in controlling immune responses, having too many Treg cells may lead to suppression of protective immunity (Belkaid & Tarbell, 2009). In epidemiological data from human populations infected with helminths, there is evidence linking the level of Treg responses during infection with clinical outcomes (Henry J. McSorley & Maizels, 2012). For instance, for humans with onchocerciasis, filariasis, human hookworm infection, and in children with schistosomiasis, asymptomatic individuals showed elevated IL-10 and TGF $\beta$  levels coinciding with suppressed Th1 cytokines (IFN- $\gamma$ ) and/or Th2 cytokines (IL-5) (Metenou et al., 2010; J. S. Satoguina et al., 2008; Wammes et al., 2010, 2012). Furthermore, infected individuals displayed higher numbers of circulating Treg cells (Metenou et al., 2010; Nausch et al., 2011; Ricci et al., 2011). Tregs isolated from infected individuals had an enhanced ability to suppress Th1 and Th2 cells *in vitro* than those isolated from uninfected individuals (Babu et al., 2006; Ricci et al., 2011; J. Satoguina et al., 2002). In mice infected with *H. bakeri* a strong Treg response occurs peaking at d28 p.i., and blocking Treg cells during infection results in increased Th2 responses and higher worm burdens (Finney et al., 2007; Grainger et al., 2010). On the other hand, depletion of Tregs during *H. bakeri* infection also results in increased severity of pathology (Rausch et al., 2008). In summary, Tregs play a central role during helminth infection in maintaining the balance between effective protective immunity and immune associated pathology.

### 1.2.5 Contribution by innate immune cells

#### *Dendritic cells*

One of the central dogmas in immunology is that dendritic cells (DCs) are required for antigen presentation to induce the adaptive branch of the immune system (T- and B-cells). While DCs are clearly required for Th1 responses, for Th2 responses the role of dendritic cells seems to be less clear cut. Mice depleted of CD11c<sup>high</sup> DCs have impaired, but not ablated, Th2 responses during helminth infection (K. A. Smith et al., 2012). However, other responses downstream of DCs such as in macrophages, ILC2, eosinophils and epithelial cells were unaltered in the gastrointestinal tract (K. A. Smith et al., 2012). These findings suggest redundancy in the multicellular response to helminths, and an innate ability to respond, although it should be noted that depletion of DCs was not complete in this model (K. A. Smith et al., 2012). While the activation signals required for dendritic cells polarise T cells towards a Th1 cell fate have been well described, the direct signals that induce Th2 priming DCs have long remained elusive (MacDonald & Maizels, 2008); Type I interferon responses have been implicated in the generation of Th2 priming DCs, and antibody blocking of the interferon receptor reduced Th2 cell induction during *N. brasiliensis* infection (Connor et al., 2017; Webb et al., 2017).

### *Macrophages*

During helminth infection macrophages are rapidly recruited to the site of infection, and in response to the milieu of Th2 cytokines become alternatively activated macrophages (AAMs) (also known as M2) (Anthony et al., 2006). Unlike their M1 counterparts, AAMs macrophages are anti-inflammatory, and have high expression of arginase-1 (Arg1), Ym1, IL4R $\alpha$ , RELM- $\alpha$  and the mannose receptor (CD206) (Anthony et al., 2006; Hesse et al., 2001). AAMs play important roles during secondary infections, where they contribute to granuloma formations surrounding L4 larvae and reduce worm burdens (Anthony et al., 2006). However, when arginase-1 is blocked the protective effect of AAMs on granulomas is significantly reduced (Anthony et al., 2006). AAM macrophages are also specialised at wound healing, and act to repair tissue damage caused by helminth invasion of various organs (Lechner et al.,

2021). AAMs repair tissues through secretion of angiogenesis factors (e.g. VEGF) which increases vascularisation of the tissue, and they induce collagen production by fibroblasts (Lechner et al., 2021; Minutti, Jackson-Jones, et al., 2017; Minutti, Knipper, et al., 2017). Finally, AAMs can also play immune regulatory roles. For example, AAMs secrete the regulatory cytokine IL-10 as well as the molecules RELM- $\alpha$  and Arg1 which can regulate Th2 cells (Pesce, Ramalingam, Mentink-Kane, et al., 2009; Pesce, Ramalingam, Wilson, et al., 2009).

### *Eosinophils, Neutrophils and Mast cells*

IL-5 is well known as an eosinophil recruitment and differentiation factor that is induced rapidly upon *H. bakeri* infections (Moro et al., 2010; Neill et al., 2010; Tominaga et al., 1991). IL-5 is also found upregulated in humans infected with *N. americanus* implicating eosinophils as an early characteristic of human helminth infection (Anthony et al., 2007; Gaze et al., 2012; Quinnell et al., 2004). Evidence from endemic regions showed that upon drug assisted helminth clearance and re-infection, initial IL-5 levels prior to treatment negatively correlate with worm burdens (Quinnell et al., 2004). Despite these findings, in mouse experimental models eosinophils do not seem to play a great role in the clearance of adult parasites in the intestine, although they may contribute to immunity through the production of IL-4 and IL-13, as well as by clearing debris, and tissue remodelling (Knott et al., 2007). Eosinophils don't seem to effect adult stage parasites, however they may play a role in the killing of early larval stage parasites (Rick M. Maizels & Balic, 2004). Indeed, eosinophils can directly kill *Trichinella spiralis* larvae *in vitro*, and in secondary challenge with *N. brasiliensis* eosinophils prevent larvae from successfully migrating from the skin to lung (Basten et al., 1970; Buys et al., 1984; Knott et al., 2007).

Neutrophils are also recruited to the site of helminth infection, and recent studies have begun to unravel their significance (Ajendra, 2021; Anthony et

al., 2007). Neutrophils can directly kill *S. stercolis* larvae *in vitro*, and in *N. brasiliensis* infection neutrophil depletion led to higher worm burdens in the gut (Bouchery et al., 2020; Galioto et al., 2006). During the larval stage of *H. bakeri* infection neutrophils play an important role in walling off larvae during the formation of granulomas, and transfer of neutrophils along with serum from infected mice to naïve mice resulted in resistance to infection (Penttila et al., 1984).

Mast cells also contribute to helminth immune responses but this is seemingly species specific, for example mast cells are important in effective clearance of *T. spiralis* worms but are not critical for parasite clearance of *H. bakeri* or *N. brasiliensis* (Anthony et al., 2006). Although mast cells are not critical for *H. bakeri* clearance, infection is associated with increased mast cell numbers suggesting they contribute to helminth immune responses in this model (Anthony et al., 2007). Indeed, mast cells contribute to *H. bakeri* responses by rapidly responding to ATP (released upon epithelial cell death during helminth infection) to produce IL-33 (Shimokawa et al., 2017). Mast cell derived IL-33 in turn acts to enhance ILC2 cytokine secretion (Shimokawa et al., 2017). Finally, mast cells express high levels of the Fc epsilon Receptor I (FcεR1) the receptor for IgE. Binding of IgE to mast cells causes degranulation and release of soluble effector molecules that regulate muscle contraction, the permeability of the intestinal epithelium, and increase mucus secretion by goblet cells (Anthony et al., 2007).

### 1.2.6 Humoral immune responses

B-cell numbers increase significantly during infection, and concentrations of the antibodies IgG and IgE correlate with protection (Ben-Smith et al., 2003; Wahid & Behnke, 1993; Wahid et al., 1994). B-cell deficiency in mice however does not alter the response to primary infection, but upon secondary infection B-cell deficient mice cannot clear their infection (Q. Liu et al., 2010; McCoy et al., 2008; Wojciechowski et al., 2009). Upon secondary helminth infection,



antibody responses are important in determining the outcome of secondary infections. B cells, which produce antibodies, are critical for parasite clearance in secondary infections as demonstrated by SCID mice (lack T- and B- cells), as well as in specific B cell knock out mice ( $\mu$ MT and JHD mice) which cannot clear secondary infections (Q. Liu et al., 2010; McCoy et al., 2008; Urban et al., 1995; Wojciechowski et al., 2009). *H. bakeri* infection as well as vaccination with total worm homogenate or HES, all result in high levels of antigen specific IgG1 and IgE (Ben-Smith et al., 2003; Hewitson et al., 2011; Wahid & Behnke, 1993; Wahid et al., 1994). Several human infective helminths including Filariasis, Onchocerciasis, *A. lumbricoides* and *T. trichuria* infections have also been associated with the isotypes IgG1, IgE and also IgG4 (Figueiredo et al., 2010; King et al., 1993; J. S. Satoguina et al., 2008). The dominant isotypes found during helminth infection can be explained by the role of IL-4 and IL-13 on antibody class switching in B cells resulting predominantly in IgG1, IgG4 and IgE isotypes (Gascan et al., 1991; Lebman & Coffman, 1988; Punnonen et al., 1993; Severinson, 2014). Antibodies that arise after multiple infections confer protection by limiting development of larvae into adult worms (McCoy et al., 2008). Antibody protection during secondary infection is mediated through enhancement of granuloma formation via antibody interactions with Fc receptors on innate immune cells, thereby increasing larval trapping (Bieren et al., 2015; Corté et al., 2017; Hewitson et al., 2015). Intriguingly, treatment with polyclonal serum from naïve mice results in a subtle decrease fecundity of *H. bakeri* but has no effect of worm development (McCoy et al., 2008). These data suggest that hosts may possess naturally occurring antibodies that target helminths, but specific antibodies that develop over multiple infections are much more effective for anthelmintic responses (McCoy et al., 2008).

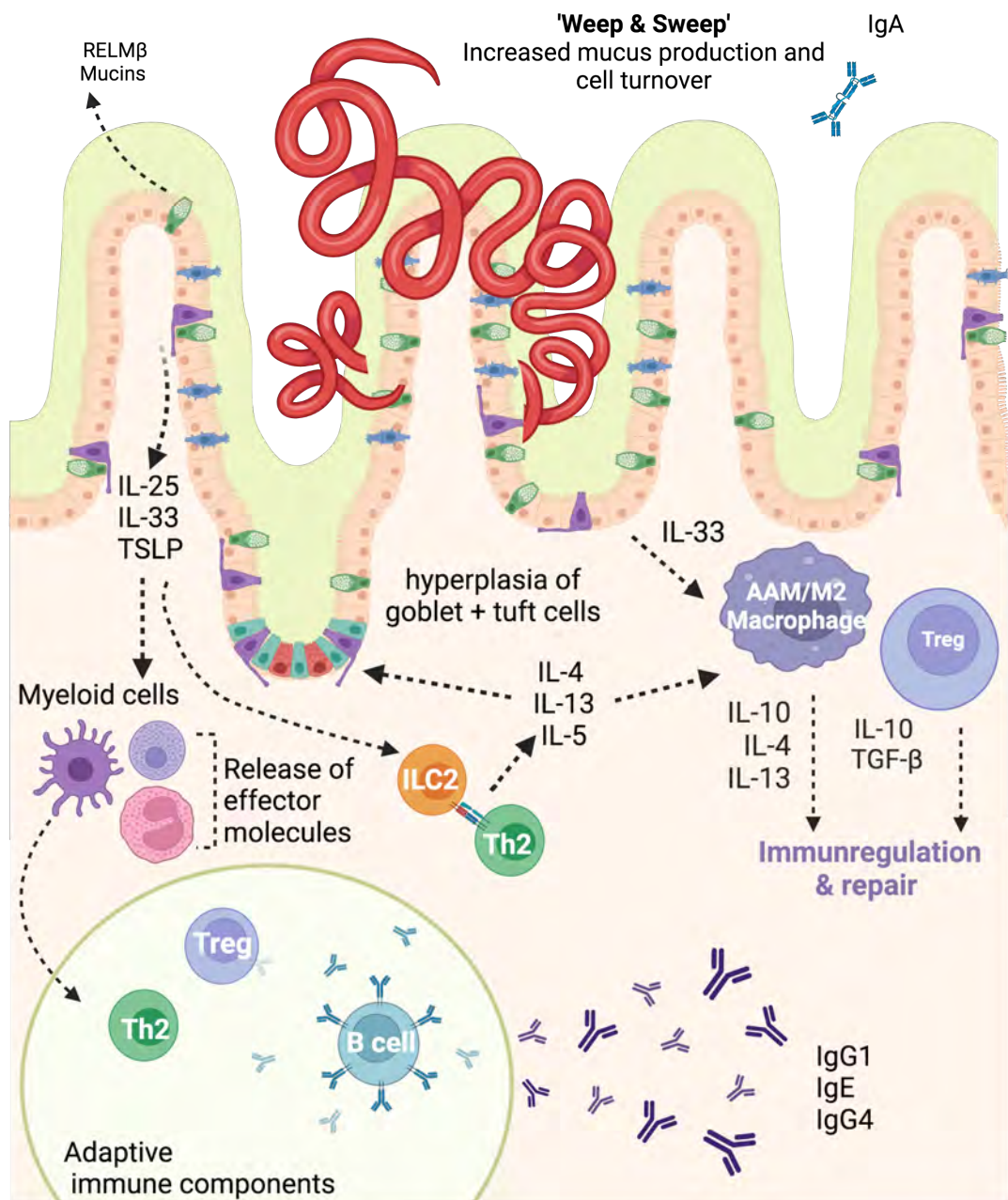


**Figure 1.3 | Summary of the immune response to *H. bakeri* infection.** During helminth infection epithelial cells sense the presence of helminths, or respond to damage signals, by release of IL-25, IL-33 and TSLP. These cytokines recruit and activate myeloid cells including eosinophils and mast cells which release anthelmintic effector molecules, and ILC2s which begin to express IL-13, IL-5 and IL-4. Dendritic cells are activated by alarmin cytokines and by antigen exposure and travel to secondary lymphoid tissue where they induce Th2 effector cells and Tregs. Th2 responses during helminth infection activate B-cells and induce class switching to IgE, IgG1 and IgG4. Th2 then traffic back to the site of infection where they interact with ILC2s, and together these two cell types produce ample Th2 cytokines IL-4, IL-13, and IL-5 leading to conversion of AAM/M2 macrophages, goblet and tuft cell hyperplasia in the epithelium, increased mucus and RELMβ secretion. Treg cells and AMM/M2 macrophages release cytokines involved in tissue repair and suppression of Th2 immune responses. Figure created using BioRender.com.

### 1.2.7 Effector mechanisms of helminth destruction and clearance in the intestinal epithelium

A culmination of multiple assaults aimed at either promoting the removal of parasites via the GI tract, or reducing the fecundity/fitness of the helminth, rather than complete killing is required for helminth clearance (Khan et al., 2001; Marillier et al., 2008; Su et al., 2011; Turner et al., 2003). The initiation and cellular drivers of immune responses during helminth infection have been summarised above. As mentioned, IL-4 and IL-13 are absolutely critical for parasite clearance, but this does not explain the mechanisms by which they mediate clearance. In the epithelium the major method of worm clearance is referred to as the 'weep and sweep' response and this is induced by IL-4 and IL-13 (Baska & Norbury, 2022). 'Weep and Sweep' describes two coordinated changes, 'Weep' refers to an increased epithelial permeability, and hyperplasia of the mucus producing goblet cells in the epithelium resulting in enhanced mucus production which can dislodge parasites (Khan et al., 2001; Marillier et al., 2008; Su et al., 2011; J. D. Turner et al., 2003). Goblet cell hyperplasia during helminth infection is thought to be dependant of IL-4 signalling, although other cytokines may also induce these cells (Khan et al., 2001; Marillier et al., 2008; J.-E. Turner et al., 2013). However, the exact mechanism of how IL-4 signalling results in goblet cell hyperplasia remains an open question. Goblet cells also release the effector molecule resistin-like molecule beta (Relm $\beta$ ) in response to IL-4/-13 signalling, which directly bind nematode chemo sensing organs and interfere with *H. bakeri* feeding leading to reduced nematode fecundity (Artis et al., 2004; Herbert et al., 2009). Other molecules secreted by specialised cells of the intestinal epithelium can negatively affect the success of helminth infection, such as angiogenin 4 (Ang4), which is increased during *T. muris* infection in response to IL-13 and correlates with worm expulsion (D'Elia et al., 2009; Forman et al., 2012). 'Sweep' refers to the increased peristalsis (Z. Chen et al., 2021), and cellular turnover in the epithelium (Cliffe et al., 2005), which helps to move parasites through the GI tract for removal (Baska & Norbury, 2022). During enteric helminth infection changes in

peristalsis is driven by epithelial derived IL-33, which is sensed by specialised endocrine cells within the epithelium called enterochromaffin cells (Z. Chen et al., 2021). Enterochromaffin cells respond to IL-33 in turn by producing serotonin (5-HT), which signals to enteric neurons cells resulting in increased peristalsis (Z. Chen et al., 2021).

### **1.3 Immunomodulation by helminths**

Although helminth infection induces a slew of host immune responses described above, generally infection leads to the tolerance of parasites rather than effective clearance (Jourdan et al., 2018). Tolerance to helminth infection reflects both the host protecting itself from immune mediated pathology, but it also the parasites ability to suppress the immune response (Rick M. Maizels et al., 2018). Hosts and helminths have co-existed for millennia, and over this time an arms race has occurred resulting in helminths becoming exceptionally well adapted to their host environment(s). These adaptations are reflected in both the aforementioned widespread and persistent STH infections seen globally (Jourdan et al., 2018), and the minimal pathology often associated with these infections. Currently, we understand that helminths secrete eloquently adapted immune modulatory molecules that act to counter the immune systems of their host(s) and the ability for helminth secreted proteins to be used as therapeutics has now been demonstrated in several studies (Rick M. Maizels & McSorley, 2016; Rick M. Maizels et al., 2018). However, given the large amount of uncharacterised helminth secreted molecules, our current understanding likely only reflects the tip of the iceberg in terms of helminth secreted molecules that have functional interactions with the host.

#### **1.3.1 Hygiene hypothesis**

The fact that helminths actively suppress the host immune system is consistent with the observation that the prevalence of helminth infections worldwide inversely correlates rates of allergic and autoimmune diseases (Smits et al., 2005). This paradigm is consistent with the well described epidemiological phenomenon born in the 1980s, known as the hygiene hypothesis, which proposed that increased hygiene could explain drastic rises in allergic disease (Strachan, 1989). The hygiene hypothesis was later modified to the 'old friends' hypothesis which proposes that many infectious organisms have developed symbiotic relationships, in which early exposure to these infectious agents trains and tolerises host immunity, thereby preventing diseases associated with hyperactive immune systems (Rook, 2012). However, in reality data from robust meta-analyses suggest that an association between helminth infection and allergic diseases in human population is not so clear cut. For example, in studies of atopy and wheezing no protective effect of helminth infection was found overall, but infections with specific helminth species (*A. lumbricoides* and *T. trichuria*) were associated with an increased risk of bronchial hypersensitivity, or wheezing (Alcântara-Neves et al., 2010; Arrais et al., 2022). Conversely, in a meta-analysis of skin allergen sensitisation, analysis of current parasite infection demonstrated protective effects, as did analysis of species specific infections with *A. lumbricoides*, *T. Trichuria*, hookworm and *Schistosomiasis* (Feary et al., 2011).

The epidemiological hypothesis that at least some species of helminths may protect against allergic disease is supported by the discovery of several mechanisms used by helminths to interfere with the host immune system (Rick M. Maizels et al., 2018; Henry J. McSorley & Maizels, 2012). As illustrated above, many helminth species induce tolerogenic immune responses, and repeated exposure early in life is thought to have bystander effects in protecting from allergic and autoimmune disease (Rick M. Maizels et al., 2018). Trials using controlled helminth infection as a therapeutic for allergic and autoimmune diseases have to date had mixed outcomes and limited efficacy, possibly due to the timing of intervention, or low dosages that are approved for these settings (Rick M. Maizels et al., 2018; Smits et al., 2005).

In recent years, it has become clear that during infection, a slew of helminth secreted molecules influences the host in different ways (Rick M. Maizels et al., 2018). Controlled infections with small doses of worms will produce only limited amounts of helminth effector molecules, while larger doses could cause detrimental side effects, for this reason infection may not be the best approach to tackle allergic and autoimmune diseases. On the other hand, defining specific immunomodulatory molecules, and identifying their potency as stand-alone therapeutics, has the potential to be much more efficacious.

### 1.3.2 Helminth immunomodulatory effector molecules

The total ES products from various helminths have been investigated for their immune suppressive roles. For example, *H. bakeri* excretory/secretory (HES) is capable of inducing Treg cells that produce IL-10 and TFG $\beta$  (Grainger et al., 2010; Johnston et al., 2017). ES from many other helminth species have also been demonstrated to modulate host immune response (Rick M. Maizels et al., 2018). The specific bioactive molecules and mechanisms by which these suppressive effects are achieved are still being elucidated, however a growing list of molecules have been defined that target some of the key immune response pathways during helminth infection.

#### *Blocking of alarmin signalling*

The importance of the alarmin cytokine IL-33 in the initiation of anthelmintic immune responses has been described above, and the role of this cytokine in helminth clearance has been demonstrated in *H. bakeri* and *N. brasiliensis* (Coakley et al., 2017; Hung et al., 2013). The role of HES in suppressing IL-33 signalling was previously shown in a mouse allergic asthma model *Alternaria*/OVA, which induces priming of Th2 responses that are later activated upon OVA exposure. Administration of HES in this model resulted in suppressed allergic responses (H. J. McSorley et al., 2014). In this allergic

asthma model HES suppressed the release of IL-33, subsequently dampening ILC2 cytokine production and abrogating eosinophilia (H. J. McSorley et al., 2014). *H. bakeri* has since been discovered to secrete at least two known proteins that interfere with IL-33 signalling (Osbourn et al., 2017; Vacca et al., 2020). The first identified secreted molecule is the *H. polygyrus* alarmin release inhibitor (HpARI) which can bind both murine and human active IL-33 protein, and tethers it to DNA within dying cells thereby inhibiting its interaction with the IL-33 receptor complex (Osbourn et al., 2017). Administration of HpARI resulted in reduced eosinophilia in the allergic asthma models, and suppressed ILC2 responses, likely due to the blocking of IL-33 release and inhibition of downstream signalling to these cell populations (Osbourn et al., 2017). During *N. brasiliensis* infection, HpARI treatment resulted in reduced eosinophilia and subsequently higher intestinal worm burdens (Osbourn et al., 2017). These findings demonstrate the potential for helminth immune modulatory molecules to be used as therapeutics in pre-clinical models, and the conservation of binding to human IL-33 gives hope for translation of helminth products to human therapeutics. Shortly after the discovery of HpARI, a second molecule termed *H. polygyrus* binds alarmin receptor and inhibits (HpBARI) was discovered, which binds the IL-33 receptor component ST2, and abrogates IL-33 signalling; resulting in similar effects on ILC2s and eosinophils as previously demonstrated for HpARI (Vacca et al., 2020). In addition to HpARI and HpBARI, extracellular vesicles (EVs) derived from *H. bakeri* can suppress the transcript IL1R1 which encodes the ST2 receptor (A. H. Buck et al., 2014). *H. bakeri* EVs administered in an *Alternaria* asthma model reduced eosinophilia, and ILC2 cytokine production, as well as reducing the expression of ST2 (A. H. Buck et al., 2014). Finally, a currently undefined *H. bakeri* ES molecule induces IL1- $\beta$  production during infection which in turn inhibits IL-25 and IL-33 production (Zaiss et al., 2013).

### *Regulatory responses*

As illustrated above, Treg cells are induced by the cytokine TGF- $\beta$  through their TGF- $\beta$  receptor during helminth infection (Grainger et al., 2010). Interestingly, number of helminths secrete TGF- $\beta$  homologues that can activate host TGF- $\beta$  receptors (Rick M. Maizels et al., 2018). For example, the filarial nematode species *Brugia malayi* (*B. malayi*) and the trematode species *Fasciola hepatica* (*F. hepatica*) both secrete conserved proteins of the TGF- $\beta$  superfamily TGH-2, and FhTLM respectively, that are able to bind host TGF- $\beta$  receptors (R. M. Maizels et al., 2001; Rm et al., 2018; Sulaiman et al., 2016). *H. bakeri* also secretes a TGF- $\beta$  mimic protein (TGM), intriguingly TGM is structurally unrelated to TGF- $\beta$  superfamily proteins, and therefore thought to have arisen by convergent evolution rather than being conserved (Johnston et al., 2017). TGM binds both murine and human TGF- $\beta$  receptors leading to induction of Treg cells *in vitro* in both species (Johnston et al., 2017). *In vivo* TGM was equally efficient at inducing Foxp3<sup>+</sup> Treg cells as murine TGF- $\beta$ , and the resulting Treg cells suppressed T-cell responses in an EAE model of multiple sclerosis equally as well as murine TGF- $\beta$  induced Treg cells (M. P. J. White et al., 2021). Finally, in a different autoimmune disease model of DSS induced colitis, TGM delayed the onset of disease equally as well as murine TGF- $\beta$  (M. P. J. White et al., 2021). As a results of these findings, it is proposed that human hookworms species may produce a similar molecule that could contribute to the increase of Treg cells which has been identified during human hookworm infection (Ricci et al., 2011).

There are many more examples of helminth secreted effector molecules that target the host immune system at various stages: from antigen processing, to T- and B- cell activation, and tissue repair (Rick M. Maizels et al., 2018). Most recently, the discovery of secreted EVs by helminth species captured the interest of helminth researchers, and investigations into whether EVs could mediate host immunomodulation has burgeoned a new field of helminth EV research.



## 1.4 Extracellular vesicles

### 1.4.1 Definition, biogenesis and cargo of extracellular vesicles

Extracellular vesicles (EVs) are a heterogeneous group of cell-derived lipid bilayer enclosed nanoparticles that cannot replicate themselves, but can contain proteins, lipids and nucleic acids from the cell of their origin (van Niel et al., 2018). The secretion of EVs by cells is a ubiquitous and conserved phenomenon found across a diverse range of organisms including mammals, archaea, plants, prokaryotes and fungi (Munhoz da Rocha et al., 2020; Woith et al., 2019). Seemingly, wherever researchers look for EV secretion it is found, suggesting that this process is universal phenomenon among living life forms.

In eukaryotes, EVs have been classified into three subtypes based on distinct biogenesis pathways: microvesicles, exosomes, and apoptotic bodies. However, due to their overlapping size and properties as well as limited techniques for separation of these populations, the umbrella term EVs is used to encapsulated all three (Théry et al., 2018). Microvesicles were initially described in platelets and arise from ectocytosis (Stein & Luzio, 1991; Wolf, 1967), a process in which the cell membrane blebs off in an outward motion. Microvesicles range in size from 50-500 nm but can be larger in some cellular contexts (van Niel et al., 2018). Apoptotic bodies similarly arise by outward budding of the cell membrane during apoptosis, leading to larger vesicles (50 – 5000 nm) (van Niel et al., 2018). Exosomes were first identified in reticulocytes, arise from the endosome and are released via the endocytosis secretion pathway. In the endosome, intraluminal vesicles (ILVs) form by inward budding resulting in multivesicular bodies (MVBs), which eventually fuse with the cell membrane releasing ILVs or exosomes into the surrounding extracellular milieu (e.g. exocytosis) (Johnstone et al., 1987; Raposo & Stoorvogel, 2013; van Niel et al., 2018).

Different biogenesis mechanisms of the EV types has implications for which protein cargo is found in a given EV. For example, proteins of the Endosomal Sorting Complex Required for Trafficking (ESCRT) which are involved in the

generation of ILVs during MVB formation, are found enriched in EVs (Beer & Wehman, 2017; van Niel et al., 2018). ESCRT proteins also play roles in microvesicles formation and therefore can be found associated with exosomes and microvesicles (van Niel et al., 2018; Wehman et al., 2011). Other proteins involved in EV biogenesis and commonly identified in EV preparations are syntenin, ALIX, tetraspanins proteins (CD9, CD81, CD82, CD63), chaperone proteins (Hsp70, Hsc70) and RNA binding proteins (AGO2, YBX1) (van Niel et al., 2018). While the majority of our understanding of EV biogenesis comes from mammalian EV studies, there is evidence of related proteins present in *H. bakeri* EVs (A. H. Buck et al., 2014) as well as in several other helminth species, suggesting conservation of EV biogenesis mechanisms in helminths (Sotillo et al., 2020). RNAi screens identified 10 ESCRT proteins involved in EV biogenesis in *C. elegans*, a non-parasitic clade V nematode of the same order (Rhabditida) as *H. bakeri* (Blaxter, 1998; Hyenne et al., 2015). In addition to ESCRT proteins, three other protein families that are commonly found in mammalian EVs were identified in *C. elegans* as well as a novel proteins i) small Rab family GTPases which are involved in intracellular vesicle trafficking, playing roles in both directing MVB to the lysosome for degradation and to the plasma membrane for release (van Niel et al., 2018); ii) SNAP receptors (SNAREs) including syntaxin 5 which form a complex that allows for fusion of MVBs with the plasma membrane allowing for EV secretion (van Niel et al., 2018); iii) V-ATPases which was previously suggested to mediate EV release (Liégeois et al., 2006); iv) RAL-1 identified by Hyenne *et al*, 2015. The overlap of proteins known to be involved in mammalian EV biogenesis that were also found to be required for EV secretion in *C. elegans*, despite their evolutionary distance from one another, suggests that EV biogenesis in helminths may utilise similar pathways to mammalian EVs.

### *EV composition and cargo*

#### *Nucleic acids*

It is well understood that nucleic acids can exist outside of the cell (Kolodny, 1971, 1972). Many nucleic acids released by cells exit within EVs, which serve as a protective barrier against nucleic acid degradation by RNases in harsh extracellular environments (Koga et al., 2011). EVs carry various nucleic acid species including small RNAs (sRNA) such as microRNAs (miRNAs), and short interfering RNAs (siRNAs), as well as longer polyadenylated mRNA (Valadi et al., 2007), and even DNA has also been described (Jin Cai et al., 2013; H. Liu et al., 2022). The shuttling of RNA/DNA for secretion in EVs is not fully understood, although at least in human primary T cells specific motifs were found within miRNAs (EXOmotifs) that mediated interaction with RNA-binding proteins and subsequent export via exosomes (Villarroya-Beltri et al., 2013). Other reports suggest EV RNA cargo reflects the RNA composition of the cell they derive from (Tosar et al., 2021). With regard to miRNAs, Argonaute (AGO) proteins which bind miRNAs has been found within EVs, and in colonic cancer cells AGO2 phosphorylation levels controlled association with the endosome and subsequent incorporation into EVs (McKenzie et al., 2016).

While many studies have characterised the nucleic acid composition of EVs from various sources, the functional assessment of how EV cargo enters the cell without getting degraded by the lysosome, and how miRNA mediate their function once in the cell has not advanced as quickly. Full length mRNA in some contexts has been shown to be translated inside recipient cells (Valadi et al., 2007). The major focus of research has been on miRNAs, perhaps due to their well described role as post-transcriptional mediators of gene regulation (Bartel, 2004). MiRNAs bind their target mRNA by sequence complementarity at their seed site (nucleotides 2-8) most often in the 3'UTR region of the target (Bartel, 2004). Binding of a miRNA accelerates de-adenylation of the target mRNA and inhibits translation (Bartel, 2004). The post-transcriptional activities of miRNAs require their association with an AGO protein, and as mentioned AGO proteins are often found within mammalian EVs. Our group characterised a worm specific AGO (WAGO) protein that is found within, as well as outside of *H. bakeri* EVs, termed extracellular WAGO (exWAGO) (A. H. Buck et al.,

2014; Chow et al., 2019). The presence of miRNAs within EVs in association with AGOs has implicated them as EV cargo molecules that could function in gene silencing in recipient cells. *H. bakeri* miRNAs have also been demonstrated to be successfully transferred to recipient cells (A. H. Buck et al., 2014). Prediction of miRNA targets can be performed computationally using knowledge of the requirements for binding, however due to the small amount of complementarity required for binding (6 nucleotides) target prediction results in large numbers of potential targets. Although predictions can be filtered based on which genes are expressed by your cell type of interest it is still not trivial to select high confidence targets for validation (Bermúdez-Barrientos et al., 2020). Target predictions are further complicated when investigating cross species interactions from non-model organisms, or other small RNA species, as the requirements for- and outcome of- binding may deviate from those described in mammalian systems.

*H. bakeri* EVs package miRNAs as has previously been described by our lab (A. H. Buck et al., 2014). EVs from several other helminth species also contain miRNAs (Eichenberger, Sotillo, et al., 2018; Sotillo et al., 2020). However, *H. bakeri* EVs were later found to contain even larger quantities of 22G secondary siRNAs, compared to the read counts of miRNAs (Chow et al., 2019). Secondary siRNAs were first discovered in *C. elegans*, and are generated via *de novo* synthesis by RNA-dependant RNA Polymerases (RdRPs), resulting in a triphosphate at their 5' end (5'PPP) (Holz & Streit, 2017; Pak & Fire, 2007; Yigit et al., 2006). Secondary siRNAs were later found in a number of other nematode species (Sarkies et al., 2015). Due to the 5'PPP on secondary siRNAs, library preparation kits for small RNA sequencing do not capture this species of small RNA, and pre-treatment with polyphosphatase is required in order to sequence secondary siRNAs (Chow et al., 2019). RNA from *H. bakeri* EVs pre-treated with polyphosphatase uncovered a dominating signature of secondary siRNAs of 22-23 nt predominantly beginning with guanine (22G siRNAs) that mostly map to novel repeats and transposable elements (Chow et al., 2019). These 22G siRNAs are not present in EVs from the clade I nematode *T. muris* (R. White et al., 2020). The absence of siRNAs within *T.*

*muris* EVs is consistent with the finding that RdRPs (which are required for secondary siRNA synthesis) are only found in helminths from clades III-V (Sarkies et al., 2015; R. White et al., 2020). The degree to which secondary siRNAs are present in other clade III-V helminth EVs has not been investigated

### *Protein*

The proteins that EVs cargo contain those involved in EV biogenesis, as well as proteins previously described are commonly found in EV preparations, but also proteins that transfer a signal to the recipient cell. For example, B cells secrete antigen loaded MHC-II EVs that are capable of inducing T cell responses (Raposo et al., 1996). The cargo detected in an EVs can also reflect the cell type of origin, physiological state of the cell, and in the context of helminths, the life stage of the parasite. For example, several nematode intestinal proteins are enriched in *H. bakeri* EVs which suggests gut cells could represent the cellular origin of EVs in HES, this was further supported by TEM of *H. bakeri* intestines (A. H. Buck et al., 2014). Although it should be noted that multiple cellular sources could exist. To date from the research in helminth species there is not one single EV membrane protein found across all helminths that could be used as a EV marker (Sotillo et al., 2020). However, within nematodes some protein families have been identified in common across several species such as M13 metallopeptidases, actin, transthyretin-like family proteins and aspartic proteases (Sotillo et al., 2020). Proteomic analysis of *H. bakeri* EVs identified enrichment of several homologues of proteins found in mammalian EVs including tetraspanins, heat shock proteins, Rab proteins and Alix (A. H. Buck et al., 2014). Interestingly, as previously mentioned *H. bakeri* EVs also contain a worm specific Argonaute protein called exWAGO loaded with secondary siRNAs, which we I hypothesise plays a role in gene silencing once within host cells (A. H. Buck et al., 2014; Chow et al., 2019). Transmembrane receptors in helminth EVs are of particular interest as they may either be required for receptor mediated uptake into recipient cells; or they could signal to host cells through interactions at the plasma membrane without uptake, similar to how B cell derived EVs can perform antigen presentation through surface MHC-II without uptake (Raposo et al., 1996).

### *Internalisation of EVs*

Whether and how helminth EVs specifically recognise a given recipient cell is not fully understood. Multiple uptake mechanisms have been described for EVs, and these may be specific to the biological context, or multiple uptake mechanisms might be utilised simultaneously (van Niel et al., 2018). Furthermore, the mechanism of uptake may affect the eventual impact of uptake on the recipient cell. For example, *H. bakeri* EV uptake into macrophages can be increased by EV specific antibodies, presumably through interactions of the Fc regions on antibodies with macrophage Fc receptors (Coakley et al., 2017). However, increased uptake by macrophages in the presence of EV specific antibodies resulted in an increased localisation to the lysosome, suggesting EVs in the presence of antibodies are no longer functional in the recipient (Coakley et al., 2017). Targeting of EVs to specific recipient cells has been shown to be mediated by interactions between EV transmembrane proteins and recipient cell membrane receptors. How helminth EVs target specific host cells is mostly unknown, although in the case of *Schistosoma mansoni* this is achieved via interactions with EV surface glycans (Kuipers et al., 2020). A proportion of *S. mansoni* EVs were observed by cryogenic electron microscopy (cryoEM) to have halo like projections subsequently identified as glycans (Kuipers et al., 2020). The surface glycans of *S. mansoni* EVs were recognised by the receptor DC-SIGN on host cells, specifically by dendritic cells which express this receptor, leading to internalisation and function effects on these cells (Kuipers et al., 2020). This study by Kuiper *et al* demonstrates that the characterisation of EV morphologies, and their surface glycans (or proteins) can help elucidate the mechanisms of EV uptake and the functions of helminth EVs.

#### **1.4.2 Helminth EV mediated immunomodulation**

Mammalian extracellular vesicles (EVs) were first discovered in reticulocytes, and were dismissed as being vehicles for disposing of cellular material during

differentiation into erythrocytes (Johnstone et al., 1987). It was not until the late 1990's, when B lymphocytes and dendritic cells (DCs) were shown to release functional EVs, that the field began to appreciate that EVs could have diverse biological roles (Raposo et al., 1996; Zitvogel et al., 1998). Although studies of mammalian systems paved the way for much of the current understanding of EV structure, cargo, and function, it is important to note that the discovery of multivesicular bodies (MVBs) and outer membrane vesicles (OMVs) in algae and plants, and bacteria, respectively had described similar structures decades prior as important players in diverse biological systems (Bishop & Work, 1965; De, 1959; Jensen, 1965).

#### *Cross-species EV mediated communication*

In the last decade alone it has become increasingly clear that EVs play an important role in inter- and intraspecies communication, including host-parasite and parasite-parasite interactions (Coakley et al., 2015; Drurey & Maizels, 2021; Eichenberger, Sotillo, et al., 2018; Woith et al., 2019). This phenomenon has been shown in diverse pathogens including leishmania (J. M. Silverman et al., 2010), trypanosomes (Garcia-Silva et al., 2014), and several species of bacteria as well as fungi have been shown to release EVs (OMVs in the case of bacteria) that interact with host cells (Munhoz da Rocha et al., 2020). Cross-kingdom EV mediated interaction has also been well demonstrated in plants, for example *Arabidopsis* secrete EVs that are taken up by the fungal pathogen *Botrytis cinera*, and use sRNA silencing to target virulence genes in the fungi (A. H. Buck et al., 2014). *B. cinera* sRNA can also enter *Arabidopsis* and induce gene silencing also, possibly trafficked in EVs, indicating a bi-directional interaction between host and pathogen (A. H. Buck et al., 2014).

#### *Helminth EVs in immune modulation*

Cross-kingdom EV uptake and modulation of host cells has been demonstrated for a number of helminth species. For example, *in vitro* murine intestinal epithelial cells take up EVs derived from *H. bakeri* (A. H. Buck et al., 2014). *H. bakeri* EV treatment of these cells resulted in modified gene expression, in particular the mRNA for IL-33 receptor component ST2, and Dusp1 which regulated MAPK signalling involved in immunity were downregulated (Buck et al., 2014). In the context of the *Alternaria* allergic asthma model (detailed in Section 1.3.1 of this thesis) treatment with *H. bakeri* EVs resulted in reduced ILC2 numbers and cytokine production, hypothesised to be mediated at least partially through suppression of IL-33 signalling via sRNA silencing (Buck et al., 2014). IL-33 initiates responses from multiple immune cell populations including macrophages. In a subsequent report, Coakley et al., then assessed the effect of *H. bakeri* EVs on macrophages *in vitro* and found suppression of both classical and alternative activation, and a reduced production of Relm $\alpha$ , Ym1, CD206 and IL-10 (Coakley et al., 2017).

Uptake of EVs from other gastrointestinal helminths has been demonstrated for *T. muris* and *N. brasiliensis* which were both taken up in small intestinal organoid cultures (Eichenberger, Ryan, et al., 2018). Intraperitoneal delivery of *N. brasiliensis* EVs prior to TNBS induced colitis in mice resulted in reduced disease severity (Eichenberger, Ryan, et al., 2018). Furthermore, reduced proinflammatory cytokines (IFN- $\gamma$ , IL-6, IL-17a, IL-1 $\beta$ ) levels were seen in the *N. brasiliensis* EV treated group, and IL-10 was markedly increased (Eichenberger, Ryan, et al., 2018). However, *T. muris* EVs had no effect on colitis severity in this model demonstrating that EVs from different helminth species induce different functional effects (Eichenberger, Ryan, et al., 2018). To further illustrate this, EVs from different helminth species in some cases display opposite effects on the host. For example, *N. brasiliensis* EVs had an anti-inflammatory effect in the colitis model above, whereas *S. mansoni* EVs increase pro-inflammatory responses (IL-6, IL-12p70) at least within dendritic cells *in vitro*, although they also increase the levels of the regulatory cytokine IL-10 (Kuipers et al., 2020). Similarly, EVs from the liver fluke *O. viverrini* have



proinflammatory effects (Chaiyadet et al., 2015). *O. viverinni* EVs enter cholangiocytes, a specialised epithelial cells of the bile duct, *in vitro* and also induce expression of proinflammatory IL-6 as well as proliferation (Chaiyadet et al., 2015). The inflammation and proliferation induced by *O. viverinni* EVs may contribute to progression of bile duct cancer that often occurs in chronically infected individuals (Chaiyadet et al., 2015). Data to date suggests the functional effects of helminth EVs from different species are not necessarily universal. However, it is thought that helminth EVs in general have functional effects on the host that will promote helminth survival (Coakley et al., 2015; Sánchez-López et al., 2021).

There is very limited evidence regarding the modulation of epithelial cells by helminth EVs. *H. bakeri* can modulate epithelial cells *in vitro* as mentioned above, in addition *N. brasiliensis* EVs have been show to enter intestinal organoid cells but the functional effect of this uptake was not directly studied (Eichenberger, Ryan, et al., 2018). *T. muris* EVs have been shown to enter organoid cells using 2-D models, and RNA seq demonstrated a suppression of IFN response genes (Duque-Correa, Schreiber, et al., 2020; Eichenberger, Ryan, et al., 2018). Given the importance of this barrier for the detection of helminths, and initiation of immune responses against them, it will be intriguing to uncover whether these cells are targeted by helminth EVs during infection.

## **1.5 Intestinal epithelium and organoids**

### **1.5.1 The intestinal epithelium**

#### *Anatomy of small intestine epithelium*

The intestinal mucosa is comprised of a contiguous epithelial cellular layer, and a secreted mucus layer containing antimicrobial peptides (Figure 1.4) (Ruby White et al., 2022). The intestinal mucosa fulfils two major biological

functions, firstly it is critical for the absorption of water (mainly the large intestine) and nutrients (mainly the small intestine); secondly, it acts as a physical barrier against incoming innocuous, and harmful intestinal assaults (Beumer & Clevers, 2020; Kiela & Ghishan, 2016). The intestinal epithelium is comprised of structurally distinct compartments, the crypts of Lieberkühn which are invaginations of epithelium into the submucosa, and villi which are protrusion of epithelium into the intestinal lumen (Beumer & Clevers, 2020). While crypts of Lieberkühn are found throughout both the large and small intestine, villi are contained to the small intestine and the large intestine has a flat epithelial surface (Figure 1.4) (Mowat & Agace, 2014).

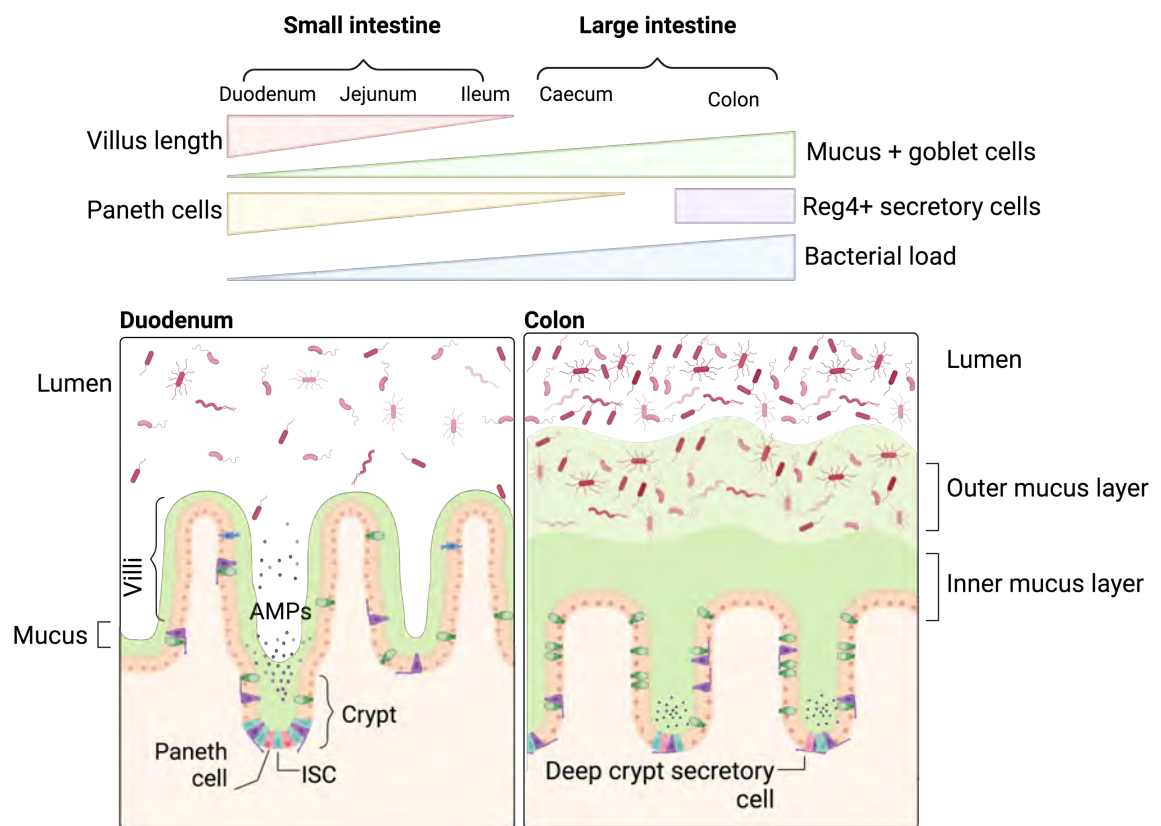


**Figure 1.4: Anatomical and physiological differences along the length of the murine intestine.** The intestine is broadly divided into two physically contiguous compartments. Firstly, the small intestine containing the specialised regions of the duodenum, jejunum and ileum. Secondly, the large intestine containing the caecum and colon. The anatomy, cellular composition, mucus structure and bacterial load change throughout different regions and are visualised using sliding scales to represent various features across the length of the intestine. In duodenum, the most proximal region of the intestine villi are their longest, a single minimal layer of mucus is present, and bacterial load is low due to high numbers of

Paneth cell which secrete antimicrobial peptide (AMPs). At the most distal end in the colon there are no villi, a high bacterial load which is physically separated from the epithelial cells by two layers of mucous, and no Paneth cells. The colon does however contain Reg4<sup>+</sup> deep secretory cells which have similar functions to Paneth cells.

Physiologically, villi help to increase the surface area of the intestine assisting in maximal absorption of intraluminal water and nutrients (Kiela & Ghishan, 2016). Along the length of the small intestine villi decrease in length, with the longest in the duodenum at the most proximal end of the small intestine (1.5 mm) thereafter they reduce in length progressively towards the distal end of the small intestine with ileal villi of 0.5 mm (Ross & Pawlina, 2011). Intestinal villi are comprised primarily of enterocyte cells (80% - 90%) which are absorptive, polarised cells that form tight junctions with neighbouring cells critical for the barrier integrity of the intestinal epithelium (Cheng & Leblond, 1974; Kiela & Ghishan, 2016). Enterocytes absorptive capabilities are assisted by microvilli protrusions on their luminal surface that, together with villus structures, multiply the surface area of the intestine by 30-600 fold (Fevr et al., 2007; Korinek et al., 1998; van Es et al., 2012). Intestinal crypts on the other hand form the anatomical boundaries of the stem cell niche, and are home to the both intestinal stem cells (ISCs) (also known as crypt-base columnar cells CBCs) and Paneth cells (Barker et al., 2007; Cheng & Leblond, 1974). ISCs constantly replenish this tissue in an escalator like fashion, new cells move upwards out of the crypt towards the villi exposing them to differentiation signals. As cells move towards the end of the villi connection with the underlying basement membrane is disrupted inducing cells to undergo a programmed cell death pathway called anoikis, and these are sloughed off into the lumen allowing for replacement by IECs below (Beumer & Clevers, 2020). At the cellular level, IECs are also organised by a strict basal-apical polarity with the basal end of the cell anchoring to the basement membrane, and the apical side facing towards the intestinal lumen and forming the actin rich brush border of microvilli (Snoeck et al., 2005). The basal side is accessible to underlying mesenchymal cells, immune cells and neurons as well as secreted factors. Some receptors, for example TLRs, have been shown to localised to either the basal or apical plasma membrane (Price et al., 2018).

The villus-crypt architecture of the intestinal epithelium is controlled by gradients of morphogens and growth factors. Two major growth factors form opposing gradients that pattern the crypt and villus structure of the epithelium: Wnt proteins and bone morphogenic proteins (BMPs) (Figure 1.5). Wnt proteins are critical for the proliferative capacity of the intestine, and are highly concentrated in intestinal crypts (Fevr et al., 2007; Korinek et al., 1998; van Es, Haegebarth, et al., 2012); while (BMPs) are highly concentrated at the villus tips and help induce differentiation (Hardwick et al., 2004; Kosinski et al., 2007). Mesenchymal cells at the villus tips secrete high levels of BMPs, while stromal cells beneath intestinal crypts such as muscle cells and myofibroblasts secrete BMP antagonists including chordin, gremlin and noggin, resulting in high BMP concentrations in the villi and low concentrations in the crypt (Kosinski et al., 2007) (Figure 1.5). Wnt proteins on the other hand are supplied in a redundant fashion by multiple cells types including Paneth cells (Wnt3a) which reside in the crypt interspersed between ISCs, as well as mesenchymal cells below the crypt (Sato et al., 2011). Additionally, R-spondin which is a potent Wnt enhancer is supplied in a non-redundant fashion by mesenchymal cells (Beumer & Clevers, 2020; de Lau et al., 2014).

#### *Maintenance of the intestinal stem cell niche*

In 2007 Barker *et al* hypothesised that due to the requirement of proliferative cells in the intestine on Wnt signalling, a Wnt target gene would allow for the identification of the elusive stem cell population within the intestine (Barker et al., 2007; Korinek et al., 1998). Indeed, although many Wnt target genes are expressed throughout the crypt, leucine-rich-repeat-containing G-protein-coupled receptor 5 (Lgr5) expressing cells were found to represent intestinal stem cells (ISCs) (Barker et al., 2007). The distribution of Lgr5<sup>+</sup> cells within the crypt also demonstrated, for the first time, that ISCs reside interlaced between the previously described Paneth cells within the crypts of the small intestine (Barker et al., 2007; Paneth, 1887). Paneth cells are terminally differentiated

secretory cells that unlike most IEC populations, are relatively long-lived (8 weeks) and provide critical signals for ISCs (Table 1.1) (Ireland et al., 2005). Wnt signalling has long been implicated in ISC maintenance, four additional known factors co-operate to control and maintain ISC stemness: i) R-spondin, ii) Notch signalling, iii) epidermal growth factor (EGF) and iv) BMPs (Beumer & Clevers, 2020). i) R-spondin in the presence of Wnt directly binds its ligand, the stem cell marker Lgr5, as well as closely related proteins Lgr4 and Lgr6 leading to internalisation (de Lau et al., 2014; Ruffner et al., 2012). In turn, once internalised this complex binds proteins Znf3 and Rnf43, in the absence of R-spondin signalling these proteins degrade the Wnt receptor Frizzled (Fzd5), therefore R-spondin binding of Znf3 and Rnf43 potentiates Wnt signalling by protecting Fzd5 (de Lau et al., 2014; Ruffner et al., 2012). R-spondin is supplied exclusively in this niche by mesenchymal cells, and as such organoid cultures are critically dependant on supplementation of exogenous R-spondin even in presence of high Wnt concentrations (Sato et al., 2009). ii) Notch signalling is supplied to ISCs through direct cell-to-cell contact between notch receptor expressing cells (in this case ISCs) and the notch ligand delta-like 1 or 4 (Dll1/4) expressing cell which in the ISC niche is supplied by interlacing Paneth cells (Beumer & Clevers, 2020; Sato et al., 2011). Sufficient notch signalling results in expression of hairy and enhancer of split 1 (HES1) which represses transcription factors involved in differentiation (T.-H. Kim & Shivdasani, 2011). iii) EGF is required for ISCs to undergo cell cycle and fulfil their proliferative capacity. Paneth cells contribute to the supply of EGF in this niche, however organoid cultures demonstrate a requirement for further EGF supplementation suggesting that *in vivo* additional cell types also supply EGF (Sato et al., 2011, 2009). iv) Finally, BMP's negatively regulate the ISC niche, BMP signalling induces downstream recruitment of histone deacetylases to stem cell genes leading to repression of their expression and inducing differentiation (Hardwick et al., 2004; Kosinski et al., 2007; Qi et al., 2017). Together these signals maintain stores of Lgr5+ ISCs (~4-6 per crypt), and result in the unmatched ability for this tissue to

rapidly renew itself faster than any other tissue in human and mice (3-5 days in mice, 5-7 days in humans) (Sato et al., 2009).

As ISCs supply the constant turnover of intestinal epithelial cells, they must be highly protected in order to avoid being damaged by the nearby digestive environment of the intestinal lumen (Gehart & Clevers, 2019). ISCs are protected firstly by the anatomical restriction of the crypt which creates a narrow entrance of ~6  $\mu\text{m}$  (Gehart & Clevers, 2019). In addition to physical protections of the crypt, Paneth cells have been described as custodians of ISCs owing to both their supplementation of critical stemness signals described above, and their secretion of antimicrobial peptides (AMPs) (H. C. Clevers & Bevins, 2013; Sato et al., 2011). Paneth cells have high secretory activity and are found only in the small intestine, where they decrease in number from proximal to distal end, and are absent in the caecum or colon except under certain conditions (Ross & Pawlina, 2011). Paneth cells secrete AMPs in response to infection including lysozyme 1 (Deckx et al., 1967);  $\alpha$ -defensins (A. J. Ouellette et al., 1992; Andre J. Ouellette et al., 1999); phospholipase A2 (Qu et al., 1996); RegIII and ribonucleases such as angiogenin 4 (Ang4) (Bevins & Salzman, 2011). Consistent with these responses, the ablation of Paneth cells results in significant changes in bacterial colonisation in the small intestine, and Paneth cell distribution (only found in the small intestine) correlates with regions of the intestine where there is lower bacterial abundance (Beumer & Clevers, 2020; Teltschik et al., 2012; Vaishnava et al., 2008). Growth of organoid cultures from single stem cells is greatly improved if co-cultured with Paneth cells, although in this artificial environment in which exogenous growth factors are also present Paneth cells are not essential (Sato et al., 2011). The necessity of Paneth cells for maintaining the ISC compartments is unclear, while these cells provide both Wnt and EGF signals which are absolutely required for ISCs, *in vivo* these can be provided by other cell types (Beumer & Clevers, 2020). Ablation of Paneth cells has been attempted in mice by knocking out several Paneth cell differentiation factors (Gfi1, Sox9 and Atoh1), or through diphtheria toxin mediated knockout of the cryptdin promoter; in these models ISCs were still

present, however a reduction of ISCs was described (Bastide et al., 2007; Durand et al., 2012; T.-H. Kim et al., 2012; Mori-Akiyama et al., 2007; Shroyer et al., 2005). Although at least for some of these models' results were confounded by shared expression of some genes with ISCs. For example, SRY-box transcription factor 9 (Sox9) is a Wnt target gene, and accordingly is expressed by both ISCs and Paneth cells which are both in high Wnt environments (Figure 1.5) (Blache et al., 2004). Sox9 expression is critical for the differentiation of Paneth cells (Bastide et al., 2007) and Sox9 conditional knockout mice have depleted ISCs. However, due to shared expression of Sox9 by ISCs and Paneth cells whether ISC depletion in Sox9 KO mice is caused by loss of Paneth cells, or by direct loss of Sox9 within ISCs is unclear (Bastide et al., 2007; Mori-Akiyama et al., 2007).

#### *Differentiation in the intestinal epithelium*

ISC have the capacity to differentiate into all terminally differentiated cells of the intestinal epithelium, which are divided into two committed lineages either secretory which gives rise to Goblet cells, Paneth cells, Tuft cells and Enteroendocrine cells; or absorptive progenitors with eventually become enterocytes (Beumer & Clevers, 2020). A seventh terminally differentiated cell originates from ISCs, the Microfold cell (M-cell). However, M-cells localise specifically to the follicle associated epithelium (FAE) surrounding gut associated lymphoid tissue (GALT) such as the Peyer's patches, and do not currently fall into either secretory or absorptive differentiation lineages (Figure 1.5) (Kobayashi et al., 2019; Mabbott et al., 2013).

ISC undergo rapid cell proliferation (24 h), as they proliferate the physical constraints of the crypt leads to one daughter cell being pushed upwards towards the villi (Ballweg et al., 2018; Christopher S. Potten, 1998; Schepers et al., 2011). As cells move out of the crypt, they are exposed to changes in the concentrations of aforementioned growth factors required for stemness

Wnt, Rspo, EGF and Noggin, and this induces transition into one of two kinds of progenitor cells. Broadly, the terminally differentiated cells of the intestinal epithelium are either i) absorptive or ii) secretory, and progenitors of each lineage are defined by the expression of mutually exclusive transcription factors Hes1 (absorptive) and Atoh1 (also known as Math1) (secretory) (Figure 1.5) (Beumer & Clevers, 2020). The determination of secretory lineage cells is controlled stochastically in response to the loss of contact mediated Notch signalling, as cells lose contact with DLL1/4 expressing Paneth cells of the crypt. Sufficient notch signalling controls the expression of Hes1, and in turn Hes1 represses the secretory lineage marker Atoh1 (Fre et al., 2005). So long as notch signals are maintained cells will remain on track to remain absorptive. The loss of notch signalling is the key fate determining step for lineage commitment, as the loss of notch signalling ablates Hes1 expression, and switches on Atoh1 resulting in a secretory progenitor (Fre et al., 2005; Yang et al., 2001).



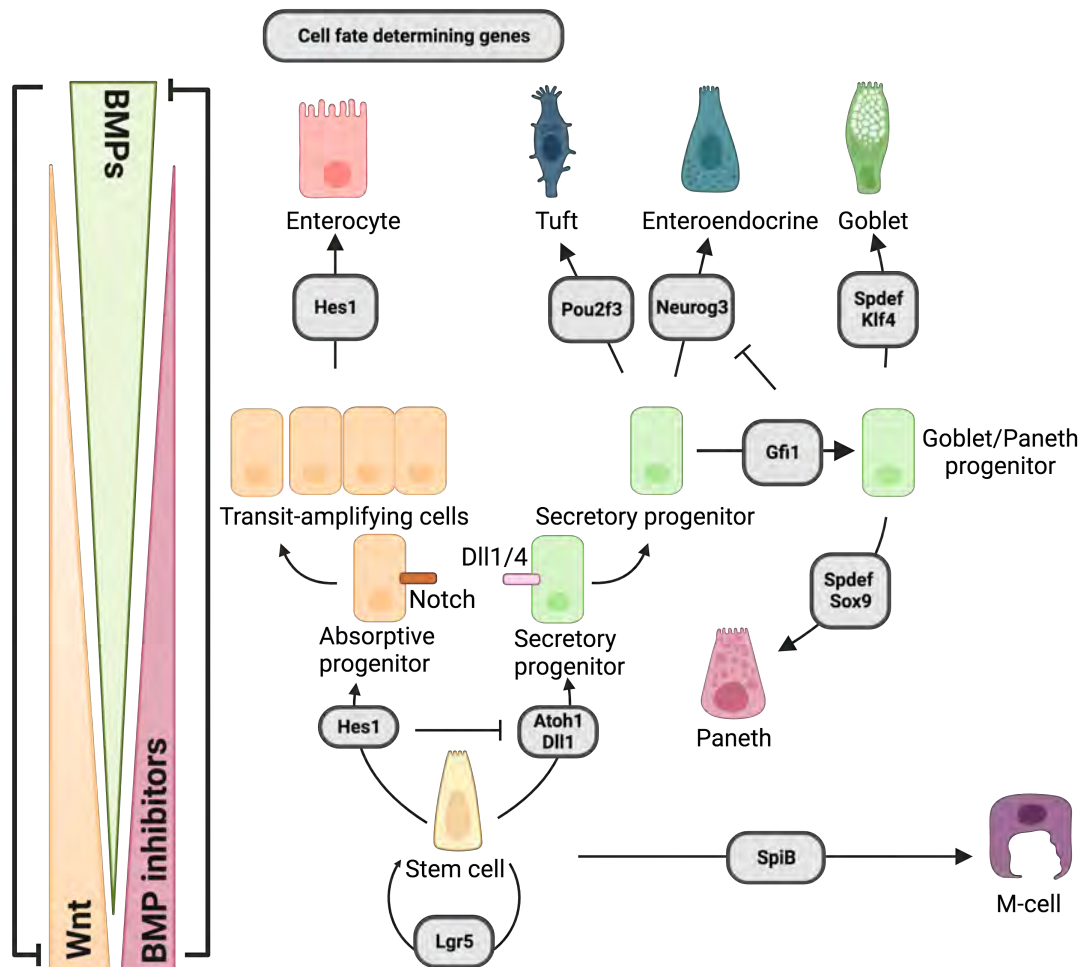


**Figure 1.5 | Major cell fate determining pathways in the intestinal epithelium.** Growth factor and morphogen gradients play a major role in controlling cellular differentiation in the small intestine. Namely, two opposing gradients Wnt ligands, which are highly concentrated in the intestinal crypt, and bone morphogenetic proteins (BMPs) which are concentrated at the villus. High Wnt concentrations are essential for maintenance of Lgr5<sup>+</sup> intestinal stem cells (ISCs) that reside in the base on the crypt. As ISCs divide, they are pushed out of the crypt and exposed to lower Wnt concentrations and higher BMP concentrations inducing differentiation. Cells leaving the crypt enter one of two differentiation pathways and this is dependent on notch signalling. Cells that express notch ligands Dll1/Dll4 provide notch signalling to their neighbouring cells. If when cells leave the crypt, they maintain notch signalling they will in turn remain expressing Hes1 and become absorptive progenitors which rapidly divide as transit-amplifying cells, and eventually enterocytes. Hes1 expression inhibits the expression of Atoh1, which is the determining factor that induces secretory progenitors. If cells lose contact with notch ligands (Dll1/4) as they leave the crypt Hes1 expression is lost, and expression of the secretory progenitor defining gene Atoh1 as well as notch ligands Dll1/4 is induced resulting in a secretory progenitor cell. Secretory progenitors give rise to several fully differentiated cell types depending on expression of particular cell fate determining genes (in grey boxes), the deletion or disruption of these genes in mouse models leads to loss or depletion of these cells from the epithelium. Fully differentiated cells that arise from secretory progenitors include tuft cells which require expression of Pou2f3; Enteroendocrine cells reliant on expression of Neurog3 for differentiation; Paneth cells which require transient expression of Gfi1, and then Spdef and Sox9; or Goblet cells which require Spdef and Klf4 for differentiation. Microfold (M) cells differentiate independent of the secretory or absorptive progenitors. M cell differentiation requires exposure to RANK ligands which induces the cell fate determining expression of SpiB. Genes in grey boxes indicate genes essential for each stage of differentiation. Made with BioRender.com

Only a small fraction of cells exiting the intestinal crypt will become secretory progenitors because notch signalling can be provided by DDL1/4 expressing secretory progenitors to its neighbouring cells, in a process termed lateral inhibition. In fact, secretory progenitors are the minority because the next 6-8 cells will receive notch signals provided by their secretory progenitor neighbour, and this maintains expression of absorptive progenitor determining transcription factor Hes1 (Figure 1.5). Lateral inhibition therefore results in a skewing of differentiation towards the absorptive lineage. Additionally, Atoh1+ secretory cells are post-mitotic limiting the numbers of secretory cells they provide (Basak et al., 2014); while the Hes1+ absorptive progenitor, also referred to as transit-amplifying (TA) cells, are able to rapidly undergo cell cycle (~12 hr) (Ballweg et al., 2018; Riccio et al., 2008). Lateral inhibition and the differential proliferative capacities of these cells lead to the skewing of cell proportions greatly in favour of enterocytes which make up ~80-90% of IECs (Cheng & Leblond, 1974; Riccio et al., 2008).

### *Enterocytes*

Enterocyte differentiation is controlled by the loss of Wnt signalling as cells leave the crypt (X. Yin et al., 2013). This is demonstrated by inhibition of Wnt in organoids resulting in increased enterocyte numbers, showing that in response to the loss of Wnt signalling which maintains stemness, differentiation occurs (Beumer & Clevers, 2020; X. Yin et al., 2013). In addition, they must receive notch signals from neighbouring cells which maintains expression Hes1 in enterocyte progenitors and suppression of Atoh1 to prevent them entering the secretory lineage (Kazanjian et al., 2010; T.-H. Kim & Shivdasani, 2011).

### *Paneth cells*

Paneth cells derive from their secretory progenitor and critically require expression of the transcription factor Sox9 (Bastide et al., 2007; Mori-Akiyama et al., 2007). Paneth cells differentiation occurs when cells are within a high

Wnt environment, leading to expression of Sox9, while simultaneously losing notch signals from neighbouring cells thus inducing Atoh1 expression (Bastide et al., 2007; Blache et al., 2004). Unlike the rest of the terminally differentiated cells of the intestinal epithelium, upon differentiation Paneth cells move retrograde back down into the crypt in order to fulfil their functional roles (described above) (Beumer & Clevers, 2020). Paneth cells quickly replace themselves even after depletion, this is logically explained by the fact that Paneth cell ablation removes notch signals within the crypt, leaving ISCs exposed to high Wnt in the absence of notch signals, the exact determining factors that induce Paneth cell differentiation (Gehart & Clevers, 2019).

### *Goblet cells*

Goblet cells reside in the villi of the intestine and are the most abundant secretory cell type (~4% in duodenum) (Cheng, 1974). Goblet cells generate mucus granules containing mainly extracellular glycosylated mucin proteins e.g., Muc2 that form the mucus barrier atop the intestinal epithelium, as well as the proinflammatory cytokine resistin-like molecule  $\beta$  (RELM $\beta$ ) and trefoil factor 3 (Tff3) (Artis et al., 2004). These granules are released into the lumen to form the mucus barrier that prevents invasion of pathogens. Goblet cells increase in abundance along the length of the intestine, in the caecum and colon higher goblet cell numbers leads to increased mucus required as stool becomes more compact, whereas in the small intestine less mucus production is needed. Goblet cells, like Paneth cells, also derive from Atoh1+ secretory progenitor cells like however goblet cells require reduced Wnt concentrations for their development (Milano et al., 2004; van Es et al., 2005). The expression of transcription factor SAM pointed domain ETS factor (Spdef) is required for goblet cell development, however there is conflicting data as to whether it may also be important for Paneth cell differentiation (Gregorieff et al., 2009; Noah et al., 2010). Klf4 is another transcription factor required for the differentiation of goblet cells in the colon, and is negatively regulated by Hes1 when notch signals are present (Ghaleb et al., 2008; Katz et al., 2002). Finally, the

cytokines IL-4 and IL-13 can also induce goblet cell differentiation, and are at least partially responsible for helminth associated goblet cell hyperplasia during infection (Khan et al., 2001; Marillier et al., 2008). Whether these cytokines act on stem cells, or on secretory progenitors, and the exact signalling cascade that induces hyperplasia is unknown (Gehart & Clevers, 2019).

### *Enteroendocrine cells*

Enteroendocrine cells (EECs) are endocrine cells which release hormones. Although EECs can be further subdivided depending on which hormones they secrete, plasticity does exist within which hormones EEC subtypes can secrete (Svendsen et al., 2015). Despite the rarity of these cells throughout the intestine (~1%), the intestine represents the largest endocrine system in the body due to its large surface area (Furness et al., 2013; Sternini et al., 2008). EEC production of hormones play important roles in many of the major functions of the intestine through their ability to act on distal organs (endocrine) (Worthington et al., 2017). For example, EEC derived hormones control responses to nutrients such as hunger, satiation, gastric emptying, peristalsis and digestion (Worthington et al., 2017). Hormones released by EECs achieve this through signalling in many cases to the surrounding nervous system, in turn relaying information to the brain, making them key communicators of the gut-brain axis. The expression of Neurogenin 3 (Neurog3) within secretory progenitors leads to differentiation of EECs, and all subtypes of EECs are depleted in Neurog3 intestinal knock out mice implicating it as a key EEC differentiation factor (Gerbe et al., 2011; Jenny et al., 2002). Neurog3 expression is repressed by the Paneth and Goblet cell specific transcription factor Gfi1 (Shroyer et al., 2005).

### *Tuft cells*









Tuft cells are very rare (~0.4%) sentinel cells specialised at sensing environmental signals and are found in other mucosal sights throughout the

body (Gerbe et al., 2012). Tuft cells play roles in both detection of helminths and initiating immune responses via the secretion of alarmin cytokines (discussed further in section 1.5.3) (Gerbe et al., 2016; Howitt et al., 2016; Von Moltke et al., 2016). Tuft cells are derived from Dll1<sup>+</sup> secretory progenitors (van Es, Sato, et al., 2012), but contradictory reports have described tufts cells as either requiring (Gerbe et al., 2011) or not requiring (Bjerknes et al., 2012) Atoh1 for their differentiation. However, disruption to Neurog3, Sox9 or Gfi1 does not ablate tuft cells suggesting they diverge from secretory progenitors by an independent lineage from that of Goblet, Paneth and EECs (Gerbe et al., 2011). Tuft cells can be identified by cell type specific markers Dckl1, Pou2f3 and Trpm5, of these genes the transcription factor Pou2f3 is required for generation of Tuft cells (Gerbe et al., 2016; Haber et al., 2017). Tuft cells, like goblet cells, are induced by the cytokines IL-4 and IL-13 through an ill-defined mechanism, although IL4-R $\alpha$  is required as KO mice are unable to induce tuft cells in response to these cytokines (Gerbe et al., 2016; Howitt et al., 2016; Von Moltke et al., 2016).

### *Microfold cells*

Microfold (M) cells are specialised cells of the intestinal epithelium that home specifically to the FAE surrounding Peyer's patches, and mediate the transcytosis of luminal antigen to underlying B- & T- cells of the Peyer's patch (Kobayashi et al., 2019; Mabbott et al., 2013). M cells differentiate directly from Lgr5<sup>+</sup> ISCs independently of secretory or absorptive progenitors. Immature M cells differentiate and express Anxa1, Marckl1 and SpiB (Kobayashi et al., 2019). For maturation however, M cells require stimulation of the receptor RANK by RANK ligand (RANKL). *in vivo* RANKL is provided by subepithelial mesenchymal cells, but can be supplemented in organoid cultures resulting in gene expression of immature M cells but not complete differentiation (Knoop et al., 2009; Kobayashi et al., 2019). RANK signalling increases the expression of M-cell signature genes SpiB and GP2 as well RANK itself (S. Kimura et al., 2015). SpiB and Sox8 play roles in the development of mature M-cells

(Shunsuke Kimura et al., 2019). In addition, signals from haemopoietic cells such as B-cells also play a role in M-cell differentiation which may explain the difficulty to induce fully mature M-cells in organoid cultures (Kobayashi et al., 2019; Mabbott et al., 2013). Although supplementation of RANKL in organoid media induces M-cells that resemble *in vivo* M-cells (Haber et al., 2017).

	Revival SC	ISC	Paneth cell	Tuft cell	EEC	Goblet cell	Enterocyte	M cell
								
<b>Differentiation signals</b>	Injury Hippo/YAP ?	Wnt + Notch +	Wnt + Loss of Notch	Wnt – Loss of Notch IL-4/IL-13	Wnt – Loss of notch	Wnt – Loss of notch IL-4/IL-13	Wnt – Notch +	RANKL
<b>Factors required</b>	Ly6a	Lgr5	Sox9, Gfi1	Pou2f3	Neurog3	Gfi1, Klf4	Hes1	SpiB
<b>Cell specific markers</b>	Clu, Ly6a,	Lgr5, Ascl2, Olfm4	Lyz1, Ang4, $\alpha$ - defensins.	Dck11, Trpm5, Pou2f3	Chga, Chgb, Sst, Grhl	Muc2, Clca1, Tff3	Alpi, Apoa1, Apoa4	Gp2, SpiB, Anxa5
<b>% of IECs</b>	unknown	4-6 cells/crypt	~4%	~0.4%	>1%	~4%	80-90%	10-20% (of FAE)
<b>Lifespan</b>	?	Life long?	8 weeks	5-7 days	5-7 days	5-7 days	5-7 days	~5 days
<b>Function</b>	Replenish epithelium after injury	Provide multipotent daughter cells to supply the epithelium	Antimicrobial activity and provide signals for stem cell maintenance	Sensor cells surveying the luminal contents. Respond to helminth infection & signal immune cells	Secrete hormones involved in regulating intestinal physiology. Signal to immune cells	Release granules containing mucus and glycosylated proteins that create the mucus barrier	Absorption of water and nutrients Create a tightly controlled barrier.	Sample luminal antigen and pass to underlying immune cells of the GALT.

**Table 1.1 | Summary of cell types of the intestinal epithelium.** Summary of the known signals that drive differentiation, and genes that are critical for the development of each cell type as well as their proportions in the epithelium, cell type specific genes, their lifespan and function. Figure made with BioRender.com. SC = stem cells; ISC = intestinal stem cells; EEC = Enteroendocrine cell; M cell = microfold cell; IEC = intestinal epithelial cell; RANKL = receptor activator of NF $\kappa$ B ligand; Lyz1 = Lysozyme 1; Ang4 = Angiogenin 4; Chga = Chromogranin A; Chgb = Chromogranin B; GALT = gut associated lymphoid tissue.

### *Recovery in the intestinal epithelium after injury*

The intestinal epithelium is incredibly robust in the face of damage. Several hypotheses of a reserve stem cell population have been proposed to describe how ISCs are rapidly replaced after damage, but there is not complete consensus on this within the stem cell field (Beumer & Clevers, 2020). Initially the idea of '4+ cells' was proposed that suggested cells positioned 4 cells above the crypt base represented a quiescent reserve stem cell population that contained the template or 'immortal' DNA strand to prevent accumulation of mutations (C. S. Potten et al., 1978). Several genes were proposed to be 4+ markers (Bmi1, Tert, Hopx, Lrig1) however these were all later found to be expressed more promiscuously by CBCs and EECs, and the 'immortal' strand hypothesis was also rejected (Haber et al., 2017; C. S. Potten et al., 1978). These 4+ cells were later found to be secretory precursors that gradually disappear over time (Buczacki et al., 2013). It is now understood that multiple cell types of the epithelium can regenerate CBCs upon damage, including secretory and absorptive progenitors which have overlapping expression of previously hypothesised 4+ cell marker (Jadhav et al., 2017; Schmitt et al., 2018; Tetteh et al., 2016; van Es, Sato, et al., 2012). Furthermore, even 'terminally differentiated' Paneth cells have been seen to replenish CBCs after damage in a process termed dedifferentiation (Murata et al., 2020; Schmitt et al., 2018; Yu et al., 2018). Dedifferentiation can be induced by notch signalling in Paneth cells (caused by Paneth cell – Paneth cell interactions after loss of interlacing CBCs). Additionally, *Ascl2* which is downstream of Wnt signalling, and the *il11ra1* have been implicated in the dedifferentiation process (Murata et al., 2020; Yu et al., 2018).



Hippo signalling is a well described pathway that regulates organ size during development. Hippo signalling initiates a kinase signalling cascade that results in the phosphorylation of YAP and TAZ, which control the expression of proliferation and cell survival genes (Moya & Halder, 2019). Expression of YAP/TAZ increases in crypts during regeneration, and loss of these transcriptional regulators results in the inability to repair the intestinal epithelium after irradiation or chemical damage (Barry et al., 2013; Jing Cai et al., 2010; Gregorieff et al., 2015; Karpowicz et al., 2010). YAP/TAZ has been shown to interact with other signalling pathways (Wnt, Notch, EGF) in the epithelium to mediate repair (Beumer & Clevers, 2020).

During L4 stage of *H. bakeri* infection (d 6), when the parasites are in the submucosa, it has been described that stem cells overlaying larvae display a loss of Lgr5+ expression (Nusse et al., 2018). Simultaneously, a specific type of reparative stem cell arises that expresses genes associated with the fetal epithelium termed revival SCs (revSC) (Karo-Atar et al., 2022; Nusse et al., 2018). revSCs were marked by a transient early expression of Ly6a (Sca1) which can be induced by interferon signalling, indeed this study found the revSC phenotype was found to be dependent on IFN- $\gamma$  at day 6 p.i. (Nusse et al., 2018). Interestingly, authors found that during *N. brasiliensis* infection revSCs were not induced, leading them to conclude that damage as *H. bakeri* burrows through the epithelium induces these changes. However a subsequent study by Karo-Atar et al, found that HES alone induced these cells which indicates that damage associated with larvae burrowing is not required (Karo-Atar et al., 2022). revSC were subsequently found to be a more generalised response to ISC damage, and appear to be induced by irradiation, dextran sodium sulphate (DSS) intestinal damage, and ablation of Lgr5+ cells (Ayyaz et al., 2019; Nusse et al., 2018).

### 1.5.2 Intestinal organoids

Research that defined the key growth factors required for intestinal epithelial renewal and differentiation has allowed for the development of *in vitro* culture of the epithelium termed organoids (Aguilar et al., 2021; Sato et al., 2009). Organoids can be generated from tissue derived from many organ sources including from the GI tract e.g. from the small intestine (enteroids), caecum (caecaloids), and colon (colonoids) (Duque-Correa, Schreiber, et al., 2020; Sato et al., 2009). Sato *et al* first demonstrated the growth of enteroids in 2009 by culturing Lgr5+ stem cells, or whole intestinal crypts, in a laminin rich hydrogel that mimics basement membrane interactions, and supplementing growth media with critical factors EGF, Noggin, Wnt and R-spondin (Sato et al., 2009). Initial intestinal organoid cultures resulted in a self-organised three-dimensional (3-D) spherical organoids with the apical membranes facing inwards, that are capable of differentiation into all terminally differentiated cell types and mimic some features of intestinal epithelium (Aguilar et al., 2021; Sato & Clevers, 2013). Although 3-D organoids recapitulate the intestinal epithelium well, a major limitation of this culture method is inaccessibility of the apical epithelium. The internal apical epithelium in 3-D organoid cultures presents two problems. Firstly, an accumulation of dead cells and mucus trapped within these enclosed structures eventually leads to organoids bursting. This can be resolved by passaging organoids for enteroids and is required approximately every 5-7 days limiting the length of culture (Sato et al., 2009). Secondly, inaccessibility of the apical lumen makes mimicking *in vivo* infection dynamics difficult as this is where most exogenous material and incoming pathogens are encountered by the epithelium (Ruby White et al., 2022). Delivering infectious agents to 3-D organoids is possible by microinjection however it has major caveats – it is laborious requiring individual injection of each organoid, the volume injected to each organoid cannot be controlled, and it requires specialised equipment and training (Ruby White et al., 2022). Additionally, the technique of microinjection is not suitable for

large multicellular pathogens such as helminths, as even the eggs or larval stages are too large for the needles (Duque-Correa, Maizels, et al., 2020).

### 1.5.3 Intestinal organoid use in helminth infection

#### *Organoids as models of GI nematode niches*

GI nematodes have a tropism for specific organs of the GI tract of their host e.g., whipworms colonise the caecum and proximal colon, hookworms and threadworms establish in the small intestine, while sheep GI parasites find a niche in the abomasum. *In vivo* the epithelium of these organs/regions vary greatly in their cell type content, mucus layer composition and thickness, size, architecture, and expression of toll-like receptors, and these features are replicated to some extent by their respective organoid cultures (Duque-Correa, Maizels, et al., 2020; Kayisoglu et al., 2021; Mowat & Agace, 2014; Price et al., 2018). Traditional organoid cultures use basement membrane extracts (BME), which mimic the laminin rich extracellular matrix, alongside the supplementation of key growth factors and morphogens that are specific to the host and organ of origin, and allow for the division and differentiation of stem cells (Beumer & Clevers, 2020; Puschhof et al., 2021; Sato & Clevers, 2013). These cultures result in self-organised three-dimensional (3-D) structures that display cellular polarisation, with the apical surface of the epithelium (basal-out) facing inwards towards the lumen, and that are capable of differentiating into multiple cell types of the epithelium of origin (Kayisoglu et al., 2021; Puschhof et al., 2021). Apical-out organoids are an alternate approach to 3-D organoid cultures that allow access to the apical surface of the epithelium. Apical-out organoids are generated by mechanical disruption of traditional 3-D organoids followed by suspension culture in the absence of BME. This procedure induces the inversion of the polarity and repair of the epithelium, thus the apical membrane faces outwards, while the organoid 3-D structure is maintained (Co et al., 2019, 2021).

Organoids can also be cultured in a 2-D conformation by dissociating 3-D organoids into single cell suspensions and then seeding into either cell culture plates, or semi-permeable membranes (transwell) coated with BME, laminin or collagen (Aguilar et al., 2021; Moon et al., 2014). 2-D organoids maintain cellular polarisation and show a degree of crypt-like spatial organisation, albeit to a lesser extent than 3-D cultures. 2-D organoids grown on semi-permeable membranes create a model with physically separated apical and basal culture compartments, which allows for greater control over delivery of growth factors, cytokines, pathogens and other cellular populations, to either the basal or apical membrane of the epithelium (Aguilar et al., 2021; Kozuka et al., 2017; Moon et al., 2014). 2-D organoids grown on semi-permeable membranes also enable longer culture lengths than 3-D models with recent studies extending culture for up to 2 months (Boccellato et al., 2019).

#### *Unravelling GI nematode invasion using organoids*

Infection by GI nematodes occurs via ingestion/swallowing of parasite eggs or infective larvae. The first crucial step for GI nematodes to establish a successful infection is the sensing by the parasites of a suitable environment to hatch and/or invade the host epithelium (Mkandawire et al., 2022). The specific cues, signalling pathways and mechanisms behind these processes are currently not well defined, but represent a key stage for intervention in the transmission of these parasites.

Organoids are an attractive model for understanding GI nematode invasion because they recapitulate many physico-chemical and cellular characteristics of the *in vivo* host niche that may promote infection. Moreover, organoids could allow real time visualisation of invasion dynamics. For example, murine caecaloids reproduce the mucus layer and cellular composition of the caecal epithelium and successfully promote the epithelium invasion and formation of syncytial tunnels by *Trichuris muris* first-stage (L1) larvae *in vitro* (Duque-Correa, Goulding, Rodgers, Cormie, et al., 2022).

When developing organoid models to study GI nematode invasion, it is critical to consider which surface of the epithelium the parasites are in contact with when interacting with their hosts *in vivo*. For GI nematodes that invade apically, modelling invasion using 3-D organoids is difficult due to the large size of the parasites. Smaller organisms such as viruses, bacteria or protists can be delivered to traditional (basal-out) 3-D organoids by microinjection, or by shearing of the organoids followed by co-incubation (Aguilar et al., 2021; Puschhof et al., 2021). However, microinjection is not suitable for delivery of any life stage of GI nematodes, as even eggs and larval stages are too large for the microinjection needles, and the luminal volume of 3D-organoids is not big enough to host the parasites (Duque-Correa, Maizels, et al., 2020). Moreover, shearing of 3-D organoids followed by co-incubation with whole parasites is unlikely to result in their successful incorporation into the organoid lumen. An alternative method to deliver live GI nematodes into the lumen of traditional 3-D organoids is to simply add these to the organoid culture media. This strategy was used to infect both ovine and bovine abomasum organoids with *Teladorsagia circumcincta* (*T. circumcincta*) and *Ostertagia Ostertagi* (*O. ostertagi*) respectively (Faber et al., 2022; D. Smith et al., 2021). Strikingly, both *T. circumcincta* and *O. ostertagi* L3 larvae migrated through the BME and transverse the organoid membrane into the lumen (Faber et al., 2022; D. Smith et al., 2021). *O. ostertagi* infection of bovine organoids additionally demonstrated L3 larvae transversing the epithelium in both directions, from the basal to apical side in order to invade the lumen of the organoid, and from the apical side to the basal side (Faber et al., 2022). However, as the authors noted, *T. circumcincta* and *O. ostertagi* are not previously described to cross the epithelial barrier during their life cycles, instead they are thought to invade through the gastric neck opening of gastric glands, and whether transversion of the epithelium occurs *in vivo* or is unique to these *in vitro* cultures is not known (Faber et al., 2022). Whether other GI nematodes co-cultured in this fashion can invade the BME and migrate across the epithelium into the organoid lumen is unknown, and this ability may be species or life-cycle-stage specific.

2-D organoids grown in semi-permeable membrane systems allow for both basal and apical delivery of GI nematodes, which is advantageous for the *in vitro* modelling of invasion by some species. For instance, L3 *H. bakeri* larvae burrow from the GI lumen through the epithelium into the submucosa, where they moult twice to reach adulthood; the adult parasites then transverse the epithelium to emerge into the duodenal lumen (Camberis et al., 2003). Therefore, apical delivery would be better suited to studies on invasion of L3 *H. bakeri* of the epithelium, while basal delivery of *H. bakeri* adult parasites could mimic conditions for re-emerging into the lumen.

2-D organoid systems also enable the study of interactions between the mucus layer and GI nematodes. The mucus layer, or layers in the case of the caecum and colon, overlays the epithelial cells and acts as a substantial physical barrier that protects the epithelium from incoming luminal contents, microbiota and pathogens (Bergstrom & Xia, 2022; Herbert et al., 2009). GI nematodes need to transverse the mucus layer(s) to reach the epithelial cells, but the mechanisms used by the parasites are not well understood. On the other hand, the mucus layer could provide uncharacterised cues for parasite egg hatching and larvae invasion. Therefore, modelling the mucus barrier in an accessible way is important for investigations of GI nematode invasion. Studying these processes *in vivo* is challenging due to the size of infective larvae and the lack of protocols to generate stably labelling nematodes for *in vivo* imaging (Duque-Correa, Goulding, Rodgers, Cormie, et al., 2022). For instance, *in vivo* studies on mucus degradation by L1 *T. muris* larvae during invasion of the caecal epithelium are impeded by the small ratio of larvae versus caecal epithelial cells, which dilutes any effects the larvae have on the mucus layer. However, using 2-D transwell caecaloid cultures in which higher numbers of L1 larvae to a smaller surface area can be achieved, degradation of mucus during early infection was detectable (Duque-Correa, Goulding, Rodgers, Cormie, et al., 2022).

*In vitro* modelling of epithelial changes and immunomodulation during GI nematode infection

A major focus of GI nematode research is on understanding the impact of parasite ES products on the modulation of host tissues (Rick M. Maizels et al., 2018). Research in this area has focussed on the effects these molecules on immune cells. However, during GI nematode infection there are significant modifications of the host GI epithelium that result either in parasite expulsion or promote parasite persistence (Coakley & Harris, 2020). As detailed above, there is also emerging data on mechanisms of regeneration of intestinal epithelium following helminth infection and the long-term effects on ISCs is unknown. Currently, little is known on the specific interactions and mechanisms by which GI nematodes and their ES molecules alter epithelial cell proliferation and differentiation (Duque-Correa, Maizels, et al., 2020; Rick M. Maizels et al., 2018).

Organoids are the perfect system to address these questions, but their use to model host– parasite interactions requires careful consideration of epithelium polarity. The apical and basolateral epithelium have different functions partly defined by the differential localisation of proteins including receptors (Weisz & Rodriguez-Boulan, 2009). Therefore, the accessibility to target receptors could influence the detection of functional effects and should be considered in terms of how parasites and their products are delivered when designing organoid experiments. Unlike live nematodes, ES products can be delivered into the organoid lumen via microinjection. For example, extracellular vesicles (EVs) derived from *T. muris*, *Ascaris suum* and *Nippostrongylus brasiliensis* have been successfully microinjected into traditional 3-D organoids (Chandra et al., 2019; Duque-Correa, Schreiber, et al., 2020; Eichenberger, Ryan, et al., 2018; Eichenberger, Talukder, et al., 2018). However, microinjection is laborious, does not allow control over the volume/dose injected, and requires specialised equipment and training (Duque-Correa, Maizels, et al., 2020). An alternative approach to study ES products interactions with traditional 3-D

organoids is to administer these molecules in the culture media in the hope that functional molecules will diffuse through the BME and find their target cells (Drurey et al., 2021; Faber et al., 2022). However, depending on the localisation of the particular parasite life stage this method may not reflect *in vivo* infection context. Apical-out organoids could facilitate the replication of interactions of GI nematodes with the apical epithelium and thus, may be used in future studies (D. Smith et al., 2021).

Teasing apart the direct effects of the parasites on the epithelium from those driven indirectly by host immune responses using *in vivo* models is difficult. For instance, several GI nematode infections induce goblet and tuft cell hyperplasia with subsequent increases in mucus and alarmin production that mediate parasite expulsion (Baska & Norbury, 2022; Coakley & Harris, 2020). The goblet and tuft cell hyperplasia is a consequence of host production of the cytokines interleukin (IL) 25, IL4 and IL13 in a feed-forward loop that is driven by tuft cell sensing of nematode infection (Howitt et al., 2016; Luo et al., 2019; Schneider et al., 2018; Von Moltke et al., 2016). In parallel, GI nematodes immunomodulatory molecules may act to minimise these responses in order to persist in their hosts. *In vivo* investigations on the mechanisms by which ES products interfere with these processes are challenging. Conversely, the reductionistic nature of organoid cultures enables the introduction of live parasites, ES products and immune factors in a controlled manner, and thus they allow the dissection of their individual effects on the GI epithelium. For example, the sole addition of adult *H. bakeri* ES products to the media of traditional 3-D enteroids resulted in suppression of tuft cell differentiation (Drurey et al., 2021). Surprisingly, this effect was observed when ES treatment was given in combination with IL4 and IL13, indicating that *H. bakeri* ES products counteracts the tuft cell hyperplasia driven by the immune response to the parasite (A. H. Buck et al., 2014). However, because adult *H. bakeri* parasites reside within the lumen of the small intestine and thus interact with the apical surface of the epithelium, it is unclear how this co-culture approach



where the ES products are in contact with the basal membrane, reflects *in vivo* interactions.

2-D organoids grown in semi-permeable membranes overcome the limitations of 3-D organoids by allowing a more accurate modelling of the stimuli the epithelial cells encounter during infection. This includes: 1) the controlled (dose and volume) co-culture of nematodes or their ES products with the apical or basal compartment that mimics the interactions of larval and adult stages with the GI epithelium, and 2) the stimulation with cytokines on the basal compartment to replicate interactions with immune cells that can occur before or after exposure to ES products.

To advance our understanding of how nematode ES interacts with the host epithelium and the functional implications of these interactions on underlying cells, it will be beneficial to introduce additional cell types such as immune and stromal cells, or microbiota, alongside organoids (Duque-Correa, Maizels, et al., 2020; Puschhof et al., 2021; Sasaki et al., 2020). Introducing immune components to 2-D organoid cultures with controlled timings could be used to model nematode-host interactions during either primary or secondary infections, or to increase numbers of rare cell types of interest for experimental purposes which are difficult to study *in vivo* due to low numbers. Similarly, micro-engineered scaffold organoids can allow for the co-culture of multiple cellular populations, but additionally have the potential to introduce vascularisation, fluid-flow and better replicate *in vivo* architecture (Nikolaev et al., 2020; Y. Wang, Gunasekara, et al., 2017). In the future these systems could allow for better understanding of interactions between helminths and their secretion products and the host epithelium.

## 1.6 Thesis aims

As detailed in this chapter, the intestinal epithelium is a key tissue for the detection of helminths, initiation of immune responses, and mediating effector functions during infection. *H. bakeri*, like many helminths, is a master manipulator of the host environment and achieves this by secreting bioactive molecules that interact with the host. HES has been discovered to contain EVs which cargo nucleic acids, proteins and lipids. Based on previous data (Buck et al., 2014) I hypothesize that *H. bakeri* EVs modulate the host intestinal epithelium.

To address our hypothesis I modelled the intestinal epithelium using 2-D enteroids which allowed us to untangle helminth induced changes from those driven by host factors (e.g., by cytokines) and allowed delivery of EVs to the apical epithelium. A proportion of the thesis therefore focused on developing methods for these studies (Aims 1&2):

1. Optimise *H. bakeri* EV preparation and labelling – this will allow for tracking of EVs within 2-D enteroids (Chapter 3)
2. Develop a 2-D enteroids model that re-capitulates the intestinal epithelium – this allows us to investigate this multicellular tissue *in vitro* (Chapter 4)

After successful progress in aims 1&2 I then investigated whether *H. bakeri* EVs modify the intestinal epithelium and characterised the host response to EVs (Aims 3&4):

3. Determine whether *H. bakeri* EVs are taken up by 2-D enteroids cells and whether specific subtypes are targeted (Chapter 5)
4. Define the host transcriptional response to *H. bakeri* EVs in 2-D enteroids cultures, and by comparison to co-cultures of 2-D enteroids with live parasites (Chapter 6)

**Chapter 2: Materials & Methods**

## 2.1 Cell culture medias

### Complete DMEM

Dulbecco's Modified Eagle Media (DMEM) (Sigma-Aldrich)

5% FBS (Gibco)

2 mM L-glutamine (Gibco)

100 U/ml Penicillin/100 µg/ml Streptomycin (Gibco)

(For HEK293 STF cells supplement with 200 µg/ml G418 (Gibco))

### Complete RPMI

Roswell Park Memorial Institute (RPMI) (Sigma-Aldrich)

5% FBS (Gibco)

2 mM L-glutamine (Gibco)

100 U/ml Penicillin/100 µg/ml Streptomycin (Gibco)

### R-spondin basal growth and selection media

Dulbecco's Modified Eagle Media (DMEM) (Sigma-Aldrich)

5% FBS (Gibco)

2 mM L-glutamine (Gibco)

100 U/ml Penicillin/100 µg/ml Streptomycin (Gibco)

(For selection media supplement with 300 µg/mL of Zeocin)

### L-Wnt-3a basal growth and selection media

Dulbecco's Modified Eagle Media (DMEM) (Sigma-Aldrich)

5% FBS (Gibco)

2 mM L-glutamine (Gibco)

100 U/ml Penicillin/100 µg/ml Streptomycin (Gibco)

(For selection media supplement with 125 µg/mL of Zeocin)

Organoid base growth media

Advanced DMEM/F12 (Gibco)  
2 mM L-glutamine (Gibco)  
1x N2 supplement (Life Technologies)  
1x B27 supplement (Life Technologies)  
10 mM HEPES (Gibco)

Organoid isolation media – used for 1 week after crypts are retrieved from *in vivo* tissue.

Organoid base media (see above) supplemented with  
100 U/ml Penicillin/100 µg/ml Streptomycin (Gibco)  
30% Wnt conditioned media – made in house  
10% R-spondin conditioned media – made in house  
1 mM N-acetylcysteine (NAC) (Merck)  
50 ng/ml Recombinant Epidermal Growth Factor (EGF) (Thermo Fisher Scientific)  
100 ng/ml Recombinant mouse noggin (PeproTech)  
10 µM Rho kinase inhibitor (ROCKi) (also known as Y-26732) (Sigma-Aldrich)  
For caecal organoids only, media was also supplemented 100 ng/ml Human Recombinant Fibroblast Growth Factor 10 (FGF-10) (PeproTech, 100-26)

Organoid expansion media – used for maintaining organoid lines after first week of culture

Organoid base media supplemented with

30% Wnt conditioned media – made in house

10% R-spondin conditioned media – made in house

1 mM N-acetylcystiene (Merck)

50 ng/ml Recombinant Epidermal Growth Factor (EGF) (Thermo Fisher Scientific)

100 ng/ml Recombinant mouse noggin (PeproTech)

For caecal organoids only, media was also supplemented with 100 ng/ml Human Recombinant Fibroblast Growth Factor 10 (FGF-10) (PeproTech, 100-26)

Organoid stem cell enrichment media – used for 4 days prior to 2-D enteroid seeding and during 2-D enteroid culture

Organoid base media supplemented with

10  $\mu$ M CHIR99021 (Cayman chemicals)

10% R-spondin conditioned media

1 mM N-acetylcystiene (Merck)

50 ng/ml Recombinant Epidermal Growth Factor (EGF) (Thermo Fisher Scientific)

100 ng/ml Recombinant mouse noggin (PeproTech)

10  $\mu$ M Rho kinase inhibitor (ROCKi) (also known as Y-26732) (Sigma-Aldrich)

Caecaloid differentiation media 1

Organoid expansion media (above) supplemented with 10% vol/vol Wnt conditioned media

Caecaloid differentiation media 2

Organoid expansion media (above) supplemented with 2.5% vol/vol Wnt conditioned media

**2.2 Buffer solutions**

FACs buffer

Phosphate buffered saline (PBS) (Sigma-Aldrich)

0.1% Bovine serum albumin (BSA) (Fisher Bioreagents)

0.1% Sodium azide (NaN<sub>3</sub>) (Sigma-Aldrich)

Sorting buffer

Phosphate buffered saline (PBS) (Sigma-Aldrich)

\*0.1% Bovine serum albumin (BSA) (Fisher Bioreagents)

\*For experiments that were sorted for the purpose of single cell sequencing BSA was reduced to 0.04%

Microscopy buffers

Paraformaldehyde (PFA) 4%

16% Paraformaldehyde (Pierce) diluted in PBS to 4%

Permeabilisation & block buffer – for 2-D enteroids & MODE-K cells

Phosphate buffered saline (PBS) (Sigma-Aldrich)

5% Fetal bovine serum (FBS) (Gibco)

0.2% Triton X (Sigma, x100-500mls)

Diluent – for 2-D enteroids & MODE-K cells

Phosphate buffered saline (PBS) (Sigma-Aldrich)

5% Fetal bovine serum (FBS) (Gibco)

0.25% Triton X (Sigma)

Permeabilisation buffer – for tissue sections

Tris buffered saline (TBS) (made in house and autoclave sterilised)

0.1% Triton X (Sigma, x100-500mls)

Block buffer – for tissue sections

Tris buffered saline (TBS) (made in house and autoclave sterilised)

5% Bovine serum albumin (BSA) (Fisher BioReagents)

Diluent – for tissue sections

Tris buffered saline (TBS) (made in house and autoclave sterilised)

Silver stain buffers

Fixation buffer

100 ml 100% Ethanol

25 ml Acetic acid (Scientific Laboratory Supplies)

125 ml dH<sub>2</sub>O

Sensitisation buffer



17 g Sodium acetate (Merck)  
10 ml Sodium thiosulfate (Sigma)  
75 ml 100% Ethanol  
Make up to 250 ml with dH<sub>2</sub>O

Silver stain buffer

25 ml of 2.5% (w/v) Silver nitrate solution (Fisher Scientific)  
225 ml of dH<sub>2</sub>O

Developing buffer

6.25 g Sodium carbonate (Sigma)  
50 µl Formaldehyde (37%) (Pierce)  
Make up to 250 ml in dH<sub>2</sub>O

Gel electrophoresis and western blot buffers

NuPAGE MOPS SDS buffer

50 ml 20x NuPAGE MOPS SDS buffer (Thermo Fisher Scientific)  
9950 ml dH<sub>2</sub>O

**2.3 Cell culture**

**2.3.1 R-spondin conditioned media**

To generate R-spondin conditioned media HA-R-spondin-1-Fc 293T cells (R-SPO1) (Amsbio) were first cultured for at least 5 days in R-spondin selection growth media containing Zeocin. Cells were passaged using trypsin-EDTA

0.25% (Thermo Fisher, C-25200072) and cultured for 10 days in R-spondin basal growth media at 37°C 5% CO<sup>2</sup>. Conditioned media was then collected after 10 days and centrifuged (Beckman Coulter) at 3000 rpm at 4°C for 15 min. Conditioned media was filtered through a 0.22 µm PES membrane filter bottle (VWR, 514-0332). R-spondin conditioned media was aliquoted and stored at -70°C.

### **2.3.2 L-Wnt3a conditioned media**

L-Wnt3a cells were gifted from Hans Clevers Laboratory. L-Wnt3a cells were cultured in L-Wnt3a selection media containing 125 µg/mL of Zeocin for at least 4 days and then passaged using TrypLE™ Express Enzyme (Thermo Fisher Scientific, 12605010). To generate L-Wnt3a conditioned media, cells were then cultured in L-Wnt3a growth media for 7 days. Conditioned media was collected and centrifuged for 5 min at 1500rpm at 4°C (Beckman Coulter) and filtered through a 0.22 µm PES membrane filter bottle (VWR, 514-0332). L-Wnt3a conditioned media was stored at 4°C.

## **2.4 Organoid culture**

### **2.4.1 3-D Organoid Isolation**

Mice were sacrificed, for small intestinal organoids the entire small intestine was dissected by cutting at junction of the stomach pylorus and duodenum, and at the ileocecal junction. For duodenal organoid lines only the first 2 inch distal to the stomach pylorus junction was dissected. Intestine sections were flushed gently with sterile PBS using a 1ml pipette to remove contents and opened longitudinally. Intestinal tissue was washed serially in a 6 well plate containing sterile PBS to further remove intestinal contents and mucus. Samples were processed from this point in a sterile TC hood on ice. Tissue sections were cut into approx. 2 mm sections and placed in a 50 ml falcon of

sterile ice-cold PBS. Washes were performed by pipetting up and down using a pre-wetted 10 ml serological pipette. Intestinal pieces were left to settle by gravity on ice, and the supernatant containing mucus and luminal contents was removed. Washes were repeated 10-15 times until the supernatant remained clear after washing. Intestinal pieces were collected by centrifugation at 600 rpm for 3 min at 4°C. Tissue pieces were digested in 25 ml of gentle cell dissociation media (Stem Cell Research, 7174) and incubated on a rocker for 15 min at RT. Tissue pieces were allowed to settle by gravity on ice and dissociation media was removed. Using a pre-wetted serological pipette tissue pieces were washed with PBS + 0.1% BSA (Fisher Bioreagents, BP9700-100) by pipetting 3 times, at this point crypts are dissociated and therefore come off with the washes. Tissue was allowed to settle by gravity and then the wash was removed and filtered through a 70 µm cell strainer (Thermo Fisher Scientific, 11597522). Washes were repeated a total of 4 times to collect 4 sequential fractions. The number of crypts in each fraction was then enumerated. The fraction(s) enriched for intestinal crypts were then centrifuged at 1200 rpm for 3 min at 4°C. Crypts were re-suspended in Matrigel® at ~50crypts/100 µl Matrigel (Corning, 35623). Crypts suspended in Matrigel® were then plated in ~50 µl domes in a 6-well cell culture plate (Corning) and incubated at 37°C 5% CO<sub>2</sub> for 10 min for Matrigel® to solidify. After which, 2.5 ml of pre-warmed organoid isolation media was added per well and incubated at 37°C 5% CO<sub>2</sub>. Organoid isolation media was replaced every second day thereafter until the organoid appearance suggested that passage was required (~ 1 week).

Caecal organoids were established by María Duque Correa at the Wellcome Sanger Institute using published methods and gifted for use in this thesis (Duque-Correa, Schreiber, et al., 2020).

#### 2.4.2 3-D Organoid maintenance

Organoid cultures were kept in isolation media until the first passage (~ 1 week) and then maintained indefinitely in organoid expansion media. Organoids were maintained in 2.5 ml of media that was replenished every second day, or in 3 mL of media over a weekend. Organoids were passaged ~5-7 days depending on the speed of growth. To passage organoids, all steps are performed on ice to prevent Matrigel<sup>®</sup> from solidifying. Organoid containing Matrigel<sup>®</sup> patties were detached from the culture plate using a cell scraper. Using a p1000 organoid containing Matrigel<sup>®</sup> was gently broken up by pipetting 3-5 times and collected into a pre-chilled 15 ml Falcon tube (Sarstedt, 62554502). Suspended organoids were washed in ~10 ml of ice-cold PBS, and then centrifuged at 2000 x g for 2 min and then the wash was aspirated to remove dead cells, debris and Matrigel<sup>®</sup>. Organoids were re-suspended in 1 ml of ice-cold Cell Recovery Solution (Corning, 354253) and incubated on ice for 40 min to dissolve remaining Matrigel<sup>®</sup> and release organoids. 1 mL of organoid base media was added to stop dissociation, and the material was centrifuged at 2000 rpm for 2 min at 4°C. The supernatant was aspirated, and the organoid pellet were re-suspended in 200 µl of organoid base growth media and broken into small cell clusters using a pipette set at 150 µl and pipetting ~200 times until there are no visible intact organoids. 2 ml of organoid base media was added, and organoid cells pelleted by centrifuge at 1500 rpm for 5 min at 4°C. Organoid pellets were re-suspended in an appropriate volume of Matrigel<sup>®</sup> for a 1/3 - 1/6 split. Organoid cells suspended in Matrigel were seeded in patties into a 6 well plate and allowed to solidify and at 37°C 5% CO<sub>2</sub> for 10 min before adding 2.5 ml of organoid growth media to the well and incubated at 37°C 5% CO<sub>2</sub>.

### 2.4.3 2-D Transwell organoid cultures

In Chapter 4 of this thesis, I optimise the growth of 2-D enteroids and trial various alterations to the culture conditions. Here I detail the methods that were

successful and implemented for subsequent experimentations in Chapter 5 & 6.

In order to enrich for stem cells, enteroids or caecaloids were grown for 4 days in stem cell enrichment media, or caecal differentiation media respectively, prior to seeding into 2-D cultures. For Collagen coated Transwell™ surfaces, 12 mm Snapwell™ cell culture inserts with 0.4 µm pores ( $1 \times 10^8$  pore/cm<sup>2</sup>) (Corning, 3407) were coated with Collagen I rat tail (Life Technologies, A10483-01) diluted in 0.2 M acetic acid (Scientific Laboratory Supplies, CHE1014) at a final concentration of 50 mg/ml and incubated at RT for 1hr prior to seeding. Collagen was then aspirated, and the transwell surface washed 3x with 500 µl of PBS at RT. The final wash was left on until cells ready to be seeded. For Matrigel® coated Transwell™ surfaces, Transwell™ were coated with a 'thin' layer of Matrigel (Corning, 35623) as described by Liu *et al*, 2018. In brief, Matrigel® was diluted at a ratio of 1:50 diluted in PBS and incubated on the Transwell™ surface for 1hr at 37°C prior to aspirating the excess volume (Y. Liu *et al.*, 2018). While Transwell™ surface coating was incubating, 3-D organoids were digested into single cell suspensions and all steps completed on ice and all washes were ice-cold unless specified. Matrigel patties containing 3-D organoids were detached from the plate surface using a cell scraper and gently broken up using a p1000 to pipette 3-5 times, these were then transferred to 15 ml falcon tubes. Organoids were washed with 5 ml ice cold PBS and centrifuged at 2000 rpm for 2 min at 4°C. Supernatant was aspirated, and organoid containing pellet was re-suspended in 1 ml PBS using a p1000, then made up to a volume of 10ml with PBS. Organoids were allowed to settle by gravity for 10 min on ice. Supernatant was aspirated to the 1 ml mark, and organoids re-suspended using a p1000 before 9 ml of PBS was added for a total volume of 10 ml and centrifuged at 2000 rpm for 2 min at 4°C. The supernatant was aspirated, and organoids were re-suspended in 3-5 ml of TrypLE™ Express Enzyme (Gibco, 12605010) (3 ml for 1 well – 5 ml for 3 wells) and incubated 37°C for 3-5 min to dissociate 3-D organoids into a single cell suspension. Suspensions were vortexed briefly to assist dissociation and checked under the microscope for complete dissociation of cell clusters aiming

for a mostly single cell suspension. Dissociation was stopped by adding 6 ml of organoid base growth media. Single cells were then centrifuged at 1,500 rpm for 5 min at RT. Cell pellets were re-suspended in 1 ml organoid base growth media and cells counted. Cell concentration was then adjusted to  $1 \times 10^6$ /ml and 200  $\mu$ l seeded into apical side of the pre-coated Transwell™ surface (200,000 cells/well). 4 ml of stem cell enrichment media, or caecal expansion media was added to the basal compartment of the Transwell™ for enteroids and caecaloids respectively. 2-D organoids were incubated at 37°C 5% CO<sub>2</sub>.

On day 1 after seeding the apical media containing dead cells that failed to adhere or proliferate was aspirated and replaced with 200  $\mu$ l of warm base growth media. Apical media was replaced every second day onwards, on day 5 of culture this was reduced to 50  $\mu$ l volume. On day 2 after seeding the basal media was aspirated and replaced, and this was repeated every second day thereafter. At day 4 the basal media was reduced from 4 ml to 2 ml for remainder of the culture. For enteroids, stem cell enrichment media was used throughout culture as enteroids demonstrated ability to differentiate even in presence of stem cell enrichment media (detailed further in Chapter 4). For caecaloid experiments I followed published protocols for lowering Wnt CM concentrations to induce differentiation (Duque-Correa, Goulding, Rodgers, Gillis, et al., 2022). In brief, on day 2 post seeding basal media was changed to caecaloid differentiation media 1 (10% Wnt CM), and again on day 4 to (2.5% Wnt CM) for the remainder of culture. For some experiments during the optimisation of this protocol the media composition during culture was modified, where relevant this is described in the text.

## **2.5 *H. bakeri* lifecycle and HES production**

CBA x C57/BL6 F1 male mice received 200 L3 larvae by oral gavage. At day 14 post infection (p.i.) mice were sacrificed and adult *H. bakeri* worms were collected from the intestine and washed following methods previously

described methods by Camberis *et al*/ before culturing in serum free RPMI 1640 at 37°C (Camberis et al., 2003). After the first 24 hr in culture the media was removed and replaced as it may contain contaminants or secreted material from the host (referred to as Day 0 HES). The culture containing *H. bakeri* excretory/secretory products (HES) was then collected every 3-4 days for a total of 2 weeks. Worms are assessed by eye under dissection microscope for changes to motility and colour changes from rust coloured to grey, which is indicative of non-viable parasites. For studies of *H. bakeri* EV function, only HES collected in the first week of culture was used. HES was centrifuged at 1,200 rpm for 5 min to pellet eggs, the supernatant was collected and filtered using a 0.2 µm syringe filter (Merck, SLGP033RS). HES was stored at -20°C until time of use. For experimental use HES was concentrated to 0.5-1.0 ml using a 5 kDa MWCO Vivaspin columns (GE Healthcare, 10646375) centrifuged at 4000 x g, if this was to use for EV isolation it was concentrated to <12.5 ml for UC isolation and ~ 1 ml for SEC isolation. If HES was to be used as total HES then it was PBS exchanged twice (total PBS volume 40 ml), concentrated to ~ 1 ml and stored at -80°C.

## **2.6 EV separation, concentration & quality control**

### **2.6.1 EV separation & concentration by ultracentrifugation**

EVs were separated from HES, for some experiment's large volumes of HES were pooled (50-100 ml) for EV separation and in these instances the HES was first concentrated to <12.5 ml before ultracentrifugation. EVs were separated by ultracentrifugation using a SW40 rotor (Beckman Coulter) and polypropylene tubes (Beckman Coulter, 331374) and centrifuged at 100,000 x g for 70-90 min at 4°C. The supernatant was collected, referred to as "EV-depleted HES" and concentrated in 5 kDa MWCO Vivaspin columns (GE Healthcare, 10646375). The pelleted EVs were washed with sterile 0.22 µm filtered PBS at 100,000 x g for 70-90 min at 4°C for a total of 2 washes. PBS

was then aspirated and the EV pellet was re-suspended in ~100-200 $\mu$ l of sterile 0.22  $\mu$ m filtered PBS, and transferred to protein LoBind tubes (Eppendorf, 0030108094) to generate a highly concentrated EV preparation. Protein concentrations were determined by Qubit. EV preparation that were to be used within 1 week of preparation they were stored at 4°C, otherwise they were stored at -70; more than one freeze thaw cycle of a given preparation was avoided.

### **2.6.2 EV separation & concentration by Sepharose size exclusion column**

Single use Sepharose (CL-2B) size exclusion columns were made in house in a sterile filtration hood using PD10 columns (Sigma-Aldrich, 17-0435-01). A glass filter was placed at the base of a PD10 column and a PD10 column reservoir (Sigma-Aldrich, 18-3216-03) was attached. Sepharose (CL-2B) was then mixed by inversion and poured into a column to a final height of 7 cm. Once Sepharose settled, 25 ml of HBSS with  $\text{Ca}^{2+}$   $\text{Mg}^{2+}$  was added to the column reservoir and allowed to drip through to remove ethanol. A second glass filter was then placed at the top of the Sepharose bed, 1 ml of PBS was added to keep column saturated and the column was capped. Columns were kept sterile in a 50 ml falcon at 4°C until use.

EVs were separated/concentrated either directly from concentrated HES (1 ml), as a secondary separation/concentration method following UC purification, or to clean up EVs after fluorescent labelling. Prior to the use, columns were equilibrated by adding 25 ml HBSS with  $\text{Ca}^{2+}$   $\text{Mg}^{2+}$  (Thermo Fisher Scientific, 14025092) using a PD10 column reservoir and allowing this to run through the column. 1 ml of EVs or HES was then added to the glass filter of a fresh SEC and a 1 ml fractions collected (representing fractions 1&2), followed by 1 ml of HBSS with  $\text{Ca}^{2+}$   $\text{Mg}^{2+}$  collected as fraction 3&4, a final 0.5 ml of HBSS with  $\text{Ca}^{2+}$   $\text{Mg}^{2+}$  was added and collected as fraction 5 for a total void volume of 2.5 ml. HBSS with  $\text{Ca}^{2+}$   $\text{Mg}^{2+}$  was then added 0.5 ml at a time and 0.5 ml fractions collected. This was repeating using 0.5 ml for fraction 6-



30 for a total volume of 12 ml of non-vesicular protein containing fractions. For some experiments, fraction 7 was combined with EV fractions. For EV depleted HES purified by SEC fractions 8-30 were pooled in equal volume and concentrated.

### 2.6.3 Qubit

Protein quantification of EV preparations was performed using the Qubit protein assay kit (Thermo Fisher Scientific, Q33211) with 3-10  $\mu$ l of neat EV preparation and measured using Qubit 3.0 Fluorometer.

### 2.6.4 Zetaview<sup>®</sup> size quantification and concentration

The Zetaview<sup>®</sup> TWIN (Particle Metrix) was used to measure particle concentration and size in EV preparations as well as labelling efficiency of fluorescent dyes. After initialisation of the machine the flow cell was rinsed with 0.2  $\mu$ m filtered dH<sub>2</sub>O and the cell quality checked before loading with 100 nm polystyrene alignment beads (Applied Microspheres, Netherlands) at a dilution of 1:250,000. Using scatter mode on the 488 laser autoalignment was performed using these diluted beads and then focus optimised. Once the Zetaview<sup>®</sup> passed the autoalignment and autosymmetry the polystyrene beads were measured to ensure machine performance. Prior to measurement the flow cell was rinsed with appropriate buffer such as 0.2  $\mu$ m filtered PBS or HBSS with Ca<sup>2+</sup> Mg<sup>2+</sup> depending on which the sample was eluted in. Samples were diluted until the number of visible particles on the Zetaview<sup>®</sup> was within the acceptable range and the concentration and size of particles was measured using scatter mode with the standardised settings of sensitivity – 85, shutter - , and 3 repeated measurement of 11 different positions were taken ensuring >1000 particles were tracked.

For fluorescent measurements, the laser (488 nm or 640/660 nm) was selected as well as the appropriate filter. Optimisation of the focus was then performed using standardised DR660 fluorescent standard beads (Zetaview<sup>®</sup>

user guide) and a measurement of the beads was taken. Fluorescently labelled EVs were then loaded into the cell and measurements performed using standardised settings of sensitivity = 95 , trace length = 7, and shutter = 100-150, with low bleaching mode selected. For determining labelling efficiency, the same EV sample was measured both in scatter mode and in fluorescent mode, however depending on the label efficiency some samples had to be measured using different dilutions for scatter and fluorescence due to the range of the machine.

### 2.6.5 Silver stain

1-5 µg of EV, EV-depleted HES or HES sample was heat inactivated at 70 for 10 min in 1x LDS sample buffer. Gel electrophoresis was performed on samples using NuPAGE SDS-PAGE gel system (Thermo Fisher Scientific) and SDS MOPS buffer. All silver stain steps were performed on a rocker. Gels were fixed in fixation buffer for 2-3 h. Fixation buffer was removed and replaced with sensitisation buffer for 30 min. The gel was then washed in dH<sub>2</sub>O 5 min for a total of 3 washes. Silver stain buffer was added to the gel for 20 min covered from light. Gels were then washed twice in dH<sub>2</sub>O for 1 min. The developing solution was added for 2-15 min and watched for the development of bands. Developing solution was removed and stopping solution added for 10 min once bands became visible (~ 8 -12 min) and gels imaged using the ChemiDoc gel imager (Bio-Rad).

### 2.6.6 Cryogenic Electron Microscopy (cryoEM)

EVs were prepared for cryoEM by Martin Singleton at the Centre Optical Instrument Laboratory (COIL) at the Wellcome Centre for Cell Biology, Edinburgh. EV samples were prepared by vitrification on lacey carbon grids (TAAB) detailed elsewhere (Dobro et al., 2010). In brief, grids were glow-discharged for 90 s at 25 mA using a Pelco EasiGlow and used immediately.

Vitrification was carried out at 4 °C, 100% humidity with no wait time. Sample was applied to the grids at approximately 0.1 – 0.2 µg/µl protein concentration and blotted for 4-5 s before plunging into liquid ethane.

Grids were examined using a Tecnai F20 microscope operating at 200 kV and Gatan Rio CMOS detector. Grids were held in a Gatan 626 cryoholder and imaged under low-dose conditions. Typically, final images were collected at a nominal magnification of 19,000x (3.2 Å/pixel) with a total accumulated dose of ~ 50 e-/Å and -4 to -6 µm defocus. Images were processed and quantification performed using FIJI ImageJ.

## **2.7 Fluorescent labelling of *H. bakeri* EVs**

### **2.7.1 TFP ester labelling (AF488) & NHS ester labelling (AF647)**

Accessible amines on EV transmembrane proteins were labelled using a tetrafluorophenyl (TFP) ester in AF488 (Thermo Fisher Scientific, A37570) or using an NHS ester/succinimidyl ester in AF647 (Thermo Fisher Scientific, A37573). For either dye reaction, EV preparations were diluted for a 1 ml labelling reaction in PBS containing 100 µl of 1M sodium bicarbonate pH 8.3 and 10 µg of TFP-AF488. Reactions were incubated for 1hr at room temperature on a spinning wheel covered from light. After labelling, excess dye was removed by SEC purification.

### **2.7.2 Memglow™ labelling**

Labelling of the bilipid membrane of EVs in PBS was achieved by adding Memglow™ 660 fluorogenic membrane probe to a final concentration of 200-400 nM in 100-200 µl total volume and incubating for 30 min at RT covered from light.

## **2.8 EV uptake assays**

### 2.8.1 MODE-K

For flow cytometry uptake experiments  $5 \times 10^4$  MODE-K cells were seeded into 24 well cell culture plates and grown overnight at 37°C 5% CO<sub>2</sub>. For microscopy uptake experiments  $5 \times 10^4$  MODE-k cells were seeded into cell culture treated 8 well  $\mu$ -slide (ibidi®, IB-81816) and grown overnight at 37°C 5% CO<sub>2</sub>. After 24 h, MODE-k cells for flow cytometry or microscopy were treated with 1-5  $\mu$ g EVs/well, depending on the experiment, equating to >10,000 EVs/cell. Cells were cultured with *H. bakeri* EVs for 16-24 h before harvesting for flow cytometry, or fixation and analysis by microscopy.

### 2.8.2 2.D Enteroids

2-D enteroids were grown as described in Section 2.4.3 of this thesis for 3 days. On day 3 the apical media was aspirated, and the apical surface was washed with 200  $\mu$ l of warm PBS. 20  $\mu$ g/ml of EVs was then given per transwell diluted in organoid base growth media containing 100  $\mu$ g/ml Primocin™ (Invivogen, ant-pm-05).

## 2.9 Microscopy

For both MODE-k cells and 2-D enteroid cells media was aspirated, and a PBS wash was performed prior to fixing with 4% PFA for 20 min at 4°C. If samples were treated with fluorescently labelled EVs they were covered from light throughout microscopy preparation. Samples were then washed 3x with PBS for 5 min per wash at RT to remove PFA. Samples were blocked using permeabilisation block buffer in Section 2.2 of this thesis for 1 hr at RT. Permeabilisation block buffer was removed and primary antibodies were then diluted in diluent to specific concentrations detailed in Table 2.1 and added incubated with samples overnight at 4°C (Table 2.1). The following day antibodies were removed, and samples were washed three times (Diluent, 5

min, 200  $\mu$ l). Any secondary antibodies, DAPI and Phalloidin were added for 1hr at RT covered from light (Table 2.1). After which, secondary antibodies were removed by washing 3 times (Diluent, 5 min, 200  $\mu$ l). For imaging, MODE-K cells 200  $\mu$ l of ibidi Mounting Medium (ibidi, 50001) was added onto the sample prior to imaging. For 2.D enteroids, all PBS was removed and the membrane carefully excised using a scalpel, the Transwell™ membrane was then placed apical side face up on a clean glass microscopy slide and 200  $\mu$ l of Prolong Gold Antifade Mountant (Thermo Fisher Scientific, P36930) pipetted on top, a glass coverslip was then used to mount the slide. Samples were left at RT overnight for prolong gold to cure and sealed with clear nail varnish the following day prior to imaging. Imaging was performed using the Zeiss LSM980 Airyscan 2, or the Zeiss LSM880 Airyscan microscope at the Centre Optical Instrument Laboratory (COIL) at the Wellcome Centre for Cell Biology, Edinburgh.

**Table 2.1: Reagents for immunofluorescence microscopy**

Reagent	Host	Dilution	Supplier	Clone	Purpose
<b>Antibodies</b>					
<b>Anti-Lysozyme 1</b>	Rabbit	1:40	DAKO (A0099)	Polyclonal	Binds lysozyme 1 expressed by Paneth cells
<b>Anti-DCAMKL1 (Dckl1)</b>	Rabbit	1:200	Abcam (ab31704)	Polyclonal	Binds doublecortin like kinase 1 expressed by tuft cells
<b>Anti-Villin</b>	Rabbit	1:100	Abcam (ab130751)	SP145	Binds villin expressed in microvilli, primarily expressed by enterocytes
<b>Anti-Chromogranin A</b>	Rabbit	1:50	Abcam (ab15160)	Polyclonal	Binds chromogranin A expressed by enteroendocrine cells
<b>Anti-ki67</b>	Rabbit	1:250	Abcam (ab16667)	SP6	Binds ki67 expressed in proliferating cells including stem cell and TA cells
<b>Anti-EV sera</b>	Rat	1:400	In house	Polyclonal	Polyclonal sera raised against <i>H. bakeri</i> EVs
<b>4',6-diamidino-2-phenylindole (DAPI)</b>	N/A	1:1000	Invitrogen (D1306)	N/A	Counter stain for A-T rich regions of DNA
<b>Secondary antibodies</b>					
<b>Anti-Rat IgG2a AF647</b>	Mouse	1:1000	Biologend (407511)	MRG2a-83	Secondary antibody used to detect primary binding
<b>Anti-Rabbit AF594</b>		1:1000	Biologend (410407)	6B9G9	Secondary antibody
<b>Counterstains</b>					
<b>Sambucus Nigra Lectin FITC (SNA)</b>	N/A	1:50	Vector laboratories (FL-1301)	N/A	Binds sialic acid in mucus on goblet cells
<b>Ulex europaeus agglutinin FITC (UEA)</b>	N/A	1:1000	Sigma-Aldrich (19337)	N/A	Binds $\alpha$ -L-fucose in mucus on goblet cells
<b>Phalloidin iFluor AF594</b>	N/A	1:2000	Abcam (ab176757)	N/A	Binds F-actin to visualise cell borders

### 2.10 Harvesting 2-D transwell organoids for flow cytometry

For flow cytometry of 2-D transwell organoids, EV treatment was the same as for microscopy. For harvesting the cells, the apical media of 2-D transwell organoids containing EVs was aspirated, and 3x washes with warm PBS were performed to remove dead cells, mucus and debris. To dissociate cells, 500  $\mu$ l of pre-warmed Trypsin 0.25% EDTA (Thermo Fisher Scientific, 25200056) containing 10  $\mu$ M ROCKi was added to the apical surface and 2 ml added to the basal side and incubated at 37°C. Dissociation was monitored and assisted by rinsing the apical transwell surface with a p1000 set to 400  $\mu$ l every 10 min; the suspended cells were then immediately collected into a falcon containing DMEM-F12 (10% FBS, 10  $\mu$ M ROCKi) on ice, and apical transwell surface replaced with fresh Trypsin. Once adequately dissociated from the membrane (~ 30 min) suspensions were transferred to a falcon tube containing DMEM-F12 10%FBS, 10  $\mu$ M ROCKi and centrifuged at 200 x *g* for 4 min at RT to pellet cells. The cell pellet was when re-suspended and washed in 10 ml of base growth media containing 10  $\mu$ M ROCKi for a total of 3 washes. At this stage large cell clusters are still present, using wide bore tips the cells were then re-suspended in 1-2 ml of pre-warmed TrypLE™ Express Enzyme containing 10  $\mu$ M ROCKi, 1 mM NAC and 10  $\mu$ g/ml DNase (STEMCELL Technologies, 7469) and incubated at 37°C for 3-5 min, once mostly single cells are present the reaction was stopped by adding 10 ml of base growth media containing 10  $\mu$ M ROCKi. Single cells were pelleted by centrifugation at 300 x *g* 5 min at 4°C. Cell pellets were then re-suspended in 1-2 ml of DMEM-F12 10% FBS, 10  $\mu$ M ROCKi using wide bore tips and filtered using a 40  $\mu$ m cell strainer. Cells were then counted if necessary, centrifuged to pellet and re-suspended in 100  $\mu$ l of PBS or an adequate volume for downstream use. For flow cytometry analysis the cells were plated in a 96-well plate (Corning) for staining. Plate containing cells were then centrifuged at 300 x *g* for 5 mins and washed with 100  $\mu$ l of PBS. In order to differentiate live cells from dead cells, samples were stained in 10 $\mu$ l of live/dead Aqua (Thermo Fisher Scientific,

L34957) at a 1:1000 dilution in PBS for 10 mins covered from light at RT. Cells were washed in FACs buffer twice before re-suspending in 200 µl FACs or Sorting buffer. Samples were acquired using the MacsQuant flow cytometer (Miltenyi Biotec) or the LSR II flow cytometer (BD Biosciences).

### **2.11 Fluorescence-activated cell sorting (FACS)**

For sorting organoid cells methods from section 2.10 were followed with the use of sorting buffer in place of FACs buffer. Sorting was performed using the FACS Aria (BD Biosciences) operated by Martin Waterfall at the Institute of Infection and Immunology Research (IIIR) Flow Cytometry Core Facility. For scRNA seq cells were sorted at 4 °C using a 70 µm nozzle at 60 psi.

### **2.12 RNA methods**

#### **2.12.1 RNA extraction**

Prior to RNA extraction, the apical membrane 2-D transwell organoids were washed with warm PBS to reduce mucus and dead cells. Cells were then lysed on the membrane using 350 µl of RTL lysis buffer (Qiagen, 79216) with 1:10 β-mercaptaethanol. Lysate was transferred to a DNase/RNase free LoBind tubes (Eppendorf, E0030108094) and RNA extracted using RNeasy micro kit (Qiagen, 74004) following manufacturer's instructions, including the on column DNase step. RNA was eluted using 14 µl of RNase free H<sub>2</sub>O, for 2-D enteroid samples RNA was eluted twice for a total volume of 28 µl.

#### **2.12.2 Reverse transcription and quantitative PCR**

Cellular RNA was reverse transcribed into cDNA using the miScript II RT kit (Qiagen, 218161) using 2 µl of 5x HiFlex buffer, 1 µl of 10x nucleics mix, 1 µl reverse transcriptase mix per reaction along with RNA diluted in RNase free H<sub>2</sub>O to a final volume of 10 µl. For sorted cells, or 2-D transwell organoids 100-



200 ng of input RNA was used for RT reactions. RT reaction was performed at 37°C for 1 hr, followed by 5 min at 95°C to deactivate RT enzymes. cDNA was stored at -20°C until use.

Subsequent cDNA was diluted 1:10 in RNase H<sub>2</sub>O for use in quantitative PCR (qPCR). qPCR was performed in duplicate using miScript SYBR green kit (Qiagen, 218075). Each reaction contained 0.7 µl forward primer, 0.7 µl reverse primer, 5 µl 2x QuantiTect SYBR green PCR master mix, 2.6 µl of H<sub>2</sub>O, and 1 µl of pre-diluted template cDNA for a final volume of 10 µl. Oligonucleotide primer sequences are details in Table 2.2. qPCR cycle conditions were, 94°C for 5 min pre-denaturation followed by 45 cycles of 10 s at 95°C for denaturation, 60°C for 10 s for primer annealing, 10 s at 72°C for elongation. Nuclease free H<sub>2</sub>O was used as in non-template control for each primer set.

Table 2.2 | Primers for RT q PCR

Target	F/R	Primer sequence	PrimerBank ID/source
<b>Lgr5</b>	F	CCTACTCGAAGACTTACCCAGT	6753842a1
	R	GCATTGGGGTGAATGATAGCA	
<b>Muc2</b>	F	ATGCCACCTCCTCAAAGAC	
	R	GTAGTTTCCGTTGGAACAGTGAA	
<b>Chga</b>	F	ATCCTCTCTATCCTGCGACAC	6680932a1
	R	GGGCTCTGGTTCTCAAACACT	
<b>Lyz1</b>	F	GAGACCGAAGCACCGACTATG	7305247a1
	R	CGGTTTTGACATTGTGTTCCG	
<b>Dckl1</b>	F	TCCACCGGAATTGAACTCGG	26328245a1
	R	GGGAGCGAACAGTCTCAGA	
<b>Pou2f3</b>	F	CTGGAACAGTAACGTCATCCTG	388914a1
	R	AGTTCATTGCTGCTTTGGAGTT	
<b>Muc13</b>	F	GGAGGCAGGTGCTAACACATT	294997231c1
	R	CCTGAGTAAGAGGGAGTAAGTGA	
<b>Olfm4</b>	F	CAGCCACTTTCCAATTTCACTG	71892419c1
	R	GCTGGACATACTCCTTCACCTTA	
<b>Sst</b>	F	ACCGGGAACAGGAACTGG	6678035a1
	R	TTGCTGGGTTTCGAGTTGGC	
<b>Ghrl</b>	F	GAAGCCACCAGCTAAACTGCAG	Origene (MP205441)
	R	CTGACAGCTTGATGCCAACATCG	
<b>Pigr</b>	F	CCGGCACACCCGGAATAC	255759935c3
	R	TGCCTGAATACTCCTTGGAGA	
<b>Actb</b>	F	GGCACCACACCTTCTACAATG	
	R	GGGGTGTGGAAGGTCTCAAAC	
<b>GAPDH</b>	F	CATGGCCTTCCGTGTTCCCTA	
	R	GCGGCACGTCAGATCCA	
<b>Spib</b>	F	GGGGGCCTTGACTCTA	(de Lau et al., 2012)
	R	CTCTGGGGGGTACACC	
<b>Gp2</b>	F	CCTGCGTTCTGACACTG	(de Lau et al., 2012)
	R	GCCGTGCAGTTATCA	
<b>Rank</b>	F	ATGCGAACCAGGAAAGT	(de Lau et al., 2012)
	R	TGCCTGCATCACAGACT	
<b>Annexin V</b>	F	AGGGCTGATGCAGAAAGT	(de Lau et al., 2012)
	R	TCCCTGCCAAACACAG	

## 2.13 Sequencing methods

### 2.13.1 10x Chromium scRNA-seq

Single cell RNA sequencing (scRNA seq) was performed on 2-D organoids treated with *H. bakeri* ES products to determine cell type specific differential gene expression. were harvested as per protocol in section 2.10 of this thesis. All 10x Chromium scRNA seq GEM generation and library preparation was performed by Susan Campbell and Elisabeth Freyer at the FACS facility in the Institute of Genetics and Cancer (IGC) at the University of Edinburgh. In brief, prior to performing scRNA seq, samples were enriched for live single cells by sorting live cells based on live/dead Aqua staining as detailed above. After sorting, cells were spun down and re-counted using a haemocytometer as the cytometer can overestimate numbers. The Chromium Next GEM chip G was then loaded with ~30,000 cells per sample (targeted 10,000 cell recovery) at 1000 cells/ $\mu$ l for Gel bead-in-emersion (GEM) generation which was performed following the reagents and manufacturer's instructions from Chromium Next GEM Single cell 3' Kit v3.1 (10x user guide). The subsequent steps of barcoding, RT, Post-GEM RT clean up, cDNA amplification and library construction were performed following the manufacturer's instructions (10x user guide) and are summarised in Figure 2.1. After library construction the quality of each sample was assessed using Aligent High Sensitivity DNA kit (Aligent, 5067-4626) on the Aligent 2100 Bioanalyzer. Sequencing of scRNA seq libraries were sequenced by the Genetics Core at the Edinburgh Wellcome Trust Clinical Research Facility (WTCRF) using the NextSeq 2000 P3 v3 for 100 cycles.

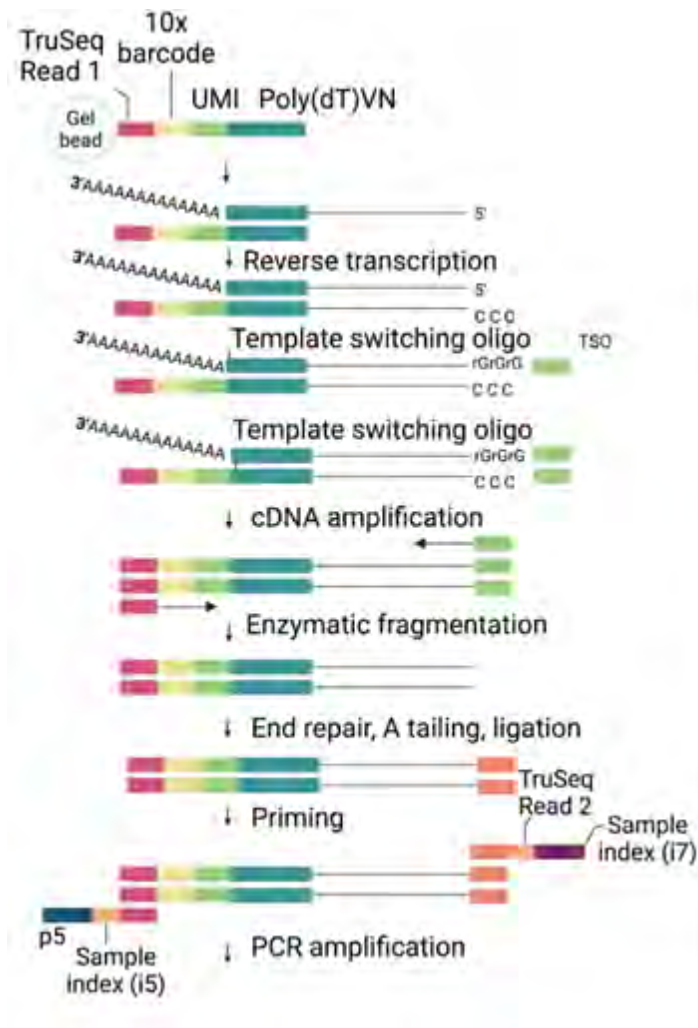


**Figure 2.1 | Schematic of steps for generation of libraries using Chromium Next GEM Single cell 3' Kit v3.1.** Figure adapted from the 10x user guide. Gel bead in emulsion (GEMs) contain attached TruSeq1 read followed by 10x barcode and the Unique Molecular Identifier (UMI) which will allow for computational identification of the single cellular identity of each read, and then a Poly(dT)VN sequence to allow for capture of polyadenylated mRNA. Single cell suspension is then mixed with GEMs on the chromium chip to allow for single cells to merge with a single bead. Reverse transcription, template switching, and extension occurs followed by cDNA amplification. Enzymatic fragmentation occurs and TruSeq Read 2 is added before addition of a sample index (this is unique for each condition e.g. mock, EV and EVdePHES to allow for computational sample identification). Finally, p7 and p5 are added which are required for Illumina bridge amplification during sequencing. Libraries are then amplified using PCR amplification and final product is depicted in Figure 6.16.

### 2.13.2 Whole transcriptome sequencing

Transcriptome sequencing of 2-D organoids co-cultured with *H. bakeri* or treated with ES products was performed to assess differential gene expression in this tissue. RNA was extracted using methods described in section 2.12.1 of this thesis. RNA was checked for quality using the Aligent 2100 Bioanalyzer and the High Sensitivity DNA kit (Aligent). Ribodepletion, library preparation and sequencing were performed by the WT CRF using the NextSeq 200 P2 for 100 cycles.

## 2.14 Bioinformatic analysis

### 2.14.1 Whole transcriptome sequencing analysis

The bioinformatic analysis of transcriptome sequencing data was performed by Roberto Jose Bermudez Barrientos Data in discussion with author. Sequencing files were first assessed for quality and filtered using FastQC, and adapter sequences removed (Andrews, 2010). Sequences that passed initial quality control were then mapped to the *mus musculus* genome from Ensembl release103 (genome GRCm39.primary\_assembly.genome.fa). Reads were aligned to the genome using hisat2 version 2.2.1 using the non-deterministic parameter. The non-deterministic parameter makes hisat2 use the current time as a seed to restart its pseudorandom generator instead of the read sequence, this may be more appropriate in situations where the input consists of many identical reads. The resulting bam files were indexed using SAMtools (release 1.13) (Danecek et al., 2021; Li et al., 2009).

#### Read counts

For generating read counts for each gene the function featureCounts was used within the package Rsubread 2.6.4 (Y. Chen et al., 2016; Liao et al., 2014). The default parameters were used with the following modification to certain parameters, as follows. geneID was used for retrieving reads to generate

counts. Multimapping reads were counted for all their reported mapping locations by setting `countMutliMappingReads` to true and `fraction` also set to true. Reads that overlapped multiple genome feature were only counted for one genome feature and this was the feature with the largest number of bases aligned.

### Differential expression analysis

Differential expression analysis (DEA) was performed using edgeR 3.34.1 on R version 4.1.1 (Y. Chen et al., 2016; Robinson et al., 2010). For pulling gene annotations (chromosome, gene symbol and description) biomaRt 2.48.3 was used. Genes with low expression which had less than 1 CPM in at least 3 libraries were filtered out of the analysis. Tagwise dispersion estimates was performed using the function `estimateDisp`. Plots of DEA results were generated in R using the packages `ComplexHeatmap` and `ggplot2` by the author.

### CAMERA pathway analysis

Competitive gene set accounting for inter-gene correlation (CAMERA) was performed using the all of the gene expression changes resulting from DEA analysis (no fold change or P-value cut offs were used). CAMERA was performed in R using the `limma` package and the function `camera` (Wu & Smyth, 2012). For CAMERA analysis using gene ontology, the gene ontology (GO) annotations were retrieved from `org.Mm.eg.db` 3.13.0. GO terms with fewer than 50 genes or more than 300 genes were removed from the analysis. For CAMERA analysis using cell type specific genes, the top 100 enriched genes for each cell type were used. Cell type specific enriched genes were retrieved from Haber *et al*, 2017 publicly available single cell RNA seq dataset of cells from *Mus musculus* intestinal epithelium (Haber et al., 2017).

### 2.14.2 scRNA-seq analysis

scRNA seq was performed by Yenetzi Villagrana Pacheco with supervision from Cei Abreu-Goodger and in discussion with the author.

#### Generating the single matrix

From the raw sequencing files (FASTQ) a single-cell expression matrix was constructed using kallisto (Bray et al., 2016) and BUSpaRse R package (Moses & Pachter, n.d.) using the *Mus musculus* reference genome. Cells that likely represented dead cells were filtered out by using a barcode rank strategy with DropletUtils (Lun et al., 2019). Further filtering was performed to remove low-quality cells and double cells using Seurat (Hao et al., 2021) based on the total number of detected genes per cell and the percent of mitochondrial genes (<20%).

#### UMAP and visualisation

Uniform Manifold Approximation and Projection (UMAP) dimensional reductions (using 20 Principal Components) were made using Seurat in R (Hao et al., 2021). UMAP methods were used because it presented the best separation between the cells by comparison to other methods tested, and preserved more of the global structure than the other methods (McInnes et al., 2018). UMAP feature plots and Violin feature plots were made in R using the package Seurat (Hao et al., 2021).

#### Identifying cell types

Cell types were predicted using SingleCellNet which employs a machine-learning approach with (Tan & Cahan, 2019). SingleCellNet is an accurate method when compared with alternative methods (Abdelaal et al., 2019), and requires a training dataset for which a published single-cell survey of intestinal cells was used (Haber et al., 2017). Finally, a differential expression analysis (DEA) between cell types was made and the agreement with the expected

biomarkers according to the databases PanglaoDB was determined (Franzén et al., 2019) and CellMarker (Zhang et al., 2019). Alternatively, I used only the cell specific markers to determine the identity of clusters obtained with Seurat and checked the agreement with previous findings (Chapter 6).

## **2.15 *In vivo* experiments**

### **2.15.1 Vaccination experiments**

To generate anti-EV polyclonal sera used for microscopy detection of EVs. CD rats ( $n = 2$ ) were vaccinated at day 0 with 70  $\mu\text{g}$  of purified EVs mixed at a 1:1 ratio with Imject alum adjuvant (Thermo, 77161). Mice then received two booster vaccinations of 15  $\mu\text{g}$  each of EV-alum (prepared as above) at day 28 post prime and day 35 post prime. Animals were sacrificed at day 42 post prime and cardiac bleeds performed by Elaine Robertson. Serum was collected from whole blood samples by incubating at RT from 30 min to allow red blood cells to coagulate. Samples were then centrifuged at 2,000  $\times g$  for 10 min at 4°C to separate the serum fraction. Serum was collected by pipette and stored at -70°C until use.

### **2.15.2 Intraluminal injections under anaesthetic**

Dr. David Donaldson at the Roslin Institute, Edinburgh performed the surgery with assistance from the author as a training experiment. C57/BL6 male mice were anaesthetised by intraperitoneal (i.p.) injection of Ketamine and medetomidine. Once non-responsive a small incision was made in the abdomen and intestine exposed. A small section of jejunum containing a Peyer's patch was exposed and ligated using sterile cotton and 50 -100  $\mu\text{l}$  of 100  $\mu\text{g}/\text{ml}$  *H. bakeri* EVs, or equivalent volume of sterile PBS was injected into ligated gut section. Incisions were closed using a bulldog clip, and animals



remained anaesthetised for 1.5 hr to allow for EV uptake. After 1.5 hr the animals were euthanised by schedule one neck break and the ligated gut tissue was dissected. Samples were fixed in 4% PFA for 4 hrs. Once fixed, the tissue was processed using following standard dehydration steps of 2x 70% Ethanol washes of 10 min and 30 min, 2x 90% Ethanol washes for 40 min each, 3x 100% absolute Ethanol washes for 40 min each and 30 min for final wash, followed by 3 x washes in xylene for 30 min each. All dehydration steps performed at all at 37°C by David Donaldson. Tissue was then washed 3x in paraffin wax for 25 min at 62°C and then paraffin embedded and stored at RT until sectioned. Sectioning of was performed by the author at the Roslin Institute under the supervision of Dr. Barry Bradford.

**Chapter 3: Optimisation of EV isolation & methods for EV labelling**

**Abstract**

Several species of helminth release extracellular vesicles (EVs) and these are hypothesised to modulate host cells during infection. However, isolating helminth EVs is technically challenging with several methods available that may result in different populations of EVs. Furthermore, assessing whether helminth EVs enter host cells *in vitro* or *in vivo* requires labelling of EVs. Fluorescent lipid dyes have been used previously to identify uptake of helminth EV into host cells, more recent studies show that dye aggregates formed by these dyes may interfere with results. In this chapter I compare ultracentrifuge (UC) and size exclusion chromatography (SEC) for *H. bakeri* EV isolation, as well as the sequential use of both these methods. Using particle tracking, cryoEM, silver stain and protein measurement I then assess the yield, purity and morphology of the resulting EV isolations. I determine that while SEC provides higher yield isolations, combining multiple methods increases purity. Finally, I investigate the use of protein reactive dyes to generate low background labelling of *H. bakeri* EVs. I then present a standardised set of protocols for the optimal isolation and fluorescent labelling for *H. bakeri* EVs.

### 3.1 Introduction

Helminth EVs have only been discovered within the last decade but, already EVs from many different species have been shown to be taken up and modulate gene expression in recipient hosts (Drurey & Maizels, 2021; Sánchez-López et al., 2021). Helminth is a broad term referring to a very large group of parasitic worms, including several evolutionarily distinct phyla including Platyhelminths, Nematoda, Cestodes and Trematodes (Coghlan et al., 2019). Each phylum is comprised of diverse species that have distinct lifecycles, passage through different host tissues, and induce distinct host immune responses (Henry J. McSorley & Maizels, 2012). Therefore, helminth EVs reflect this diversity with regard to both their composition and host interactions (Sánchez-López et al., 2021; Sotillo et al., 2020). For example, *Schistosoma japonicum* (*S. japonicum*) EVs polarise macrophages towards a pro-inflammatory M1 phenotype which protect against fibrosis during the adult stage of infection (L. Wang et al., 2015). Conversely, *H. bakeri* EVs suppress activation of both M1 and M2 macrophages (Coakley et al., 2017).

The protein and miRNA composition of EVs from various helminth species has also been compared, and while some common EV proteins and miRNAs exist within phylum's, no universal pan-helminth EV markers have been identified across all four phylum's (Sotillo et al., 2020). To add to the complexity, the term EVs encapsulates a heterogeneous population of vesicles that vary in size, protein content and biogenesis pathways (van Niel et al., 2018) and the choice of EV isolation method may bias towards isolation of particular EV populations (Théry et al., 2018). At least for *F. hepatica* EVs, as is well documented for mammalian EVs (Veerman et al., 2021), the choice of isolation technique influences the population of EVs that are isolated (Davis et al., 2019). The Minimal Information for Studies of Extracellular Vesicles (MISEV) 2018 guidelines, which outline best practice for EV research, do not recommend one particular EV isolation method. However they strongly recommend the use of combining multiple isolation methods to achieve high purity EV preparations

(Théry et al., 2018). Combinational approaches have been gaining traction in the EV field (Stam et al., 2021), however high purity comes at the cost of reduced yield, which is problematic when ES products are already limited (Appendix IV).

In this chapter I aimed to compare the methodologies used for isolation of *H. bakeri* EVs. Prior work in our lab primarily used ultracentrifugation (UC) isolation which has been the gold standard approach, more recently size exclusion chromatography (SEC) has been favoured as being a higher purity method (Davis et al., 2019; Monguió-Tortajada et al., 2019; Théry et al., 2018). UC uses high speed centrifugation (100,00 x *g*) to pellet particles including EVs based on their sedimentation coefficients, while this method greatly increases EV concentrations it also contains non-vesicular protein contaminants from ES (Davis et al., 2019). Despite being the most utilised method UC is a low efficiency, and low recovery method (Monguió-Tortajada et al., 2019). Size exclusion chromatography (SEC) separates EVs from non-vesicular components of HES by running HES through a porous polymer (e.g. Sepharose) under gravity (Böing et al., 2014). Larger particles such as EVs do not enter particle pores, and therefore move quickly through the column and are eluted first. Whereas smaller molecules (e.g. proteins) become trapped by pores and elute in subsequent fractions (Böing et al., 2014). I aimed to identify how UC and SEC isolation compared in yield and purity of *H. bakeri* EVs isolated.

MISEV 2018 state that for functional studies a combination of sequential methods to EV isolation is strongly encouraged. Therefore, in addition to comparing UC vs. SEC, I also investigated the EV populations yielded by sequential isolation. EVs were isolated first using UC followed by SEC, with the aim of increasing purity. Most EV isolation methods also result in some loss of EVs, therefore whilst sequential approaches are preferable in terms of purity come with the trade-off of lowered yield. As it is understood that UC EV isolation is low yield, I also investigated the presence of EVs within EV depleted HES (EVdepHES), which represents the non-vesicular components of HES present in supernatant after EV depletion. In functional studies

EVdepHES is used as a comparison to identify the effects of EVs. Therefore, as well as investigating sequential EV isolations I also investigated sequential EV depletions from HES. I characterise further the successful depletion of EVs from HES upon both UC, and subsequent SEC purification.

An overarching goal of this thesis was to understand the cell specificity for uptake and the functional effects of *H. bakeri* EVs within the intestinal epithelium *in vitro* and *in vivo*. However, the ability to detect EV uptake is not straightforward and optimisation of methods for detection was required. A gold standard approach for fluorescent labelling of mammalian EVs is genetic modification to introduce fluorescent tagging of EV associated proteins (e.g. CD9) (Chow et al., 2019; Coakley, 2017). However, genetic modification of nematodes is notoriously challenging (Hagen et al., 2021). Previously, studies have used lipid intercalating dyes such as PKH67 for tracking EVs, but later PKH67 was found forms fluorescent aggregates that have a similar size to EVs leading to confounding results (Pužar Dominkuš et al., 2018). Therefore, in this chapter I investigated alternative fluorescent labelling techniques for *H. bakeri* EVs.

## 3.2 Results

### 3.2.1 EV preparation methods

In order to determine the best methodology for EV isolation in this thesis I first wanted to determine which of the available methods would yield i) high purity EVs and ii) high yields of EVs. Our lab had previously implemented UC for purification which was golden standard at the time the research started, however more recently SEC had risen in popularity (2.6.1). I first aimed to compare UC and SEC isolation of EVs for yield and quality. HES was pooled and split equally with half being purified following our standard protocol for UC purification and the other half was fractionated using SEC (2.6.2) (Figure 3.1 A). To determine which SEC fractions contained EVs I quantified these by flow cytometry using the Attune Nxt Cytometer which is capable of detecting particles as small as ~500 nm. EVs were briefly labelled with Violet Ratiometric Membrane Asymmetry Probe/Dead Cell Apoptosis Kit (Thermo Fisher) which is a lipid intercalating dye in order to differentiate EVs from other small particles and background. Due to the size limitations (> 500 nm), this is not a highly accurate method of EV quantification but was used to first quickly assess the presence of EVs in each fraction from SEC. Fractions 7-10 were found to contain fluorescent particles indicative of EVs, and all other fractions contained only very low numbers of these particles close to the background measurement seen in HBSS buffer (Figure 3.1 B&C). UC isolated EVs were also measured by flow cytometry for comparison (Figure 3.1 B&C). UC EVs had a similar profile by flow cytometry to SEC isolated EVs (Figure 3.1 B). SEC isolated EVs appear less concentrated in flow cytometry plots (Figure 3.1. B) as they re-suspended in a larger volume (0.5 ml) over four fractions for a total of 2 ml, whereas UC EVs were re-suspended in 200  $\mu$ l so are ~10-fold more concentrated than SEC EVs. Total EV yields based on flow cytometry were calculated to account for total sample volume (UC = 200  $\mu$ l, SEC = 0.5 ml) and SEC isolation showed higher EV yields by flow cytometry (Figure 3.1 C). I also

measured SEC EV containing fractions 7-10, and UC isolated EVs by nanoparticle tracking analysis (NTA) using the Nanosight LM10 (Malvern Panalytical). NTA uses light scattering properties and Brownian motion of small particles to give accurate measurements of both particle size (20 nm – 1000 nm range) and concentration. NTA showed similar results to flow cytometry, however particle numbers are much higher owing to the enhanced accuracy and ability to detect smaller particles compared to flow cytometry. Quantification of all SEC fractions 7-10 combined yielded higher total particles ( $2.7 \times 10^{11}$ ) than those isolated by UC isolation ( $5.4 \times 10^{10}$ ) from equivalent volumes of the same starting material (Figure 3.1 E).

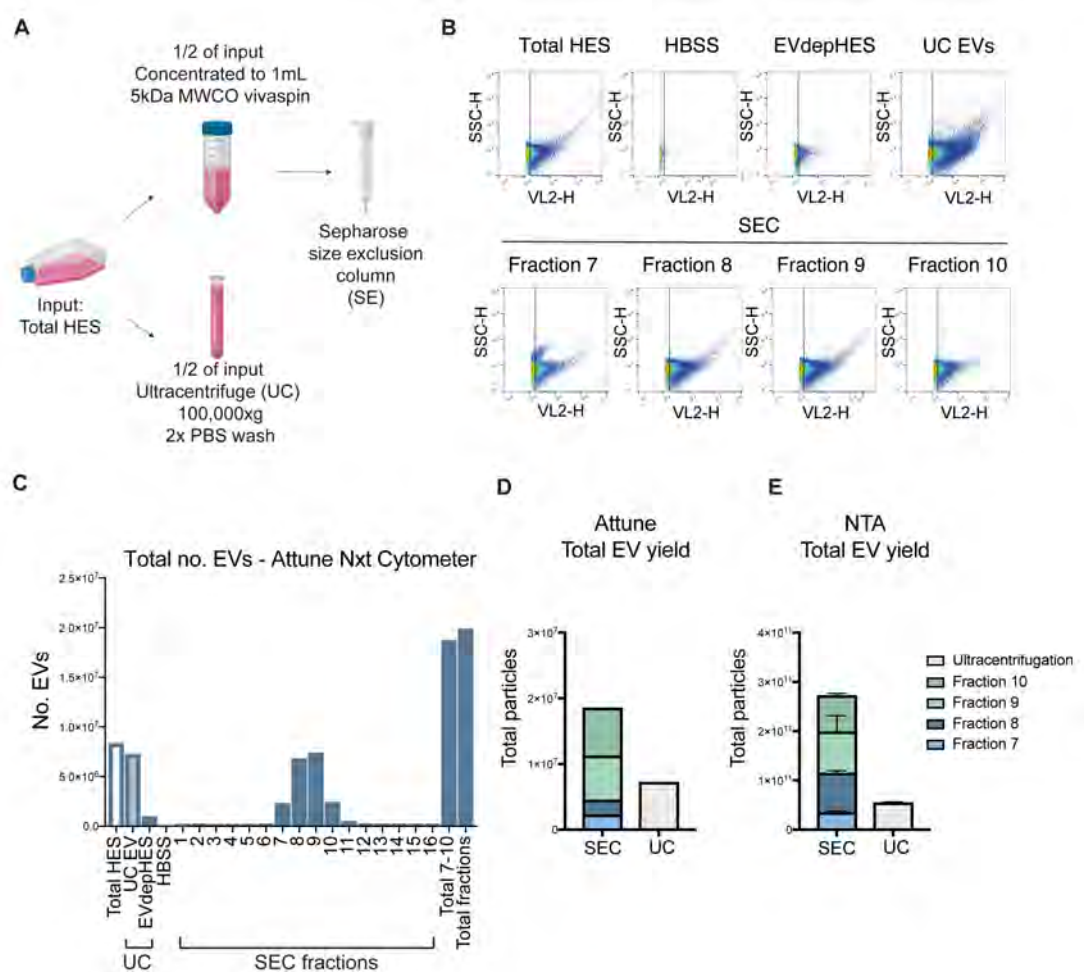


**Figure 3.1 | Comparison of EV isolation by UC or SEC. A)** Schematic of EV isolation comparison between UC and SEC purification. Total HES from multiple batches was pooled and split equally (100 ml per isolation) for UC or SEC isolation. **B)** Flow cytometry analysis using performed on the Attune NXT Cytometer. Presence of EVs was gated using side scatter (SSC) on the y-axis and violet lipid intercalating dye was measured on the x-axis (VL2-H). On the top row from left to right is the initial total HES used for isolation, HBSS buffer, UC supernatant/EVdepHES, UC EVs. Bottom row left to right fraction 7 – 10 of SEC purification. **C)** Quantification for each sample of number of EVs from flow cytometry data. **D&E)**



Total EV yield by **D**) flow cytometry or by **E**) Nano tracking analysis (NTA) from size exclusion chromatography (SEC) isolated EVs coloured by EV containing fractions, or from ultracentrifuge (UC). n = 1.

I wanted to assess not only the quantity of EVs isolated by both methods, but also the sample composition. Silver stain analysis of EV and EVdepHES protein profiles has been routinely used in our lab as a quality control assessment (2.6.5) (Chow et al., 2019; Coakley, 2017). I implemented this method to assess which SEC fraction of HES gave the expected EV associated profile and which had EVdepHES associated profiles. Silver stain was also performed for the UC isolated EVs from this experiment however the amount of UC EVs was limited, and I was not able to load sufficient protein for visualisation. Instead for comparison, a representative silver stain of UC isolated EVs showing the expected banding profile in three independent sample preparations, as well as for their matched EVdepHES (Figure 3.2 A). Silver stain analysis showed that EV associated protein profiles were present in fractions 7-10, but primarily within fractions 8 & 9 with 6 & 10 showing differential intensity of certain bands; perhaps suggesting different subpopulations of EVs that have specific protein cargos (Figure 3.2 B). Clear separation was detected between EVs (frac 7-10) and the majority of non-vesicular proteins (frac 16-27) (Figure 3.2 B). Protein profiles give us an indication of purity of preparations, but transmission electron microscopy (TEM) allows better qualitative assessment of the morphology of EV isolations. By TEM I found numerous EVs from both isolation methods. UC EVs showed a higher amount of non-vesicular electron dense staining which could be protein contaminants, while SEC EVs were highly pure although dense with EVs. All four SEC fractions assessed (7 – 10) contained numerous EVs (Figure 3.2 C). It is worth noting that the UC isolated EVs were diluted to achieve approximately similar particle concentration to the most concentrated SEC fractions, particle concentrations for each sample is provided (Figure 3.2 D).

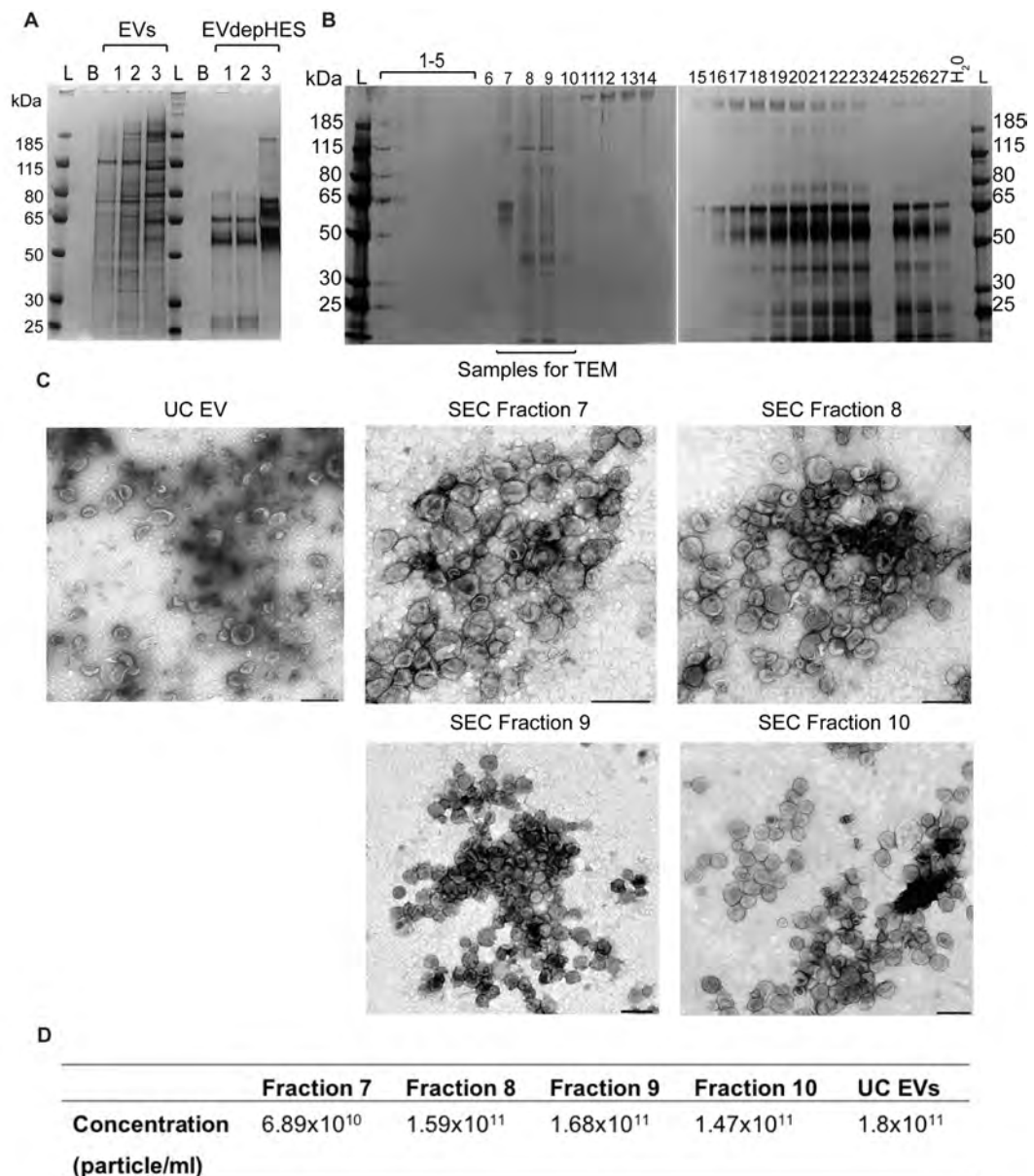


**Figure 3.2 | QC of *H. bakeri* EVs purified by UC or SEC.** **A)** An example of representative silver stain banding patterns in three independent UC isolated *H. bakeri* EVs samples, and their matched EVdepHES (1  $\mu$ g of protein loaded per sample). **B)** Silver stain of SEC fractionated HES, 5  $\mu$ l of each fraction was loaded. Well numbers refer to each 0.5 ml fraction. **C)** Transmission electron microscopy of UC isolated EVs and EVs isolated by SEC in fractions 7 – 10 (same experiment as Figure 3.1). **D)** Table describes concentration (particles/ml) for each sample used for TEM. Scale bars = 200 nm. L = Ladder, B = blank well, EVs = extracellular vesicles, EVdepHES = EV depleted HES kDa = kilodalton. n = 1.

During the sample preparation process for TEM samples are fixed and then dehydrated, as a result EVs appear with a cup like morphology (Chuo et al., 2018). By contrast, cryogenic electron microscopy (cryoEM) embeds EV

samples in vitreous ice (which does not form ice crystals), and maintains the spherical structure of hydrated native EVs (2.6.6) (Chuo et al., 2018). In addition, because cryoEM maintains spherical structure the diameter of EVs is usually large than those visualised by TEM. A subsequent experiment in which EVs were purified either by SEC or UC for cryoEM analysis was performed. This yielded qualitative data that gives insight into the heterogeneity of morphology within our EVs isolations from either method. For all cryoEM images in this Chapter, there are regions that capture the vitreous ice sections,, and regions that capture the carbon grid. Example images illustrating the appearance of the ice layer compared to the carbon grid, and where the formation of ice crystal contamination has occurred, are shown in in Figure 3.3 A&B.Both UC and SEC showed similar EV populations, however due to low numbers of EVs imaged in this experiment, quantification and comparison was not possible.

Previous publications have used cryo-EM to describe various morphologies found in EVs from cerebrospinal fluid (Emelyanov et al., 2020). Similar morphologies were identified for *H. bakeri* EVs in this study and therefore used similar terminology: i) 'bare' EVs showed defined lipid bilayer with no electron dense proteins at their surface (Figure 3.3 C) ii) 'decorated' EVs showed electron dense staining at their surface indicative of proteins (Figure 3.3 D) iii) 'double' EVs showed two lipid bilayers (Figure 3.3 (E) iv) 'multiple' EVs have >2 lipid bilayers forming concentric circles (Figure 3.3 (F) v) 'electron dense' EVs are single layer circular EVs with electron dense contents (Figure 3.3 G) vi) 'polymorphous' EVs had non-circular morphology (Figure 3.3 (H) and vii) 'incomplete' EVs did not have a completely intact lipid bilayer (Figure 3.3 I).

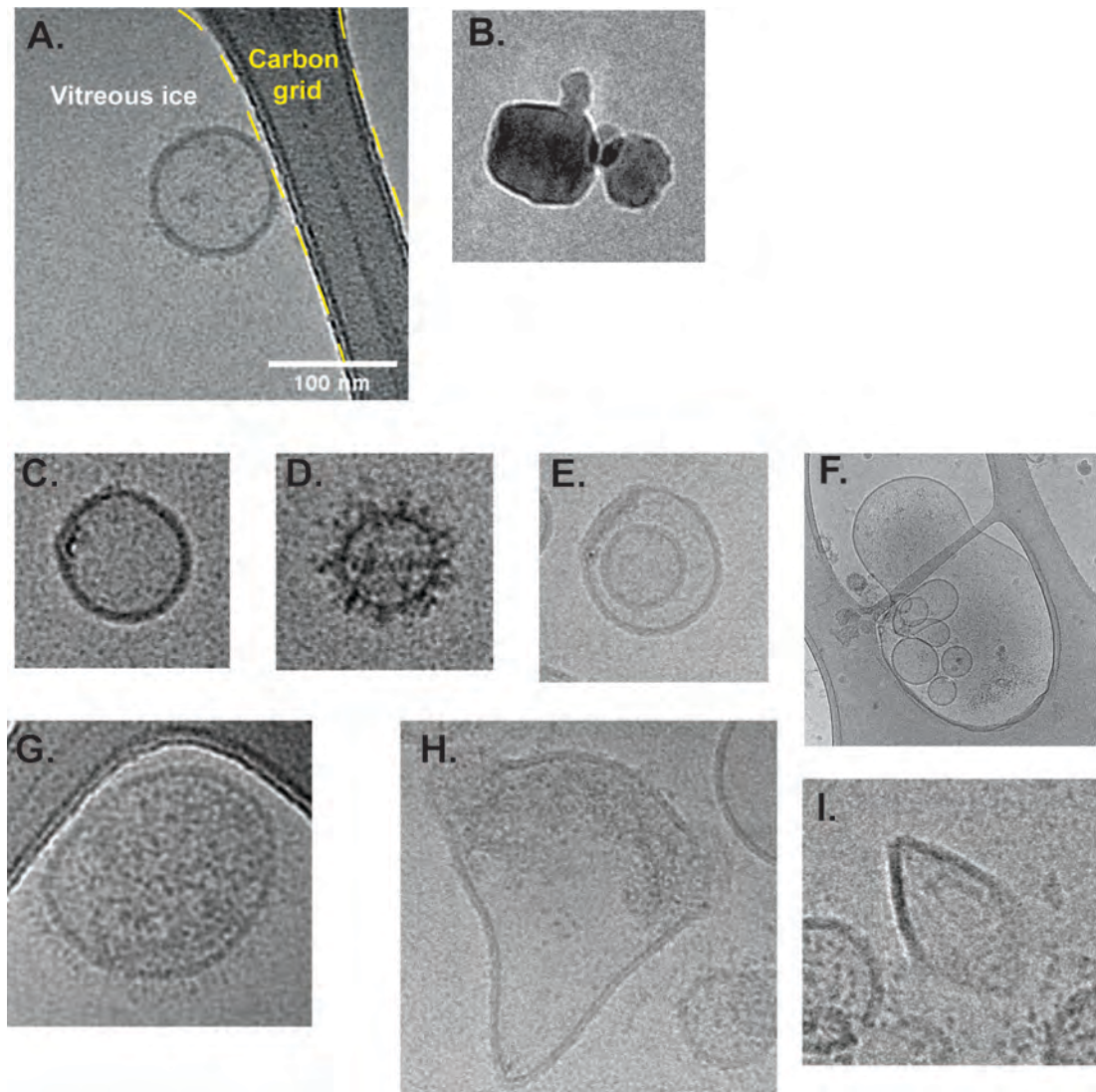


**Figure 3.3 | Example of EV morphologies identified by cryoEM in this study.** Example images of **A)** Example of carbon grid (within the yellow dotted lines) and vitreous ice sheet. **B)** ice crystal contaminant that are present in some cryoEM images. **C)** A 'bare' EV, **D)** a 'decorated' EV. **E)** EV with double membrane, **F)** Multiple membrane EV, **G)** Electron dense EV, **H)** Polymorphous EV & **I)** an incomplete EV.

Both incomplete and polymorphous EVs may be the result of damage during EV isolation, freezing and thawing of samples, processing samples for cryo-EM, or these could be present in native HES.

The majority of EVs isolated both by UC were circular in formation and approximately between 60 – 100 nm, some were seemingly bare (Figure 3.4 A-E). EVs were also found that were decorated with electron dense halos

similar to previously described EV coronas (Palviainen et al., 2020; Tóth et al., 2021) (Figure 3.4 F-H).

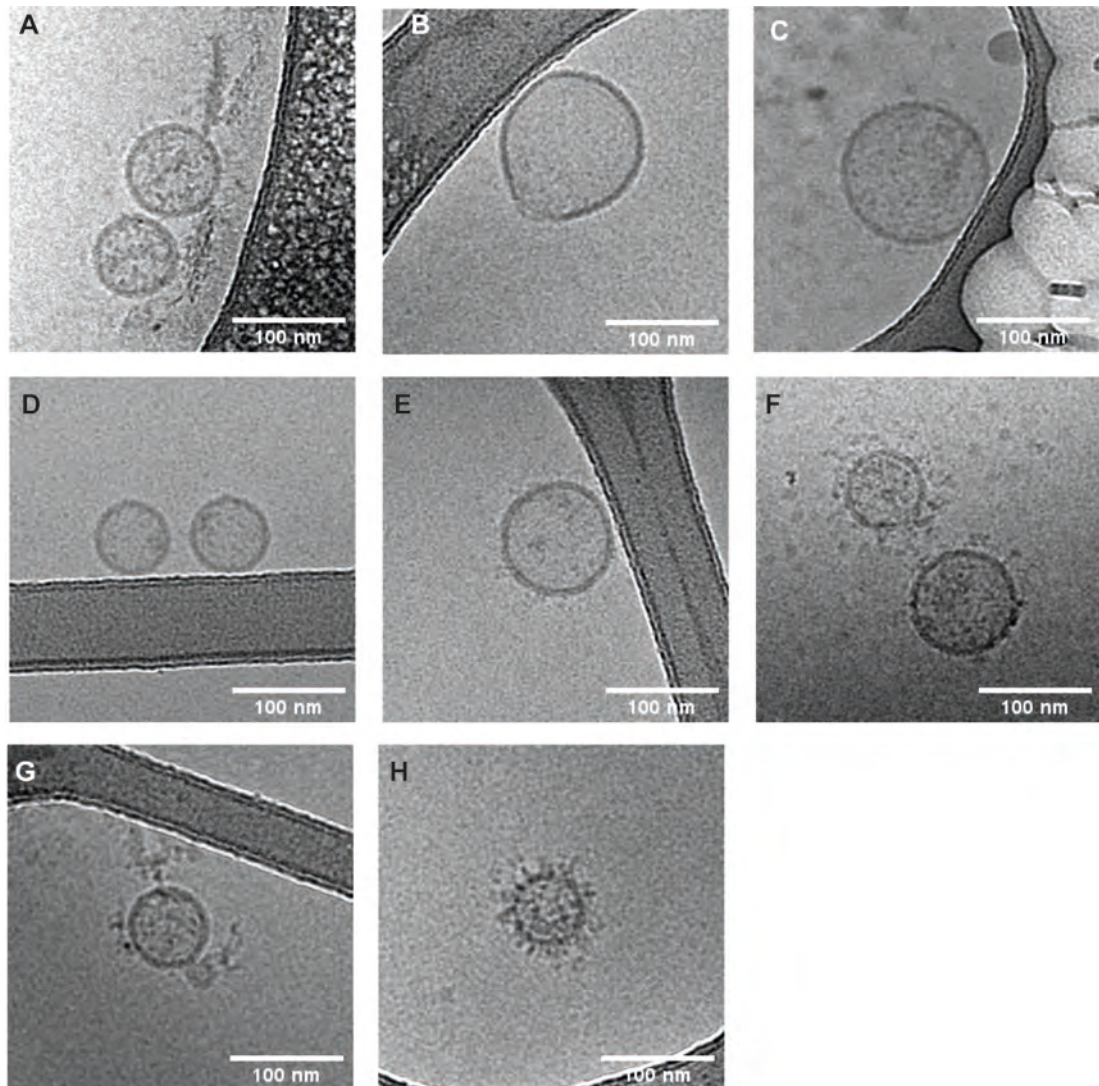


**Figure 3.4 | Representative cryoEM images from UC isolated EVs.** CryoEM of UC isolated EVs showing heterogeneity. **A- E)** Bare EVs **F-H)** Decorated EVs Scale bars = 100 nm. n = 1.

Initial SEC preparations by cryoEM were not highly concentrated so this was repeated this experiment with higher EV concentrations, which allowed more quantitative assessment of EV diversity in SEC EV isolations (Figure 3.5). CryoEM images confirmed the majority of EVs are small circular EVs, however a diverse range of EV sizes and morphologies were also identified including polymorphous EVs (Figure 3.5).

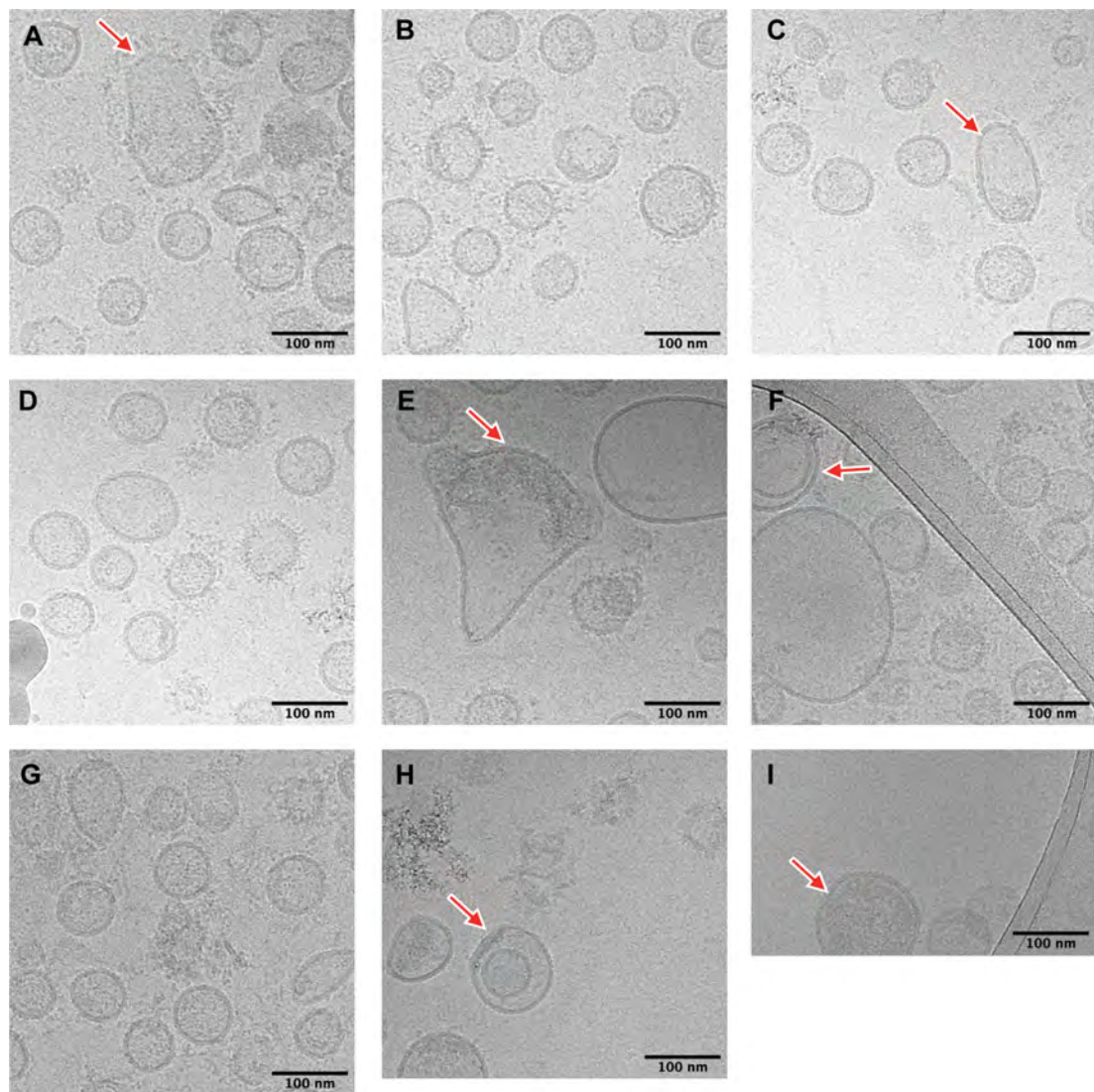


**Figure 3.4 | Representative cryoEM images of SEC isolated EVs. A-I)** SEC isolated EVs were imaged by cryoEM showing the diversity of EV morphology present in these preparations. Arrows indicate **A)** Large polymorphic EV and small oval EV. **B)** many circular EVs of variable sizes, some demonstrate protein coronas **C)** Oval EV **D)** Coated **E)** Large polymorphous and incomplete EV, large EV. **F)** Double concentric EV **G)** Unknown contaminant, double concentric EV. **I)** Electron dense EVs. n = 1.

### 3.2.2 Sequential isolations of *H. bakeri* EVs

MISEV 2018 recommends the sequential isolation of EVs using multiple methods for highly pure EV isolations free of non-vesicular contaminants (Théry et al., 2018). The use of two isolation methods for EVs should generate higher purity and specific EV subpopulations but has significant drawbacks with regard to EV yield and could impact diversity of EVs isolated. Standard

UC isolation was performed which resulted in an EV pellet and EV supernatant (also termed “EVdepHES”). Upon NTA performed on the Zetaview (Particle Metrix) a significant number of particles was found in both the EV pellet after UC, and the EVdepHES (the supernatant generated during UC) which led us to hypothesis that UC EV isolation might be highly inefficient such that many EVs remain present in EVdepHES (data not shown). To assess the presence of EVs within EVdepHES, and to identify whether non-vesicular protein contaminants were isolated by UC alongside our EV pellet, I performed SEC fractionation of both UC products (EV and EVdepHES) as summarised in schematic Figure 3.5 A. Silver stain of fractionated UC EVs yielded EV associated protein profiles in neat samples from fractions 7 – 10, as expected. For EVdepHES, while I also identified an EV associated profile by pooling and concentrating fractions 7-10 (EVs), neat fractions 7-10 showed only very faint staining (Figure 3.5 C). Suggesting that although EVs were present in fractions 7-10 of fractionated EVdepHES, they were not as abundant as in fractionated UC purified EVs (Figure 3.5 C). For UC isolated EVs that were fractionated, small amounts of non-vesicular proteins were recovered in fractions 15-30 with the exception of fraction 25-26 which yielded a large amount of protein, suggesting indeed UC EV isolations could contain non-vesicular contaminants that are further separated upon sequential SEC isolation (Figure 3.5 B).

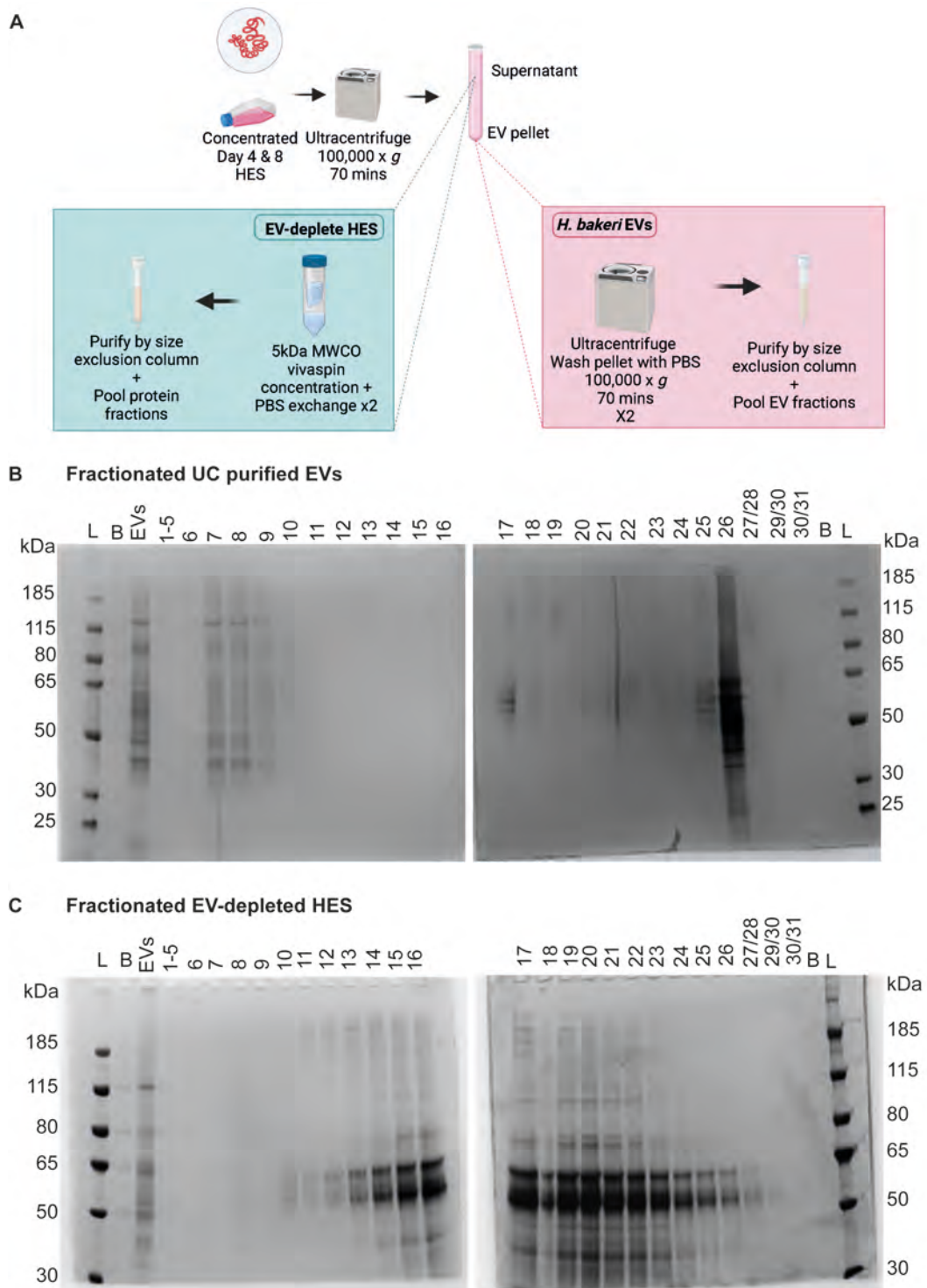
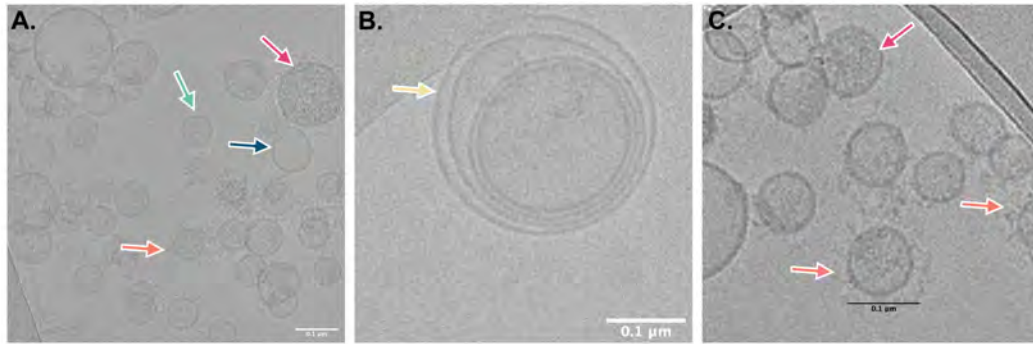


**Figure 3.5 | Double isolation of *H. bakeri* EVs.** **A)** Schematic of methodology for *H. bakeri* EV isolation (pink) and preparation of EV-dep HES (green). **B)** Representative silver stain of 1 batch of UC isolated EVs fractionated by SEC. **C)** Representative silver stain of 1 batch of UC prepared EV-depleted HES fractionated by SEC **L** = Ladder, **B** = blank well, **EVs** = fractions 7-10 of UC +SEC isolated EVs were pooled and concentrated. **kDa** = kilo Daltons, numbers refer to fraction number. 1-5 represents a total of 2.5 ml of void volume, subsequent fractions are all 0.5 ml. Some fractions were combined for purpose of running silver stain (as noted).  $n = 1$ .

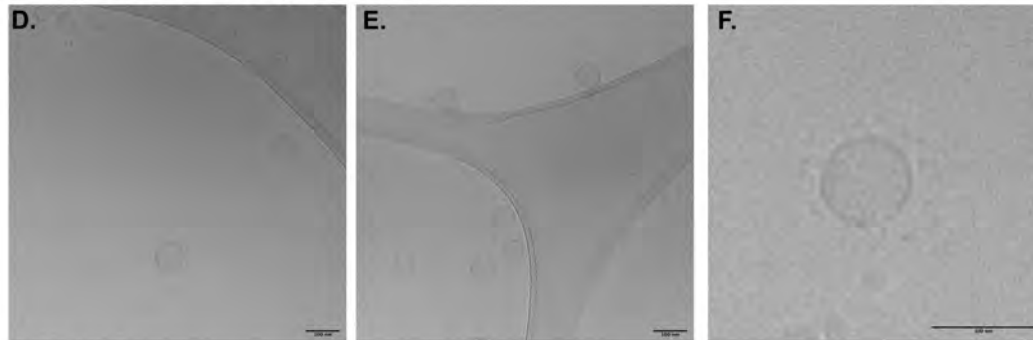


While initial particle measurement by Zetaview measurement of EVdepHES suggested EVs were abundant in these fractions, silver stain analysis of fractionated EVdepHES (fractions 7-10) did not show strong banding patterns associated with EVs. Finally, I assessed the resulting EV populations that were isolated by sequential UC then SEC fractionation by cryoEM. CryoEM of putative EV populations isolated by SEC fractionation from EVdepHES was also performed. Fewer images were able to be obtained of EVs isolated from EVdepHES indicating they were only present in low numbers (Figure 3.7 A-F). The large number of images that was obtained in this experiment from sequentially isolated EVs allowed for quantification of EV diameters and morphologies represented (Figure 3.7 G&H). The EVs isolated from EVdepHES had a smaller mean diameter (60.59 nm) compared to sequentially isolated EVs (79.26 nm) and were predominantly 'bare' EVs (80.49%) (Figure 3.7 G&I). For sequentially isolated EVs, a greater diversity of morphologies was found with the most represented morphologies being 'decorated' EVs (62.9%) followed by 'bare' EVs (28.8%) (Figure 3.7 G&I). Other morphologies described in previous sections of this Chapter were also found but at lower proportions (Figure 3.7 G&I). Finally, previous data indicated EVdepHES containing substantial particles by Zetaview however although silver stain and cryoEM evidenced the presence of EVs within EVdepHES they were not very abundant. I then measured our sequentially isolated EVs (UC + SEC) as well as the EVs isolated from EVdepHES by SEC (fractions 7-10) (Figure 3.7 I). I still found abundant particles in the putative EV sample isolated from EVdepHES by SEC (fractions 7-10) with overlapping size profile to sequentially isolated EVs (Figure 3.7 I). For batch 1, the particle concentration was much higher for EVs isolated from EVdepHES by SEC than it's sequentially isolated EV counterpart. Taken together data from this section suggests that while EVdepHES contains some EVs, Zetaview measurements likely capture other molecules present in HES that have similar light scattering and Brownian motion properties to EVs. This also has ramifications for our understanding of EV isolation purity, as contaminants from HES may be difficult to distinguish by Zetaview measurement alone.

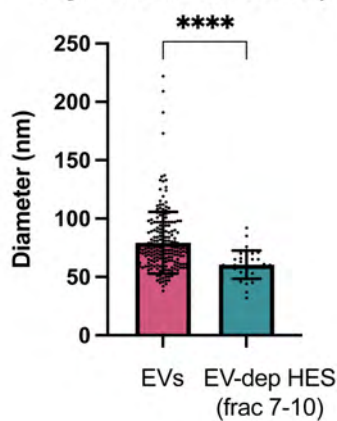
## EVs UC + SEC



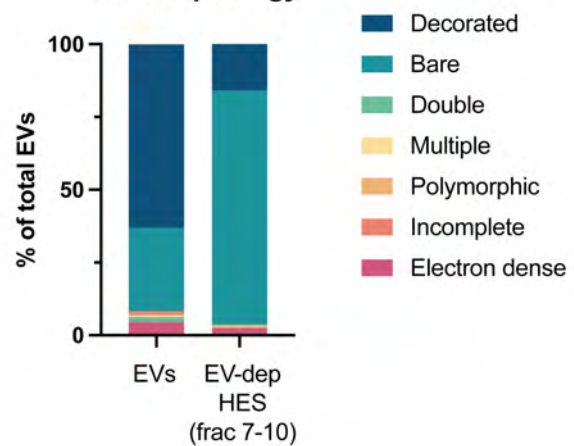
## EV-dep HES UC + SEC (Fracs 7-10)



## G. CryoEM EV diameter (nm)



## H. EV morphology



## I.

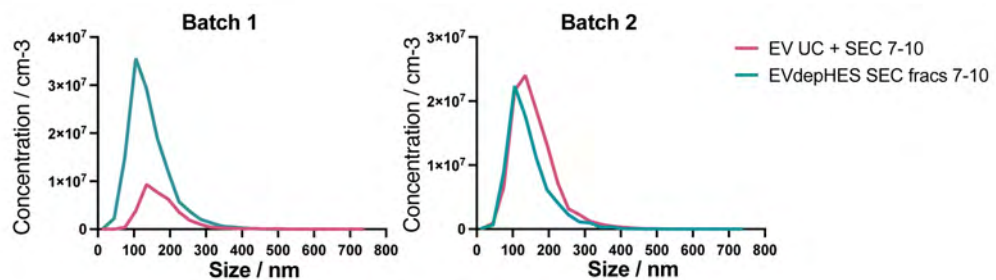


**Figure 3.6 | CryoEM of *H. bakeri* EVs double isolated by UC & SEC. A-F) Representative images of EVs A) Red arrow highlights electron dense EV with surrounding corona. B) Red arrow highlights instance of EV with concentric circles G & H) Quantification of G) EV diameter and H) proportions of various EV morphologies present, using cryoEM images for two batches of sequentially isolated EVs**

(pink) and double purified EV-dep HES fractions 7-10 (green). Data was pooled for quantification (n = 2). Quantification performed using ImageJ software. **I)** Zetaview measurements of particle concentration and size in sequentially isolated EVs (pink) and EVs isolated by SEC fractionation from EVdepHES (fractions 7-10) (green) from two independent batches. n = 1.

### 3.2.3 CryoEM of EVs in native HES

EV isolation methods are inherently biased and may remove certain EV subtypes. Additionally, multiple isolation steps may alter the morphology of EVs or remove associated molecules. Therefore I aimed to assess the morphology of EVs in native HES. The need to first concentrate the HES in order to increase EV concentration in the hope of capturing EVs by cryoEM could not be avoided. To do this HES was concentrated by ultrafiltration using 5 kDa MWCO vivapspin columns at 4°C. Despite concentration, only a handful of EVs in native HES was found at these concentrations. EVs that were imaged were small and circular, representing previous findings from isolated EVs which are mostly small circular EVs. I did not find any polymorphic EVs, double EVs or multiple concentric EVs in these samples, but this likely reflects the low numbers of EVs imaged, and not their absence from native HES.

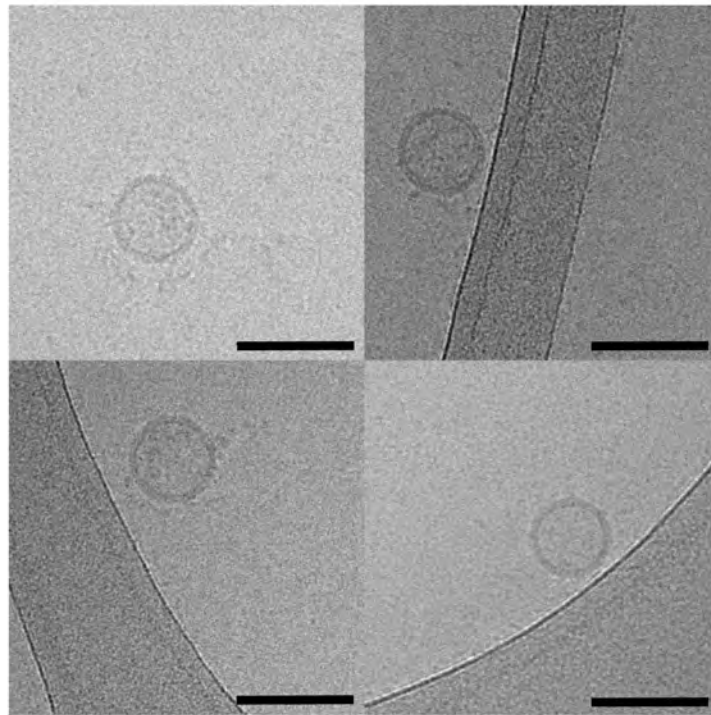


**Figure 3.7 | Native *H. bakeri* EVs in HES.** CryoEM of *H. bakeri* concentrated HES to identify morphology of native EVs. Scale bar = 100 nm.

### 3.2.4 Methods of fluorescent EV labelling for *in vitro* & *in vivo* use

A major aim of this project was to study *H. bakeri* EV interactions with the host intestinal epithelium using 2-D organoid models which is described in subsequent chapters. In order to assess *H. bakeri* EV uptake in this system a method for labelling *H. bakeri* EVs for detection upon uptake into host cells was required, that demonstrated low background signal. UC isolated *H. bakeri* EVs were then isolated by SEC to remove any non-vesicular protein before labelling using a tetrafluorophenyl ester (TFP) AF488 which reacts with primary amine residues (R-NH<sub>2</sub>) on proteins, presumably in this case on the surface of intact EVs based on previously published studies (Ferguson et al., 2022). EV fluorescent labelling protocols require a clean-up step to remove excess dye aggregates that could be misidentified as labelled EVs. Additionally, because non-specific dyes were used that could also react with mammalian cells upon treatment the excess dye needs to be adequately

removed to minimise this. To control for 'background' staining that could arise as a result of excess dye, buffer was labelled (HBSS or PBS depending on experiment) and clean-up protocols were performed side-by-side with EVs and delivered to host cells. A protein labelling strategy was trialled using UC isolated EVs followed by SEC isolation to remove non-vesicular contaminant proteins, labelling was then performed as per established methods (methods detailed in Chapter 2) (Figure 3.9 A). After the labelling reaction excess dye was removed by SEC clean-up (Figure 3.9 A). In subsequent experiment throughout this thesis, it was decided sequential isolation prior to labelling was excessive and would increase EV loss. For future experiments EVs were UC isolated and then directly labelled before SEC clean-up to remove both excess dyes, as well as non-vesicular contaminants in a single step.

NTA showed some particle loss after labelling and SEC clean up, this is expected as all EV isolation methods can lead to some particle loss (Figure 3.8 B & C). Labelled EVs had with similar size profile to unlabelled input EVs (Figure 3.8 B). I tested the ability to detect AF488 signal in a dose dependant manner in treated MODE-K cells, which have been shown to take up *H. bakeri* EVs previously (Buck et al., 2014). I found detectable uptake at doses of  $5 \times 10^7$  particles and above (Figure 3.9 D). Treatment with  $1 \times 10^8$  EVs resulted in 62.6% of live single cells being EV-AF488 positive and the greatest separation from the HBSS-AF488 which showed 8.2% of cells were AF488 positive (Figure 3.9 E). These data demonstrate this methodology to effectively label *H. bakeri* EVs that can be detected in host cells upon uptake, with HBSS-AF647 control showing minimal background (MFI = 251) although fluorescence was slightly above naïve cells (MFI = 189) indicating this to be a necessary control (data not shown).

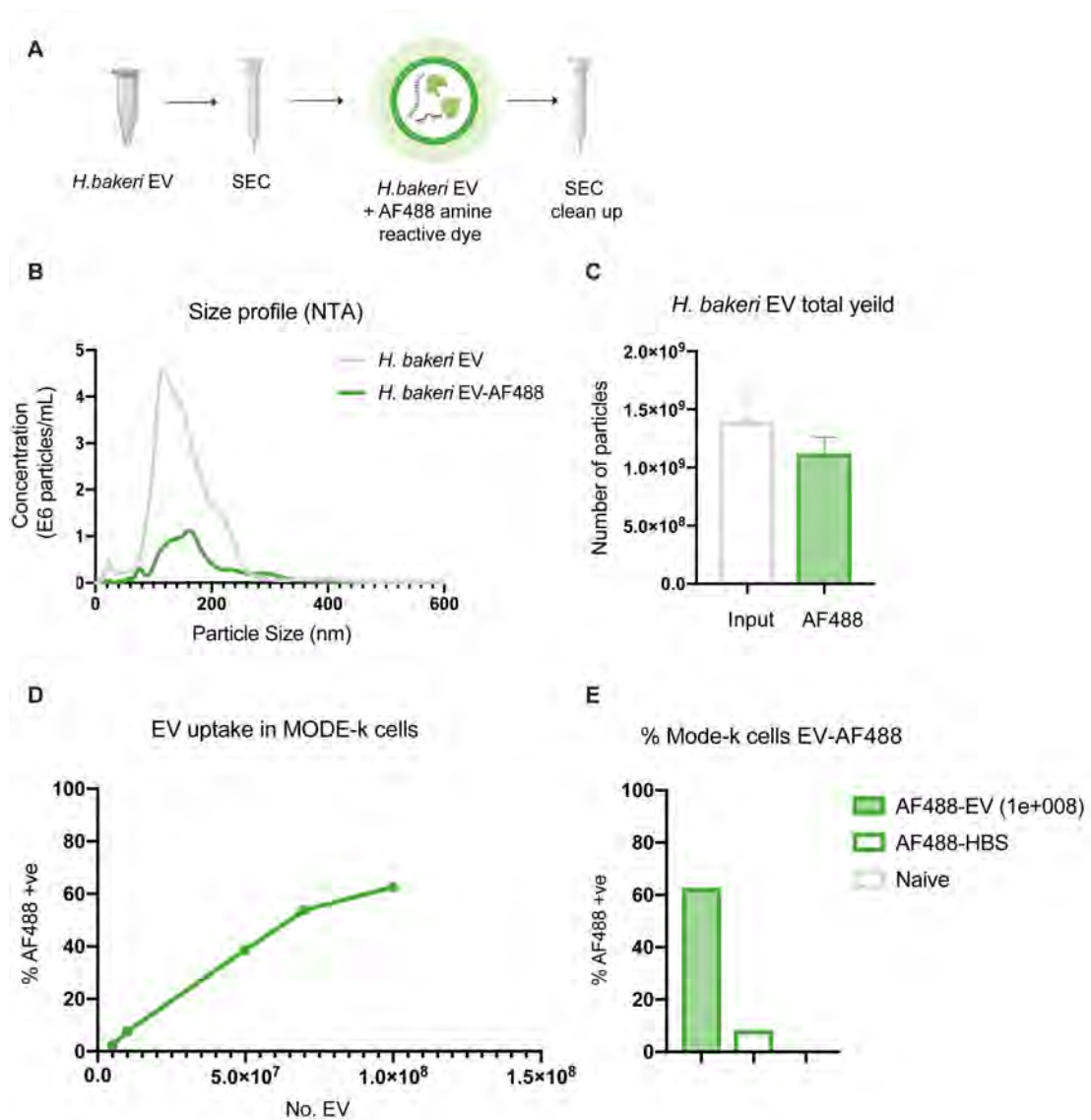


**Figure 3.8 | Fluorescent labelling of EV proteins.** **A**) Schematic of labelling protocol. **B**) Nano tracking analysis (NTA) of input *H. bakeri* EV preparation (grey) and AF488 labelled and cleaned up *H. bakeri* EV (green) **C**) Total yield by NTA of input (grey) and AF488 labelled *H. bakeri* EV (green). **D&E**) MODE-K cells treated with AF488 labelled EVs for 24 h and then analysed by flow cytometry for uptake of EV-AF488 **D**) Percentage of live single MODE-K cells positive for AF488, gating based on fluorescence of naive samples at differing doses (n =1). **E**) Percent of live single MODE-K cells AF488 positive treated with  $1 \times 10^8$  EVs (green filled), treated with AF488 labelled HBSS buffer (green line, white fill) or Naïve (grey line).

Initial results with TFP AF488 were promising, however our eventual aim was to detect *H. bakeri* EVs within organoid cultures. The intestine as well as intestinal organoids are notoriously auto fluorescent tissues particularly in the green channel (GFP, AF488). Therefore, from the onset I was aware AF488 would not be a suitable fluorophore choice for downstream application. I trialled a succinimidyl ester (NHS ester) available in AF647 dye, which has

very similar chemistry to TFP AF488. I labelled EVs using the same methodology and found minimal loss with SEC clean up and higher loss with UC clean up, consistent with previous findings that SEC isolation is higher yield (data not shown). This labelling strategy was utilised in subsequent chapters and yielded detectable uptake in MODEK cells and 2-D enteroid cultures (Chapter 5 of this thesis).

For our earlier experimentation, *H. bakeri* EV particle measurements were performed using the Nanosight LM10 which only allows measurement of scattered light to determine particle concentration and size. Later on, a twin laser Zetaview (Particle Metrix) was purchased allowing us to directly measure particles in two ways: using scattering of light, and by fluorescence. This allowed measurement of both total particles and the proportion of EVs that were successfully labelled with the various dyes. I first assessed the proportion of EVs that were AF647 labelled using our standardised methods. Surprisingly, it was found that a relatively low proportion of total particles were labelled (19%) (Figure 3.10 A). In addition, I identified an increase in the mean diameter and diameter of highest peak after protein labelling and in the standard deviation of the measurement (Figure 3.10 B). This new data suggested that NHS-AF467 is inefficient at labelling EVs, but is low background and detectable in host cells.

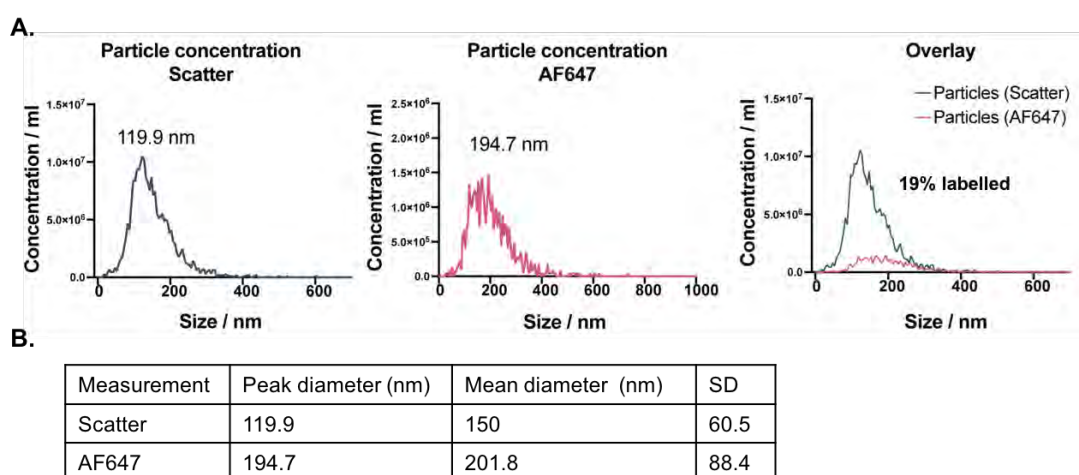


**Figure 3.9 | Labelling efficiency of *H. bakeri* EVs with NHS-AF647.** Zetaview measurements were performed on the same sample using scattered light to measure total particles and fluorescence (660 nm) to measure fluorescent particles **A)** Concentration and size distribution of measured particles for (left to right) scatter measurement (blue line), fluorescent measurement (pink line), and overlaid scatter

with fluorescent measurement. The diameter (nm) of the peak size is annotated on each measurement. For the overlay the percentage of fluorescent particles of the total particles is annotated on the graph. **B)** Table displaying the peak diameter (nm), mean diameter (nm) and standard deviation (SD) for scatter and fluorescent measurements. SD = Standard deviation, nm = nanometre, nM = nanomolar, ml = millilitre.

This chapter aimed to investigate best approaches for isolating and fluorescently labelling EVs that allows for high confidence detection in host cells. To summarise, I developed a pipeline for optimal isolation and concentration of fluorescently labelled EVs that results in high quality EV-647 preparations (Figure 3.11). Three EV isolation and concentration methods are combined namely, UC, ultrafiltration and SEC and mandatory QC to measure protein and particle concentration are routinely carried out. CryoEM is an additional QC method that is carried out for some experiments.

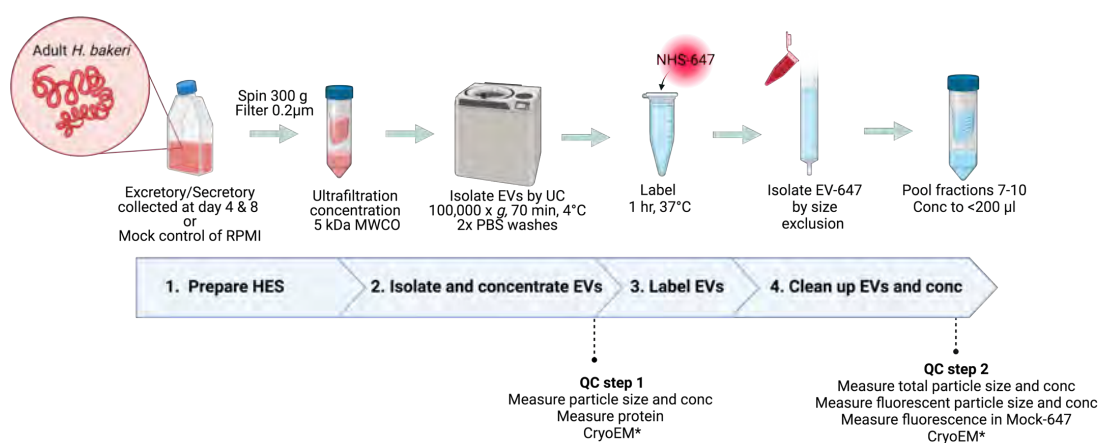


**Figure 3.11 | Optimal EV isolation and labelling methods.** 1. Describes the preparation of HES by culturing adult *H. bakeri*, as a mock control RPMI media of equal volume is used. HES is concentrated prior to EV isolation to a volume of <12 ml by ultrafiltration 2. EVs are isolated by a primary method in this study I used ultracentrifuge followed by two PBS washes to remove HES protein contaminants 3. EVs are labelled using NHS-ester 647 4. After labelling EV-647 are isolated from excess dye using a secondary isolation method for clean up in this study this is size exclusion chromatography. EV containing fractions are then concentrated by ultrafiltration to a volume of ~ 200 µl resulting in highly concentrated and pure EV-647. Mandatory QC steps should be performed between stage 2&3 as well as after stage 4, astricks indicates optional QC steps. Conc = concentration.



### 3.3 Discussion

This chapter focuses on the comparison of different EV isolation methods; identifies heterogeneity within *H. bakeri* EV morphologies; and tested strategies for fluorescently labelling *H. bakeri* EVs with the goal of tracking their uptake into host cells. Our project aim was to investigate the interactions of *H. bakeri* with the intestinal epithelium. To address this aim I required pure EV isolations in order to attribute functional responses to EVs, and high confidence low background labelling methods were needed to confidently assess uptake in host cells. While MISEV 2018 does not recommend a specific isolation method (Théry et al., 2018), there has been a growing use of SEC isolation as it produces high yield and high purity EVs preparations (Davis et al., 2019; Monguió-Tortajada et al., 2019). I found SEC isolation to give higher yields by comparison to UC (Figure 3.1). MISEV encourages the use of multiple isolation methods to enhance purity. *H. bakeri* EVs that were sequentially isolated first by UC followed by SEC I identified by silver stain the presence of non-vesicular contaminants in later fractions suggesting UC alone co-purifies non vesicular protein (Figure 3.5). By cryoEM, heterogenous morphologies were identified with *H. bakeri* EV isolations from sequentially isolated EVs, but the majority are small either bare or decorated EVs (indicating a protein corona), although multi-layered EVs were also found (Figure 3.6). I also identified the presence of EVs in UC sup referred to as EVdepHES, these were smaller in diameter and mostly bare and could represent a population of EVs that is not captured by UC (Figure 3.6). Finally, methods for labelling *H. bakeri* EVs were investigated I found protein labelling using NHS-AF647 to successfully label EVs with minimal background (Figure 3.8). To summarise, I developed a rigorous pipeline of optimal methods for isolating highly pure fluorescently labelled *H. bakeri* EVs which was used for later chapters (Figure 3.11).

### 3.3.1 Considerations and limitations of EV isolation

Several EV isolation methods have been described that were not tested in this thesis. A method that is encouraged for highly stringent isolations of EVs is the use of sucrose cushions or sucrose density gradients during UC (Monguió-Tortajada et al., 2019; Théry et al., 2018). Sucrose gradients are required for the isolation of different EV subpopulations. However, it is difficult to assess the contributions of different EV subpopulations when a well characterised functional read out has not yet been established as in this project, therefore we choose not to discriminate between different *H. bakeri* EV subpopulations. Furthermore, when comparing sRNA cargo of *H. bakeri* EVs we found a very high correlation between the sRNA content of EVs isolated using either UC alone, or in combination with sucrose gradient suggesting that these methods may isolate very similar EVs (Appendix I). One advantage of sucrose cushions and gradients is their improved ability to remove non-vesicular protein contaminants over other methods (Monguió-Tortajada et al., 2019). The increased purity that sucrose gradients offer comes as a cost to EV yield, and this technique requires substantially longer (20 h) to perform. For reasons listed above in this study I did not use sucrose gradients or cushions.

Some techniques, such as antibody based immunoaffinity purification are not currently applicable for *H. bakeri* EVs due to a lack of well characterized antibodies, and even when antibodies are available result in highly specific subpopulations of EVs (Monguió-Tortajada et al., 2019; Théry et al., 2018). Other techniques were prohibitive either because of cost or specialist equipment such as asymmetrical flow field-flow fractionation (AF4). Finally, ultrafiltration is recognised as an EV isolation method, however it is a crude method based on molecular weight cut offs (MWCOs) and results in highly impure preparations. Ultrafiltration is utilised in this thesis (where stated) for the concentration of total HES prior to EV isolation by other methods.

Emphasis in the EV field has been put on ensuring increased EV purity, although it is described that entirely pure preparations are not realistic (Théry et al., 2018). While minimising contaminants is important, this comes at a cost to total yield as all isolation methods led to some loss (van Niel et al., 2022). Therefore, regarding EVs purified from HES, which is already a limited resource that requires laborious work to generate, EV yield is a priority. Additionally, multiple isolation steps likely limit the population of EVs isolated – this is supported by the presence of smaller EVs that are not captured by UC but upon SEC fractionation of EVdepHES could be identified (Figure 3.6).

The initial HES is also factors to consider when preparing *H. bakeri* EVs. For example, although we qualitatively assess worms by eye, we did not routinely perform standardised worm viability tests on each batch of *H. bakeri* parasites. Future studies could be strengthened by implementing this in future studies. Other HES preparations steps may also remove functionally relevant EV subtypes and may need to be reconsidered. For example, during HES collection a standard first step used to remove *H. bakeri* eggs also present is filtration through a 0.2 µm filter, and then concentration with using vivaspin column. Filtering will likely remove any larger EV populations (> 200 nm) from HES.

Sequential isolation enhanced EV isolation purity by combining UC and SEC methods demonstrated by silver stain which showed some protein contamination removed by SEC fractionation (Figure 3.6). Sequential isolation was used for later where the research question regarded the functional effect of EVs, for example in Chapter 6 where I aimed to distinguish the functions of EVs from non-vesicular fractions. Experiments that required labelled EVs (Chapter 5) were isolated by UC, and SEC was used as a method to both clean-up excess dye, and as a sequential isolation method. While highly pure EV preparations may be useful for demonstrating EVs functions from other components of HES, on the other hand they could remove EV populations that themselves induce functional effects on the host. Additionally, as EV mediated cross-species communication is a young field it is not fully understood whether EV-associated proteins (those commonly isolated with EVs) have roles in their

uptake and function. For example, it may be that vesicle associated proteins (as demonstrated by cryoEM (, Figure 3.4, Figure 3.6) play a role in attachment and invasion of host cells. To address these concerns, cryoEM of native concentrated HES was attempted to identify whether I see similar proportions of EV morphologies, however even when HES was concentrated only very few EVs were able to be imaged by cryoEM making comparison difficult.

### 3.3.2 Morphology of *H. bakeri* EVs

CryoEM demonstrated the heterogeneity of *H. bakeri* EVs present in our isolations. The majority of EVs purified from *H. bakeri* by UC, SEC or by sequential UC then SEC approach were small and circular. The mean EV diameter measured by cryoEM was (79.06 nm) which is smaller than the typical diameter peak measured by NTA (120-150 nm), this could be explained by two factors i) NTA measurements captures more events (> 1000 traced particles) than captured by cryoEM and ii) cryoEM images capture a cross-section of each EV, and not all EVs will be captured at their centre EV leading to bias in the data to underestimate size.

A few non-standard EV morphologies were identified in my *H. bakeri* EV preparations which is interesting to note as only a handful of papers have performed cryoEM on EVs derived from helminths, and of those none described non-standard EV shapes (Boysen et al., 2020; Kuipers et al., 2020). However, many of these morphologies have been described for EVs derived from human cells including polymorphic EVs, incomplete EVs, double EVs, EVs with electron dense centres (Zabeo et al., 2017) and EVs containing multiple concentric circles (Emelyanov et al., 2020). EVs containing double lipid bilayer and EVs with multiple-concentric lipid bilayers could represent additional protection for EVs as they travel between cells. Additionally, how EVs are taken up or deliver cargo molecules to the recipient cell is still an area of active research, especially in cross-species contexts (Woith et al., 2019). One proposed mechanism is via membrane fusion, and the presence of double or multiple layered EVs could provide a mechanism in which the outer

membrane fuses with the host cell membrane resulting in the release of the inner EVs into the cytoplasm intact; However, this hypothesis requires further investigation outside the scope of this thesis.

The presence of EVs coated in proteins has been described as EV protein coronas, or “decorated EVs” elsewhere (Palviainen et al., 2020; Tóth et al., 2021). I also found evidence of a substantial proportion of EVs containing electron dense ‘decoration’ which is likely to be proteins on their surface, 62.91% in sequentially isolated EVs. A substantial proportion of *S. mansoni* EVs have been shown to have a filamentous glycosylated surface which can be seen by cryoEM and results in a peak at 350 nm when EVs are measured by NTA (Kuipers et al., 2020). The glycosylation on *S. mansoni* EVs binds C-type lectin receptor DC-sign on host dendritic cells (Kuipers et al., 2020). I did not see any evidence of multiple peaks in *H. bakeri* EV isolations by NTA, although during HES collection I perform a 0.2 µm filtration step to remove eggs and this may also remove these; nor did I detect any filamentous projections similar to those described by Kuipers *et al* around our EVs by cryoEM (, Figure 3.4, Figure 3.6).

### 3.3.3 Fluorescent labelling of *H. bakeri* EVs

Fluorescent labelling of *H. bakeri* EVs using NHS esters was successful and led to detectable uptake in host cells (Figure 3.6). I implemented protein labelling for the detection of EV uptake in later chapters, however I later discovered that this method as well standard lipid dyes inefficiently labelled only a low proportion of all particles detected by scatter NTA (< 20%) (Figure 3.10). There are several possible reasons for this, firstly total scatter particle measurement likely measures some non-vesicular particles that are similar in size and motion to EVs, as demonstrated in EVdephES and this could account for some proportion of unlabelled particles (Figure 3.10). Secondly, in the case of lipid dyes specifically cell mask which is reported to label ~80% for mammalian serum plasma EVs, I found very low labelling efficiency suggesting

a fundamental difference in lipid composition of helminth EVs as opposed to mammalian EVs (data not shown) (Carnell-Morris et al., 2017). The lipid composition of *H. bakeri* EVs has been analysed and supports the claim that *H. bakeri* EV lipid content is different from mammalian EVs (Simbari et al., 2016). One factor I didn't investigate was optimisation of the dye:particle ratio for NHS-AF647 labelling of *H. bakeri* EVs. Our protocol was based on established protocols for labelling mammalian EVs, and because at the time I did not have the capability to measure the proportion of particles labelled I did not test various concentrations of dye. NHS-AF647 labelled EVs were detectable in host cells with minimal background (Chapter 5), therefore in the future it would be worth optimising the dye:particle ratio for increased labelling efficiency to determine if this could still be a suitable labelling method for *H. bakeri* EVs. Finally, even in the mammalian EV field all dye options are not entirely efficient, and the highest efficiency approach is genetic modification of one, or multiple, EV specific transmembrane proteins (Verweij et al., 2021). Successful genetic modification of *H. bakeri* has yet to be achieved and even for facultative parasitic helminth species where successful modification has been achieved the results were limited (Hagen et al., 2021), making this an impractical choice for this project.

Use of antibody to detect *H. bakeri* EVs in infected tissue is an obvious alternative to the other approaches described in this Chapter. I had minimal success with antiserum raised against HPOL000582001 (a CD9 orthologue). Instead, I generated  $\alpha$ -EV serum against EV isolations, this antibody is used in subsequent chapters (Chapter 5). More recently, antibodies have been generated against EV specific proteins by our lab. For example, an orthologue of SID2 (an RNA transporter protein enriched in EVs), and against the EV cargo protein exWAGO which is hypothesised to be involved in cross-species RNA silencing. Although, exWAGO can also be secreted out with vesicles so it is not entirely EV specific. In the future, development of EV-specific antibodies and successful genetic modification of helminths will drastically improve our ability to track *H. bakeri* EVs through host tissues *in vivo*.

**Chapter 4: Development of 2-D enteroid cultures**

**Abstract**

Organoids are capable of self-renewal and differentiation in a regional specific manner that closely represents their *in vivo* tissue of origin. Intestinal organoids (enteroids) traditionally grow into 3-D spherical structures that are constricted by size and length of culture. The spherical structure of 3-D limits the use of this model for study of *H. bakeri* which is substantially larger than individual organoids. Furthermore, 3-D organoids have their apical epithelium facing inwards making it inaccessible for treatment with helminth excretory secretory products. In studies using colon (colonoids) or caecal organoids (caecaloids) others have developed methods to grown organoids in 2-D structures using transwell plates. In this chapter I optimise and develop a protocol for growing 2-D enteroids that replicates key features of the small intestinal epithelium. The methods presented in this chapter allow for investigation of host-helminth interactions explored in later chapter of this thesis and are applicable to studies beyond this thesis.



## 4.1 Introduction

Helminth infection is well known to modify the host environment, including changes to the intestinal epithelium (Coakley & Harris, 2020; Rick M. Maizels, 2020; Henry J. McSorley & Maizels, 2012). Most studies rely on animal models to investigate helminth-host interactions. However, these have limitations such as requiring defined end points to assess host changes because helminths are not tractable during infection. Additionally, during infection it is difficult to distinguish which changes are a result of helminth modulation and which reflect the host response to infection (Ruby White et al., 2022). Organoid cultures, which are simplified recapitulations of their organ of origin, have begun to be utilised for the study of host-pathogen interactions for example with microbial species (Dutta & Clevers, 2017; Puschhof et al., 2021). Helminths are much larger macroparasites and though organoid technologies have promise for the helminth field, advancement of current organoid methods is needed to address questions in helminth-host interactions, including those raised in this thesis (Ruby White et al., 2022).

3-D intestinal organoids are grown from adult stem cells cultured within artificial basement membrane extracts (BME), which acts as a replacement for the extracellular matrix (ECM) found *in vivo* (Puschhof et al., 2021). Organoids can be cultured from distinct regions of the intestine by isolating adult stem cells from specific regions e.g., small intestine (enteroids), caecum (caecaloids) and colon (colonoids) (Ruby White et al., 2022). Organoids are then grown in culture media supplemented with specific combinations of the critical growth factors and morphogens required, and these will vary depending on region identity of the organoids (Dutta et al., 2017). Intestinal organoids are usually grown with various concentrations of four main factors, Wnt CM (W), EGF (E), Noggin (N), and R-spondin (R) (Sato & Clevers, 2013). The media used throughout this chapter is referred to using acronyms e.g., WENR, to denote the media composition. Wnt concentrations vary depending on the specific intestinal region being cultured, for example the small intestine produces exogenous Wnt3a and therefore it is not critically required like it is for large intestinal cultures (Sato & Clevers, 2013). In these aforementioned

conditions, 3-D organoids will form spherical enclosed structures of polarised epithelial cells with their apical surfaces facing inwards to a central 'lumen', and their basal surface accessible (Puschhof et al., 2021).

Organoid cultures have recently begun to be used as a model for helminth epithelial interactions, demonstrated for example by studies investigating the effect of HES on these cultures (Drurey et al., 2021; Karo-Atar et al., 2022; Nusse et al., 2018). 3-D cultures however are limited by the fact that the apical epithelium is inaccessible. During the adult stage of infection delivery of HES components, including *H. bakeri* EVs, will come in contact with the apical epithelium, however delivery to the apical epithelium using 3-D organoid is possible only by microinjection. Microinjection delivery of helminth EVs to 3-D colonoids has previously been demonstrated for *N. brasiliensis* and *T. muris* (Eichenberger, Ryan, et al., 2018). However, microinjection has significant draw backs such as the dose injected cannot be controlled, and it is a laborious method that requires specialised equipment.

We aimed to generate 2-D enteroid cultures that would provide an improved experimental model of the small intestinal epithelium over 3-D models, recapitulate the cellular populations of the small intestinal epithelium and fulfil two requirements: i) an accessible and contiguous apical epithelium that allows for practical delivery of *H. bakeri* EVs, or other HES components ii) a physically separate basal compartment allowing for delivery of basally localised proteins e.g., cytokines. Prior to this project 2-D systems (also referred to as monolayers) were described for colonoids (Ahmad et al., 2014; Y. Wang, DiSalvo, et al., 2017), and for caecaloids (Duque-Correa, Goulding, Rodgers, Gillis, et al., 2022). Publications in 2018 and 2019 demonstrated various methods for 2-D enteroid culture, although these showed variable success in achieving complete monolayers (summarised in Table 4.2). I therefore began by modifying 2-D caecaloid protocols through collaboration with Maria Duque-Correa at the Wellcome Sanger Institute. In this chapter, I demonstrate the growth of 2-D enteroid cultures that successfully fulfil our pre-defined requirements and allow us to address our downstream research questions (Chapter 5 & 6).

## 4.2 Results

### 4.2.1 Defining the conditions for 2-D enteroid growth

Primary enteroid cultures were generated from the small intestine of mice using established protocols (2.4.1). 3-D enteroids demonstrated round cystic morphology in the the first two days of culture and then formed branching morphology described from day 4 through 7 (Figure 4.1 A). These cultures grew similarly following their first passage (Figure 4.1 B)

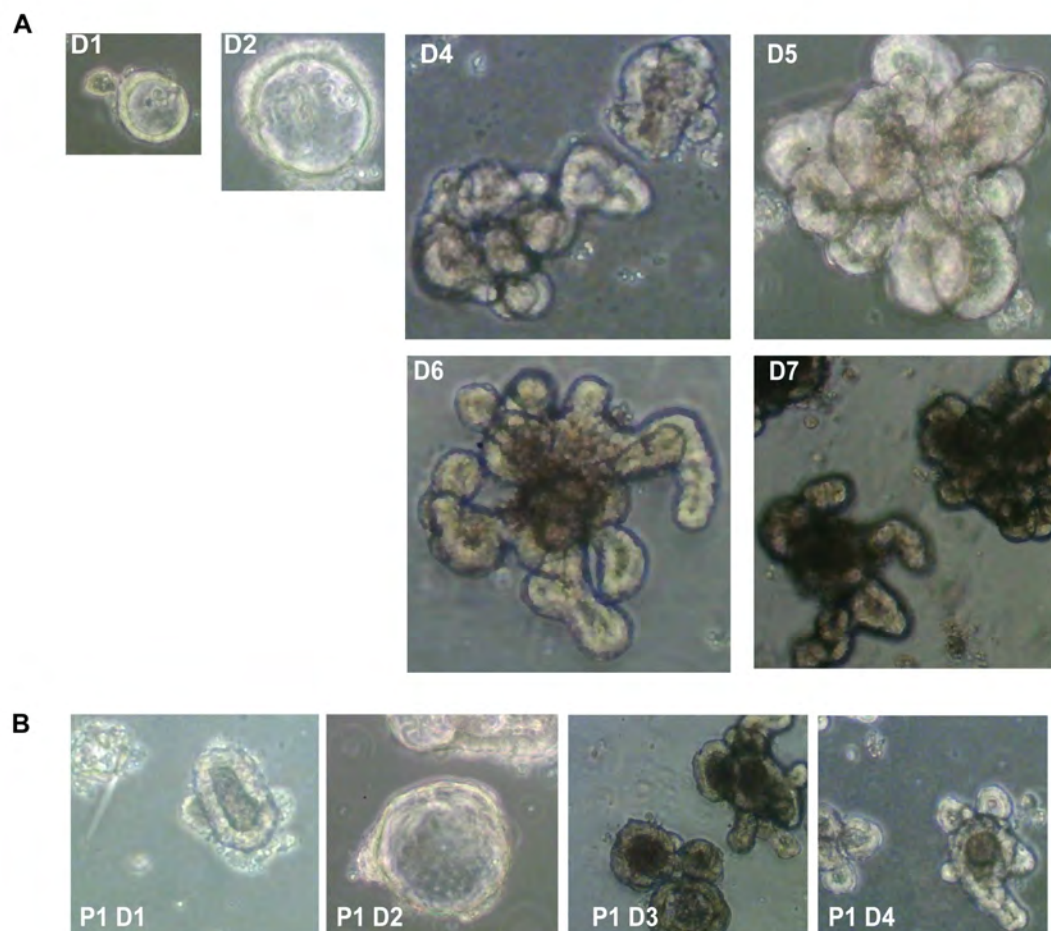


**Figure 4.1 | 3-D enteroid growth over time.** Representative images of 3-D enteroid in culture **A)** with isolation media over the first week in culture **B)** in organoid growth media after the first passage. P = passage, D = day

We began by adapting 2-D caecaloid methods through collaboration with Dr. María Duque-Correa for the generation of 2-D enteroid cultures (Duque-Correa, Goulding, Rodgers, Gillis, et al., 2022). The overall design of our 2-D culture system is summarised by a schematic (Figure 4.2). In brief, 3-D organoids are passaged and cultured for 4 days before being dissociated and seeded on transwell plates (0.4  $\mu\text{m}$  pore) coated with an ECM mimic (Figure 4.2). The lower transwell compartment is supplied with growth media containing required growth factors and morphogens simulating the basal environment, while the top compartment receives 200,000 enteroid cells in 200  $\mu\text{l}$  of base media simulating the intestinal lumen. After 24 h in culture, the non-adherent cells are removed from the top compartment, and media replaced and changed every second day onwards. On day 2 in culture the growth media in the lower chamber is changed and every second day onwards. Cultures were initially maintained for 7 days after seeding, however later I modify the length of culture which is discussed further below.

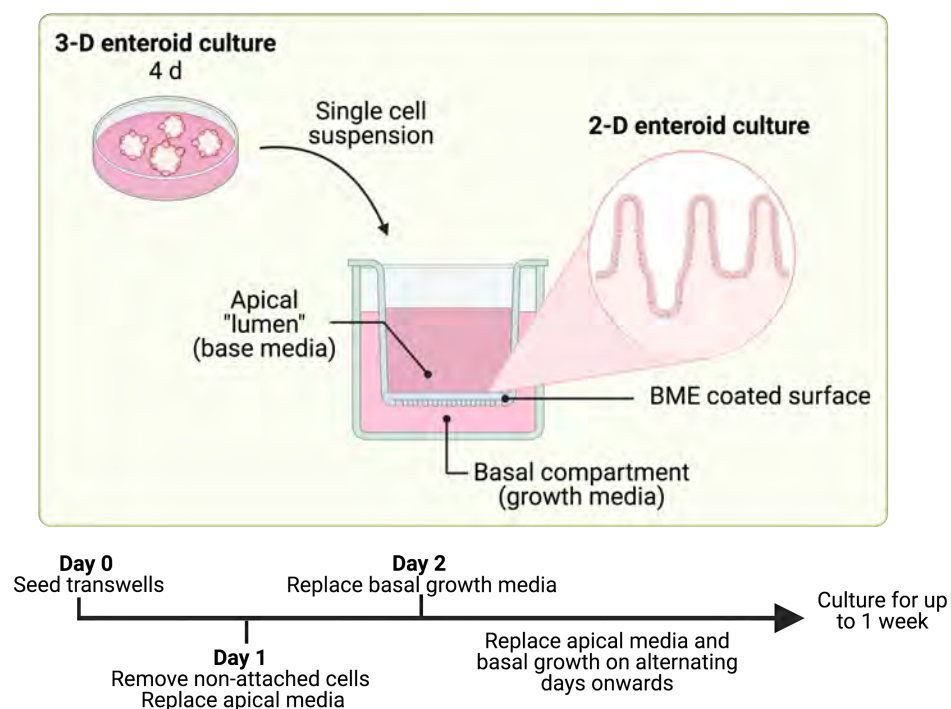


**Figure 4.2 | Summary of 2-D enteroid culture model.** 3-D organoids were grown as per established protocols based on Sato *et al*, 2009 with modifications detailed throughout this Chapter for 4 days. After which cells were dissociated using protocols from Duque-Correa *et al*, 2022 and seeding in base growth

media (200  $\mu$ l) into the apical chamber of transwell plates coated with an ECM mimic to encourage adherence. Growth media (4 ml) was supplied in the basal compartment, the conditions of this media were optimised throughout this Chapter. Non adherent and dead cells were removed from apical compartment after 24 h and apical media replaced every second day onwards. After 48 h the basal media was changed as well as every second day thereafter. Cultures were maintained initially until day 7 after seeding.

To achieve 2-D enteroid cultures, I modified 2-D caecaloid methods by optimising two major features i) the composition of growth media and ii) the ECM mimic used for coating the transwell surfaces. This chapter details several modifications, a summary table is provided with the media composition and outcome of each (Table 4.1). The growth media of caecaloid cultures requires supplementation with fibroblast growth factor (FGF-10), as this is secreted by the caecal mesenchyme *in vivo* (Burns et al., 2004; Duque-Correa, Schreiber, et al., 2020). FGF-10 is not required for 3-D enteroid growth, therefore this was omitted from all 2-D enteroid growth medias trialled (Burns et al., 2004; Duque-Correa, Schreiber, et al., 2020; Sato et al., 2009) (Table 4.1). Wnt ligands initiate signalling cascades that result in expression of stem cell genes, and therefore are crucial for stem cell maintenance (H. Clevers et al., 2014; Fevr et al., 2007). In the small intestinal epithelium Wnt ligands can be provided by Paneth cells, as well as by mesenchymal cells, while in the caecum and colon Paneth cells are thought not to be present, although they may arise in response to inflammation (H. C. Clevers & Bevins, 2013). Paneth cells provide an epithelial intrinsic source of Wnt ligands in enteroid cultures, specifically Wnt3a. Intestinal organoids containing Paneth cells (enteroids) therefore do not require supplementation; while in the Paneth cell devoid caecaloid or colonoid cultures Wnt3a supplementation with Wnt3a CM is absolutely required (Duque-Correa, Schreiber, et al., 2020; Sato & Clevers, 2013; Sato et al., 2009). Therefore, during culture caecaloids require relatively high Wnt CM, 30% vol/vol, to support stem cell proliferation and monolayer formation, concentrations are then successively reduced during culture to 10% and then 2.5% to stimulate differentiation of the monolayer (Table 4.1). Although, Wnt supplementation is not essential for enteroid growth, Wnt3a conditioned media (CM) has been shown to enhance enteroid culture and is required for long term cultures (Wilson et al., 2021). Initially, I trialled caecaloid culture methods for 2-D enteroid culture (without FGF-10) using Wnt CM

starting at a lower vol/vol concentration than caecaloids of 10% for 48 h, 2.5% for 48 h, and 0% for remaining culture (Table 4.1). Our second trial repeated this except used the same Wnt concentration schedule used for 2-D caecaloids. However, both attempts failed to result in monolayer cultures (summarised in Table 4.1) and instead resulted only in small patches of cells (data not shown).

Table 4.1 | Summary of conditions trialed in this study for the optimisation of 2-D enteroid cultures.

Culture & origin	Base media	Growth media Schedule	ECM	Figure(s)	Complete monolayer (Y/N)
2-D Caecaloid (Duque-Correa, Goulding, Rodgers, Gillis, et al., 2022)	Advanced DMEM/F12 2mM L-glutamine 1x N2 supplement 1 x B27 supplement 10 mM HEPES	<b>WENRF</b> <b>W</b> - Wnt CM (50% – 2.5% vol/vol)* <b>E</b> - EGF (50 ng/ml) <b>N</b> - Noggin (100 ng/ml) <b>R</b> - R-spondin CM (10% vol/vol) <b>F</b> – FGF-10 (100 ng/ml) N-acetylcysteine (NAC) (1 mM) made up with base medium to total volume required <i>*Wnt was reduced every 2 days from 50%, 10%, 2.5%</i>	Collagen rat tail I	Figure 4.2	Y
2-D Enteroid		<b>WENR</b> <b>W</b> - Wnt CM (10% – 0% vol/vol)* <b>E</b> - EGF (50 ng/ml) <b>N</b> - Noggin (100 ng/ml) <b>R</b> - R-spondin CM (10% vol/vol) N-acetylcysteine (NAC) (1 mM) made up with base medium to total volume required <i>*Wnt was reduced every 2 days from 10%, 2.5%, 0%</i>	Collagen rat tail I	Data not shown	N
		<b>WENR</b> Wnt was reduced every 2 days from 30%, 10%, 2.5%	Collagen rat tail I	Data not shown	N
		<b>WENR</b> Wnt kept at 30% throughout cultures ( <b>30% WENR</b> )	Collagen rat tail I	Figure 4.2, 4.3	N
		<b>ENR</b> 0% Wnt throughout cultures ( <b>ENR</b> )	Collagen rat tail I	Figure 4.2, 4.3	N

Culture & origin	Base media	Growth media Schedule	ECM	Figure(s)	Complete monolayer (Y/N)
		<b>WENR</b> Wnt kept at 30% throughout culture ( <b>30% WENR</b> )	"Thin" Matrigel® (1:50 in PBS)	Figure 4.2, 4.3	N
		<b>ENR</b> 0% Wnt throughout cultures ( <b>ENR</b> )	"Thin" Matrigel® (1:50 in PBS)	Figure 4.2, 4.3	N
		<b>ENR + CR</b> + CHIR99021 (10 mM) + Y-27632/ROCKi (10 μM)	"Thin" Matrigel® (1:50 in PBS)	Figure 4.5, and subsequently throughout this thesis	Y
		Intesticult™	"Thin" Matrigel® (1:50 in PBS)	Figure 4.5	Y



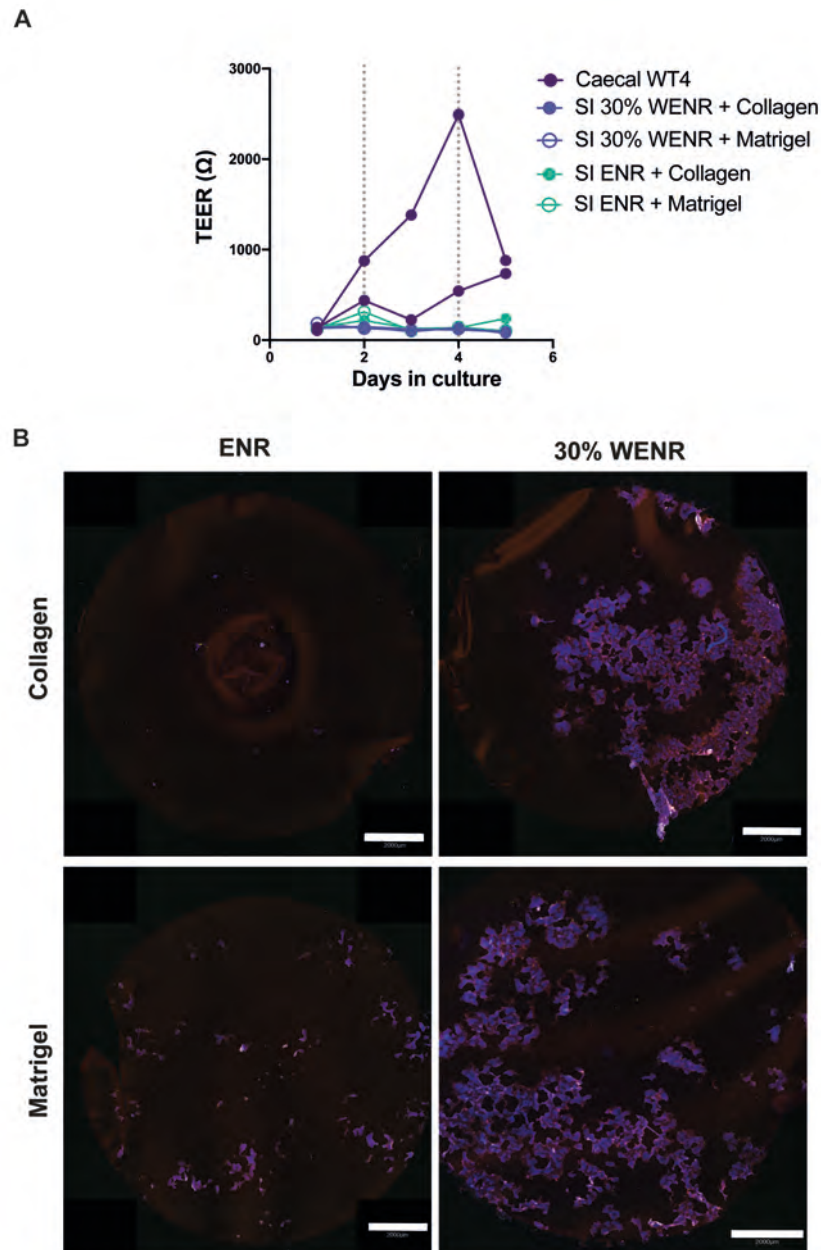
3-D enteroids only contain a proportion of cells that are able to proliferate (stem and TA cells), and these stochastically differentiate during culture into post-mitotic terminally differentiated cells that are unable to undergo cell cycle (Gehart & Clevers, 2019). Additionally, in our hands even in high concentrations of Wnt CM, organoids quickly showed signs of differentiation. Therefore, I reasoned that in order to form a successful monolayer during 2-D organoid growth I must seed transwell with a high density of proliferating cells capable of forming a monolayer and covering the transwell surface and this could be our major problem. Additionally, recent literature had also described similar approaches to 2-D enteroids with variable success (summarised in Table 4.2). Another variable that proved important for successful generation of monolayers by other groups was the choice of ECM coating of transwell surfaces prior to seeding (Table 4.2). Published methods used either Collagen which was what I had previously trialled (Duque-Correa, Goulding, Rodgers, Gillis, et al., 2022; Y. Liu et al., 2018; Thorne et al., 2018), or Matrigel<sup>®</sup> (Altay et al., 2019; Thorne et al., 2018) and found Matrigel<sup>®</sup> to improve results (Table 4.2). I therefore trialled side-by-side collagen coated or Matrigel<sup>®</sup> coating in combination with enteroids grown in the presence of Wnt (30% WENR) without modifying concentrations throughout culture, or when it was removed all together (ENR) (Table 4.1, Figure 4.2).

Table 4.2 | Summary of murine intestinal 2-D organoid publications.

Reference	ECM	Media	Time (d)	Monolayer	Seeding density	Conclusions
(Thorne et al., 2018)	Matrigel® poly-L-lysine Collagen	ENR CHIR99021 Y-27632	5	Claim monolayer but holes present in microscopy images	50-100 crypts/well 50,000 cells/well	Single cells better than crypts Matrigel® coating best CHIR99021 + ROCKi (Y-27632) improved culture but switched back to ENR after 4-6 hr
(Y. Liu et al., 2018)	Collagen I Matrigel®	ENR Blebbistatin LDN-193189 (LDN) CHIR99021. ROCKi (Y-27632)	4	Monolayer forms but do not report on coverage	500 crypts/well	No cells adhered to Collagen I coated plate. Blebbistatin & CHIR99021 improved culture Noggin can be replaced with LDN-193189 (LDN)
(Altay et al., 2019)	Matrigel® 'thin' and 'thick'	ENR Wnt3a ISEMF CM CHIR99021 Valproic acid	7-21	~100% by 10 d	100,000x cm <sup>2</sup>	'Thin' Matrigel® Grew best with all media components combined

Measurement of transepithelial electrical resistance (TEER) gives an indication of monolayer growth, and over the course of culture should increase as monolayers form (Altay et al., 2019). I found TEER indicates minimal differences between culture conditions for enteroids, however our caecaloid control showed consistent increase in TEER followed by rapid decline indicating differentiation (*María Duque-Correa, personal communication*) (Figure 4.3 A). Consistent with recently published papers, coating with collagen I resulted in poor adherence of enteroid cells (Figure 4.3 B) (Thorne et al., 2018) despite resulting in successful monolayers for caecaloid cultures (Duque-Correa, Goulding, Rodgers, Gillis, et al., 2022). 'Thin' Matrigel® coating described by Altay *et al*, resulted in improved coverage of the transwell surface in both ENR media and 30% Wnt WENR media compared to those coated with collagen (Figure 4.3 B). Microscopy showed that while supplementation of

30% Wnt WENR improved the coverage of transwell cultures compared to growth in ENR media, complete coverage was not achieved (Figure 4.3 B).



**Figure 4.3 | Growth of 2-D enteroids.** 2-D enteroid cultures on collagen I coated or Matrigel<sup>®</sup> coated transwell and grown in the presence or absence of 30% Wnt CM. Caecal organoids were grown side-by-side as a comparison using published methods. **A**) transepithelial electrical resistance (TEER) measured each day of culture for caecaloid monolayer (purple), enteroids generated from the entire small intestine grown in 30% WENR (light purple), and enteroids from entire small intestine grown in ENR (green). Filled circles indicate collagen coated and empty circles indicate Matrigel<sup>®</sup> **B**) Fluorescence microscopy of enteroid monolayers, image is an overlay of fluorescent channels of DAPI staining nuclei (blue), actin stained using phalloidin for visualisation of cell boundaries (red), lectins SNA/UEA which binds mucus on goblet cells (green), and ki67 for proliferative cells (yellow). Tiled image of transwell surfaces coated with collagen I (top row) or Matrigel<sup>®</sup> coated (bottom row) grown in presence of 30% Wnt (WENR) (right-hand column) or in absence of Wnt (ENR) (left-hand column). Scale bars = 2 mm.

An explanation for failure to achieve a complete monolayer could be that not enough proliferative cells were seeded. Yet, despite unsuccessful coverage of the transwell surface, the presence of proliferative cells was demonstrated by immunofluorescence microscopy staining of Ki67+ proliferative cells (Stem and TA cells). Ki67+ proliferative cells were present in all conditions, with the exception of collagen coated transwell grown in ENR media in which no cells adhered (Figure 4.4). Proliferative cells did not form foci as described for 2-D organoid cultures elsewhere (Altay et al., 2019; Duque-Correa, Goulding, Rodgers, Gillis, et al., 2022). I identified goblet cells using the fluorescent lectins *Ulex europaeus* agglutinin (UEA) and *Sambucus nigra* (SNA) which bind mucus on goblet cells. Goblet cells were present in all conditions where there were cells present, indicating differentiation of stem cells was occurring in these cultures even in the presence of high concentrations of Wnt. These data suggested that I had successfully seeded proliferative cells, but either i) too few proliferative cells were seeded to achieve coverage or ii) differentiation occurs too quickly hampering the ability of these cells to achieve complete coverage or iii) both factors play a role.

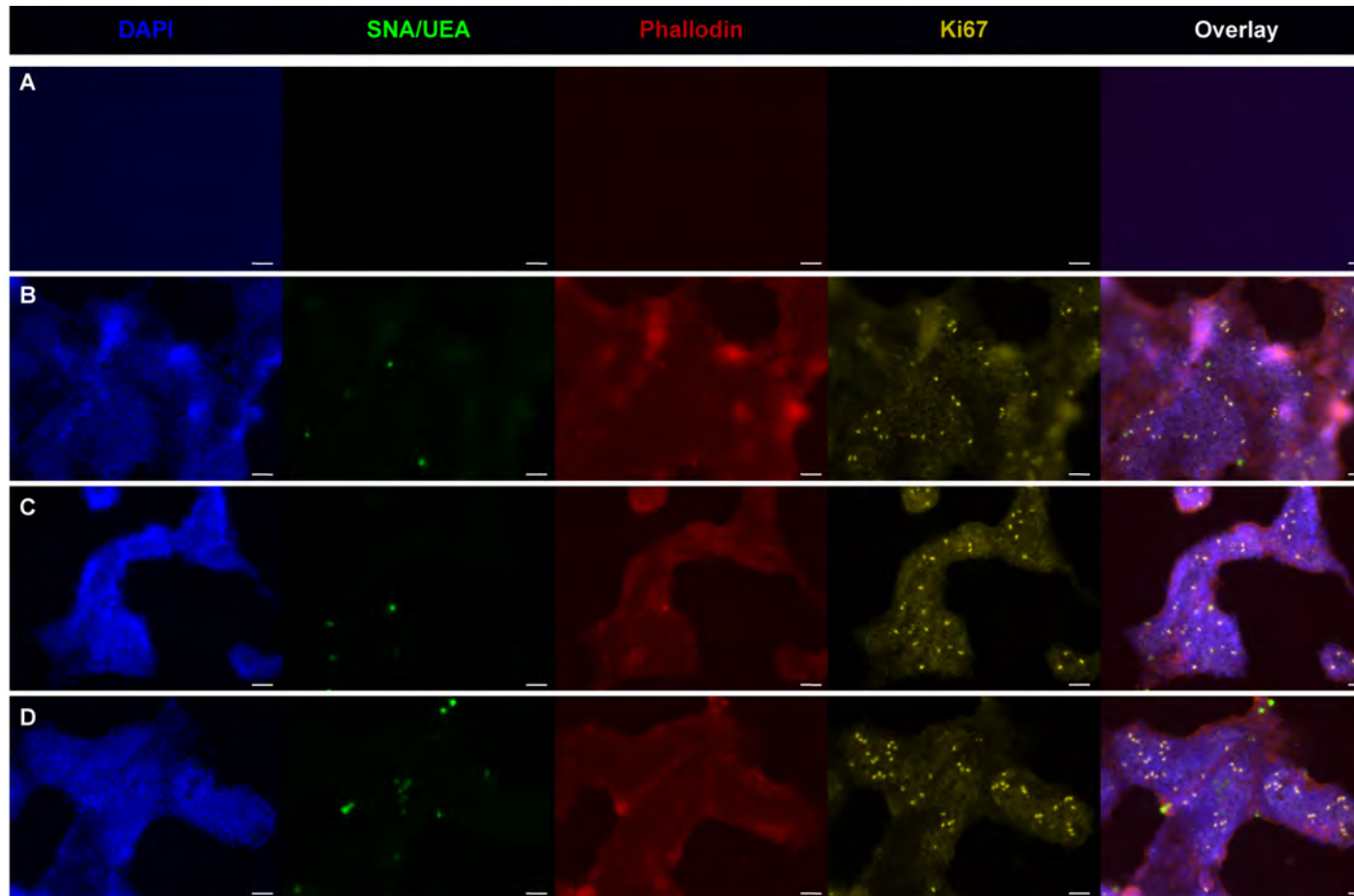


**Figure 4.4 | 2-D enteroid cultures contain proliferating cells.** Fluorescence microscopy of monolayers, DAPI staining nuclei (blue), actin stained using phalloidin for visualisation of cell boundaries (red), lectins SNA/UEA which binds mucus on goblet cells (green), and ki67 for proliferative cells (yellow). **A&B**) Collagen I coated transwell in **A**) ENR media **B**) 30% Wnt3a CM (vol/vol) ENR media or **C&D**) Matrigel® coated transwell in **C**) ENR media **D**) 30% Wnt3a CM (vol/vol) ENR media. Scale bars = 100  $\mu$ m.

The generation of large 3-D organoids that yield sufficient numbers of cells for seeding 2-D cultures requires at least 3-4 day of culture however our 3-D enteroid cultures rapidly differentiated even in 30% CM WENR media by Day 3-4 (Appendix I). Therefore, I tested alternative methods to strongly enrich for stem cells firstly in our 3-D organoid so that when seeded into transwell plates these would be enriched. Publications summarised in Table 4.2 used a variety of combination of growth factors, morphogens, and growth factor CM, some of which I were using already (WENR) and others I decided to trial. Y-27632 is a Rho-associated protein kinase inhibitor (ROCKi) that helps prevent anoikis that occurs when epithelial cells lose contact with basement membrane, and in general improves epithelial survival during dissociation and culture. I added this to our media for 4 days prior to 2-D enteroid cultures, and during the course of 2-D cultures to enhance overall survival. Even at relatively high Wnt CM concentrations (30%) our 3-D enteroids differentiated. Another way to activate Wnt signalling is through the use of the molecular agonist CHIR99021 (An et al., 2012). CHIR99021 is an inhibitor of the protein kinase GSK $\beta$ , which functions to phosphorylate  $\beta$ -catenin in the absence of Wnt signalling, labelling it for destruction (An et al., 2012) (Figure 4.5). Inhibition of GSK $\beta$  by CHIR99021 subsequently leads to increased activation and translocation of  $\beta$ -catenin to the nucleus to enhance expression of stem genes (An et al., 2012) (Figure 4.5). Some papers use the BMP inhibitor LDN-193189 (LDN) as an alternative to Noggin (Table 4.2), however as I already included the BMP inhibitor Noggin, I proceeded with to use this. Alternatively, some researchers use Intesticult<sup>TM</sup> media to grow organoids, which is a pre-defined media sold by Stem Cell Technologies that does not specify which growth factors it contains, or their concentrations. I also trialled Intesticult<sup>TM</sup> for the growth of 2-D enteroids.

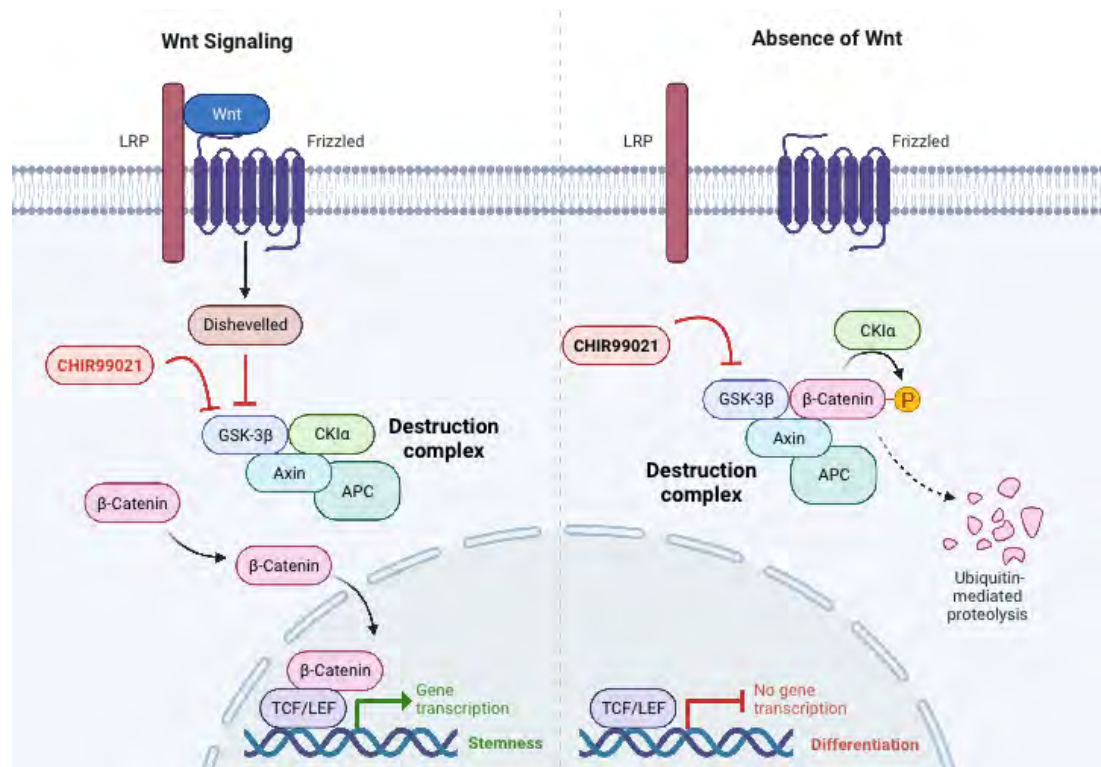


**Figure 4.5 | Schematic of Wnt signalling pathway demonstrating effect of CHIR99021 inhibitor.** In the presence of available Wnt (right-hand side of image) Wnt binds its receptor and co-receptors Frizzled (Fzd) and Lrp respectively, upon binding this leads to activation of dishevelled. Activated dishevelled then inhibits a protein complex termed the destruction complex which is comprised of APC, Axin, CK1 $\alpha$  and GSK-3 $\beta$ . Dishevelled mediated inhibition of the destruction complex allows  $\beta$ -catenin to enter the nucleus and transcribe genes involved in stemness. In the absence of Wnt signalling (left-hand side) the destruction complex phosphorylates  $\beta$ -catenin which leads to ubiquitin mediated proteolysis and no transcription of stemness related  $\beta$ -catenin target genes. CHIR99021 inhibits GSK-3 $\beta$  of the destruction complex in the presence and absence of Wnt and this leads to an inability to phosphorylate  $\beta$ -catenin, allowing translocation to the nucleus and active gene transcription of  $\beta$ -catenin target genes. This figure was adapted from “Wnt signalling pathway Activation and Inhibition” by BioRender.com.

3-D enteroids were grown in either 30% Wnt WENR media, ENR media supplemented with 10  $\mu$ M CHIR99021 and 10  $\mu$ M ROCKi (ENR + CR), or Intesticult<sup>TM</sup> media (Figure 4.6, Table 4.1). High concentrations of CHIR99021 induced very large cystic organoids indicative of stem cell enrichment, as did culture in Intesticult<sup>TM</sup> media (Figure 4.6).



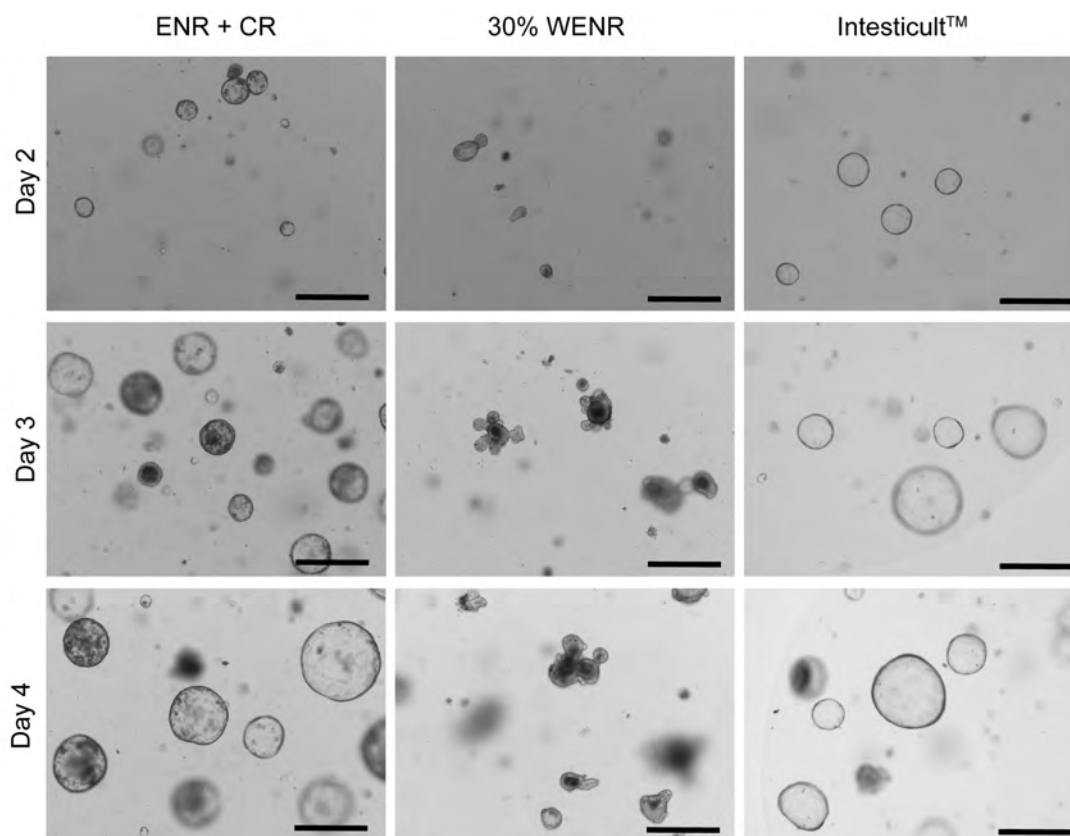
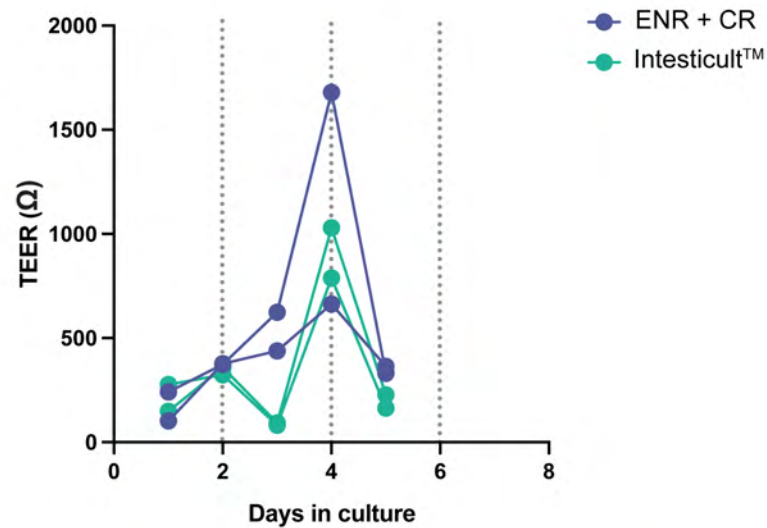


**Figure 4.6 | 3-D organoid growth in stem cell enriching media.** 3-D enteroid morphology when grown in ENR media + 10  $\mu\text{m}$  CHIR99021 (right-hand column), 30% Wnt3a (vol/vol) ENR media (middle column), or Intesticult™ (right-hand column) at days 2 (top-row), 3 (middle row) and 4 (bottom row) of post passaging. Scale bars = 500  $\mu\text{m}$ .

We then dissociated 3-D organoids grown in ENR + CR for 4 days, and seeded cells into transwell plates coated with ‘thin’ Matrigel® layers. 2-D enteroid cultures were then maintained in stem cell enriching media, either ENR + CR or Intesticult™ media for the entire length of culture (7 days). TEER values increased over the course of growth in both media conditions, indicating monolayer coverage of transwell surfaces (Figure 4.7 A). DAPI staining of nuclei demonstrated successful coverage in both media conditions of the entire transwell surface (Figure 4.7 B). Coverage was complete for ENR + CR, or nearly complete for Intesticult™ (Figure 4.7 B). Due to the architecture of these cultures some areas appear to have less DAPI fluorescence, and appear as holes, but upon subsequent investigation using confocal microscopy these

were found to contain cells on different planes. Intesticult™ media showed no advantage over ENR + CR, and since it is costly and does not allow for controlled modification of various growth factors, I did not proceed with using this media further.

**A**



**B**

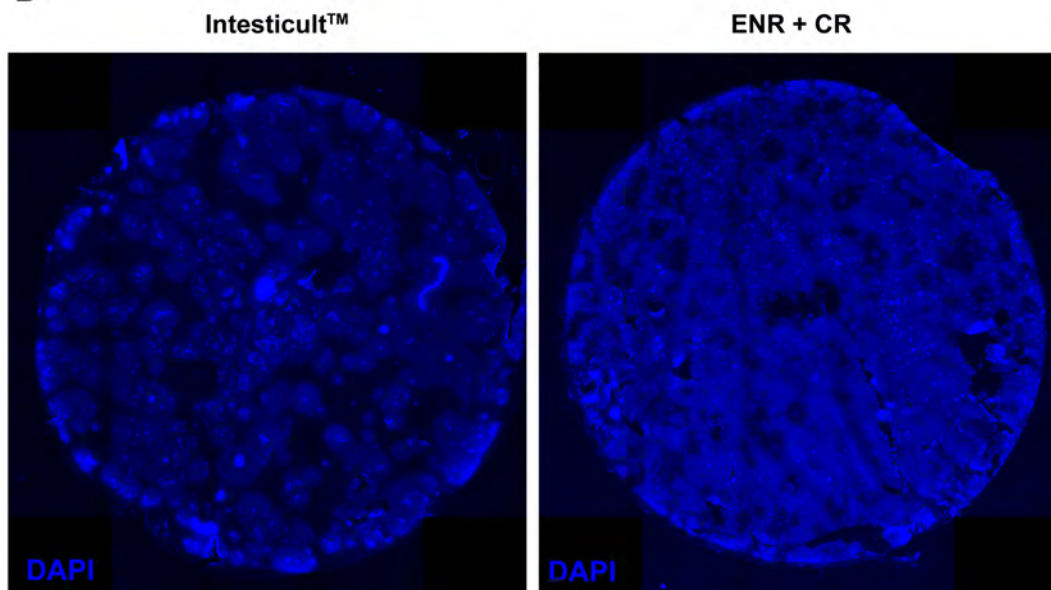


**Figure 4.7 | CHIR99021 leads to successful transwell coverage with SI enteroids. A&B)** 2-D enteroids were grown in ENR + 10  $\mu$ m CHIR99021 **A)** Trans epithelial electrical resistance (TEER) measurements for first 5 days of 2-D enteroids culture. **B)** Immunofluorescence of DAPI staining enteroid cell nuclei.

We initially cultured 2-D enteroids for 7 days post seeding which was based on methods developed for caecaloid culture by our collaborator Dr. Maria Duque-Correa (Duque-Correa, Goulding, Rodgers, Gillis, et al., 2022). Upon successful monolayer growth I then aimed to determine the growth dynamics specific to 2-D enteroid cultures. I performed a time course experiment using two separate enteroid organoid lines, one originated from the murine duodenal tissue, and one from the entire length of the murine small intestine (2.4.1). 2-D enteroids were grown as previously described and a well was taken for microscopy at each day from day 2-7 post culture. Full coverage of the transwell surface was demonstrated as early as day 2 as well as substantial Ki67+ staining of proliferative cells. By day 3&4 the numbers of proliferative cells has increased and clear proliferative foci had spontaneously formed (Figure 4.8 and Figure 4.9) as described for 2-D enteroid and caecaloid cultures (Altay et al., 2019; Duque-Correa, Goulding, Rodgers, Gillis, et al., 2022). Using the fluorescent lectins *Ulex europaeus* agglutinin (UEA) and *Sambucus nigra* (SNA) which bind mucus and thereby marking goblet cells, I identified terminally differentiated goblet cells. Surprisingly these were present as early as 2 days in culture, even in the presence of this highly stem enriching media, demonstrating the strong ability of these enteroid cultures to differentiate (Figure 4.8). Growth dynamics between duodenal organoids and SI organoids were consistent (data not shown).

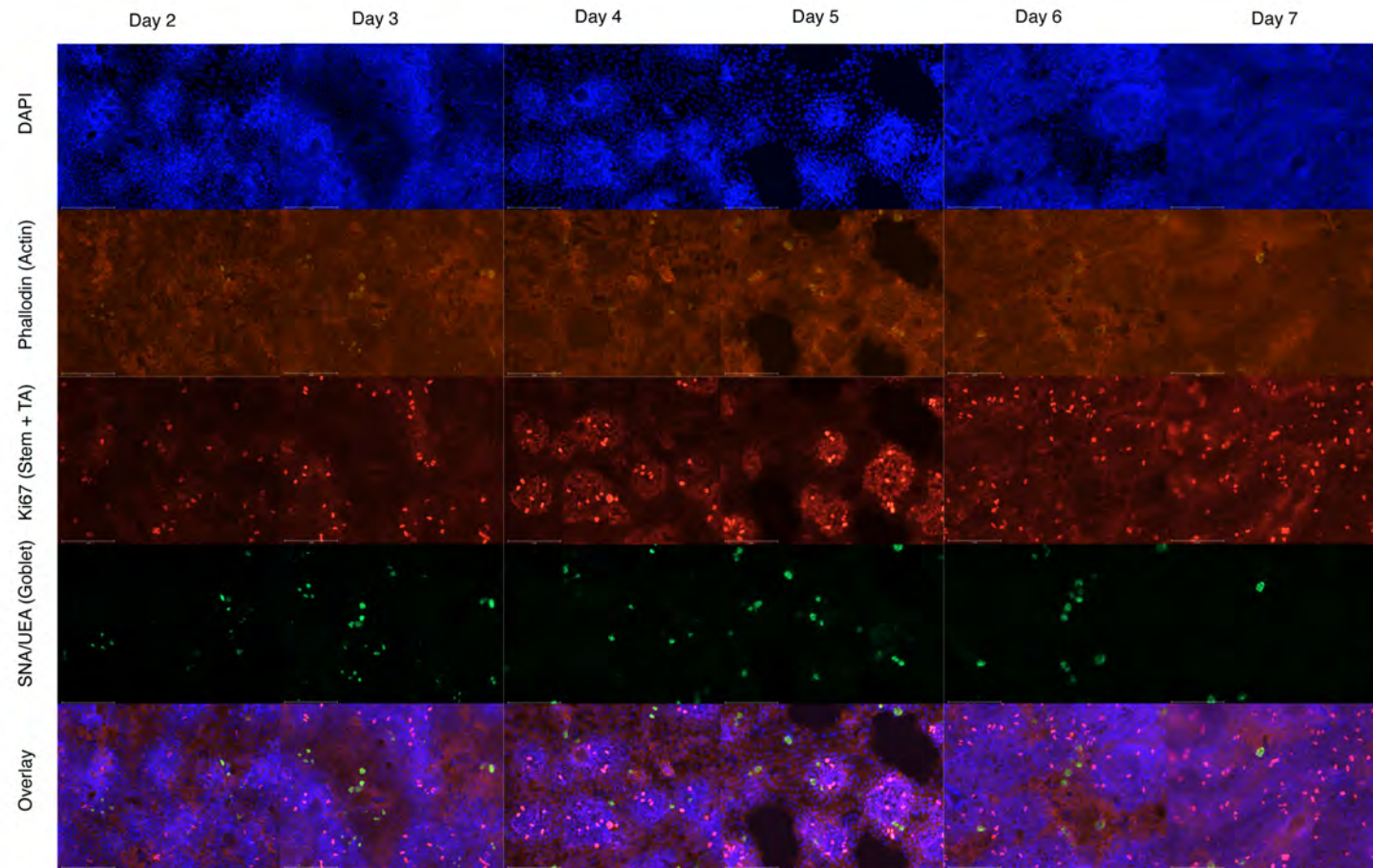


**Figure 4.8 | Growth and differentiation dynamics of 2-D enteroid cultures.** Immunofluorescence of duodenal 2-D enteroids from each day 2-7 of culture. DAPI = Nuclei, orange = Phalloidin staining actin, red = Ki67+ cells (Stem and TA cells), green = Lectins SNA/UEA bind mucus on goblet cells and overlay of channels.

#### 4.2.2 2-D enteroid cultures recapitulate the host intestinal epithelium

We illustrate 2-D enteroid cultures spontaneously form proliferative foci of densely clustered cells that are positive for Ki67, as described by others for caecaloid and enteroid cultures (Altay et al., 2019; Duque-Correa, Goulding, Rodgers, Gillis, et al., 2022; Y. Liu et al., 2018; Thorne et al., 2018) (Figure 4.9). In addition, goblet cells were identified by SNA/UEA staining and localised to regions where cells were distributed away from densely packed proliferative loci (Figure 4.9 and Figure 4.10). I aimed to determine whether the remaining terminally differentiated cell types of the intestinal epithelium, that are known to be present in 3-D organoids, are present in our 2-D enteroid model. I used immunofluorescence microscopy to detect Dck11 (Dcam1) specific to tuft cells, lysozyme 1 (Lyz1) specific to Paneth cells, Chromogranin A (ChgA) specific to enteroendocrine cells and villin which is highly expressed in the microvilli of enterocytes (Figure 4.10 A&B). In addition to goblet and proliferative cells, the presence of all other cell types investigated was confirmed (Figure 4.10). Tuft and enteroendocrine cells are rare cell types within these cultures. M cells are the only remaining cell type that I did not quantify as they require RANK signalling to induce their differentiation (Knoop et al., 2009). When 2-D and 3-D enteroid growth media was supplemented with RANKL I observed M cell specific genes by qPCR for the 3-D setting only and did not pursue this further (data not shown). The presence of differentiated cell types was also supported by the identification of well established cell type specific marker genes of specialised intestinal epithelial cells using RT qPCR in both 2-D and 3-D organoid cultures (Figure 4.10 C&D). In Chapter 6 of this thesis, single cell RNA seq (scRNA seq) was performed and further confirms the presence of different cell populations as well as indicates the proportions of each cell type. Finally, by confocal microscopy these cultures did not form

flat monolayers and instead demonstrated a 'hill and valley' like structure (Supplemental file 1 and Supplemental file 2).

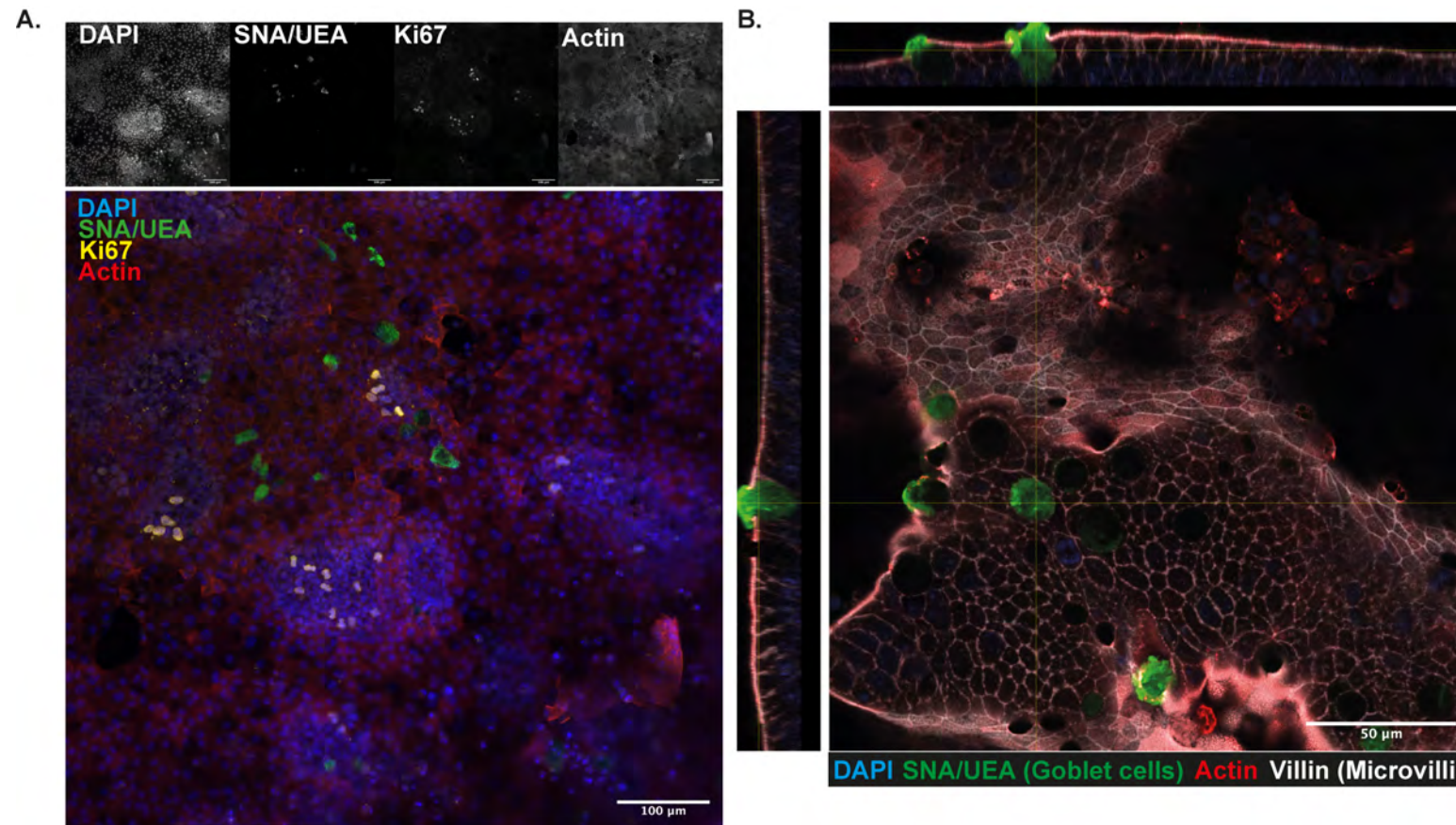


**Figure 4.9 | 2-D enteroids spontaneously form proliferative foci and generate terminally differentiated cells.** Immunofluorescence microscopy of 2-D enteroid cultures after 7 days. DAPI staining of cell nuclei (blue), SNA/UEA bind lectins present within mucus of goblet cells (green), Actin visualises cell boundaries and microvilli (red). **A)** Ki67 labels proliferative cells (yellow). Scale bar = 100 μm. **B)** Z-stack image showing orthogonal view of 2-D enteroid cultures, villin was labelled to identify microvilli at the apical surface (white). Scale bar = 50 μm

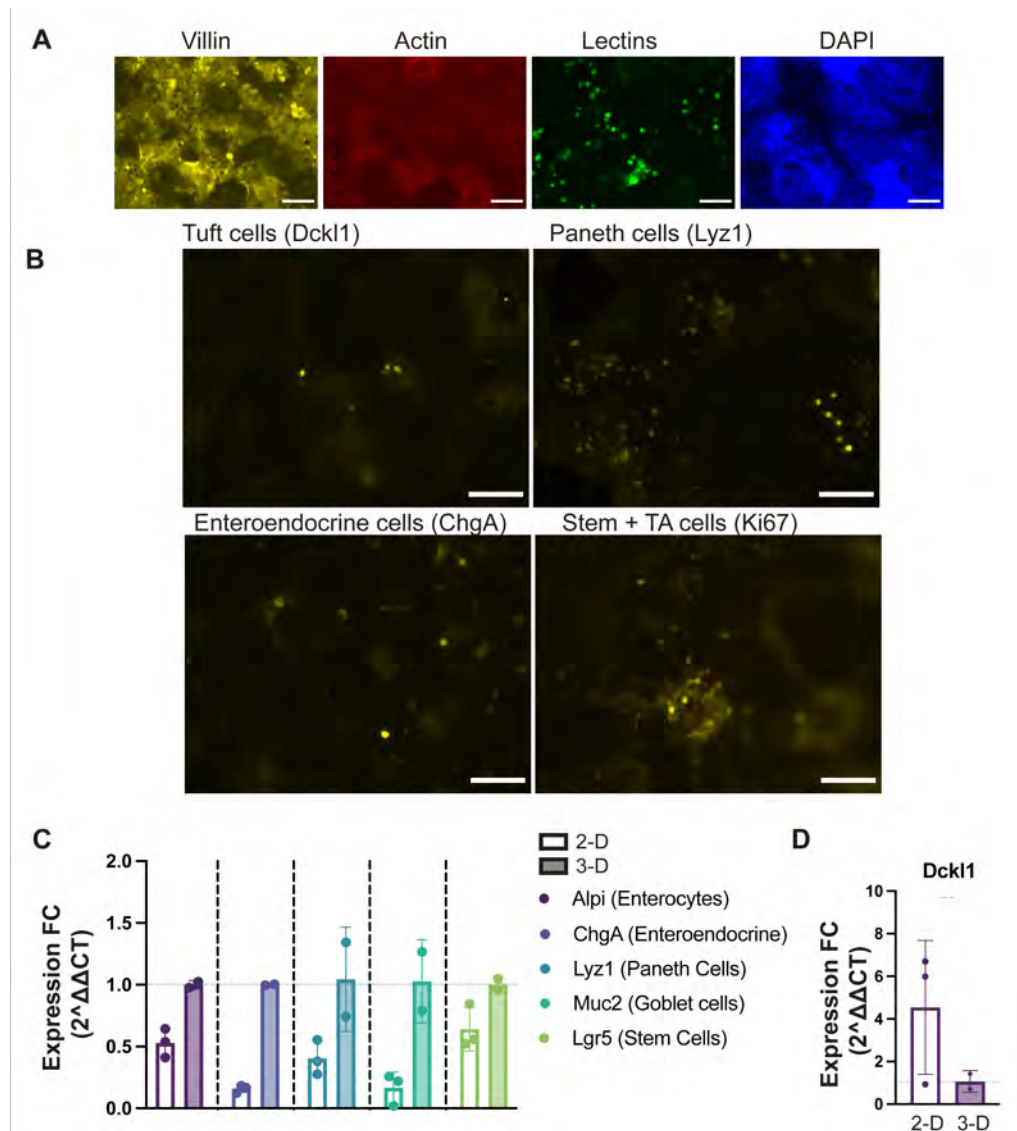


**Figure 4.10 | Validation of 2-D enteroid cultures. A)** Immunofluorescence microscopy of villin labelling enterocytes (yellow), actin to identify cell boundaries (red), lectin+ goblet cells (green) and DAPI stained nuclei (blue). **B)** Representative immunofluorescence microscopy of Dck1+ tuft cells, Lyz1+ Paneth cells, Chga+ enteroendocrine cells and Ki67+ proliferative cells (stem and TA cells). **C)** RT qPCR analysis of RNA from 2-D (empty columns) and 3-D organoid (shaded columns) cultures for cell type specific marker genes purple = Alpi (enterocytes), violet = Chga (Enteroendocrine cells), blue = Lyz1 (Paneth cells), turquoise = Muc2 (Goblet cells) and green = Lgr5+ (Stem cells). Y-axis shows normalised (GAPDH) mRNA expression fold change ( $2^{-\Delta\Delta CT}$ ) of 2-D organoids vs. 3-D organoids. **D)** as in C but for expression of Dck1 (same experiment). **C&D)** mean values  $\pm$ SD plotted; points plot individual biological replicates; for 2-D (n = 3), 3-D (n = 2).



In summary, the methods trialled in this chapter that allowed for growth of 2-D enteroids were using CHIR99021 and ROCKi to supplement enteroid media both 4 days prior to seeding transwells and throughout culture (2.4.3) (Figure 4.11). Matrigel® coating of 2-D transwells was required for monolayer formation, and both apical and basal media requires changing every other day on alternating days (Figure 4.11). In this study cultures were grown for a maximum of one week but the monolayer is established by day 4, longer culture lengths were not investigated (Figure 4.11).

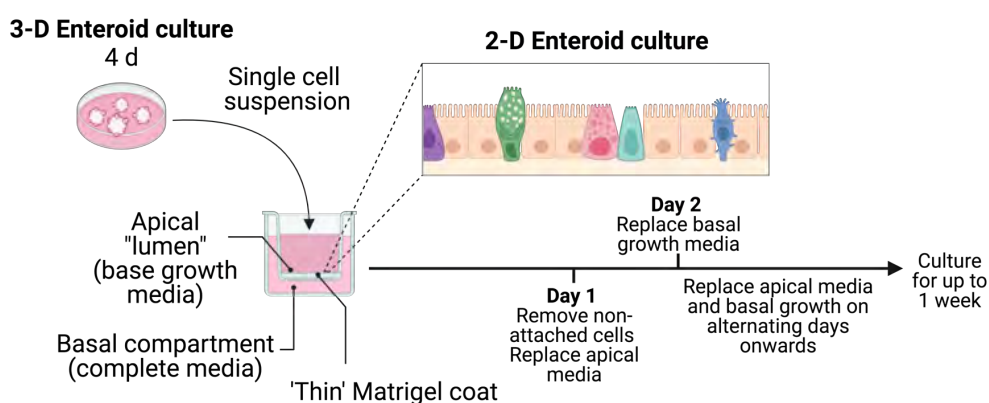


**Figure 4.11 | Summary of 2-D enteroid protocol.** 3-D enteroids are grown for 4 days in stem cell enriching media. 3-D enteroids are then digested into a single cell suspension in base growth media and seeded into the upper compartment of a 0.4  $\mu\text{m}$  pore transwells pre-coated with a 'thin' layer of Matrigel®. Stem cell enriching media is added to the bottom compartment. After 1 day of culture, the media and non-adherent cells in the upper compartment are aspirated and replace with fresh media, and every other day onwards. On day 2 of culture the basal media is aspirated and replaced, and every other day onwards. In this thesis cultures were maintained for up to one week.

#### 4.2.3 Modulating the cellular composition of 2-D enteroids

Th2 cytokines IL-4 and IL-13 drive both goblet (Khan et al., 2001; Marillier et al., 2008) and tuft cell (Gerbe et al., 2016; Howitt et al., 2016; Von Moltke et al., 2016) hyperplasia in the intestinal epithelium during helminth infection, and addition of these cytokines to 3-D enteroid cultures also induces goblet and tuft cell differentiation (Druerey et al., 2021; Karo-Atar et al., 2022; Lindholm et al., 2022). I seeded 2-D enteroids, allowing 48 h for cells to adhere and form a monolayer before supplementing growth media with 50 ng/ml of IL-4 and 50

ng/ml of IL-13 and culturing for a further 48 h. As expected, I found hyperplasia of tuft and goblet cells by fluorescence microscopy (Figure 4.12 A). I also found higher background fluorescence; I predict this is a result of increased mucus production by goblet cells. RT qPCR was used to assess the expression of cell type specific genes in response to cytokines IL-4 and IL-13 after 72 h. I assessed the mucus component Muc2 specifically expressed by goblet cells, and the tuft cell specific marker Dckl1 after 72 h of growth in the presence of IL-4 and IL-13. While I saw an increase in goblet and tuft cells by microscopy, qPCR analysis of goblet and tuft cell specific genes Muc2 and Dckl1 showed no significant difference (Figure 4.12 B). Interestingly, this experiment also revealed that in response to IL-4 and IL-13 the expression of Lgr5 is strongly downregulated and could not be detected in 2-D enteroids grown with cytokines (Figure 4.12 B).

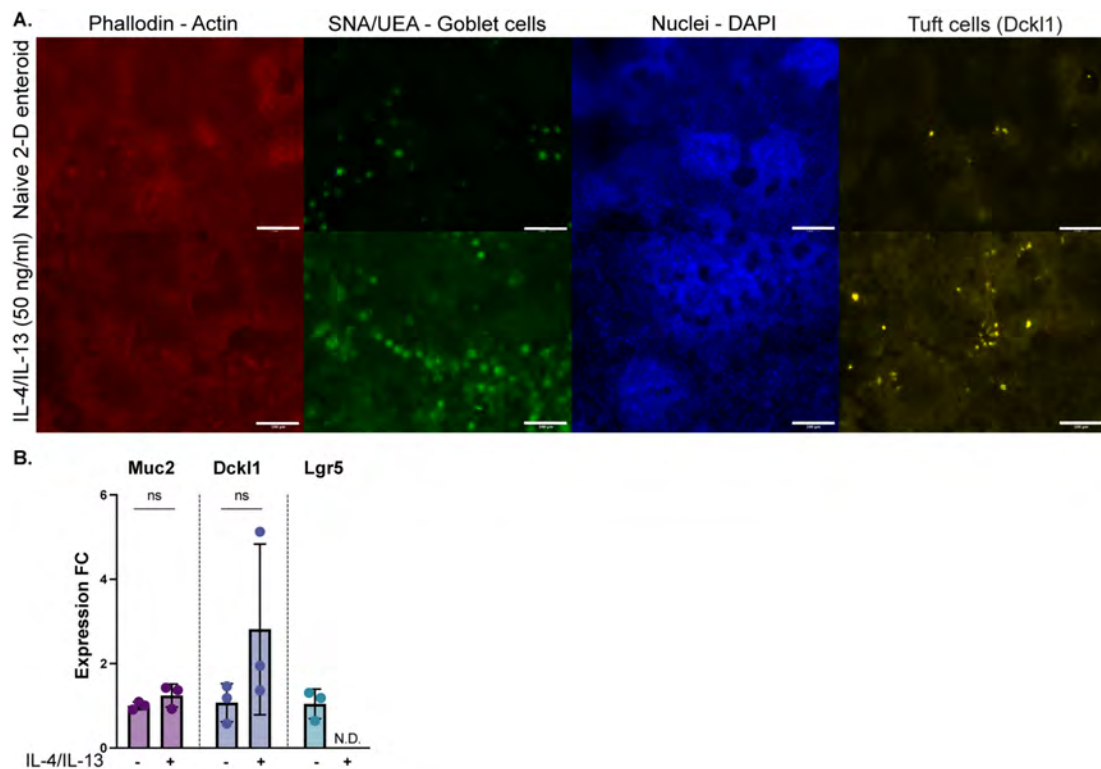


**Figure 4.12 | 2-D enteroid composition in presence of IL-4 and IL-13. A)** Immunofluorescence of 2-D enteroids grown without (top row), or with (bottom row) IL-4 (50 ng/ml) and IL-13 (50 ng/ml) for 48 hr stained for Actin (red), goblet cells using lectin binding dyes UEA and SNA (green), nuclei (DAPI) and tuft cells using Dckl1 (yellow). Scale bars = 100  $\mu$ m. **B)** normalised (GAPDH) mRNA expression fold change ( $2^{-\Delta\Delta CT}$ ) of Muc2, Dckl1 and Lgr5 in 2-D enteroids grown in presence or absence of IL-4 (50 ng/ml) and IL-13 (50 ng/ml) for 72 h. Mean  $\pm$  SD is plotted. Statistical test student t test, ns = non-significant, (n = 3). N.D. = not detected.



### 4.3 Discussion

In this chapter 2-D enteroid cultures that form contiguous monolayers of polarised cells epithelial cells were developed (Figure 4. and Figure 4.). Our 2-D enteroid cultures self-organise into proliferative loci (Figure 4.) and spontaneously differentiate into all specialised cells of the intestinal epithelium with the exception of M cells (Figure 4. and Figure 4.10 ). Enteroid cells require BME substitutes for adherence to transwell surfaces, unlike caecaloid cells which adhere well to rat collagen type I. The biology underpinning this difference is unknown (Figure 4.). Furthermore, despite enteroids possessing Paneth cells which can provide an endogenous source of Wnt ligands, in order to enrich for stem cells, I required the use of Wnt agonist CHIR99021 and ROCKi to enhance survival and monolayer formation (Figure 4.). Our 2-D enteroids exhibit some degree of architecture with a 'hill and valley' appearance, however a caveat of these cultures is that they do not reflect well the *in vivo* structures of crypts and villi which may impact cellular differentiation within these cultures. Nevertheless, these 2-D cultures provide an advantage over 3-D enteroids specifically for the delivery of *H. bakeri* EVs to the apical epithelium, and for subsequent studies of the host intestinal epithelial response to helminth parasites and their secreted products (Chapters 5 & 6).

#### Limitations

While 2-D organoids have many advantages over 3-D organoids especially for the study of large multicellular pathogens, they don't necessarily replicate all of the features that 3-D organoids do. For example, 3-D organoids replicate much more closely the structure of the intestinal epithelium while 2-D organoids poorly represent crypts and villi. In the future 2-D organoids may be supported by the use of scaffolds to better replicate the architecture of the epithelium.

Another limitation of this study was the small number of biological replicates used to generate enteroid lines. This study could have been strengthened by generating enteroids from several mice to determine variability between biological sources.

To date a handful of publications have utilised 3-D organoids for the study of helminths or their ES products (Drurey et al., 2021; Faber et al., 2022; Karo-Atar et al., 2022; D. Smith et al., 2021). However, 2-D models circumvent many of the limitations that 3-D organoids have for studying helminth-host interactions. For example, livestock infective L3 larvae from both *T. circumcincta* and *O. ostertagi* have been co-cultured with ovine, or bovine, 3-D abomasum organoids respectively (Faber et al., 2022; D. Smith et al., 2021). In these studies a small proportion (<2%) of L3 *O. ostertagi* larvae could invade BME domes (in this case Matrigel®) that contained organoids, but not the Matrigel® only dome controls (Faber et al., 2022). Of those L3 larvae that successfully invaded organoid containing Matrigel®, 50% (*T. circumcincta*) or 61% (*O. ostertagi*) were able to transverse the epithelium and enter organoid lumens (Faber et al., 2022; D. Smith et al., 2021). These studies suggest that epithelial cells provide at least some of the cues required for L3 larval invasion, although it should be noted these species are not known to transverse the epithelium *in vivo* as noted by the authors (Faber et al., 2022; D. Smith et al., 2021). While these studies are the first to allow for *in vitro* studies of epithelial invasion by these species, further investigations would be limited by the small fractions of L3 larvae that successfully invaded organoids. On the other hand, 2-D organoid models can provide an enhanced platform for similar studies of helminth invasion and interactions at the epithelium because burrowing through Matrigel® and transversing the epithelium is not required. The use of 2-D organoids has recently been exemplified for *T. muris* (Duque-Correa, Goulding, Rodgers, Gillis, et al., 2022). Co-culture of L3 *T. muris* larvae with 2-D caecaloids allowed for in-depth monitoring of the early stages of invasion and development of syncytial tunnels previously difficult to assess *in vivo* (Duque-Correa, Goulding, Rodgers, Gillis, et al., 2022).

Another major benefit of 2-D models for co-culture studies is their open confirmation and larger format compared to 3-D organoids. For instance, studies that demonstrate burrowing of L3 larvae into 3-D organoids modified the organoid structure in order to accommodate these large parasites, which

does not reflect the physiological interactions during infection (H. J. Kim et al., 2012; J. Yin et al., 2021). Furthermore, as helminths develop through subsequent life cycle stages like L4 larvae and eventually adult parasites, worms increase in size and many helminths are larger even than an individual 3-D organoids (Ruby White et al., 2022). Finally, 3-D organoids accumulate dead cells and mucus within their lumen, requiring passaging and therefore limiting the longevity of co-cultures. However, 2-D enteroids and caecaloids have demonstrated the potential to be cultured for extended periods of time (several weeks) (Altay et al., 2019; Ruby White et al., 2022). Therefore 2-D organoid-helminth co-cultures could be maintained long enough to even allow for the transition between parasite life stages e.g., *H. bakeri* takes ~10 days to reach adulthood p.i. (Camberis et al., 2003; Reynolds et al., 2012).

An alternative method that has been described by others but was not used in this study is the Apical-out method (Co et al., 2019). Apical-out organoids are generated by mechanical disruption of 3-D organoids before placing in suspension culture, this process forces a reversion of epithelial polarity of the 3-D organoids (Co et al., 2019). This method may be applicable for some research questions, such as studying uptake of helminth derived EVs, and could be explored in the future. However, some limitations pertaining to traditional 3-D organoids also apply to Apical-out organoids. For example, Apical-out organoids are limited by their size, and have limited culture length. Therefore, for studies co-culturing live helminths, 2-D organoid models are advantageous (Ruby White et al., 2022).

2-D enteroids may eventually lead to *in vitro* replication of parasite lifecycles, although further bioengineering of more complex models will likely be required, at least for some species. For example, vascularisation or other blood sources would likely be crucial for the culture of hematophagous helminths (e.g., human hookworm species *N. americanus* and *A. duodenale*). Technologies are already on the horizon such as 'organ-on-a-chip' models which introduce features such as vascularisation (Zhao et al., 2021), microfluidics and fluid flow (H. J. Kim et al., 2012); sheer or contractile forces stimulating peristalsis (H. J. Kim et al., 2012; J. Yin et al., 2021); and gradients of oxygen or growth factors

(R. Kim et al., 2019). Some 2-D organoid models are beginning to use scaffolds to force epithelial growth into the configuration of crypts and villi (Bein et al., 2018; Nikolaev et al., 2020). One constraint of the currently developed organs-on-a-chip systems for helminth research is the physical size of these chips, which in most cases are too small for helminth co-culture. However, through modifications of these technologies it is possible that replication of helminth life cycles *in vitro* could be achieved (Ruby White et al., 2022).

An *in vitro* reproduction of helminth lifecycles has long been desired, and attempted many times (P. H. Silverman, 1965; P. H. Silverman & Hansen, 1971). The field has seen minimal success in completing helminth life cycles *in vitro* for most species, with the exception of *Strongyloides spp* which is able to complete its lifecycle free-living, or through infection (Heyneman et al., 1984). For example *H. bakeri* eggs can develop into L3 larvae *in vitro* which was first detailed in 1969 (P. H. Silverman, 1965). Since then, researchers remain reliant on animal infections to progress *H. bakeri* through the remaining life stages (L3 to Adults) (Heyneman et al., 1984; P. H. Silverman & Hansen, 1971). The ability to culture helminths out with animal hosts has big implications for the field, including the reduction of experimental animal use and associated costs; and allowing for tractable methods to investigate host-helminth interactions. Most importantly it could eventually allow for the *in vitro* culture of human infective helminth species most of which currently require human volunteers for lifecycle maintenance and remain a significant global health concern (Chapman et al., 2021; Loukas et al., 2016; WHO, 2020). Excitingly, 2-D enteroids cultures advanced by bioengineering of additional host physiology represent a new frontier for the culture of helminth parasites *in vitro*.

The 2-D enteroid methods developed in this chapter is used as a model system in subsequent chapters of this thesis to investigate the uptake and function of *H. bakeri* EVs in the host intestinal epithelium. In addition, I use 2-D enteroids to co-culture live *H. bakeri* parasites at different life stages. 2-D enteroids allowed for replication *in vivo* localisation of *H. bakeri* and its ES products, which is a unique advantage of this model.





**Chapter 5: *H. bakeri* EV uptake by intestinal epithelial cells**

**Abstract**

Extracellular vesicles (EVs) from several helminth species enter host cells *in vitro*. *H. bakeri* EVs can enter the enterocyte cell line MODE-K, and at much higher proportions bone marrow derived macrophages (BMDMs) suggesting cell type specificity. The intestinal epithelium is a heterogeneous tissue comprised of specialised cells and a mucus layer, whether *H. bakeri* EVs enter cells in the epithelia during infection is not known. In this chapter I aimed to determine the uptake dynamics of *H. bakeri* EVs in the intestinal epithelium using 2-D organoids which in comparison to MODE-K cells better models the intestinal epithelia. I use microscopy and flow cytometry to demonstrate that 2-D organoids take up *H. bakeri* EVs but at lower proportions than side-by-side with MODE-K cells. Furthermore, I assessed the uptake of *H. bakeri* EVs *in vivo* by delivering EVs using intraluminal injection, and detecting uptake using anti-EV sera. *H. bakeri* EVs may enter intestinal epithelial cells *in vivo* but further investigation is required to support this.

## 5.1 Introduction

One of the major aims of this thesis was to define the specificity of *H. bakeri* EV uptake within the host epithelium. In chapter 4 the methodology for generating 2-D enteroids was defined, which reflect the heterogenous cell type composition of the intestinal epithelium and enable studies that address cell type specificity for uptake. In this Chapter I investigated the uptake dynamics and specificity of *H. bakeri* EVs using MODE-K cells, 2-D enteroids and also begin to assess uptake *in vivo*.

Evidence of cross-kingdom EV mediated communication has been demonstrated in various contexts, including between fungus and plants (Q. Cai et al., 2018; M. Wang et al., 2016; Weiberg et al., 2013), animals and fungus (Gehrmann et al., 2011; Vargas et al., 2015), and animals and bacteria (Codemo et al., 2018; Deo et al., 2018; Kaparakis et al., 2010; Koeppen et al., 2016; Macdonald & Kuehn, 2013; Rivera et al., 2010). While helminth EVs have been shown to have immunomodulatory functions in many contexts (Sánchez-López et al., 2021), the majority of work has focused on *in vitro* co-culture with homogenous cell lines, or with isolated immune cells (Sánchez-López et al., 2021). As such, little is understood regarding the specificity of EV uptake in complex tissues comprised of multiple cell types, and several questions remain unanswered. Are *H. bakeri* EVs targeted to specific host cells? What underpins EV specificity, is it defined by the molecular mechanism used for uptake e.g., endocytosis or membrane fusion; or the inherent ability of the recipient cell to uptake EVs? Conversely, is uptake ubiquitous and does this reflect the ubiquity of EV uptake pathways across various cell types?

Previously, in side-by-side comparisons bone marrow derived macrophages (BMDMs) demonstrated an enhanced ability to uptake *H. bakeri* EVs compared to MODE-K cells (A. H. Buck et al., 2014; Coakley et al., 2017). These findings could represent a targeting of *H. bakeri* EVs to macrophages, however they could also be explained by the fact that macrophages are

phagocytic and inherently specialised at engulfing foreign material (Metchnikoff, 1905). Little is known of the true fate of *H. bakeri* EVs during infection. During the adult stage of infection, when the parasites reside in the lumen, the most proximal tissue barrier is the intestinal epithelium. As described in earlier chapters of this thesis (Chapter 1), the intestinal epithelium is involved in parasite detection and response. Upon helminth infections with cellular composition of the epithelium changes and has been associated with hyperplasia of the secretory cell types e.g., Paneth cells (Kamal et al., 2002), goblet cells (Khan et al., 2001; Marillier et al., 2008; J.-E. Turner et al., 2013), and tuft cells (Gerbe et al., 2012; Howitt et al., 2016; Von Moltke et al., 2016). Of these secretory cells, goblet and tuft cells are associated with helminth expulsion, through their role in mucus secretion or alerting the immune system respectively (Baska & Norbury, 2022; Gerbe et al., 2012; Howitt et al., 2016; Von Moltke et al., 2016). I therefore hypothesised that EVs may target these specific cell types during infection or target the stem cells to interfere with their differentiation. To address these questions, I treated MODE-K and 2-D enteroids with *H. bakeri* EVs labelled with AF647 (EV-AF647). Uptake was assessed using fluorescence and confocal microscopy, as well as flow cytometry. In comparison to *H. bakeri* EV uptake by MODE-K cells, I found lower proportions of EV-AF647 in cells from 2-D enteroids, which could suggest cell type specificity within these cultures.

Finally, tracking uptake of helminth EVs *in vivo* is challenging as helminths cannot easily be genetically modified to generate fluorescent EVs. Additionally, delivery of isolated helminth EVs *in vivo* requires large doses that can be prohibitive. Furthermore, delivery of intact EVs to the intestine by oral gavage must overcome the highly acidic environment of the stomach. Antibodies that detect of *H. bakeri* EVs within infected tissue have been limited. I raised antibodies against isolated *H. bakeri* EVs by immunising rats and collecting serum, referred to as  $\alpha$ -EV serum (detailed in Chapter 3) to detect EVs in infected gut tissue. While  $\alpha$ -EV serum strongly detects worms and surrounding EV sized particles, identification of EVs within host epithelial cells was not demonstrated. One reason that identifying uptake in infected tissue is

challenging could be the low abundance of EVs in a given section of tissue. Therefore, I performed intraluminal injections of isolated *H. bakeri* EVs into the small intestine of mice under aesthesia to assess *in vivo* uptake after 1.5 h. Tissue from intraluminal injections showed promising evidence of uptake into villi epithelial cells, although further investigation of these samples is required for confirmation. In this chapter I demonstrate *H. bakeri* EVs can enter host intestinal epithelium using 2-D enteroids. I begin to investigate uptake *in vivo* however subsequent work is required to convincingly demonstrate that this phenomenon occurs *in vivo*.

## 5.2 Results

### 5.2.1 *H. bakeri* EV-647 uptake properties in the MODE-K cell line

The main aim of this chapter was to determine whether *H. bakeri* EVs are taken up by cells of the intestinal epithelium using 2-D enteroids, and if so by which cellular subtypes. Previously, MODE-K were shown to take up *H. bakeri* EVs labelled using PKH67 as early as 1 h, but were highest at 24 h of co-culture, timepoints after 24 h have not been assessed (Buck et al., 2014; Coakley et al., 2017). PKH67 labelling forms dye aggregates that are similar in size to EVs, therefore I first confirmed whether I could detect uptake of EV-647 in MODE-K epithelial cells. MODE-K cells are an immortalised cell line that was originally derived from the mouse intestinal epithelium of the duodenum/jejunum, and most closely represents enterocytes (Vidal et al., 1993). MODE-K cells serve as a good model of intestinal enterocytes but critically lack many features found in organoid culture. For example, MODE-K cells cannot differentiate into other subtypes of the epithelium, they do not produce mucus, and they lack expression of many intestinal epithelial genes associated with non-enterocyte cells.

I performed a dosage experiment using two batched preparations of EVs. Two batches of HES (Batch A & Batch B) were split in half for isolation by either UC or SEC. I had carried out substantial assessment of the EV populations isolated by SEC and UC (Chapter 3). I aimed to assess whether isolation method affects uptake into host cells. EVs were labelled using NHS-AF647 and excess dye removed using SEC (Chapter 3 of this thesis). HBSS buffer, which was used to re-suspend EV isolations, was also labelled using the same protocol (HBSS-AF647) in order control for dye aggregates, or unintentional labelling of host cell proteins by excess dye. For batch A, each isolation method had an input of 52.5 ml HES, while batch B had an input of 77.5 ml per isolation method. MODE-K cells were co-cultured with EV-AF647 from each batch in a 2-fold serial dilution: the highest dose was 4 µg and the lowest dose

was 0.5  $\mu\text{g}$ . Due to limited amounts of Batch B (UC), I treated cells with only two doses (4  $\mu\text{g}$  or 1  $\mu\text{g}$ ). MODE-K cells were imaged by fluorescence microscopy at 16 h post treatment to visualise uptake (Figure 5.1). Treatment with EV-AF647 with all batches showed detectable EV uptake by 16 h by fluorescence microscopy (Figure 5.1). Based on the (qualitative) microscopy, uptake varied between batches, and also individual MODE-K cells demonstrated higher levels of uptake than other cells (Figure 5.1).

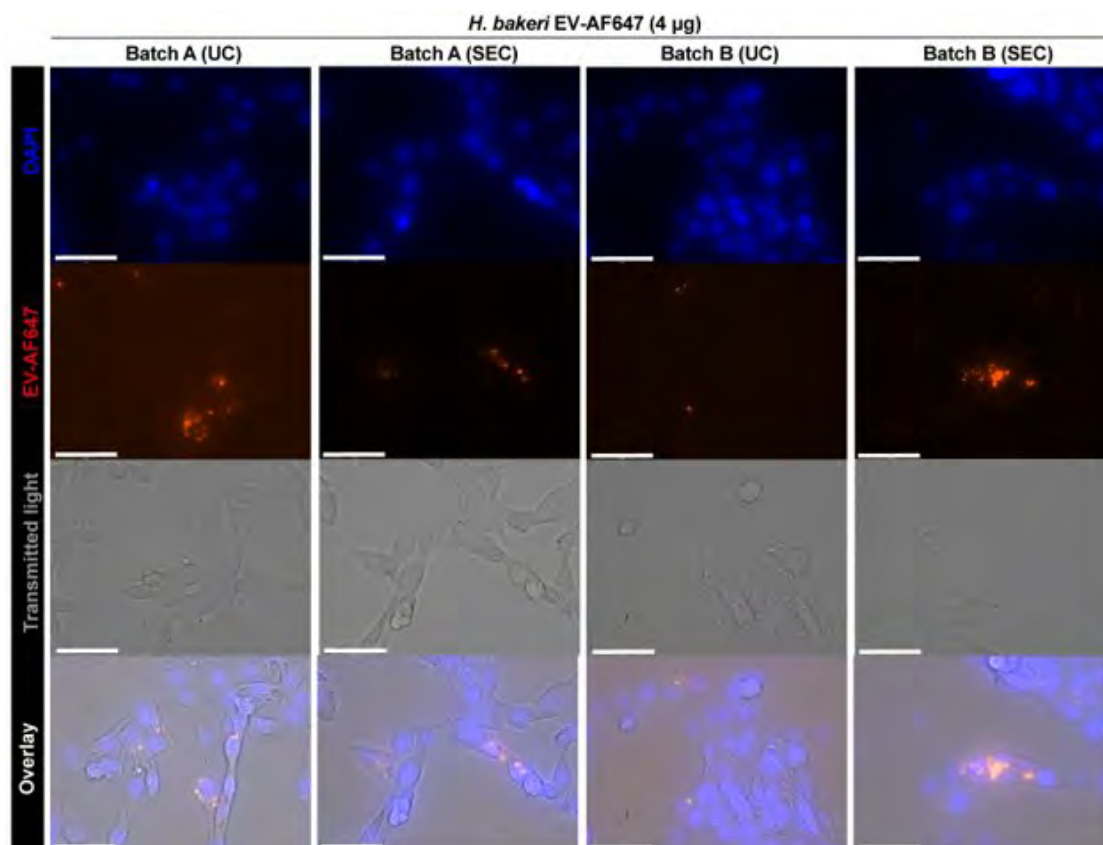


**Figure 5.1 | *H. bakeri* EV-647 uptake in MODE-K cells by fluorescence microscopy.** Fluorescence microscopy of MODE-K cells cultured with 4  $\mu\text{g}$  of *H. bakeri* EV-AF647 for 16 hr. Left to right columns, Batch A (UC), Batch A (SEC), Batch B (UC), Batch B (SEC). Rows top to bottom, DAPI staining of cell nuclei (blue), EV-AF647 labelled EVs (red), transmitted light for visualisation of cell boundaries (grey), overlay. Scale bar = 50  $\mu\text{m}$ .

Cells were then washed to remove EV-647 containing media and harvested for flow cytometry analysis of uptake. MODE-K cells showed dosage dependant EV-647 uptake detectable by flow cytometry (Figure 5.2 A, B & C) indicated by both an increase in median fluorescence intensity (MFI) (Figure 5.2 D) and the percentage of live single cells that were positive for EV uptake

(Figure 5.2 B) compared to untreated or HBSS-647 treated cells. HBSS-AF647 showed similar AF647 fluorescence to untreated MODE-K cells, indicating that there was little carry over of dye during purification (Figure 5.2). Uptake of EV-647 was dose dependant for all treatments, however the percentage of EV positive cells varied between isolation batches. An observable, but subtle shift of the population in AF647 fluorescence was noticed for EV-AF647 treated cells compared to controls, for all batches except Batch B (UC) (Figure 5.2 A&C). However, a proportion of cells demonstrated much higher fluorescence compared to the median of the population (Figure 5.2 A). This finding is interesting as it suggest that although a high proportion of MODE-k cells take up EV-AF647, some cells seem to have much higher propensity for uptake consistent with imaging data (Figure 5.1& Figure 5.2). I did not see large differences in proportions of uptake between UC or SEC isolated EVs for Batch A, but for Batch B SEC isolated EVs showed higher uptake than those isolated by UC. It should be noted that, Batch A was used freshly after labelling, whereas Batch B was frozen after labelling for practical purposes and thawed prior to treating cells (Figure 5.1 & Figure 5.2). EV batches that were labelled freshly prior to treatment (Batch A) showed higher detectable uptake than batches that were labelled and frozen until use (Figure 5.2 B&D). In hindsight this may have affected our results, as freeze thawing EVs has been described to damage EVs (Bachurski et al., 2019; Théry et al., 2018). However, because these isolations came from two independent batches of HES it is difficult to discern whether this reflects batch to batch variation in starting material, or whether this is a result of freeze thawing. Irregardless, for our future experiments I minimised freeze thaws for all experiments to one cycle and always labelled EVs fresh prior to use.



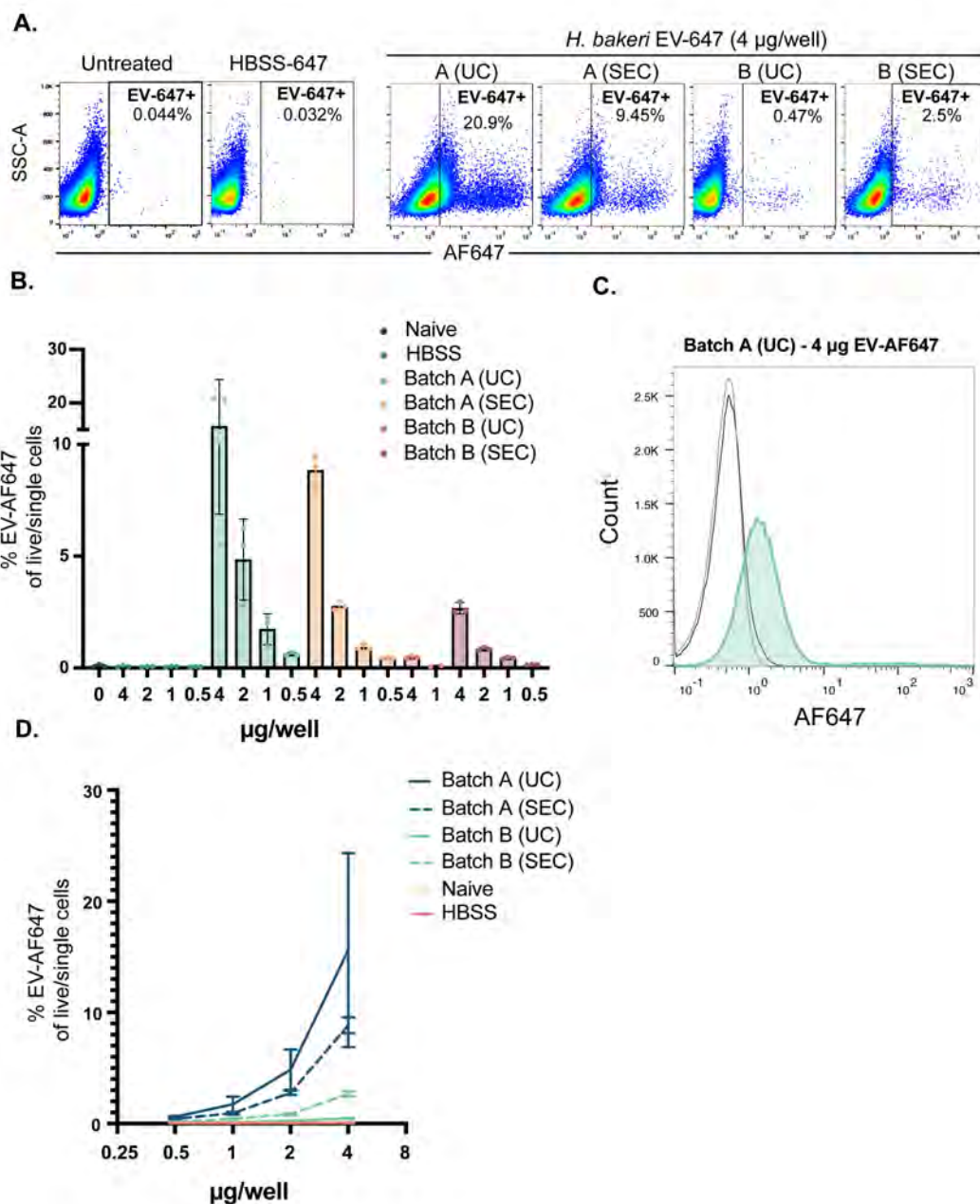


**Figure 5.2 | Uptake properties of *H. bakeri* EV-647 in MODE-K cells.** Flow cytometry analysis of EV-AF647 uptake in MODE-K cells at 24 h post treatment **A)** Representative FCS plots of AF647 fluorescence (x-axis) against SSC (y-axis) for single live cells in (left to right) naïve MODE-K cells, HBSS-AF647 treated, *H. bakeri* EV-AF647 treated for each batch treated with 4  $\mu$ g/well. EV-647+ gate was drawn based on AF647 fluorescence in the untreated MODE-K population. **B)** Percentage EV-AF647 positive cells of single live cells from each batch at each dose. **C)** Representative histogram for AF647 for naïve MODE-K cells (black line), HBSS-AF647 (grey line), Batch A (UC) EV-AF647 treated (green). **D)** Percentage EV-AF647+ cells as in C graphed against EV dose ( $\mu$ g/well).

## 5.2.2 Caecaloid cells take up *H. bakeri* EVs

We aimed to determine whether our 2-D enteroid cultures described in Chapter 4 of this thesis would take up *H. bakeri* EVs as hypothesised. Previously, experiments from former Buck lab members suggested that addition of *H. bakeri* EVs labelled with PKH67 to 3-D enteroid culture medium could be detected within 3-D enteroids after (Coakley, 2017). Prior to the development of 2-D enteroids cultures (Chapter 4 of this thesis) I first received training on 3-D and 2-D organoid culture methods from Dr. María Duque-Correa at Wellcome Sanger Institute using caecaloids. The experiments in this section (5.2.2) were performed during this time. Initially, I began by determining *H. bakeri* EV uptake in 3-D caecaloid cultures. Caecaloid cultures have many similarities to enteroids, however in the caecum Paneth cells are very rare, and the number of goblet cells are higher than in the caecum than the small intestine (Mowat & Agace, 2014). These regional differences are reflected in caecaloid and enteroids cultures (Duque-Correa, Schreiber, et al., 2020).

3-D caecaloid cultures were microinjected with *H. bakeri* EV-647 (at  $1.5 \times 10^8$  particles/ml). As a comparison I also injected AF647 labelled EVs derived from *T. muris*, a clade I nematode that naturally resides in the murine caecum (at  $1.7 \times 10^7$ /ml). Microinjected organoids were cultured for 24 h prior to fixing these cultures for immunofluorescence microscopy (Figure 5.3 & Figure 5.4). I detected evidence of *T. muris* uptake in 3-D caecaloids, while *H. bakeri* EV-AF647 were detected near to nuclei on the basolateral side of 3-D organoids it was less clear if uptake had occurred, furthermore it was more difficult to identify instances of uptake (Figure 5.3 & Figure 5.4). Signal of EV-AF647 was also identified in the central lumen where dead cells and mucus accumulate (Figure 5.3, Supplemental file 3 & Supplemental file 4). Z-stack images were taken of microinjected 3-D caecaloids and images were converted into video files that can be viewed for greater detail (Supplemental file 3 & Supplemental file 4).

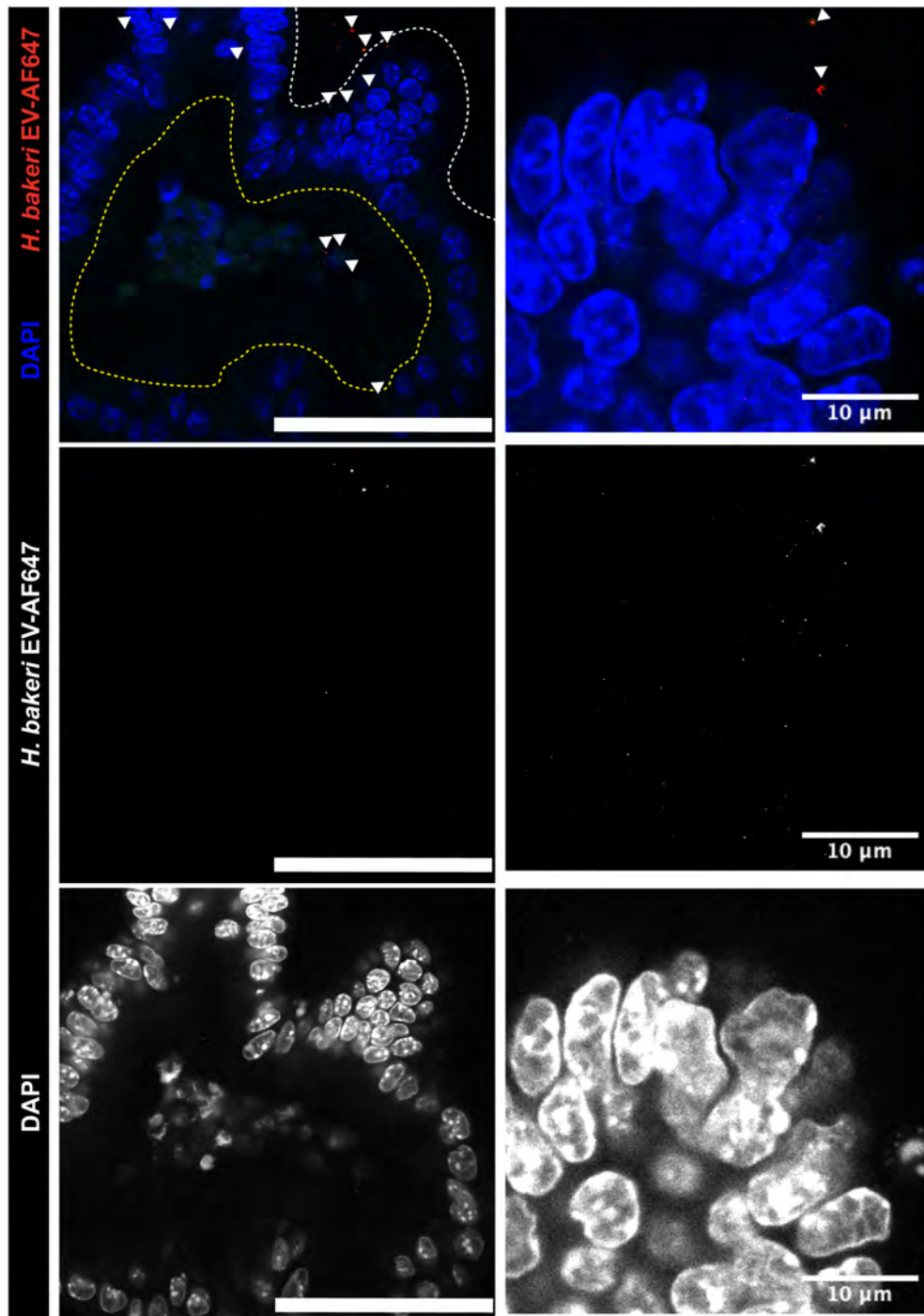


**Figure 5.3 | *H. bakeri* EV-AF647 microinjection of 3-D caecaloids.** 3-D caecaloids microinjected with *H. bakeri* EV-AF647 ( $1.5 \times 10^8$  particles/ml) and processed for microscopy 24 h later. Top row overlay of DAPI staining nuclei (blue), *H. bakeri* EV-AF647 (red). Middle row shows the single channel of *H. bakeri* EV-AF647 (grey), and bottom row shows single channel image of DAPI staining nuclei (grey). Right hand column is a zoom in of the left-hand column. Right hand column scale bar = 50  $\mu\text{m}$ , left hand column scale bar = 10  $\mu\text{m}$ . Yellow dotted line = approximation of caecaloid lumen, white dotted line = approximation of basal boundary of caecaloid, white arrows indicate *H. bakeri* EV-AF647.

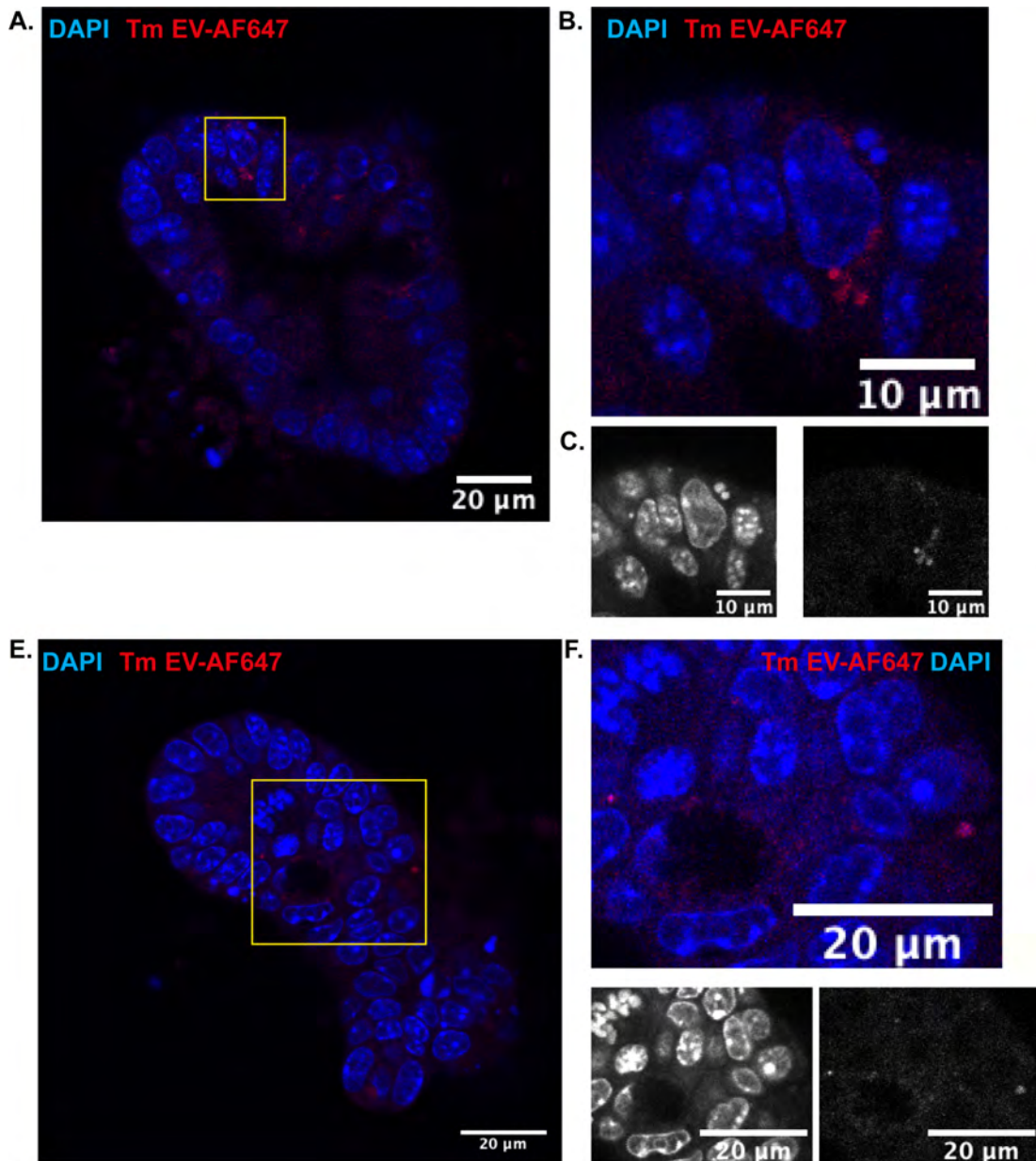


**Figure 5.4 | *T. muris* EV-AF647 microinjection of 3-D caecaloids.** 3-D caecaloids microinjected with *T. muris* EV-AF647 ( $1.7 \times 10^7$  particles/ml) and processed for microscopy 24 h later. **A)** Overlay of 3-D caecaloid DAPI staining nuclei (blue) and *T. muris* EV-AF647 (red). Uptake highlighted by yellow box. **B)** Zoom in of yellow box in A. **C)** Single channel image of DAPI staining nuclei (left-hand side) and *T. muris* EV-AF647 (right-hand side) **D-F)** Same as A-C, of another organoid. Scale bars length indicated on each image.

Finally, I also treated both flat caecaloids and transwell 2-D caecaloids with  $7 \times 10^8$  particles/ml of *H. bakeri* EV-AF647, or *T. muris* EV-647, for 24 h and assessed uptake by microscopy. Flat organoid cultures are grown by dissociating 3-D organoids into single cells before seeding onto ibidi  $\mu$ -slides pre-coated with Collagen I (Duque-Correa, Maizels, et al., 2020). Flat caecaloid cultures demonstrated uptake of both *H. bakeri* EV-AF647 and *T.*

*muris* EV-AF647 (Figure 5.5). However, in flat cultures I stained for goblet cells using the lectins SNA/UEA and could not identify any differentiation of these cells. For 2-D caecaloids I did not find evidence of uptake of *H. bakeri* EV-AF647 in this experiment. For *T. muris* EV-AF647 I could easily identify labelled EVs on 2-D caecaloids, but most appeared to not be within epithelial cells (Supplemental Figure 2).

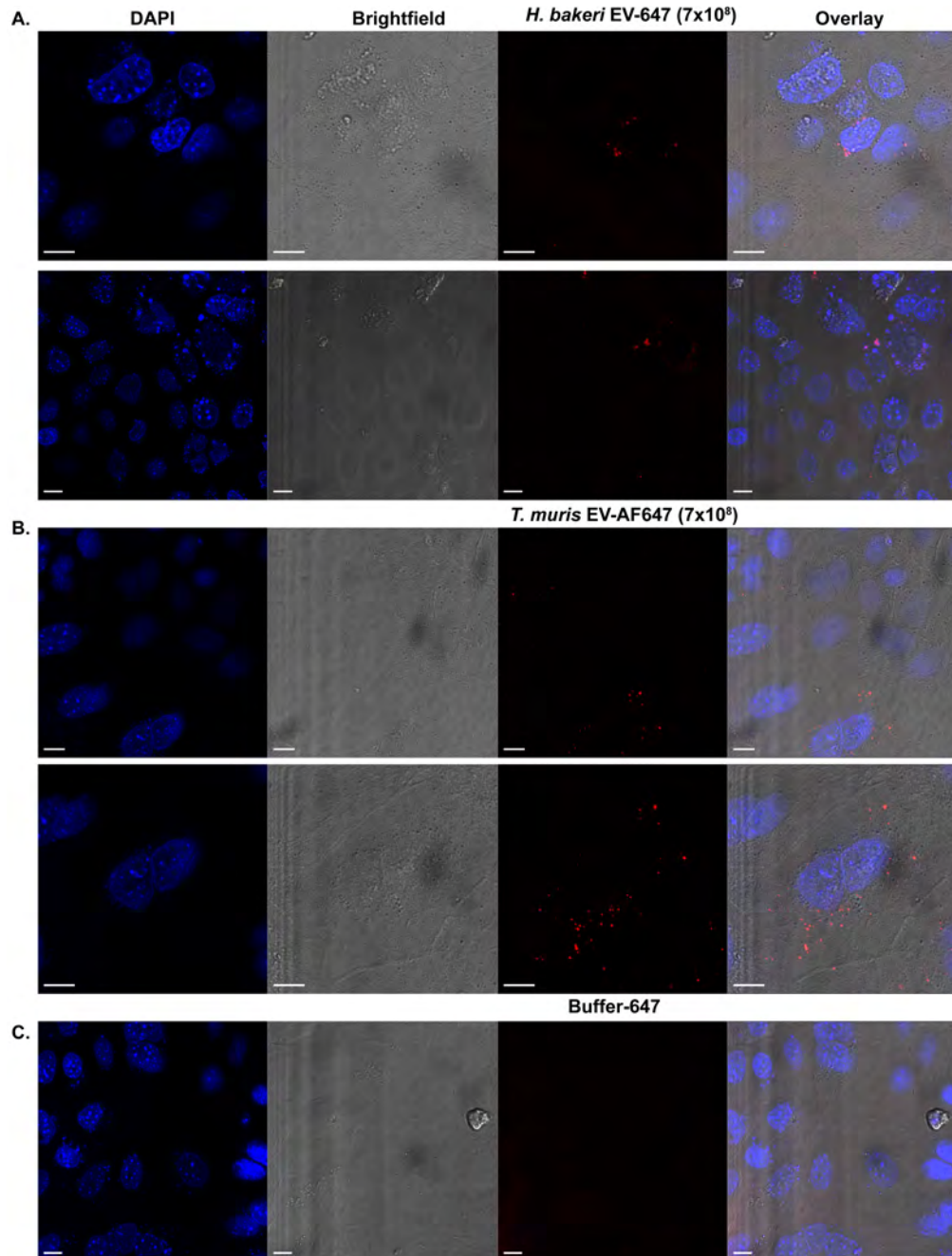


**Figure 5.5 | *H. bakeri* EV-647 uptake in flat caecal organoids.** Confocal microscopy of flat caecaloid cultures treated with **A&BH. bakeri EV-647 (7x10<sup>8</sup> particles per well) for 24 h **C**) Flat caecal organoids**

treated with equivalent volume of HBSS buffer AF647 labelled for 24 h. Columns from left-hand side to right-hand side DAPI (nuclei) in blue, Brightfield in grey, EV-647 in red, overlay image.

### 5.2.3 *H. bakeri* EVs enter 2-D enteroid cells

Once 2-D enteroid cultures were validated to recapitulate the major features of the small intestinal epithelium (Chapter 4), I aimed to assess whether *H. bakeri* EV-AF647 enter cells within these cultures. Previous data showed that by day 3 post seeding, 2-D enteroids have formed complete monolayers, proliferative cells have formed loci and goblet cells have differentiated (Chapter 4). I therefore grew 2-D enteroids for 3 days before treating with 20 µg/ml of *H. bakeri* EV-AF647 (this is equivalent to 4 µg/ well in 200 µl media) for 24 h before washing, harvesting and analysing the cells by flow cytometry (Figure 5.6 A). A major question in this thesis is whether *H. bakeri* EVs target specific cell types for uptake. I reasoned that tuft and goblet cells, which are critical for anthelmintic responses, could be targeted by *H. bakeri* EVs for uptake in order to modify their function. To be able to test this, I grew organoids in the presence or absence of IL-4 and IL-13 (50 ng/ml each) from day 2 post seeding which induces the differentiation of tuft and goblet cells (Chapter 4). I assessed whether organoids grown with cytokines IL-4 and IL-13 demonstrate *H. bakeri* EV uptake which would implicate goblet and/or tuft cells as target populations. Here I present two independent experiments side-by-side, these were not pooled due to using different cytometers. Furthermore, each batch of *H. bakeri* EV-AF647 was compared for uptake in 2-D enteroids and in MODE-K cells for a minimum of one replicate. MODE-K uptake of EV-AF647 serves as a positive control and as demonstrated in these data, accounts for batch-to-batch variation seen for EV-AF647 batches. Representative FCS plots and gating of EV-AF647 positive cells showed a subtle shift in AF647 of the population in *H. bakeri* EV-AF647 treated samples compared to untreated 2-D enteroids (Figure 5.6 B). In two independent experiments *H. bakeri* EV-AF647 treated 2-D enteroids showed a significant increase in the percentage of EV-AF647 positive single live cells compared to both the naïve and HBSS-AF647

controls, evidencing EV uptake in 2-D enteroids (Figure 5.6 C). MODE-K cells showed consistently higher uptake of *H. bakeri* EV-AF647 than 2-D enteroids by percentage of live single cells EV-AF647 positive and AF647 fluorescence (Figure 5.6 C&E). Interestingly, the percentage of EV-AF647 positive cells was much higher within the dead 2-D enteroid cells (20-80%) (Supplemental Figure 3). This raised the question of whether *H. bakeri* EV treatment induced cell death, however I found no evidence that *H. bakeri* EVs induced higher amounts of death (Supplemental Figure 3). Dead and dying cells expel their contents and DNA, which is sticky and could trap *H. bakeri* EVs. *H. bakeri* EV-AF647 uptake in 2-D enteroids grown in the presence of IL-4 and IL-13 had contradicting effects on uptake in two independent experiments, leading to inconclusive findings. Experiment 1 (Expt 1) indicated no significant difference was seen for the percentage of live single cells that were EV-AF647 positive (Figure 5.6C). However, experiment 2 (Expt 2) showed a significantly lower EV-AF647 uptake when 2-D enteroids were grown in presence of cytokines by the percentage of single live cells that are EV-AF647 positive (Figure 5.6 C). MODE-K cells treated with EV-647 demonstrated a strong shift in fluorescence of the entire population, while 2-D enteroids treated with EV-647 results in only a minimal shift in fluorescence compared to naïve or HBSS-647 (Figure 5.6 E)

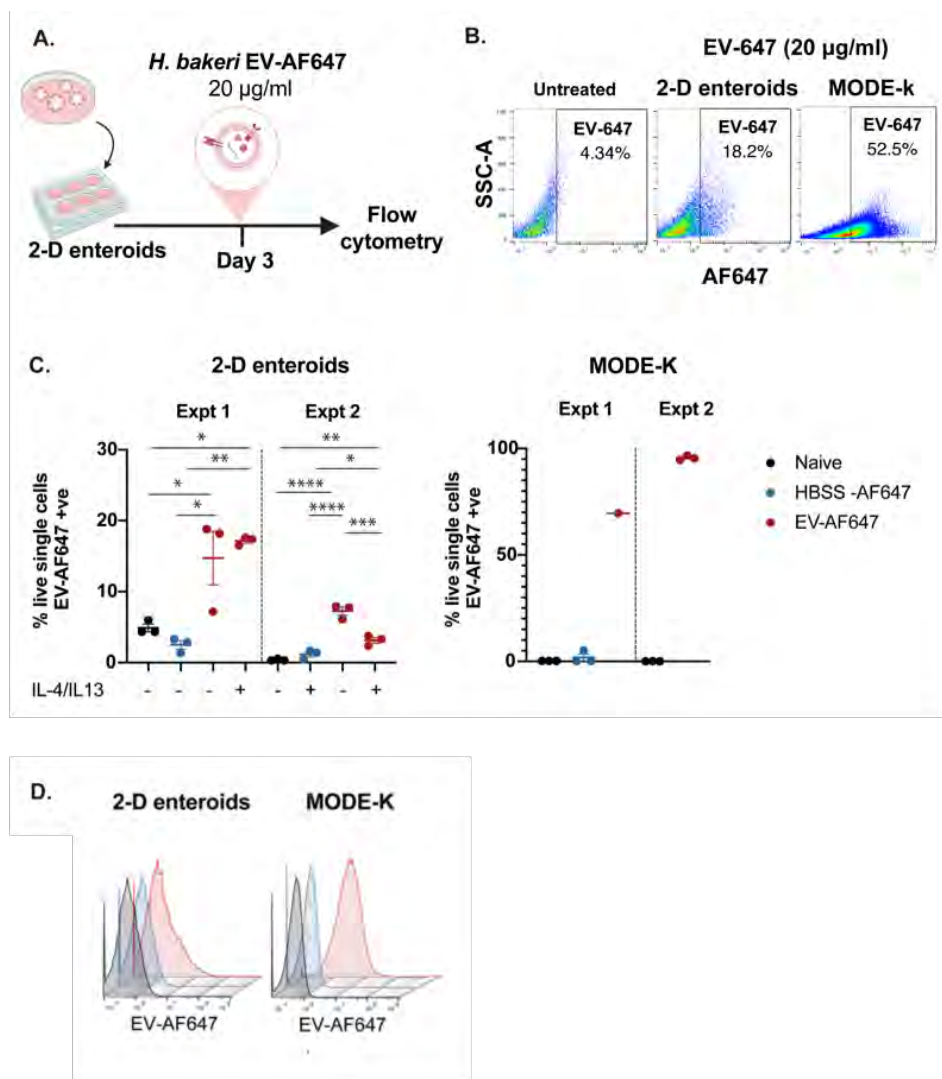


**Figure 5.6 | *H. bakeri* EVs are taken up by cells in 2-D enteroid cultures.** **A)** Schematic of experimental design **B)** Representative samples demonstrating gating of EV-647 positive of live single cells in untreated or 2-D enteroids and MODE-K cells treated with 4 µg of *H. bakeri* EV-647. **C)** Percentage of live single cells that are EV-647 positive in either 2-D enteroids (left-hand side) or MODE-K cells (right-hand side) each condition, blue = untreated 2-D enteroids, green = HBSS-647, pink = EV-647 the presence of IL-4 & IL-13 in enteroid culture is signified along the x-axis. **D)** Representative histograms of naïve (black), HBSS-AF647 (blue) and EV-AF647 (red) treated 2-D enteroids or MODE-K cells. **C-D)** Mean values  $\pm$  SD are plotted for each group (n = 1-3). One-way ANOVA used for significance testing. \* =  $p < 0.05$ , \*\* =  $p < 0.01$ , \*\*\* =  $p < 0.001$ , \*\*\*\* =  $p < 0.0001$ .

#### 5.2.4 Searching for evidence of *in vivo* *H. bakeri* EV uptake

Identifying *H. bakeri* EV uptake *in vivo* is not trivial, as EVs cannot be easily genetically modified to express fluorescent proteins and antibodies that



recognise *H. bakeri* EVs are not currently available (Lendner et al., 2008). I generated  $\alpha$ -EV serum as previously described (Chapter 3), in brief rats were immunised with isolated *H. bakeri* EVs and serum collected. A-EV serum has since been shown by other lab members to successfully label single EVs (Thomas Fenton, personal communication). I aimed to identify *H. bakeri* EVs within host cells by immunofluorescence microscopy of infected intestinal tissue (d 14 p.i.) using  $\alpha$ -EV serum on the ZEISS Airyscan (LSM880). A-EV serum combined with a secondary antibody which recognises rat IgG (AF555) successfully detects *H. bakeri* parasites within the intestinal lumen of infected mice compared to naïve rat serum, although naïve rat serum showed some non-specific background (Figure 5.7).  $\alpha$ -EV serum detected small particles which I define putatively as secreted EVs in the surrounding region (Figure 5.7). However, when I interrogated intact epithelial villi nearby to worms were unable to confidently identify EV signal (data not shown).

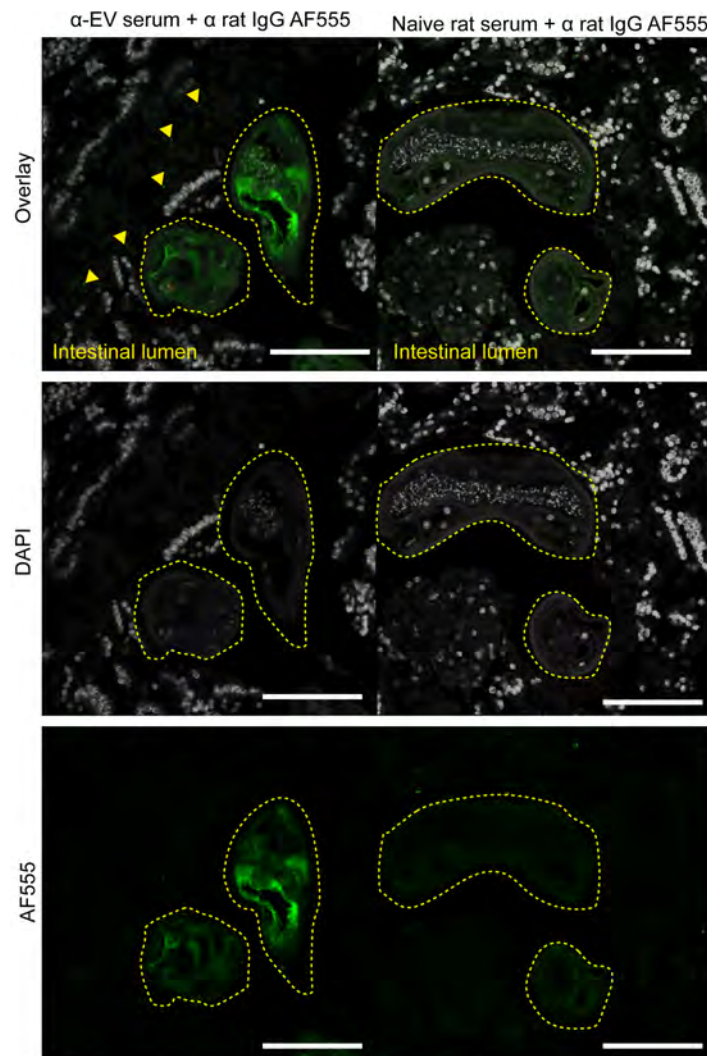


**Figure 5.7 |  $\alpha$ EV sera recognises *H. bakeri* parasites.** Immunofluorescence Airyscan microscopy of *H. bakeri* worms in the intestinal lumen of infected mice at day 14 p.i. Left-hand column  $\alpha$ -EV serum AF555 (green), nuclei stained with DAPI (grey). Right-hand column naïve rat serum control and  $\alpha$ -rat IgG AF555 (green). Rows top to bottom, overlay, single channel DAPI, single channel AF555. Scale bars = 100  $\mu$ m. Yellow dotted line indicates parasites boundaries; yellow triangles indicate putative EV signal outside of worms.

In order to enrich for signal, I performed intraluminal injection of *H. bakeri* EVs into small intestinal ligated loops (referred to as “gut loops”) under anaesthesia (Fukuda et al., 2011). Mice were anaesthetised surgically, and a section of small intestine was ligated surrounding a Peyer’s patch. Each mouse (n = 6) received two ligations: one was injected with PBS as a control, and the second with unlabelled *H. bakeri* EVs. Mice remained anaesthetised for a total of 1.5 h prior to sacrifice and harvesting and processing of tissue for microscopy. I detected *H. bakeri* EV within the lumen of *H. bakeri* EV injected tissue (Figure

5.8 A). EVs were detected at the surface of intestinal epithelium villus cells, however it was difficult to confirm if these represent internalised EVs as I did not include a stain for cell surface such as phalloidin, or for the brush border such as villin (Figure 5.8 B). The control of naïve rat serum showed a low level of none specific background (Figure 5.8 C).

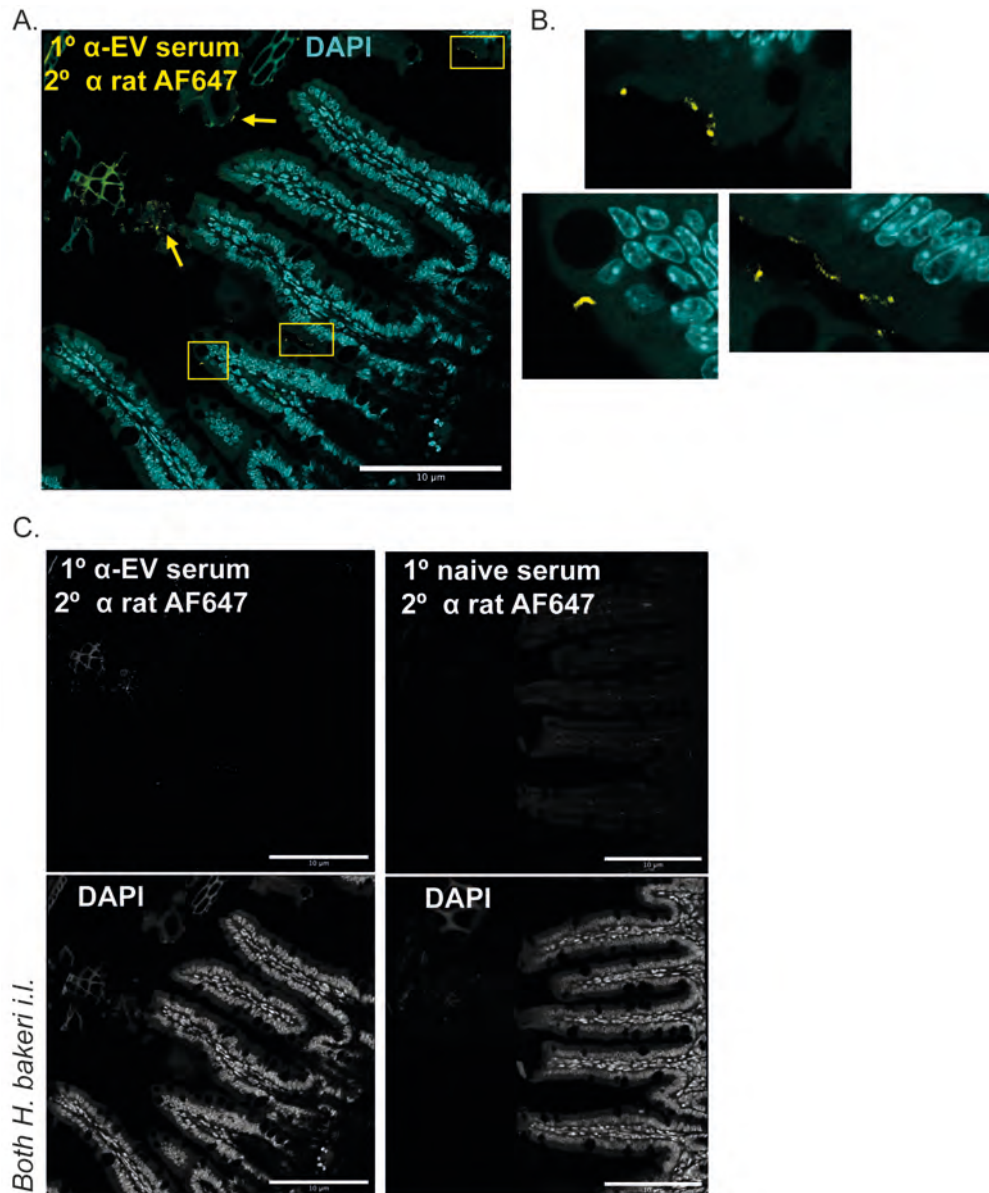


**Figure 5.8 | Searching for *H. bakeri* EV uptake in gut loop tissue.** Immunofluorescence Airyscan microscopy of gut loop sections injected with *H. bakeri* EVs. DAPI staining cell nuclei in the intestinal epithelium (cyan), **A**) *H. bakeri* EVs injected intraluminally and detected by anti-EV antibody. Yellow arrows indicate EVs and potential uptake indicated by yellow boxes **B**) Close up images of yellow boxes from A showing possible uptake **C**) Grey scale images of *H. bakeri* EVs detected by (top right-hand column) α-EV serum primary antibody or (top left-hand column) naïve rat serum control primary antibody followed by α-rat IgG AF555 secondary and DAPI staining for each (bottom row). Scale bars = 10 μm.

### 5.3 Discussion

A growing number of publications demonstrate the ability of helminth derived EVs to enter and modify host cells in various contexts (Drurey & Maizels, 2021; Sánchez-López et al., 2021). The majority of research to date has focused on *in vitro* homogenous cell line cultures, with only minimal instances of systems that contain multiple cell populations such as organoids (Eichenberger, Ryan, et al., 2018). There are now several examples of helminth EVs modulating host immune responses *in vivo* (Drurey & Maizels, 2021; Sánchez-López et al., 2021). Furthermore, the idea that EVs play an important role during infection, possibly through immune modulation, is supported by the fact that vaccination of animals using EVs results in protective immunity (Coakley, 2017). Yet, the true cellular target of helminth EVs during natural infection, and their functional role remains unknown. In this chapter I aimed to further understanding of *H. bakeri* EV uptake within the intestinal epithelium. I used multiple models for this investigation increasing in complexity from the homogenous cell line MODE-K, to organoid models, and finally I searched *in vivo* within the small intestine for evidence of *H. bakeri* EV uptake.

We found that *H. bakeri* EVs are taken up by MODE-K cells in a dosage dependant manner (Figure 5.1 & Figure 5.2). *H. bakeri* EVs uptake events in organoid cultures were shown as proof-of-principle using flat and 3-D caecaloid cultures by microscopy (Figure 5.3 & Figure 5.5) however events were rare, and I did not find uptake in 2-D caecaloid models (data not shown). *H. bakeri* EVs are taken up by at least a proportion of cells within 2-D enteroids evidenced by flow cytometry (Figure 5.6). *In vivo* intraluminal injections of *H. bakeri* EVs was performed and may show EV uptake (Figure 5.8). However, progression of current methods for antibody-based detection of *H. bakeri* EVs is required to further investigate these tissue samples.

2-D enteroids are capable of taking up *H. bakeri* EVs exemplified by flow cytometry analysis, however 2-D enteroids displayed lower uptake than MODE-K cells in side-by-side comparisons (Figure 5.6). These data suggest that *H. bakeri* uptake occurs in a cell type and context dependant manner

consistent with previous findings which showed that *H. bakeri* EV uptake is higher in macrophages than epithelial cells (Coakley et al., 2017). Even within homogenous cultures of MODE-K cells there is evidence of a population of 'high' uptake cells qualitatively observed by fluorescence microscopy and confirmed by flow cytometry (Figure 5.1 & Figure 5.2). It is intriguing that within a homogenous cell line some cells take up higher amounts of *H. bakeri* EVs than the bulk of the MODE-K population (Figure 5.2). Evidence from cancer-cell derived EVs has suggested that the cell cycle stage of recipient cells can affect EV uptake, authors saw increased EV uptake when recipient cells were in G<sub>2</sub>/M phases of cell cycle (A. H. Buck et al., 2014; Vidal et al., 1993). As MODE-K cells were not synchronised for experiments, cell cycle could be one explanation for the presence of high uptake cells, however further investigation would be required to confirm this hypothesis. Extending this hypothesis to the context of 2-D enteroids, this could be one explanation for the lowered uptake in these cultures, as only a proportion of cells are capable of undergoing cell cycle (stem cells, TA cells and to a lesser extent secretory progenitors). Whether cell cycle influences uptake in 2-D enteroid cultures could be investigated further by similar flow cytometry analysis combining Ki67 staining and other cell cycle markers, with EV-AF647.

There are several other reasons that may explain why 2-D enteroids may display lower *H. bakeri* EV uptake in these experiments than MODE-K cells. Firstly, uptake could be specifically targeted to a certain cell type. MODE-K cells are immortalised intestinal epithelial cells derived from murine duodenum, and most closely represent the enterocyte fraction of the epithelium (Vidal et al., 1993). On the other hand, organoid cultures contain mixed population of cells including enterocytes, CBCs, TA, Paneth, goblet, enteroendocrine and tuft cells, but enterocytes constitute the bulk of these cultures (Chapter 4 & Chapter 6 of this thesis). Therefore, if enterocytes were specifically targeted by *H. bakeri* EVs, it is unlikely that changes in cell composition alone would explain such differences in uptake when compared to MODE-K cells. At the same time, 2-D enteroids produce a mucus layer, and due to their rapid proliferation and turnover dead cells accumulate on their surface. These two

factors together could present a substantial barrier to EV uptake, and indeed in both experiments I identified a high proportion of dead cells that were EV-AF647 positive (Supplemental Figure 3). Dead cells are well known to have increased autofluorescence which could be confused for true EV-AF647 signal, however AF647 fluorescence in naïve cells gives us an indication of background fluorescence and is much lower than EV-AF647 treated cells (Supplemental Figure 3). It is likely that dead cells indeed capture *H. bakeri* EVs, consistent with observations by microscopy (data not shown) but EV treatment itself did not induce differences in the proportion of dead cells (Supplemental Figure 3).

We hypothesised that goblet and tuft cells could be targets of EVs due to their role in anthelmintic responses. Addition of cytokines IL-4 and IL-13 in 2-D enteroid basal growth media successfully induces tuft and goblet cells (Chapter 4). I compared uptake of *H. bakeri* EV-AF647 in the presence or absence of cytokines to identify whether higher proportions of these cells would increase overall EV-AF647 uptake. It is important to note that culturing 2-D enteroids in the presence of these cytokines has other implications on the cultures, alongside goblet cell induction you also have increased mucus production that could trap EVs preventing uptake. I also observed a strong reduction in stem cell specific marker gene (*Lgr5*) in these cultures when grown in the presence of IL-4 and IL-13 suggesting a reduction of stem cells, or a change in their functions (Chapter 4). Results were inconclusive, in two independent experiments I observed opposing effects, the first showed only a significant increase in uptake by MFI, while the second showed a significant reduction of uptake in the presence of cytokines by both the percentage of single live EV-AF647 positive cells and MFI (Figure 5.6).

Finally, 2-D enteroids unlike MODE-K cell cultures have an underlying ECM mimic provided by a thin layer of Matrigel® and below this a physically separated basal compartment. It is possible that 2-D enteroid models therefore allow for transcytosis of material from the apical epithelium to the underlying basal compartment. It is possible that EVs could be internalised in 2-D models and re-released into the basal compartment. Recent work using EVs derived

from HEK293T cells demonstrated as proof-of-principle that EVs can be internalised by HeLa cells, and re-released intact (O'Brien et al., 2022). Enterocytes and more recently, goblet cells, have known functions in transcytosis for the delivery of antigen across the intestinal epithelium however whether transcytosis of intact *H. bakeri* EVs could occur is unknown (Gustafsson et al., 2021; Zimmer et al., 2016).

### 5.3.1 Limitations

Data in this chapter was mostly generate prior the discovery of low labelling efficiency (described in Chapter 3) and this likely limited our ability to detect uptake. This also likely underpinned difficulty identifying uptake by microscopy. If only a small fraction of 2-D enteroid cells take up AF647 labelled EVs, it is not trivial to identify these instances, this difficulty is amplified by the fact that high magnification lens (60x – 100x) are required for high confidence identification of these nano particles meaning only small areas can be scanned at a time.

An alternative approach is identification of *H. bakeri* EVs using EV specific antibodies. At the time of this work, I had only generated  $\alpha$ -EV serum for EV detection. Our  $\alpha$ -EV serum successfully identified worms, and surrounding EVs, in infected tissues (Figure 5.7), as well as specifically binding single *H. bakeri* EVs in super resolution microscopy experiments (*Thomas Fenton, personal communication*). I used this to detect intraluminal injected *H. bakeri* EVs in paraffin embedded tissue sections and found detection of EV size particles within the lumen (Figure 5.8). Detection of uptake was low and close to background in control samples. Furthermore, the time constraints for which animals could be anaesthetised (1.5 h) may also limit detection. Previously, while some *H. bakeri* EVs are taken up by 1 h post treatment in MODE-K cells uptake was low compared to 24 h (A. H. Buck et al., 2014). In contrast studies using latex beads of a similar size to EVs, or studying uptake of intraluminally

injected bacteria do see quick uptake into the Peyer's patch and suggesting this may not be the key limiting factor effecting detection of EVs.

### 5.3.2 Future directions

*H. bakeri* EVs are taken up within 2-D enteroids, however whether specific cells are targeted remains an open question. Advancements have been made recently in our laboratory in antibody detection of *H. bakeri* EVs through development of antibodies against EV cargo proteins (SID2, exWAGO). Tissue from intraluminal injected mice can be re-assessed using these antibodies for detection of EV uptake. Additionally, thus far I have only focused on assessing *H. bakeri* EV uptake in the epithelium of intraluminal injected tissue. However, it is possible that this is not a major target of *H. bakeri* EVs during infection, analysis of sections containing Peyer's patches and overlaying M cells from the same tissue will provide insight into cell type specificity for *H. bakeri* EVs in these sites.



**Chapter 6: Functional effects of *H. bakeri* on 2-D enteroids**

**Abstract**

The intestinal epithelium plays important roles in the immune response to helminths and is the primary tissue associated with *H. bakeri* during infection. Only a limited number of studies have used organoids to investigate interactions between helminths and the host epithelium and all have used 3-D models. I aimed to investigate the host epithelial response to both *H. bakeri* parasites, its purified excretory/secretory (ES) products or isolated EVs to determine direct effects of helminths on the epithelium. I used bulk RNA sequencing of treated 2-D organoids to identify changes to specific cell types of the intestinal epithelium. Many changes induced by live parasites were also replicated by delivering ES or EVs alone but to a lesser extent. Changes induced by *H. bakeri* primarily reduced cell cycle, antimicrobial response genes, and suppressed key genes related to stemness. The data in this chapter adds to existing knowledge of how helminths modify the host intestinal epithelium during infection.

## 6.1 Introduction

Over the last decade mounting evidence has emerged demonstrating that EVs derived from a diverse range of helminth species can modulate host cells; supporting the hypothesis that helminth EVs represent a mechanism of host-parasite communication (Drurey & Maizels, 2021; Sánchez-López et al., 2021). EVs released by *H. bakeri* can enter the murine epithelial cell line model MODE-K, which most closely represent the enterocytes of the host epithelium, resulting in differential gene expression and suppression of immune related genes *Il1rl1* (ST2) and *Dusp1* (Buck et al., 2014; Vidal et al., 1993). Additionally *H. bakeri* EVs can also enter bone marrow derived macrophages (BMDMs), repress expression of ST2 and abrogate their activation *in vitro* (Coakley et al., 2017). Abrogated activation was maintained in BMDMs from ST2 KO mice treated with *H. bakeri* suggesting additional mechanisms are involved in macrophage suppression (Coakley et al., 2017). Collectively those data demonstrate a role for *H. bakeri* EVs in immune suppression *in vitro* (Coakley et al., 2017). *In vivo* delivery of *H. bakeri* EVs reduced the severity of allergic asthma in the *Alternaria* model (described Chapter 1 of this thesis); resulted in fewer lung eosinophils, and a reduction in both the number and function of ILC2s in the lung (Buck et al., 2014). Immunomodulation in the lung demonstrates the *in vivo* capabilities of *H. bakeri* EVs, however during the natural infection adult *H. bakeri* parasites reside in the duodenum of the intestine and here we know relatively little about the natural targets of *H. bakeri* EVs.

During chronic infection when adult *H. bakeri* reside in the intestinal lumen, parasites are faced with the complex barrier of the intestinal epithelium. Several factors make the intestinal epithelium a likely target of *H. bakeri* EVs i) it is the most proximal tissue during the adult stage of *H. bakeri* lifecycle (Camberis et al., 2003) ii) it forms a multi-layered (mucus layer and cellular layer) contiguous barrier that tightly regulates what can pass through it (Beumer & Clevers, 2020; Sharpe et al., 2018) ii) it plays a key role in sensing the presence of helminths and relaying this information to immune cells

(Coakley & Harris, 2020; Howitt et al., 2016; McGinty et al., 2020; Von Moltke et al., 2016) and iii) during infection it significantly modifies its cellular composition (Kamal et al., 2002; Khan et al., 2001; Nusse et al., 2018; Von Moltke et al., 2016), mucus production and physiology to mediate parasite clearance (Coakley & Harris, 2020). Many alterations to the epithelium during infection have been reported to be driven by the Th2 cytokines IL-4 and IL-13 that are released by ILC2s, Th2 cells and AAMs (Anthony et al., 2007; Coakley & Harris, 2020). A number of studies in recent years have also shown that the excretory-secretory products from *H. bakeri* modulate the intestinal epithelium (Drurey et al., 2021; Karo-Atar et al., 2022). Whether *H. bakeri* EVs enter the intestinal epithelium and interfere with infection processes in this tissue is not well understood. Although *H. bakeri* EVs can enter MODE-K cell line *in vitro* this homogenous cell line does not reflect the cellular diversity and physiology of the intestinal epithelium *in vivo*.

Organoid models offer enhanced recapitulation of the intestinal epithelium as detailed in chapter 4 of this thesis. Our lab, in collaboration with Maria Duque-Correa at the Sanger institute, had previously generated pilot data by microinjection of 3-D organoids with *H. bakeri* EVs suggesting they modified the stem cell niche (Buck lab, unpublished). Recent publications have utilised organoids to unravel the effects of *H. bakeri* infection, or of total HES on the intestinal epithelium. Organoids isolated from *H. bakeri* infected mice during the L4 larval stage (day 6 p.i.) and adult stage of infection (day 14 p.i.) are morphologically distinct displaying higher proportion of cystic phenotypes compared to those from naïve mice (Drurey et al., 2021; Karo-Atar et al., 2022; Nusse et al., 2018). Concordantly, *H. bakeri* infection results in a transcriptional reprogramming of stem cells characterised by downregulation of classic ISC genes *Lgr5* and *Olfm4*, and expression of genes associated with the fetal epithelium (*Clu*, *Ly6a*, *Il1rn*, *Anxa1*) resulting in the conversion to revival stem cells (revSCs) (Karo-Atar et al., 2022; Nusse et al., 2018). revSCs are enriched in organoids derived from intestines of infected mice, at both day 6 and 14 p.i. with higher numbers of these cells at day 14 p.i. (Karo-Atar et al., 2022). Culturing organoids in the presence of HES also replicates the cystic

morphology and induction of revSC seen in organoids derived from infected tissue (Drurey et al., 2021; Karo-Atar et al., 2022). These data suggest that effects on the intestinal epithelium during infection are mediated by secreted products (Drurey et al., 2021; Karo-Atar et al., 2022). HES treatment of organoids also modifies the transcription of genes that are critical for differentiation of certain cell types. For example, HES downregulated gene markers of secretory cell subtypes such as tuft cells (*Dckl1*, *Pou2f3*), Paneth cells (*Lyz1*), goblet cells (*Spdef*, *Muc2*, *Clca1*), and enteroendocrine cells (*Neurog3*) as well as *Atoh1* which is critically required for their upstream secretory progenitor (Drurey et al., 2021; Karo-Atar et al., 2022). Consistent with this data HES treatment upregulated the absorptive marker gene *Hes1*, which is expressed in a mutually exclusive fashion with *Atoh1* (Drurey et al., 2021; Karo-Atar et al., 2022). Subsequent investigation confirmed the suppression of tuft cell differentiation by *H. bakeri* in organoids and *in vivo* (Drurey et al., 2021).

While it is clear that HES are capable of inducing substantial changes in the intestinal epithelium, the individual molecules that induce these changes is unknown and the specific contribution by *H. bakeri* EVs has not been investigated. One limitation of previous studies is the use of 3-D organoids, in which the apical epithelium is not easily accessible and therefore basal delivery is required which does not reflect the localisation of adult worms *in vivo* (Ruby White et al., 2022). To understand the host response in the intestinal epithelium to *H. bakeri* EVs, I treated 2-D organoid cultures with either *H. bakeri* EVs, or HES depleted of EVs (EVdepHES) and performed RNA-sequencing (RNA-seq) analysis. Differential gene expression in host intestinal epithelium after *H. bakeri* EV treatment was then used to understand i) which genes and processes are modified in this host tissue by *H. bakeri* EV and by non-vesicular components of EVdepHES ii) provide a physiological dataset of host gene expression for target prediction between *H. bakeri* 22G RNAs and host genes.

In parallel, I also compared the effect of co-culture with *H. bakeri* with our 2-D organoids. *In vivo* it is difficult to untangle helminth driven changes in the

epithelium from those driven by the host immune response. For example although HES abrogates and constrain tuft cell differentiation, overall tuft cell numbers are increased in infected mice compared to naïve due to the high levels of IL-4 and IL-13 cytokines (Drurey et al., 2021). Therefore, live co-culture allows investigation of the response to whole parasites in the absence of immune drivers, and can be compared to changes induced by purified ES products such as EVs and EVdepHES.

Prior to this thesis, other investigators had infected ovine and bovine abomasum 3-D organoids with live larval stage parasites from *T. circumcincta* and *O. ostertagi* respectively, and showed they can invade into the lumen of 3-D organoids (Faber et al., 2022; D. Smith et al., 2021). However, invasion to the apical side is inefficient, doesn't reflect infection dynamics and causing damage to the organoid limiting the length of these studies (Ruby White et al., 2022). Our 2-D organoids uniquely allows for the co-culture of helminths either on the apical epithelial surface, or in the basal compartment depending on the life stage and helminth (Ruby White et al., 2022). To investigate the impact of apical or basal delivery, adult worms were co-cultured either apically or basally, in addition I co-cultured L4 stage *H. bakeri* in the basal compartment reflecting *in vivo* localisation. Demonstrating for first-time co-culture of live *H. bakeri* with organoids. After 24 h worms were removed and RNAseq performed on the intestinal epithelium.

Finally, one of our major aims was to determine if *H. bakeri* EVs specifically target certain cell subtypes within the epithelium. Our RNAseq analysis showed changes to several cell type specific genes indicating EVs may either target or have a specific affect for certain populations. To address this hypothesis, I performed scRNA-seq after treatment with *H. bakeri* EVs, EVdepHES or a mock control (n = 1). In addition, because I know tuft cells are rare in our 2-D organoids in the absence of Th2 cytokines IL4 and IL13, I performed this experiment in the presence of this cytokines in order to also assess whether I saw any effects of *H. bakeri* EVs on these rare cells.



## 6.2 Results

### 6.2.1 Gene expression changes in 2-D enteroids in response to *H. bakeri* ES products

We aimed to characterise the transcriptional response within murine intestinal epithelium to *H. bakeri* EVs. Total HES (which contains EVs) is known to modify the intestinal epithelium (Drurey et al., 2021; Karo-Atar et al., 2022). In order to determine whether EVs are responsible for specific host changes in the epithelium, 2-D organoids were grown as per our established methods (Chapter 4 of this thesis), and after 3 days of growth apical media was removed and surfaced washed once with PBS before treatment with either EVs, EVdepHES or mock control in quadruplicate (Figure 6.1). RNA was extracted after 24 h and used for RNA-seq (Figure 6.1). Previous data showed uptake of *H. bakeri* EVs at 16, 18 and 24 h (Buck et al, 2014; Chapter 5 of this thesis) I choose to assess transcription after 24 hrs when I was confident that *H. bakeri* EVs had entered cells and to allow adequate time to capture changes in gene expression. The average RNA yield across all samples was 2.6 µg and demonstrated high RNA integrity (Supplemental Figure 3). Library preparation, which included a ribosomal depletion step, and sequencing were performed by the Wellcome Trust Clinical Research Facility in Edinburgh.



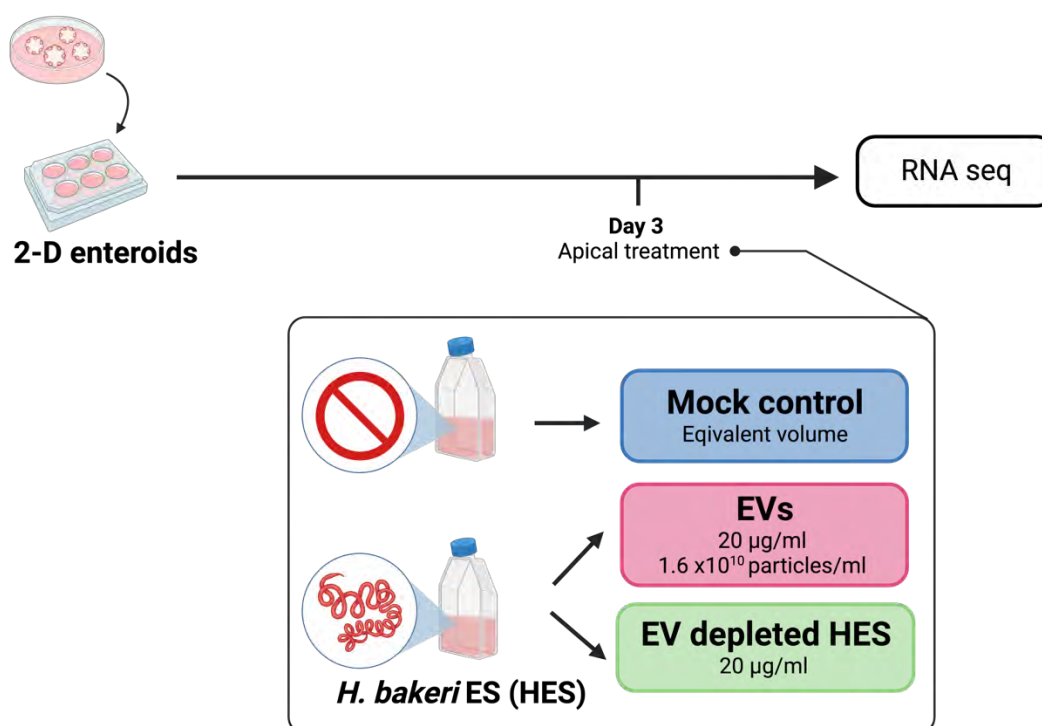


**Figure 6.1 | Schematic of experimental design.** 2-D enteroids were cultured for a total of 4 days. IL-4 (50 ng/ml) and IL-13 (50 ng/ml) were added to growth media on day 2 onwards. On day 3 of culture, organoids were treated on their apical surface with either i) mock control, ii) Sequentially isolated (UC followed by SEC) EVs at 20 µg/ml which equated to 1.6x10<sup>10</sup> particles/ml or iii) EVdepHES at 20 µg/ml representing double the dose of HES used by Drurey *et al*, 2021. After 24 h media was removed, and RNA extracted from cells for subsequent RNA-sequencing. All conditions were performed in quadruplicate (n = 4).

Global assessment of gene expression across all samples was performed using principal component analysis (PCA) as a dimensionality reduction method of the top 10% most variable genes. PCA analysis showed that EVdepHES replicates clustered further from both EVs and the mock control and this was captured in PC1 which explains 27% of the variance (Figure 6.2). *H. bakeri* EV treated replicates did not separate from the mock control by PC1, however PC2 which captures 21% of the variance partially separates these two treatments (Figure 6.2). Overall, stronger global gene expression changes were induced by EVdepHES compared to mock than EV treatment, while *H. bakeri* EVs induced more subtle effects compared to the mock control (Figure 6.2). Replicates for all treatments did not cluster closely together suggesting substantial variability within groups, even for the mock control. This could suggest 2-D organoid models are inherently more variable than tissue, or 3-D

organoids based on published literature (Figure 6.2) (Drurey et al., 2021; Karo-Atar et al., 2022).

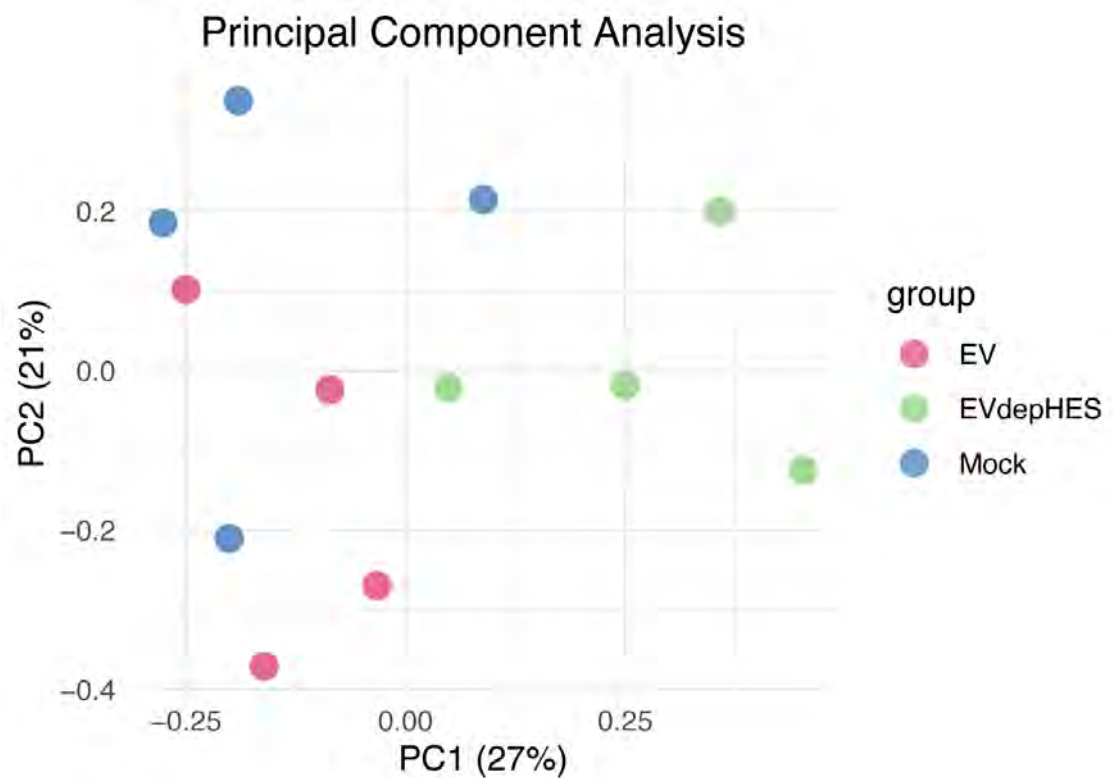


**Figure 6.2 | Principal component analysis of 2-D organoids treated with *H. bakeri* ES products.** PCA showing PC1 (x-axis) compared to PC2 (y-axis) of the top 10% most variable genes in the dataset *H. bakeri* EVs (pink), EVdepHES (green) and mock control (blue).

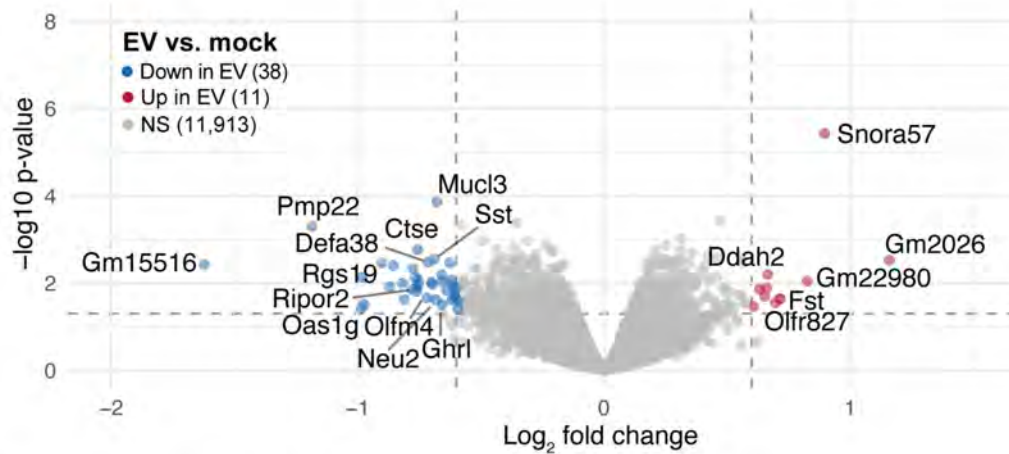
We next identified differentially expressed genes in EV, or EVdepHES, treatment compared to mock using edgeR 3.34.1. Genes with <1 CPM in  $\geq 3$  libraries were removed. Differential expression was then assessed using a log<sub>2</sub>FC cut off of  $\pm 0.589$ , and a false discovery rate (FDR) adjusted P-value cut off of 0.05. These log<sub>2</sub>FC cut offs represents a 50% increase/decrease in expression similar to cut offs previously applied for EV treated MODE-K cells by Buck *et al* (2014). Using these cut offs, I identified one upregulated snoRNA transcript (snora57) in the EV vs. Mock comparison (Supplemental file 6.1). For EVdepHES vs. Mock using the same cut offs, 28 upregulated and 41 downregulated genes were identified (Supplemental file 6.1). These differential expression results are consistent with PCA results, that together demonstrate EVdepHES induces stronger changes in 2-D enteroids than EVs, however I anticipated that only a proportion of cells will take up *H. bakeri* EVs (based on

data from Chapter 5 of this thesis) thereby diluting effects of gene expression. I then proceeded to analyse this dataset using lowered statistical cut off of raw P-value  $<0.05$  and  $\log_2FC \pm 0.589$  in order to cautiously interpret the changes that occur upon EV treatment. In section 6.2.4, differential expression was assessed in 2-D enteroids in response to co-culture with live parasites, I chose to analyse these data separately in order to apply more robust statistical cut offs for the latter.

Differentially expressed genes that had a  $\log_2FC \pm 0.589$  and raw P-value  $\leq 0.05$  were defined as upregulated or downregulated respectively and were visualised by volcano plot (Figure 6.3). *H. bakeri* EV treatment compared to the mock control resulted in more downregulated genes (38) than upregulated genes (11) (Figure 6.3 A). All upregulated and downregulated genes in EV vs. mock are listed in Table 6.1. Among the downregulated genes was *Olfm4* a marker of intestinal stem cells seen to be downregulated by HES (Karo-Atar et al., 2022) (Figure 6.3 B, Table 6.1). In addition, I identified down-regulation of a number of genes with likely roles in the barrier defence (*Defa38*, *Muc13*), roles in immunity (*Irak3*, *Ctse*), antiviral response (*Oas1g*), genes that encode hormones (*Ghrl*, *Sst*), as well as a number of histone encoding genes and mitochondrial genes (Table 6.1). Of the few genes significantly upregulated by *H. bakeri* EVs, Follistatin (*Fst*) was up regulated, which has a role in binding and neutralises activins and TGF $\beta$  family members that orchestrate proliferation of the intestinal epithelium (W. Chen & Ten Dijke, 2016) (Table 6.1). However, the majority of the upregulated genes were uncharacterised. EVdepHES treatment induced vs. mock controls resulted in 62 downregulated genes and 91 upregulated, consistent with PCA that suggests stronger effects on transcripts by EVdepHES. The full list of these genes is provided in Supplementary Table 6.1. Genes involved in induction of, or induced by, type I interferon response were upregulated (*Ifit3b*, *Ifit3*, *Isg15*, *Bst2*, *Ifi44*, *Oasl*), genes encoding cytokines, chemokines, or involved in controlling their function were also induced (*Cxcl10*, *Cxcl9*, *Dusp1*, *Il18rl*, *Il34*, *Csf1*) (Figure 6.3 B and Supplemental file 6.1). Downregulated genes included genes related to mucus secretion by goblet cells (*Clca1*), genes involved in kinetochore formation

during mitosis (*Kntc1*, *Kif2c*, *Rmi2*), as well as a small number of genes regulated consistently between EVdepHES vs. mock and EV vs. mock, including hormone encoding genes (*Ghrl*, *Sst*) and the stem cell gene (*Olfm4*).

**A.**



**B.**

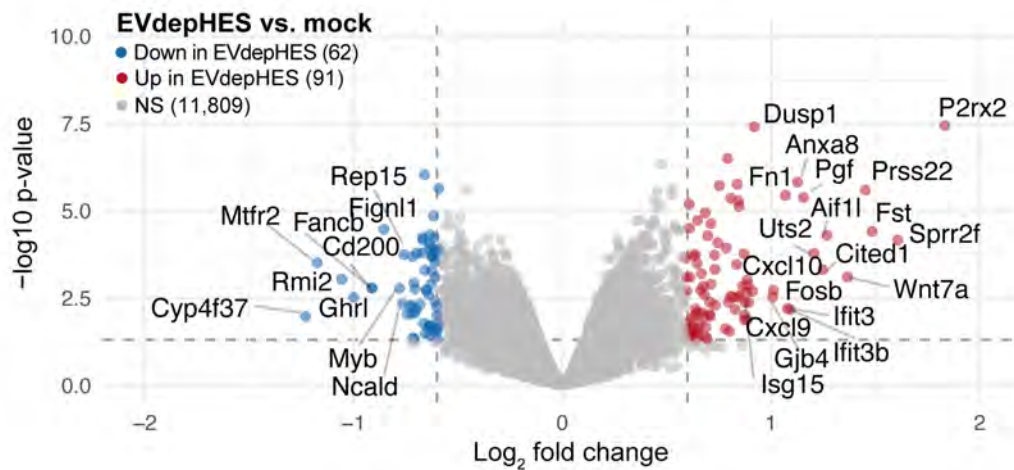


**Figure 6.3 | Differentially expressed genes in EV and EVdepHES treatment.** Differential expressed generated using edgeR analysis by Jose Roberto Bermudez Barrientos. **A)** Genes differentially expressed in EV treatment compared to mock plotted by  $-\log_{10}$  P-value (y-axis) against  $\text{Log}_2$  fold change (x-axis). Genes defined as upregulated with a  $\text{log}_2$  FC of  $> 0.589$  and a raw P-value of  $< 0.05$  in red and genes defined downregulated with a  $\text{log}_2$  FC of  $> -0.589$  and a P-value of  $< 0.05$  in red defined as down in EV followed by no. of genes. Genes with P-value  $> 0.05$ , or those that don't meet  $\text{log}_2$ FC cut off in grey are defined non-significant (NS). **B)** Differentially expressed genes as in EVdepHES compared to mock plotted as in A. Volcano plots generated in Rstudio using the ggplot2 package.

**Table 6.1 | Differentially expressed genes (DEGs) in EV vs. Mock.** DEGs defined as having a Log<sub>2</sub> fold change of  $\pm 0.589$  and a raw P-value of  $\leq 0.05$  ranked by log<sub>2</sub> FC. 11 genes were significantly up regulated and 38 were significantly downregulated.

Gene	Description	Direction	Log <sub>2</sub> FC	P-Value
<b>Gm2026</b>	predicted gene 2026	UP	1.16	2.99E-03
<b>Snora57</b>	small nucleolar RNA, H/ACA box 57	UP	0.90	3.73E-06
<b>Gm22980</b>	predicted gene, 22980	UP	0.83	9.01E-03
<b>Fst</b>	Follistatin	UP	0.72	2.30E-02
<b>Gm6083</b>	predicted gene 6083	UP	0.71	2.31E-02
<b>Olfir827</b>	olfactory receptor 827	UP	0.70	2.84E-02
<b>Ddah2</b>	dimethylarginine dimethylaminohydrolase 2	UP	0.67	6.37E-03
<b>9330160F10Rik</b>	RIKEN cDNA 9330160F10 gene	UP	0.66	1.30E-02
<b>Gm26202</b>	predicted gene, 26202	UP	0.65	2.00E-02
<b>C730034F03Rik</b>	RIKEN cDNA C730034F03 gene	UP	0.63	1.38E-02
<b>Abca14</b>	ATP-binding cassette, sub-family A (ABC1), member 14	UP	0.61	3.43E-02
<b>Mns1</b>	meiosis-specific nuclear structural protein 1	DOWN	-0.59	2.56E-02
<b>Nt5c1a</b>	5'-nucleotidase, cytosolic IA	DOWN	-0.59	3.96E-02
<b>mt-Nd4</b>	mitochondrially encoded NADH dehydrogenase 4	DOWN	-0.60	1.31E-02
<b>Irak3</b>	interleukin-1 receptor-associated kinase 3	DOWN	-0.61	1.97E-02
<b>H2bc7</b>	H2B clustered histone 7	DOWN	-0.61	1.97E-02
<b>H3c15</b>	H3 clustered histone 15	DOWN	-0.61	1.13E-02
<b>H3c1</b>	H3 clustered histone 1	DOWN	-0.62	2.43E-02
<b>Gm6180</b>	predicted pseudogene 6180	DOWN	-0.62	8.62E-03
<b>Mutyh</b>	mutY DNA glycosylase	DOWN	-0.63	3.45E-03
<b>Gm10263</b>	predicted gene 10263	DOWN	-0.64	1.47E-02
<b>Lars2</b>	leucyl-tRNA synthetase, mitochondrial	DOWN	-0.66	9.29E-03
<b>Neu2</b>	neuraminidase 2	DOWN	-0.66	3.11E-02
<b>Rpl7-ps8</b>	ribosomal protein L7, pseudogene 8	DOWN	-0.66	6.44E-03
<b>Muc13</b>	mucin like 3	DOWN	-0.68	1.36E-04
<b>Ghrl</b>	ghrelin	DOWN	-0.68	2.41E-02
<b>Defa38</b>	defensin, alpha, 38	DOWN	-0.69	2.82E-03
<b>H2bc24</b>	H2B clustered histone 24	DOWN	-0.70	1.07E-02
<b>H2bc23</b>	H2B clustered histone 23	DOWN	-0.70	9.50E-03
<b>Gm10136</b>	predicted pseudogene 10136	DOWN	-0.71	3.33E-03
<b>Olfm4</b>	olfactomedin 4	DOWN	-0.72	2.19E-02
<b>H2bc11</b>	H2B clustered histone 11	DOWN	-0.75	1.05E-02

<b><i>mt-Nd4l</i></b>	mitochondrially encoded NADH dehydrogenase 4L	<b>DOWN</b>	-0.76	8.19E-03
<b><i>Ctse</i></b>	cathepsin E	<b>DOWN</b>	-0.76	1.71E-03
<b><i>Rps27rt</i></b>	ribosomal protein S27, retrogene	<b>DOWN</b>	-0.76	1.22E-02
<b><i>H2ac5-ps</i></b>	H2A clustered histone 5, pseudogene	<b>DOWN</b>	-0.76	1.55E-02
<b><i>Gm10222</i></b>	predicted gene 10222	<b>DOWN</b>	-0.77	7.27E-03
<b><i>Sst</i></b>	somatostatin	<b>DOWN</b>	-0.78	4.64E-03
<b><i>Ripor2</i></b>	RHO family interacting cell polarization regulator 2	<b>DOWN</b>	-0.78	1.42E-02
<b><i>Rpl27a-ps4</i></b>	ribosomal protein L27A, pseudogene 4	<b>DOWN</b>	-0.81	2.39E-02
<b><i>mt-Atp8</i></b>	mitochondrially encoded ATP synthase 8	<b>DOWN</b>	-0.82	1.02E-02
<b><i>H2bc3</i></b>	H2B clustered histone 3	<b>DOWN</b>	-0.85	3.95E-03
<b><i>Rgs19</i></b>	regulator of G-protein signaling 19	<b>DOWN</b>	-0.87	1.21E-02
<b><i>H2bc22</i></b>	H2B clustered histone 22	<b>DOWN</b>	-0.90	3.47E-03
<b><i>Oas1g</i></b>	2'-5' oligoadenylate synthetase 1G	<b>DOWN</b>	-0.97	3.08E-02
<b><i>mt-Tl1</i></b>	mitochondrially encoded tRNA leucine 1	<b>DOWN</b>	-0.98	7.41E-03
<b><i>Gm5431</i></b>	predicted gene 5431	<b>DOWN</b>	-0.98	3.75E-02
<b><i>Pmp22</i></b>	peripheral myelin protein 22	<b>DOWN</b>	-1.18	5.00E-04
<b><i>Gm15516</i></b>	predicted gene 15516	<b>DOWN</b>	-1.62	3.82E-03

### 6.2.2 EV and EVdephES induce concordant changes as well as unique changes 2-D organoids

An aim of this experiment was to identify gene expression changes occur in 2-D enteroids that are specific to *H. bakeri* EVs compared to non-vesicular components of HES e.g., EVdephES. Only a handful of genes that were identified in Section 6.2.2 were consistently differentially expressed in both the EV vs. mock and the EVdephES vs. mock comparisons. Of these, 3 were upregulated (Figure 6.4 A) and 4 were downregulated (Figure 6.4 B). These data therefore suggest that the EVs induce different gene expression changes compared to EV-depleted HES. However, EdgeR analysis resulted in a substantial number of genes were differentially expressed but did not meet the FC cut offs to be defined up- or down- regulated. Therefore, many genes may be concordantly regulated by EVs and EVdephES but were removed from the list used for comparison due to cut off requirements. To compare the global

gene expression changes induced by EVs and EVdepHES across all genes that were identified by edgeR analysis I performed linear regression analysis (Figure 6.4 C&D). Pearson correlation coefficient describe the strength and direction of linear relationship, where  $R = 0$  indicates no correlation, positive values and negative values indicate positive and negative correlation respectively (Whitlock, 2015). I found a positive correlation between all genes from edgeR analysis in both comparisons with a Pearson correlation coefficient of  $R = 0.41$  ( $P\text{-value} = <2.2 \times 10^{-16}$ ) (Figure 6.4 C). Stratifying the analysis by significance level drastically improved the positive correlation, when considering only the genes that were significantly differentially expressed (raw  $P\text{-value} \leq 0.05$ ) in both comparison a strong positive correlation was found ( $R = 0.87$ ) (Figure 6.4 D). These data suggest that overall, the genes dysregulated in 2-D enteroids in either EV vs. mock or EVdepHES vs. mock treatment are concordant.

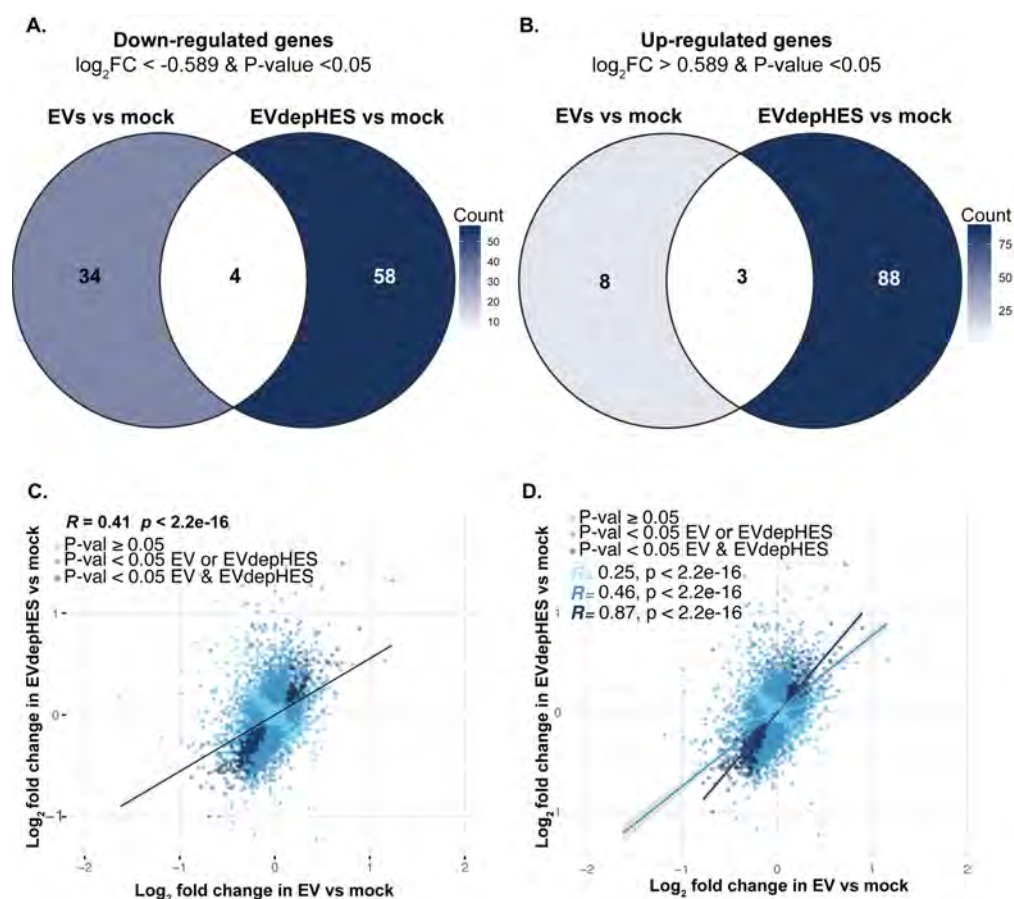


**Figure 6.4 | Correlation of gene expression changes in EV and EVdepHES treatment. A&B)** Venn diagram of **A)** downregulated genes or **B)** upregulated genes in EV vs. mock and EVdepHES vs. mock.

Colour indicates number of genes **C&D**) Scatter plot of  $\log_2FC$  of all differentially expressed genes in EV vs. mock (X-axis) and  $\log_2FC$  in EVdepHES vs. mock (Y-axis). Genes coloured by significance, raw P-value  $\geq 0.05$  (pale blue),  $< 0.05$  in either EV vs. mock or EVdepHES vs. mock (blue), and  $< 0.05$  in both comparisons (navy). Linear regression was performed either **C**) on all genes (black line), or **D**) stratified by non-significant in both comparisons (pale blue), significant (raw P =  $< 0.05$ ) in EV vs. mock or EVdepHES vs. mock (blue), and significant in both EV vs. mock and EVdepHES vs. mock (navy). Confidence intervals are shaded in grey. Pearson's correlation coefficient  $r$  and P-value for Pearson's correlation indicated on plot. Correlation plots and regression analysis performed in RStudio using the package `ggpubr` and the function `ggscatter`.



### 6.2.3 *H. bakeri* EVs & EVdepHES modifies expression of genes integral to the intestinal epithelium and immune response

To further assess the functional effects that EVs and EVdepHES may have on 2-D enteroids cells I highlight a number of gene expression related either by function, or due to their cell type specific expression within the intestinal epithelium (Figure 6.5). Type I interferon response genes (ISGs) were upregulated in EVdepHES vs. mock (*Isg15*, *Ifit3*, *Cxcl10*) additionally one of the significantly downregulated genes upon EV treatment was *Oas1g*, a known ISG (Nair et al., 2017). Furthermore, ISGs have been shown to be suppressed by EVs from the clade I nematode *T. muris* in caecal 2-D organoids (Appendix II) (Duque-Correa, Schreiber, et al., 2020). These lead us to further investigate the presence of other known ISGs in our dataset. I found an induction of genes involved in either sensing of nucleic acids, induction of type I interferon response, or genes induced by type I interferons in the EVdepHES condition (Figure 6.5). In contrast, EV treatment did not have effects on the expression of these same genes, and these genes are some of the most differentially expressed genes between EVs vs and EVdepHES suggesting these treatments induce opposing effects on the intestinal epithelium interferon response (*data not shown*).

Genes associated with endocytosis, vesicle uptake and synaptic vesicle uptake were among the upregulated genes upon EV treatment, with some also upregulated in EVdepHES treatment (Figure 6.5). I hypothesised that EVs modify the intestinal stem cell niche based on pilot data and published data on HES treatment of organoids. Indeed, I identified a down-regulation of many key stem cell genes in both EV and EVdepHES treatment (Figure 6.5) most notably *Ascl2*, a transcription factor that controls expression of *Lgr5* (Figure 6.5). In addition, clusterin (*Clu*) which is a marker of revSC was upregulated by EVdepHES but EVs induced an opposite effect on this gene (Figure 6.5).

We noticed two of the genes significantly downregulated by EV treatment encoded the secreted hormones somatostatin (*Sst*) and Ghrelin (*Ghrl*), which are specifically produced and secreted in the intestinal epithelium by enteroendocrine cells. Expression of other enteroendocrine specific genes and hormones was also subtly downregulated by EV treatment however, EVdepHES induced a much stronger down-regulation of many of these genes (Figure 6.5).

A number of alpha defensin (*Defa*) genes were downregulated by EV treatment. Alpha defensins are antimicrobial peptides, also known as cryptdins, are secreted in the intestinal epithelium by Paneth cells, and have bactericidal effects against gram-negative and gram-positive bacteria, fungi and some viruses (Andre J. Ouellette, 2005). I identified a suppression of these genes after EV and EVdepHES treatment, however EV treatment induced strong downregulation than EVdepHES (Figure 6.5). In addition, EV treatment suppressed the antimicrobial peptide angiogenin 4 (*Ang4*) which has been previously implicated in *T. muris* infection (D'Elia et al., 2009; Forman et al., 2012). Finally, I identified a downregulation of the polymeric immunoglobulin receptor (*Pigr*) after EV and EVdepHES treatment, which allows transcytosis of secreted antibodies (IgA and IgM) from the basal side across the epithelium membrane where they protect mucosal surfaces (Wei & Wang, 2021) (Figure 6.5).

Previous publications suggested that HES alters the differentiation of intestinal epithelial cells by suppressing the secretory progenitor marker *Atoh1* (Drurey et al., 2021). I assessed expression of *Atoh1*, and other known regulators of differentiation in the intestinal epithelium. For EVdepHES, the only significant suppression in these key differentiation factors was for *Spdef* which is required for the differentiation of goblet cells (Figure 6.5). For EV treatment, I identify a subtle but significant suppression of the notch ligand *Dll1* ( $\text{Log}_2\text{FC} = -0.15$ ) which is expressed by secretory progenitor and Paneth cells as well as *Sox9* ( $\text{Log}_2\text{FC} = -0.29$ ) which is a transcription factor critical for Paneth cell differentiation (Bastide et al., 2007) (Figure 6.5).

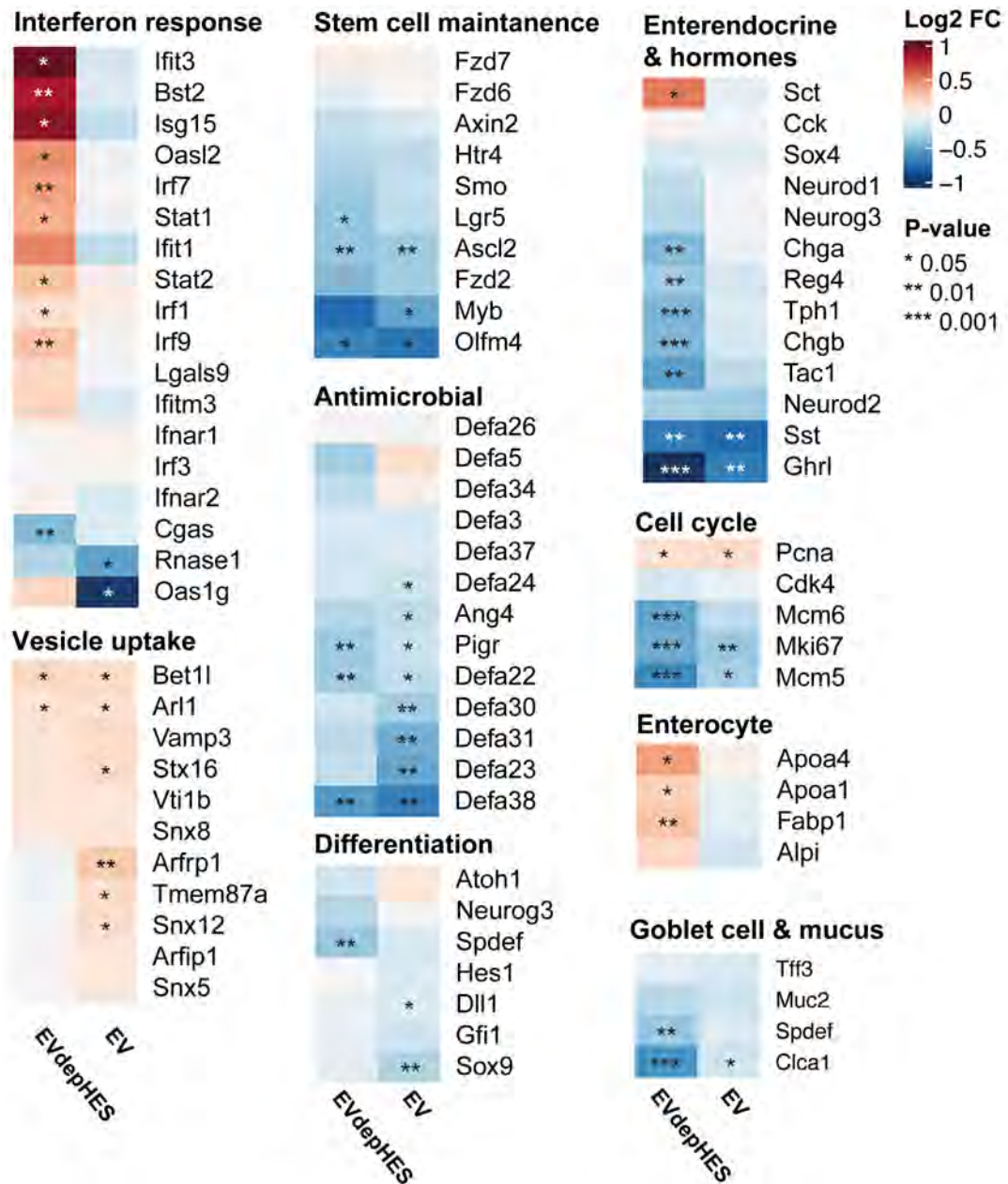


**Figure 6.5 | Gene expression changes related to epithelial function and immune responses.** Heatmap of  $\log_2$  fold change in selected genes (rows) in EVdepHES vs. mock (left-hand column), or in EV vs. mock (right-hand column). Cells coloured by  $\log_2$  fold change from 1 (dark red) to -1 (dark blue) key on graph. Genes were selected from those differentially expressed based on biological relevance with no  $\log_2$  fold change cut off applied. Raw P-value =  $< 0.05 = *$ ;  $< 0.01 = **$  and  $< 0.001 = ***$

We identified differential expression of intestinal stem cell genes or genes involved in Wnt signalling in our *H. bakeri* EV microinjected 3-D organoid pilot data (Buck lab, unpublished). I therefore hypothesised that *H. bakeri* EVs modify intestinal stem cells. I found the well-established ISC marker gene *Olfm4* to be significantly downregulated after EV and EVdepHES treatment

(Figure 6.5). The transcription factor *Ascl2* is controlled by Wnt signalling, and regulates the expression of several stemness genes including *Lgr5* (Schuijers et al., 2015) (Figure 6.5). *Ascl2* was downregulated after EV (Log<sub>2</sub>FC -0.36) and EVdepHES (Log<sub>2</sub>FC -0.39), while its target *Lgr5* itself was also downregulated although only statistically significant in EVdepHES vs. mock (Figure 6.5).

During my PhD, seminal papers demonstrated that during the larval stage of *H. bakeri* infection (day 6) while parasite still reside within the submucosa modulation of proximal stem cells occurs (Nusse et al., 2018). ISCs transition into clusterin (*Clu*) positive cells that express genes associated with the fetal epithelium and lose expression of classic markers *Olfm4* and *Lgr5* (Nusse et al., 2018). These fetal-like stem cells were later termed revival stem cells for their role in repair of the epithelium after various damage models including but not limited to *H. bakeri* infection (Ayyaz et al., 2019; Nusse et al., 2018). Emergence of these cells is replicated in 3-D organoids that are treated with adult HES (Drurey et al., 2021; Karo-Atar et al., 2022). I investigated the differential expression of genes defined by Karo-Atar *et al* as enriched in revSCs and identified an anticipated upregulation in these genes for the EVdepHES treatment (Figure 6.6). However, induction of revSC genes was not replicated by EV treatment alone suggesting that EVs do not play a role in the induction of genes required for revSCs (Figure 6.6).

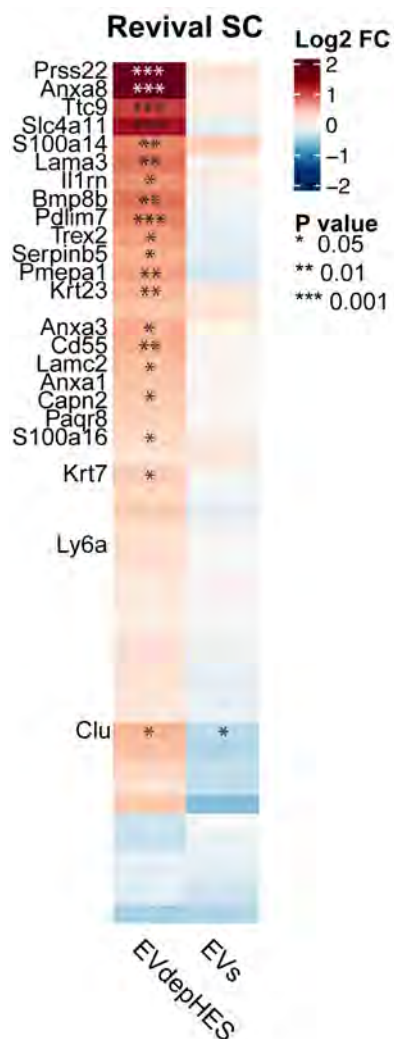


**Figure 6.6 | Differential expression of genes identified in revSC signature after *H. bakeri* ES treatments.** Differential expression of each gene (rows) in EVdepHES vs. mock (left-hand column) and EV vs. mock (right-hand column). Cells coloured by log<sub>2</sub> fold change from 1 (dark red) to -1 (dark blue) key on graph. Significance of differential expression indicated for each gene in each comparison < 0.05 = \*, <0.01 = \*\* and <0.001 = \*\*\* only genes that reach a P-value significance of <0.05 are labelled with gene names, as well as Ly6a.

To understand how these gene expression changes may act cumulatively to modify a specific pathway I performed a competitive gene set test accounting for inter-gene correlation (CAMERA) analysis using the output from edgeR analysis to identify gene ontology (GO) terms enriched in our dataset. GO categories with fewer than 50 genes and more than 300 genes were removed. CAMERA pathway analysis produced many enriched GO terms and an extensive table for all comparisons is found in Supplemental file 6.2. GO terms enriched for EV vs. mock were predominantly downregulated. Of those enriched pathways many had overlapping genes and functions, the topmost 20 enriched pathways in EV vs. mock are summarised in Table 6.2 and represented three major processes i) antimicrobial and humoral immune response (downregulated) driven by alpha defensins, *Ang4* and *Pigr* ii) DNA replication and repair / DNA-protein interactions (downregulated) and iii)

Pathways related to uptake, and transport of endosomes or vesicles which were the only pathways that were upregulated (Table 6.2, Figure 6.7).

**Table 6.2 | Top 20 enriched pathways using CAMERA pathway analysis for EV vs. mock.** Pathway analysis was performed using a competitive gene set test accounting for inter-gene correlation (CAMERA) pathway analysis in R. CAMERA analysis was performed by Jose Roberto Bermudez Barrientos. Pathways were ranked in descending order by their FDR value

<b>Rank</b>	<b>GO term</b>	<b>Direction</b>	<b>P-value</b>	<b>FDR</b>
1	Antimicrobial humoral response	Down	3.83E-07	0.001
2	nucleosome assembly	Down	9.58E-07	0.001
3	defence response to Gram-positive bacterium	Down	5.41E-06	0.003
4	humoral immune response	Down	6.27E-06	0.003
5	nucleosome organization	Down	9.88E-06	0.003
6	DNA-dependent DNA replication	Down	2.27E-05	0.005
7	protein-DNA complex assembly	Down	2.18E-05	0.005
8	retrograde transport, endosome to Golgi	Up	2.01E-05	0.005
9	DNA packaging	Down	4.62E-05	0.008
10	protein-DNA complex subunit organization	Down	5.22E-05	0.009
11	chromatin assembly	Down	7.23E-05	0.011
12	chromatin assembly or disassembly	Down	1.15E-04	0.014
13	organelle fusion	Up	1.07E-04	0.014
14	organelle membrane fusion	Up	1.97E-04	0.023
15	cytosolic transport	Up	2.68E-04	0.029
16	vesicle fusion	Up	3.16E-04	0.032
17	endosomal transport	Up	3.90E-04	0.037
18	metaphase/anaphase transition of mitotic cell cycle	Down	4.80E-04	0.039
19	DNA replication	Down	4.93E-04	0.039

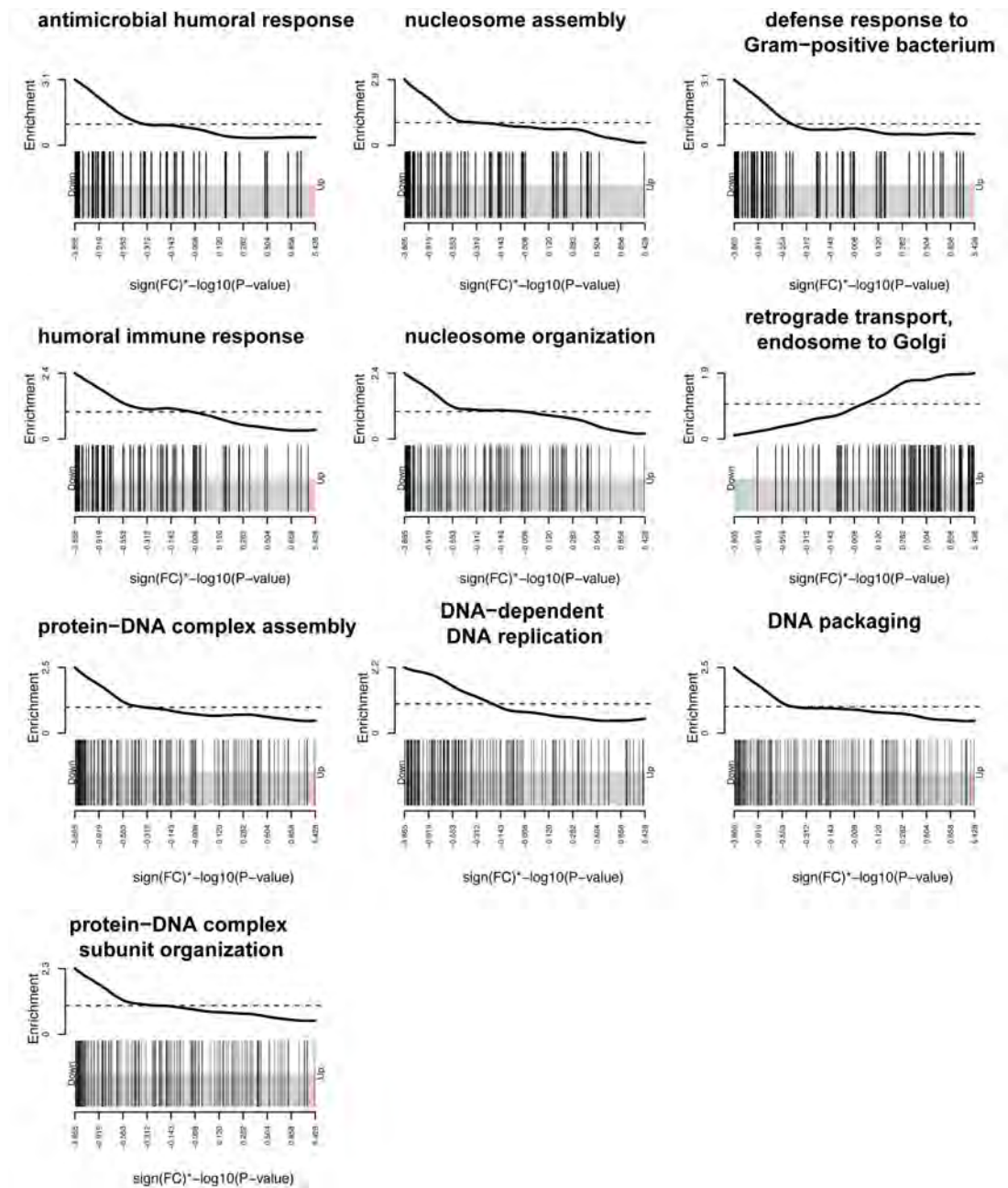


**Figure 6.7 | Pathways enriched in DEGs from EV vs. Mock.** Barcode plots individual genes in my dataset are compared to genes belonging to a particular GO term for biological processes. Differentially expressed genes in EV vs. mock are ranked from most downregulated to most upregulated and represented by black lines indicating their position on the x-axis showing their  $\text{sign}(\text{FC}) \cdot -\log_{10}(\text{P-value})$ . Left-hand side are the most downregulated genes in this GO term and on the right-hand side the more upregulated genes for this GO term. Enrichment score indicates at each position enrichment level of each pathway.



Enrichment of pathways related to DNA-protein interactions and DNA repair were predominantly driven by genes encoding histones, and many of the lower ranked pathways related to cell cycle (Supplemental file 6.2). Additionally, consistent with our hypothesis that EVs modify intestinal stem cells, the GO term for stem cell population maintenance was also enriched and downregulated but was non-significant in our CAMERA pathway analysis ranked 55, FDR 0.234 (Supplemental file 6.2).

Pathway analysis for EVdePHES vs. mock pathway analysis yielded a larger list of significantly enriched pathways (Supplemental file 6.2) with a very strong enrichment of pathways related to DNA replication and cell cycle comprising the majority of the topmost enriched pathways with the exception of RNA transport from the nuclei (Table 6.3). Pathways related to immunity such as T-cell mediated immunity and antigen presentation were also significantly upregulated but ranked lower in the list (Supplemental file 6.2).

**Table 6.3 | Top 15 enriched pathways using CAMERA pathway analysis for EVdepHES vs. mock.** Pathway analysis was performed using a competitive gene set test accounting for inter-gene correlation (CAMERA) pathway analysis in R. Pathways were ranked by their FDR value

Rank	GO term	Direction	P-value	FDR
1	DNA-dependent DNA replication	Down	2.78E-14	4.54E-11
2	sister chromatid segregation	Down	6.07E-14	4.95E-11
3	DNA replication	Down	1.48E-13	8.05E-11
4	mitotic sister chromatid segregation	Down	8.90E-13	3.63E-10
5	nuclear chromosome segregation	Down	5.32E-12	1.74E-09
6	chromosome segregation	Down	2.35E-11	6.41E-09
7	DNA conformation change	Down	6.56E-11	1.53E-08
8	recombinational repair	Down	3.93E-10	8.02E-08
9	double-strand break repair via homologous recombination	Down	4.69E-10	8.50E-08
10	DNA recombination	Down	8.49E-10	1.29E-07
11	RNA export from nucleus	Down	8.71E-10	1.29E-07
12	DNA packaging	Down	1.76E-09	2.05E-07
13	metaphase/anaphase transition of mitotic cell cycle	Down	1.69E-09	2.05E-07
14	meiotic cell cycle	Down	1.52E-09	2.05E-07
15	mitotic sister chromatid separation	Down	2.13E-09	2.31E-07

Our analysis identified several genes that have cell type restricted expression within the epithelium, for example  $\alpha$ -defensin genes which are expressed by Paneth cells. I then aimed to investigate using our RNA-seq data whether I could identify enrichment or depletion of specific subpopulations of cells within our data. To achieve this, I used the top 100 cell type specific genes identified from published scRNA-seq data (Haber et al., 2017) and used CAMERA analysis to assess whether genes for each cell type were enriched in the differentially expressed genes from our dataset (the extended results are accessible in Supplemental file 6.3).

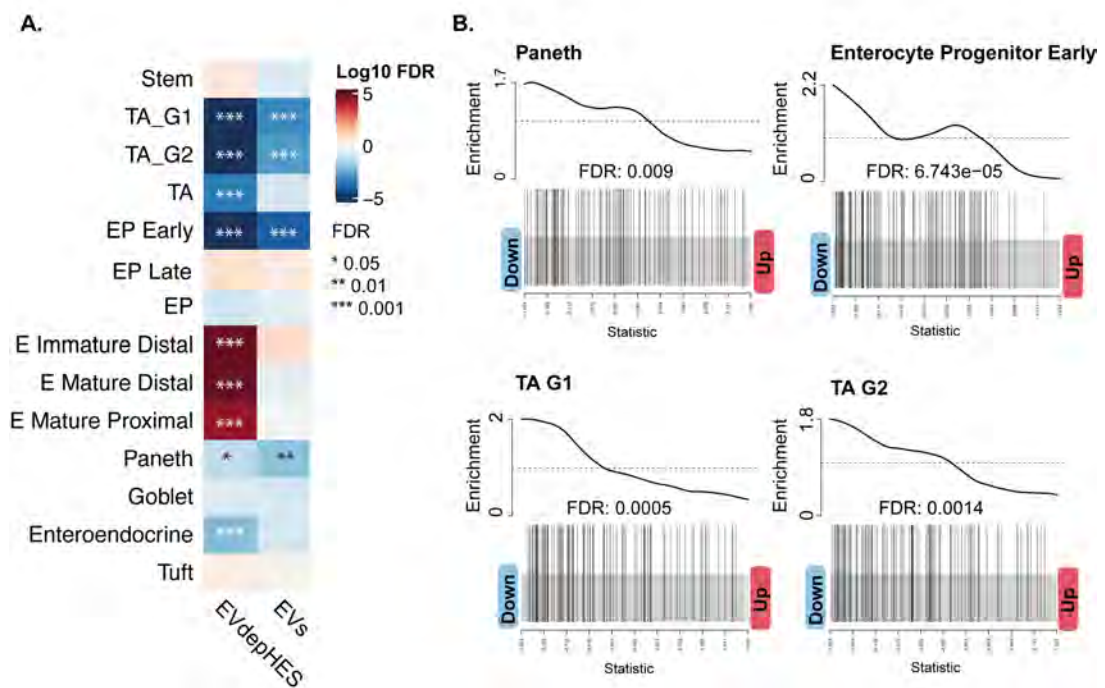


**Figure 6.8 | Positive and negative enrichment of cell type specific genes in EV or EVdepHES treatment.** CAMERA analysis was performed using edgeR results for EV vs. mock (right-hand side) or EVdepHES vs mock (left-hand side) against the top 100 cell type specific genes for each intestinal epithelial cell type identified in Haber *et al*, 2017. **A)** For upregulated pathways FDR values were transformed by  $-\log_{10}(\text{FDR})$  and for pathways going down these were transformed by  $-1 * -\log_{10}(\text{FDR})$  to visualise both the direction of change and significance, these values were then visualised in a heatmap using the package ComplexHeatmap in RStudio. Significance values are indicated by \* <math><0.05</math>, \*\* <math><0.01</math> and \*\*\* <math><0.001</math>. EP = enterocyte progenitor, E = enterocyte, TA = Transit-amplifying, G1 = Gap 1 phase of cell cycle, G2 = Gap 2 phase of cell cycle **B)** Barcode enrichment plot for each of the significantly enriched cell populations differentially expressed genes from EV vs. mock are ranked by differential expression from down (left-hand side) to up (right-hand side) those that are present in the comparison dataset (Haber *et al*, 2017) are plotted along the X-axis (black lines) by their statistic =  $\text{sign}(\text{FC}) * -\log_{10}(\text{P-value})$ . Skewing of genes towards down regulation results in an enrichment score denoted on the left-hand side.

We found a significant downregulation of Paneth cell specific genes in our EV treated 2-D enteroids which is consistent with previous results showing a downregulation of antimicrobial peptides specifically produced by Paneth cells (Figure 6.8 & Figure 6.4). I also identified a downregulation of TA cells undergoing cell cycle and enterocyte progenitors. For EVdepHES several cell type expression signatures were downregulated including TA cells, enterocyte progenitor cells, Paneth cells and a strong downregulation enteroendocrine cells consistent with findings in Figure 6.4. EVdepHES upregulated mature enterocyte population. It should be noted that despite other studies demonstrating that HES restricts the differentiation of tuft cells (Drurey *et al.*, 2021), our dataset only captured some tuft cell marker genes (*Pou2f3*, *Dclk1*)

with low CPMs <1. In the absence of IL-4 and IL-13 cytokines tuft cells are likely not highly represented in 2-D enteroids (Chapter 4 of this thesis) therefore I cannot confidently interrogate the effects of ES products on this cell type using this dataset.

#### **6.2.4 2-D organoids co-culture with live worms drastically modifies the epithelium**

In parallel to ES treatments, I performed co-culture of live *H. bakeri* worms with 2-D enteroids in order to compare the effects of EVdepHES or EV treatment, with the effects induced by whole parasites (which also produce ES products). Additionally, in contrast to data from infection models, our approach allows for separation between direct effects caused by *H. bakeri* and those driven by non-epithelial host responses (e.g., cytokines). As our 2-D enteroids system has physically separate apical and basal compartments, I aimed to assess transcriptional changes during different stages of infection by co-culturing of 2-D organoids with live *H. bakeri* adults on the apical side, or with L4 larvae in the basal compartment. Additionally, as all currently available datasets where organoids are treated with HES have used 3-D organoids and HES was therefore delivered to the basal epithelium, I also wanted to compare between the effect of basal delivery and apical delivery of *H. bakeri*. For each condition I used a dose of 10 worms, though it should be noted that the volume of the apical compartment is 200  $\mu$ l whereas the basal compartment is 2 ml which means ES products secreted by the worms should be more dilute in the basal conditions than the apical. This generated a novel dataset that captures the intestinal epithelial response to *H. bakeri* worms in the absence of immune driven changes.

2-D enteroids were co-cultured with either adult worms on apical surface, adult worms in the basal compartment, or L4 larvae in the basal compartment for 24 hr before removing the parasites and harvesting samples for transcriptomic analysis. Using PCA to assess the global gene expression changes, PC1

(43%) partially separated *H. bakeri* co-cultured samples from the mock condition (Figure 6.9). However, PC2 (17%) separated the worm co-culture conditions from the mock strongly with the exception of 1 replicate of the *H. bakeri* adult apical co-culture (Figure 6.9). The effect of co-culture was stronger for basal conditions either treated with adults or L4's, than for the apical adult condition. This suggests that apical delivery induces weaker changes side-by-side than basal delivery. L4 *H. bakeri* induced the strongest effect on host transcription by PCA.

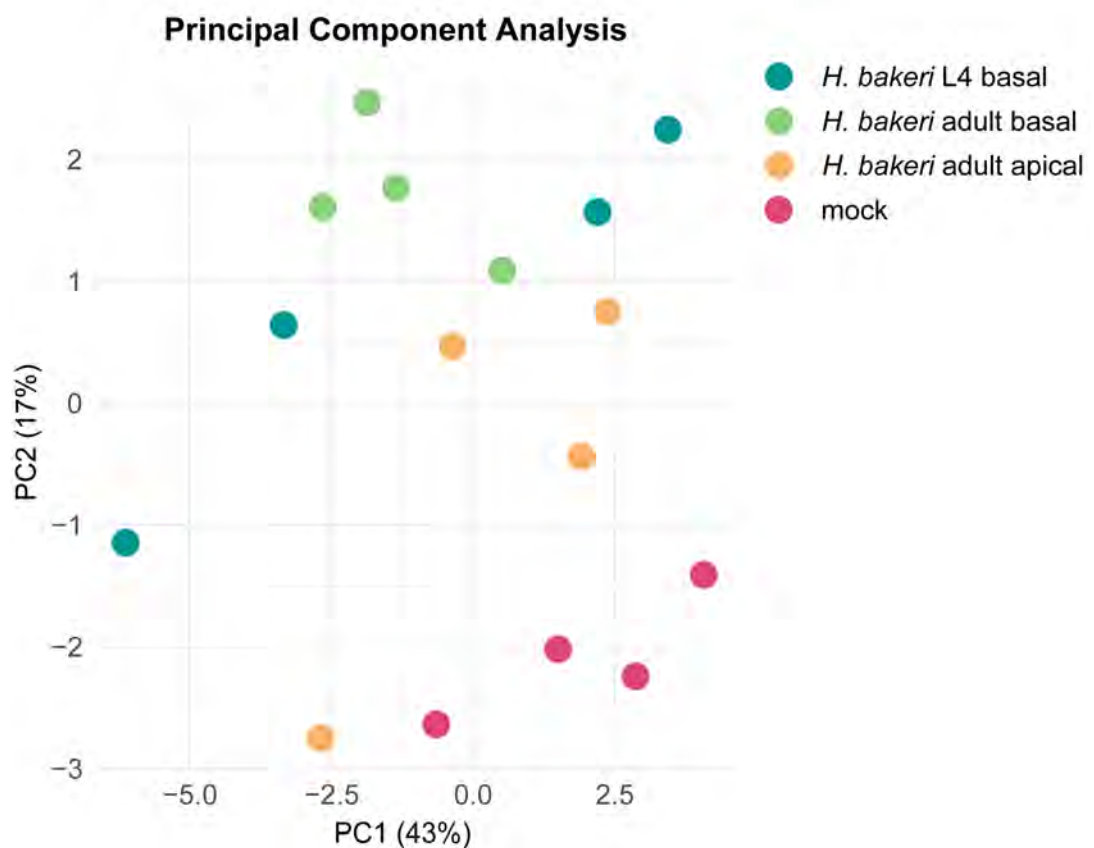


**Figure 6.9 | Principal component analysis (PCA) of 2-D organoids co-cultured with live *H. bakeri* worms.** *H. bakeri* L4 (teal), *H. bakeri* adult basal (green), *H. bakeri* adult apical (peach), and mock (pink). PC1 on x-axis representing 43% of variation and PC2 on y-axis representing 17% of variation. PC1 = Principal component 1; PC2 = Principal component 2. All conditions in quadruplicate (n = 4).

We then performed differential expression analysis using edgeR. Differential expression results were then filtered to remove genes with <1 CPM in  $\geq 3$  libraries. Differentially expressed genes were determined using a  $\log_2$  FC cut off of  $\pm 0.589$ , and false discovery rate (FDR) adjusted P-value cut off of 0.05.

Using these cut offs, I identified for i) Adult *H. bakeri* apical vs. mock 142 upregulated and 248 downregulated genes ii) Adult *H. bakeri* basal vs. mock 337 upregulated and 718 downregulated genes iii) L4 basal vs. mock 432 upregulated and 808 downregulated genes (Figure 6.10). An extensive list of the genes defined as up- and downregulated using these cut-offs for worm co-cultures are provided in Supplemental file 6.4. In addition, the unfiltered edgeR results for all ES and worm co-culture conditions are provided in Supplemental file 6.5.

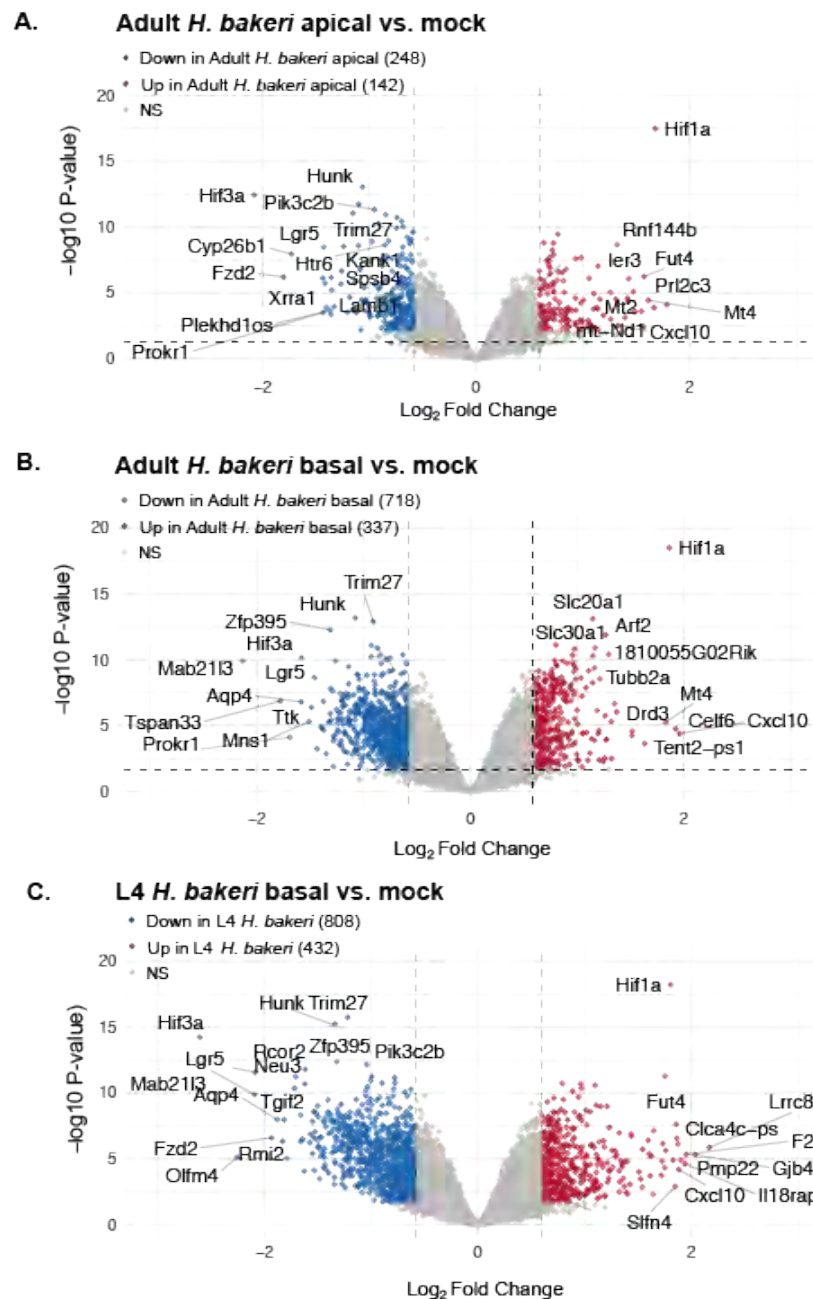


**Figure 6.10 | Differentially expressed genes in *H. bakeri* co-culture.** Differential expression generated by Jose Roberto Bermudez Barrientos. **A-C)** Genes differentially expressed in **A)** Adult *H. bakeri* apical vs. mock, **B)** Adult *H. bakeri* basal vs. mock, **C)** L4 *H. bakeri* basal vs. mock. Y-axis represents  $-\log_{10}$  P-value and X-axis shows  $\text{Log}_2$  fold change genes. Genes with a  $\text{log}_2$  FC of  $\pm 0.589$  and FDR adjusted P-value of  $< 0.05$  are defined as either upregulated (red) or downregulated (blue). Genes that do not meet these cut-offs are defined as NS (grey). Volcano plots made in RStudio using the ggplot package. NS = non-significant; Down = downregulated; Up = upregulated, NS = non-significant.

We identified differences in how many genes were differentially expressed after different co-culture conditions. Next, I wanted to compare how similar or different the changes in gene expression were between treatments. To do so

I performed linear regression analysis on all genes identified by edgeR analysis and found that all three conditions correlated well with each other. Moderate correlation was found between adult basal vs. mock, and adult apical vs. mock ( $R = 0.69$ ) (Figure 6.11). I found stronger correlations between the basal conditions, adult basal vs. mock and L4 vs. mock ( $R = 0.76$ ) (Figure 6.11). The strongest correlation was between the two comparisons that most closely represent *in vivo* localisations, which are the adult apical vs. mock and L4 basal vs. mock ( $R = 0.77$ ) (Figure 6.11).



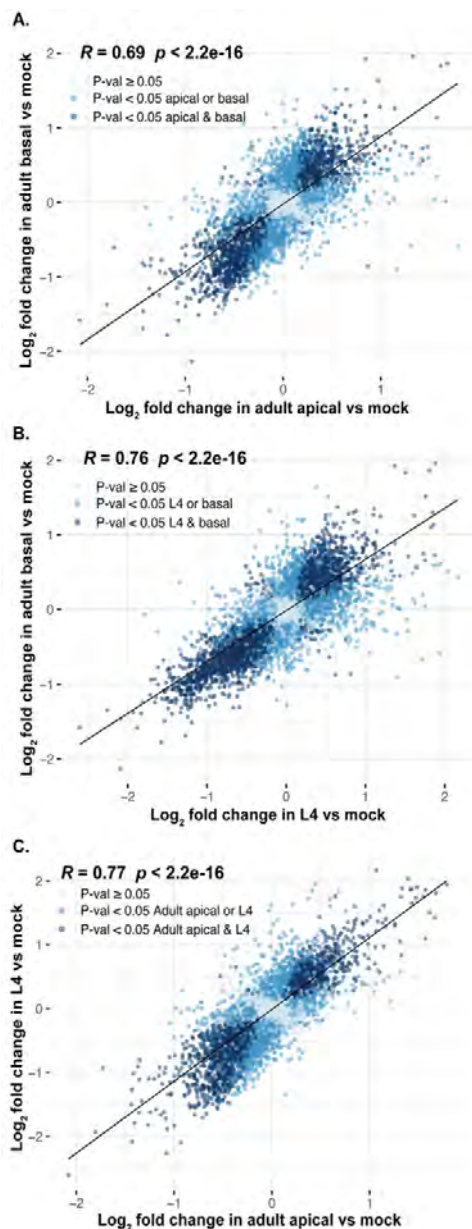


**Figure 6.11 | Correlation of gene expression changes between live worm treatments. A-C)** Scatter plot of all differentially expressed genes in **A)** adult apical vs. mock  $\text{log}_2\text{FC}$  (X-axis) and  $\text{log}_2\text{FC}$  in adult basal vs. mock (Y-axis). **B)** L4 basal vs. mock  $\text{log}_2\text{FC}$  (X-axis) and  $\text{log}_2\text{FC}$  in adult basal vs. mock (Y-axis). **C)** adult apical vs. mock  $\text{log}_2\text{FC}$  (X-axis) and  $\text{log}_2\text{FC}$  in L4 basal vs. mock (Y-axis). **A-C)** Genes coloured by significance, P-value  $\geq 0.05$  in both comparisons (pale blue),  $< 0.05$  in one of the two comparisons (blue), and  $< 0.05$  in both comparisons (navy). Linear regression was performed (black line) and Pearson's correlation coefficient shown on graph ( $R$ ). Correlation plots and regression analysis performed in R using the function ggscatter from the package ggpubr.

We next assessed how co-culture with the live parasites impacted expression of the genes that were previously identified as differentially expressed in our ES treated samples (using different significance cut-offs) (Section 6.2.3). I found a strong induction of interferon response genes in both L4 and adult basal co-cultures that was not present in the apical adult condition, which was consistent with the observation that EVdepHES treated 2-D enteroids induced ISGs (Figure 6.12). Similarly, vesicle uptake was induced in L4 basal and adult basal conditions, but changes were less striking in the adult apical condition (Figure 6.12). As described above, EVs and EVdepHES both play a role in

modifying expression of genes involved in stem cell maintenance (6.2.3), and published data supports modification to stem cells by HES (Drurey et al., 2021; Karo-Atar et al., 2022) or during infection (Nusse et al., 2018). However, I see an even stronger suppression of stem cell maintenance genes after co-culture with either adult or L4 *H. bakeri* than with ES products alone (Figure 6.12). Enteroendocrine cells and their secreted hormones, particularly ghrelin and somatostatin, are repressed in the basal co-culture with adults or L4's (Figure 6.12). I identified a subtle repression of antimicrobial genes in all conditions, but the FC decrease was strongest for EV conditions (Figure 6.12). The polymeric immunoglobulin receptor (*Pigr*) was strongly suppressed by both adult basal and L4 basal co-cultures. Finally, I also assessed expression of key differentiation factors within the intestinal epithelium. I found stronger effects on many of these host genes when co-cultured with the worms compared to co-culture with the ES treatments. For example, there was a strong induction of the enterocyte progenitor gene *Hes1* in all co-culture conditions suggesting skewing toward enterocyte lineage, supported by an increase in enterocyte specific genes (Figure 6.12). However, I did not see the expected inverse effect on *Atoh1*, which is expressed in a mutually exclusive fashion (Figure 6.12). The only differentiation factor significantly downregulated was the enteroendocrine cell determining factor *Neurog3*, which was suppressed in L4 vs. mock (Figure 6.12). Cell cycle, like in ES treated 2-D enteroids, was downregulated (Figure 6.12). Finally, genes encoding proteins integral to the mucus barrier were also downregulated (Figure 6.12).

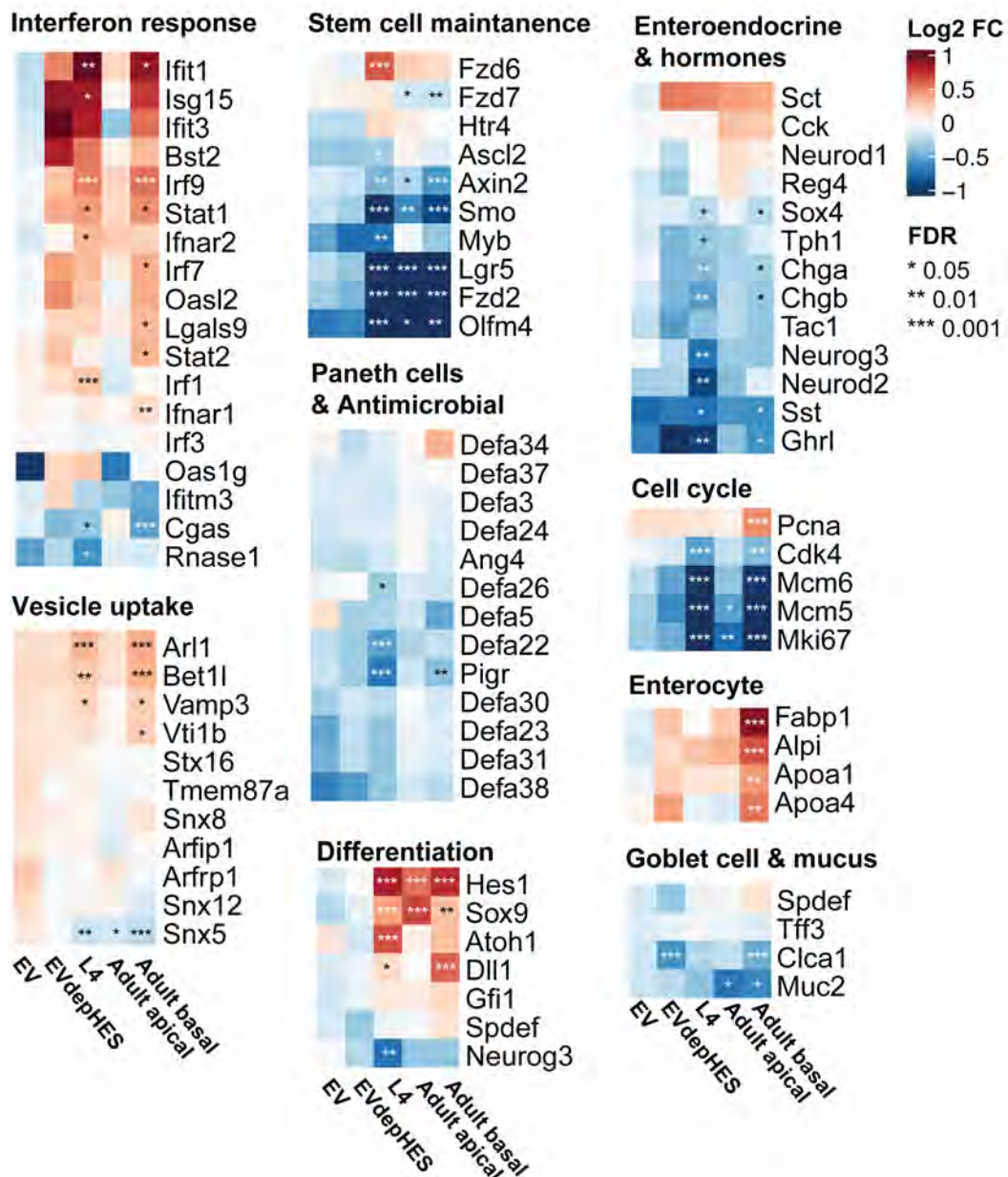


**Figure 6.12 | Gene expression changes related to immune response and epithelial function during *H. bakeri* co-culture.** Heatmap of log<sub>2</sub> fold change in selected genes (rows) in L4 basal vs. mock (L4, left-hand column), apical adult vs. mock (centre column), or basal adult vs. mock (right-hand column). Cells coloured by log<sub>2</sub> fold change from 1 (dark red) to -1 (dark blue) key on graph. Significance of differential expression indicated for each gene in each comparison FDR adjusted p-value < 0.05 = \*, < 0.01 = \*\* and < 0.001 = \*\*\*

As previously reported intestinal epithelial tissue from infected mice, as well as 3-D organoids treated with HES, results in revSC conversion. I assessed whether this was also seen in our co-culture experiment. As expected, I saw a strong induction of this response in all co-culture conditions most notably in the L4 condition, although a strong induction was also seen in adult apical co-

culture. Interestingly, basal adult co-culture induced a more subtle induction (Figure 6.13).

## Reserve stem cells

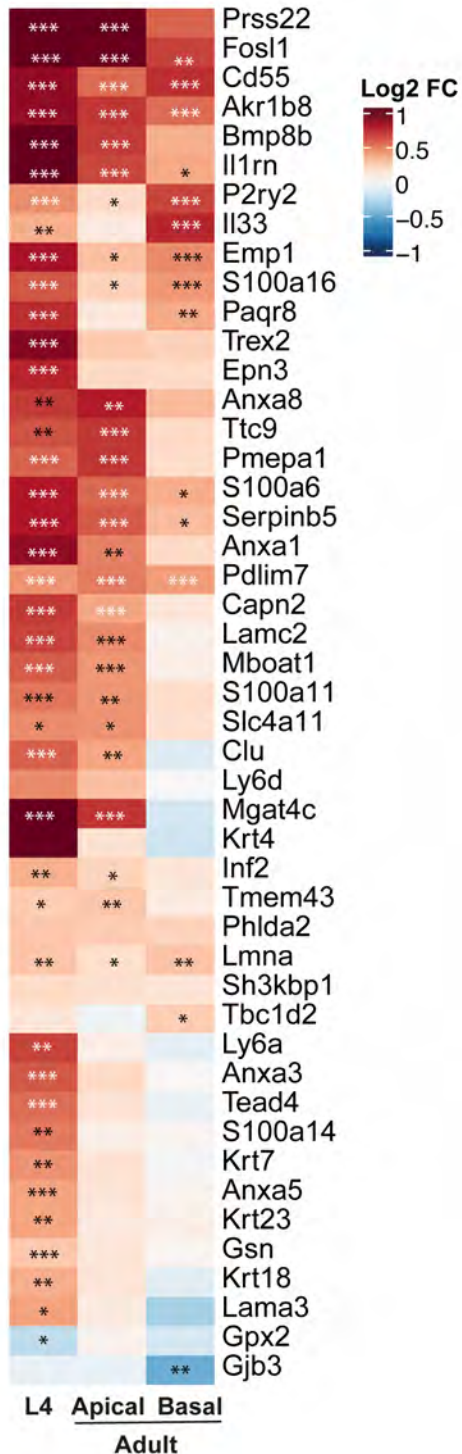


**Figure 6.13 | Differential expression of genes identified in revSC signature after *H. bakeri* co-culture.** Heatmap of  $\log_2$  fold change in genes identified as fetal-associated enriched in revSC (Karo-Atar et al., 2022) (rows) in L4 basal vs. mock (L4, left-hand column), apical adult vs. mock (centre column), or basal adult vs. mock (right-hand column). Cells coloured by  $\log_2$  fold change from 1 (dark red) to -1 (dark blue) key on graph. Significance of differential expression indicated for each gene in each comparison  $< 0.05 = *$ ,  $< 0.01 = **$  and  $< 0.001 = ***$

CAMERA analysis was performed using the edgeR results for live worm co-cultures and I found a number of pathways enriched. The majority of the most significantly enriched pathways (ranked by FDR) were downregulated and

related to cell cycle, DNA replication and chromosome segregation, suggesting a strong effect on cell proliferation (Table 6.4). Conversely, the upregulated pathways related to metabolism (Table 6.4). The full list of enriched pathways can be found in Supplemental file 6.2.

**Table 6.4 | Top 20 ranked pathways enriched using CAMERA pathway analysis for live worm co-cultures.** Only pathways that rank in the top 20 pathways for at least one comparison are included in this table. Pathway analysis was performed using a competitive gene set test accounting for inter-gene correlation (CAMERA) pathway analysis in R. Pathways were ranked by their FDR value in L4 vs. mock.

GO term	Direction	P-value	FDR	Rank in L4 vs. mock	Rank in Adult apical vs. mock	Rank in Adult basal vs. mock
DNA-dependent DNA replication	Down	9.31E-14	7.60E-11	1	9	2
mitotic sister chromatid segregation	Down	2.00E-13	9.17E-11	2	2	3
sister chromatid segregation	Down	4.74E-14	7.60E-11	3	1	1
DNA replication	Down	2.81E-13	9.17E-11	4	14	5
nuclear chromosome segregation	Down	2.38E-13	9.17E-11	5	3	4
chromosome segregation	Down	1.00E-12	2.73E-10	6	6	6
DNA recombination	Down	8.54E-12	1.74E-09	7	19	8
meiotic cell cycle process	Down	2.56E-10	2.46E-08	8	4	17
mitotic nuclear division	Down	3.90E-07	9.09E-05	9	7	21
meiotic nuclear division	Down	3.39E-10	2.83E-08	10	5	19
metaphase/anaphase transition of mitotic cell cycle	Down	1.94E-10	1.98E-08	11	13	16
meiotic cell cycle	Down	7.56E-11	1.03E-08	12	8	12
metaphase/anaphase transition of cell cycle	Down	2.96E-10	2.69E-08	13	12	18
regulation of mitotic sister chromatid separation	Down	5.74E-06	0.00052734	14	17	22
recombinational repair	Down	8.82E-11	1.03E-08	15	24	13
mitotic sister chromatid separation	Down	2.69E-11	2.71E-09	16	21	26
double-strand break repair via homologous recombination	Down	9.78E-11	1.06E-08	17	23	15
nucleosome assembly	Down	3.42E-11	3.11E-09	18	63	53
DNA conformation change	Down	5.81E-11	4.99E-09	19	72	25
regulation of mitotic metaphase/anaphase transition	Down	8.13E-11	6.50E-09	20	27	32
double-strand break repair	Down	1.74E-11	2.58E-09	21	11	10
meiosis I cell cycle process	Down	5.27E-06	0.00052734	23	18	28

<b>regulation of sister chromatid segregation</b>	Down	9.04E-06	0.000703 2	25	20	24
<b>regulation of chromosome segregation</b>	Down	3.46E-10	2.83E-08	26	16	20
<b>meiosis I</b>	Down	4.81E-06	0.000524 1	27	15	27
<b>glutathione metabolic process</b>	Up	3.50E-12	8.17E-10	88	10	7
<b>cholesterol metabolic process</b>	Up	1.15E-11	2.08E-09	114	68	9
<b>sterol metabolic process</b>	Up	1.67E-11	2.58E-09	118	79	11
<b>secondary alcohol metabolic process</b>	Up	8.39E-11	1.03E-08	135	74	14

To assess whether gene expression changes in response to co-culture with live *H. bakeri* may modify the proportions of cellular subpopulations within 2-D enteroids, I performed CAMERA analysis against top 100 gene specifically expressed by each cell type (retrieved from scRNA-seq data from Haber *et al*, 2017). I found similar effects to when 2-D enteroids were treated with EVdepHES or EVs, with a strong negative enrichment of TA cell specific genes, especially those undergoing cell cycle, and enterocyte progenitors (Figure 6.14). Conversely, more mature enterocyte populations were increased which could reflect an abrogated ability to generate new enterocyte progenitors while those present at time of treatment continued to mature (Figure 6.14). Stem cells were significantly suppressed only by adult *H. bakeri* basal co-culture, despite identifying significant suppression of key stem genes in other comparison (Figure 6.14). Paneth cells were suppressed by adult and L4 basal co-culture (Figure 6.14).



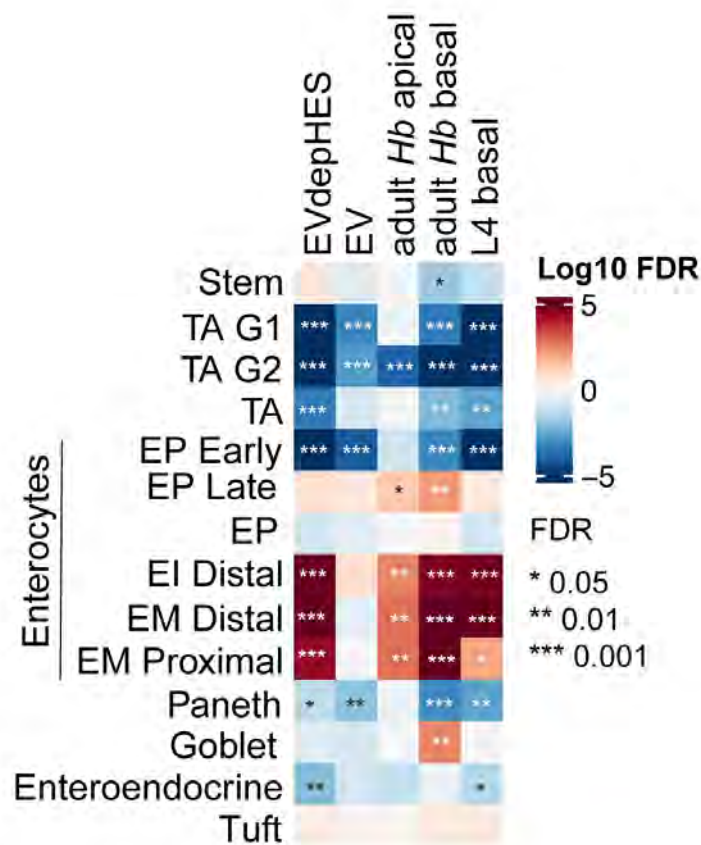


**Figure 6.14 | Positive and negative enrichment of cell type specific genes in 2-D enteroids after co-culture with *H. bakeri*.** CAMERA analysis was performed using edgeR results for (left to right) EVdepHES vs mock, EV vs. mock, adult *H. bakeri* apical vs. mock, adult *H. bakeri* basal vs. mock, L4 basal vs. mock, against the top 100 cell type specific genes for each intestinal epithelial cell type identified by scRNA-seq in Haber *et al*, 2017. **A)** For upregulated pathways FDR values were transformed by  $-\log_{10}(\text{FDR})$  and for pathways going down these were transformed by  $-1 * -\log_{10}(\text{FDR})$  to visualise both the direction of change and significance, these values were then visualised in a heatmap using the package ComplexHeatmap in RStudio. Significance values are indicated by FDR \* <0.05, \*\* <0.01 and \*\*\* <0.01. EP = enterocyte progenitor, E = enterocyte, EI = enterocyte immature, TA = Transit-amplifying, G1 = Gap 1 phase of cell cycle, G2 = Gap 2 phase of cell cycle

### 6.2.5 scRNA-sequencing of treated 2-D enteroids

A major goal of this thesis was to determine whether *H. bakeri* EV uptake in the 2-D enteroids is cell type specific, or whether *H. bakeri* EVs have a tropism for certain cellular subpopulations with the intestinal epithelium. RNA-seq data (Section 6.2.3) indicated that *H. bakeri* EVs induce gene expression changes on genes that are specifically expressed by certain cell types in the intestinal epithelium, namely Paneth, TA cells and enteroendocrine cells. To further investigate the cell type specific gene expression signatures upon EV, or EVdepHES treatment I designed a scRNA-sequencing experiment. Based on the low detection of tuft cell marker genes in our previous RNA-seq data (Section 6.2.3), and the well described role of tuft cells in detection and response to helminth infection (Drurey et al., 2021; Gerbe et al., 2016; Howitt et al., 2016; Von Moltke et al., 2016) I decided to enrich for these cells to improve our chances of capturing this population. Therefore, this experiment was performed under IL-4 and IL-13 conditions, which I have shown induce goblet and tuft cell differentiation in 2-D enteroids (Chapter 4 of this thesis). I treated grew 2-D enteroids in the presence of IL-4 and IL-13 from day 2 after seeding and on day 3 treated the apical epithelium with either the mock control, EVs, or EVdepHES for 24 h before performing scRNA-seq summarised in Figure 6.15.

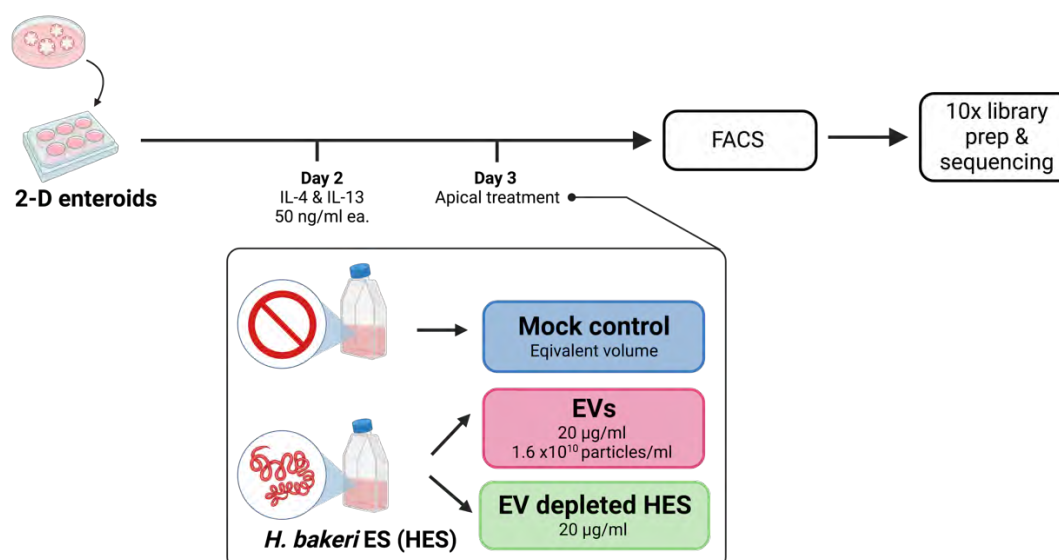


**Figure 6.15 | Schematic of scRNA-seq experimental design.** 2-D enteroids were cultured as previously described. After seeding cells were maintained in stem cell enriching media for 2 days after which media was replaced with 2-D culture media containing 50 ng/ml each of IL-4 and IL-13. On day 3 in culture apical media was removed and apical surface washed once with PBS before treated with either i) mock control volume equivalent to EVs, ii) double isolated EVs (20 µg/ml equating to 1.6x10<sup>6</sup> particles) or iii) double depleted EVdepHES (20 µg/ml). Samples were left for 24 h before harvesting cells for FACS sorting of live cells and 10x library preparation (Chapter 2 of this thesis) before sequencing. FACS = flow cytometry assisted cell sorting. Sequencing of each conditions was performed on a pool of 6 replicates in order to have enough cells for 10X scRNA seq.

Prior dissociations of 2-D enteroids into single cell suspensions resulted in relatively high proportions of dead cells as evidenced in Chapter 5 of this thesis, I therefore chose to sort for live cells using FACS prior to library preparation. Despite retrieving a low proportion of live cells (<35%) I was able to sort enough cells of each condition to load 30,000 on the 10x chromium aiming for a targeted cell recovery of 10,000 cells (Table 6.5).

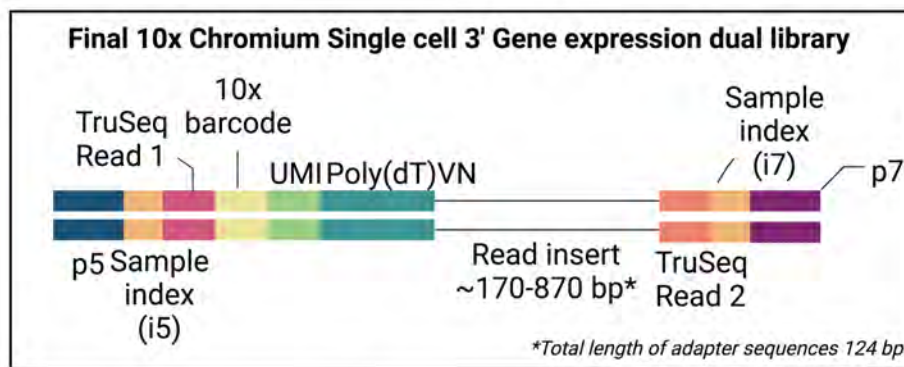
**Table 6.5 | Summary of percentage live of samples and sorted cell numbers for 10x scRNA-seq.** Sample (Left-hand column), number of live cells sorted total (middle column) and the percentage of single cells that were live within each sample (right-hand column).

Sample	Live cells recovered	% live
Mock	43,381	32.06
EVs	74,368	32.19
EVdepHES	82,315	22.01

10x chromium scRNA-sequencing libraries were made by Elisabeth Freyer at the FACS facility in the Institute of Genetics and Cancer (IGC) at the University of Edinburgh using the Chromium Next GEM Single cell 3' Kit v3.1 (10x user guide). A schematic describing the steps of 10x library generation is provided

in Chapter 2 of this thesis, and the resulting 10x read structure is summarised here (Figure 6.16). Quality control was performed using a High Sensitivity DNA bioanalyzer chip of the resulting single cell DNA fragment libraries. Our libraries showed a size range of ~ 300-1000 bp with a peak of 400-600 bp. The 10x genomics adapter components comprise a total of 124 bp, meaning the DNA insert in a given read ranges from ~176–876 bp (10x user guide). I achieved high quality library preparations from all three samples based on the yield and size of DNA (peak 400-600 bp) (Figure 6.16).

A.



B.

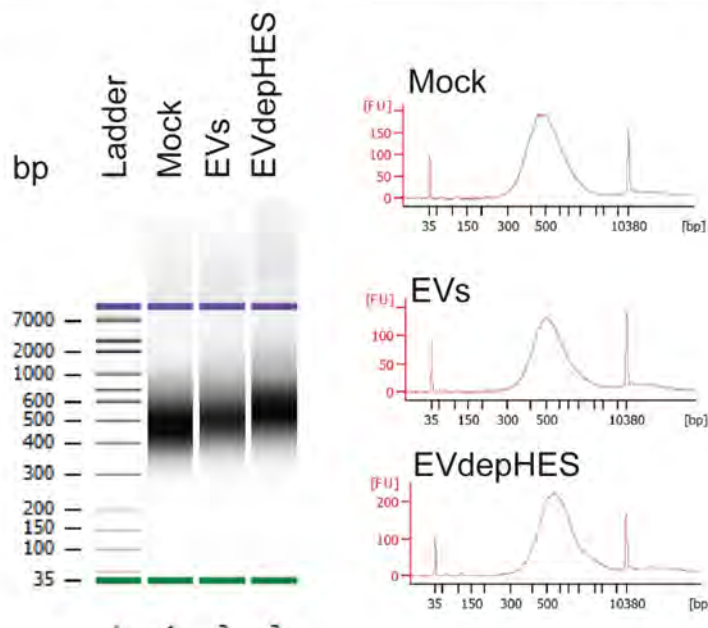


**Figure 6.16 | Quality control of 10x scRNA-seq libraries.** **A)** Schematic of final libraries generated by Chromium Next GEM Single cell 3' Kit v3.1. The total length of adapter sequences is 124 bp and genomic insert should therefore be between ~170-870 bp. Figure adapted from the 10x user guide. **B&C)** DNA

High Sensitivity Bioanalyzer analysis of Mock, EV and EVdepHES treated 2-D enteroid 10x single cell libraries showing library size range and peak size. bp = base pairs.

After sequencing, scRNA-seq data underwent computational quality control. In brief, cells deemed to be empty, or cells that represented doublets were removed as were cells that were likely dead based on barcode rank. An additional filter was used to remove low quality cells >20% UMIs associated with mitochondrial (mt) genes. This is a more relaxed filter than the standardised threshold (5%) (Satija et al., 2015), owing to the fact that scRNA-seq data from intestinal epithelium has a higher % mt reads than other tissues (Osorio & Cai, 2021). It should be noted our % mt cut off is stricter than previously published intestinal epithelial data (<30%) (Duque-Correa, Goulding, Rodgers, Gillis, et al., 2022; Triana et al., 2021). For visualisation of the distribution of single cells dimensionality reduction was performed using Uniform Manifold Approximation and Projection (UMAP) with 20 principal components and identified 10 separate clusters (Figure 6.17 A&B). When our UMAP was coloured by treatment I can immediately see that the different conditions have differing patterns of distribution for certain clusters. For example, mock cells are only lowly represented in clusters 0, 3 & 7 and instead these are comprised mostly of cells that were EV or EVdepHES treated (Figure 6.9 A&C-E). After filtering, retrieved variable numbers of cells for each condition 1,096 cells for mock, 2,835 for the EV treatment and 1,962 for the EVdepHES treatment.

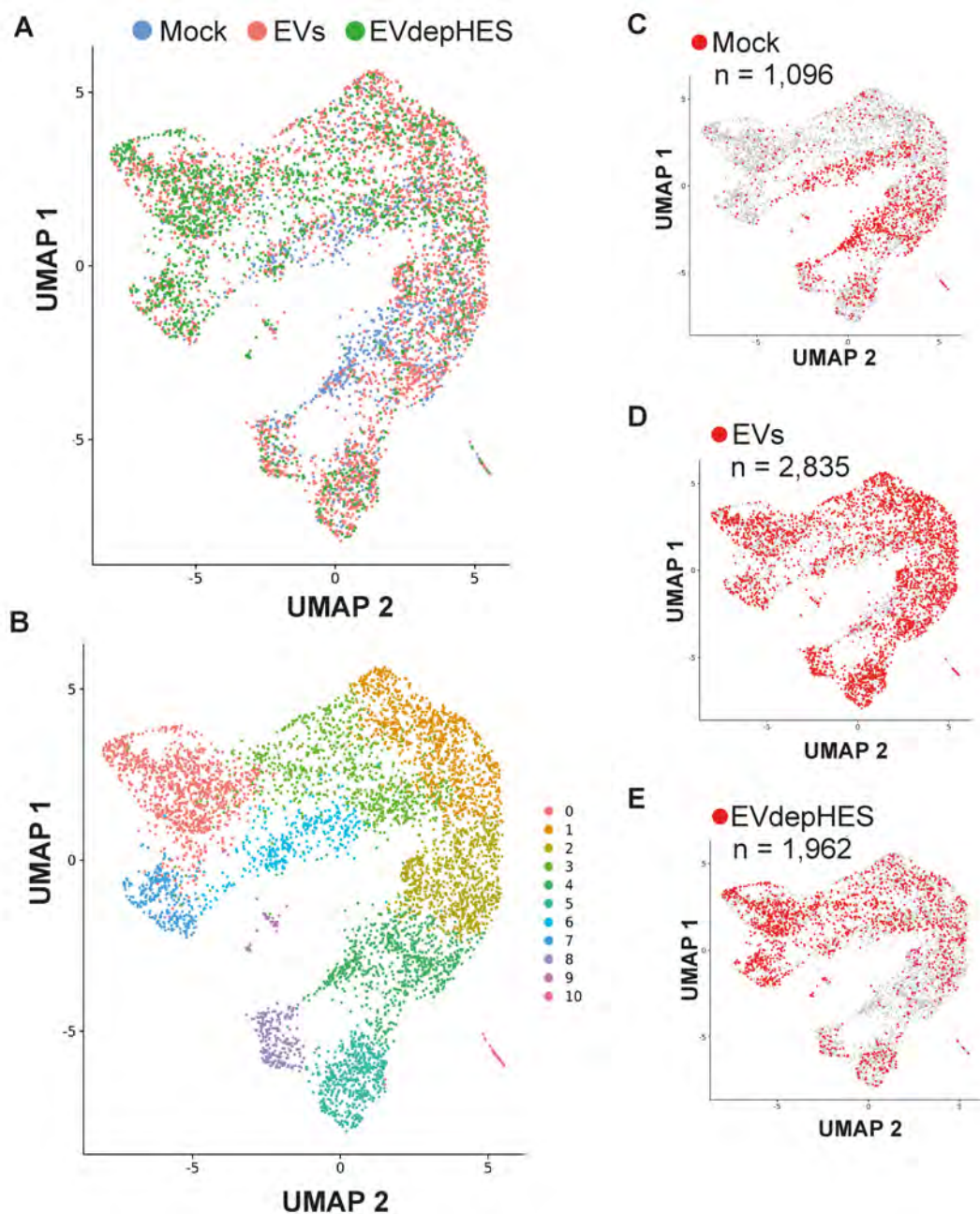


**Figure 6.17 | scRNA-seq of *H. bakeri* ES treated 2-D enteroids.** Uniform Manifold Approximation and Projection (UMAP) was used for dimensional reduction and visualisation of the distribution of cells from all conditions using 20 principal components. Cell clustering was performed by Yenetzi Villagrana Pacheco using Seurat **A**) Coloured by conditions. Mock (blue), EV (pink) and EVdepHES (green). **B**) Coloured by cell clusters identified using the Seurat functions FindNeighbors and FindClusters detailed in Chapter 2 of this thesis **C&E**) UMAP coloured by each condition in red all remaining cells in grey, number of cells per condition identified **C**) Mock **D**) EVs **E**) EVdepHES. n = total number of cells for each condition after filtering steps.

We next identified cell cluster identities using SingleCellNet machine learning algorithms to determine cell types. SingleCellNet requires a training data set,

for this I used scRNA-seq analysis of intestinal epithelium from tissue as a training dataset (Haber et al., 2017). I found the presence of all cell types of the intestinal epithelium, with the exception of M cells known to be absent from our 2-D enteroids (Chapter 4 of this thesis). By performing differential expression of the genes in each cluster identified by Seurat compared to expression in all clusters I generated a list of enriched genes for each Seurat cluster. I then manually checked the cell identifications made by SingleCellNet against the genes enriched for each cluster by Seurat to confirm cluster identities. I were confident in the identification of most clusters cell types identified by SingleCellNet, which overlap with expression of cell specific markers for enterocyte populations, enterocyte progenitors, tuft, goblet and Paneth cells (Figure 6.18). Due to some uncertainty in some of the SingleCellNet cell identifications (discussed below) I choose to show expression of marker genes across the dataset to better represent the data (Figure 6.18). Cluster 9 represents a small mixed population of cells expressing markers of both Paneth, goblet and enteroendocrine cells that owing to the fact they express many genes in common (Karo-Atar et al., 2022), and the low numbers captured in this dataset likely affected our ability to separate these cells (Figure 6.17, 6.18,). However, cluster 0 and 5 were identified by SingleCellNet as enteroendocrine (EEC) but were not enriched for typical EEC marker genes (e.g., *Neurog3*, *Neurod1* and *Neurod2*). Cluster 9 on the other hand had enrichment of these EECs specific genes, and I predict our true EECs are within Cluster 9 but were only captured in very small numbers (Figure 6.18). I investigated clusters 0&5 which were identified by SingleCellNet as EECs, however I were not confident in this identification, and discovered these clusters to display the higher expression of revSC specific genes than other cluster and I identify them as putative revSCs (Figure 6.20). revSC were not classified by the Haber *et al*, 2017 study and therefore revSC were not included in the training dataset which could have led to misidentification. In the presence of IL4/IL13 I see a small, but clearly detectable population of tuft cells in our scRNA-seq data (Cluster 10) (Figure 6.17 & Figure 6.18). These data taken together confirm the heterogeneity of

cell types in 2-D enteroids and show the presence of all differentiated cell types even if only captured at low numbers, with the exception of M cells.

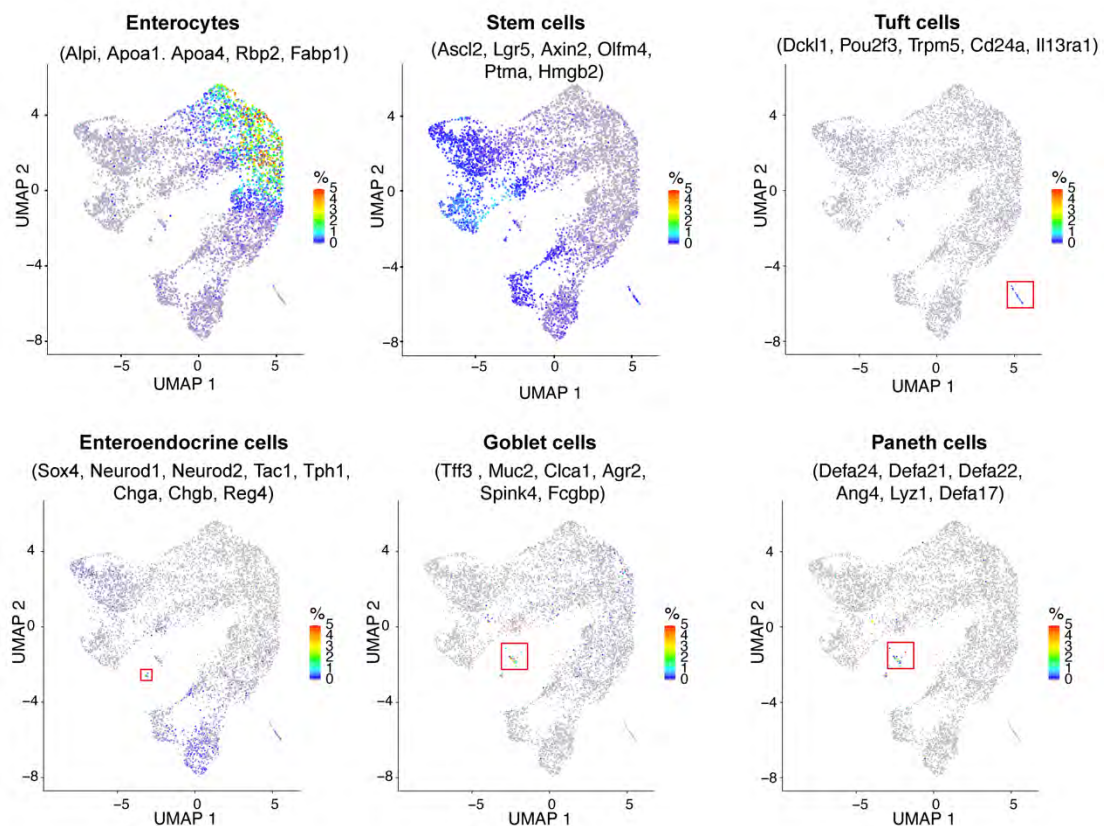


**Figure 6.18 | Expression of cell type specific genes in scRNA-seq of 2-D enteroids.** UMAP plot of dataset coloured by percentage of reads that map to the genes listed on each plot. Each plot shows cell type specific genes on the top row left to right enterocyte genes, intestinal stem cell genes, and tuft cell genes. Bottom row left to right enteroendocrine genes, goblet cell genes and Paneth cell genes.

The expression of several key cell type specific genes was qualitatively assessed for each condition (mock, EV, EVdepHES) (Figure 6.19). I identify a pattern of lower expression of tuft cell specific genes (*Dckl1*, *Trpm5*, *Pou2f3* and *Il13ra1*) in EV and EVdepHES treated 2-D enteroids than in the mock control (Figure 6.19). It should be noted that while the IL-13 receptor (*Il13ra1*) is expressed by tuft cells, it is also expressed by enterocytes in our dataset. For EEC specific genes while I detect well characterised EEC genes, only very few cells were identified as expressing these genes making comparison difficult (Figure 6.19). The stem cell associated genes *Lgr5*, *Axin2* and *Ascl2* displayed lower expression in EV or EVdepHES treated 2-D enteroids than in the mock control, while for *Olfm4*, which was detected in fewer cells, this was



less convincing (Figure 6.19). Paneth cell specific antimicrobial peptides (*Lyz1* and *Defa17*) also showed lowered expression in EV or EVdepHES treated, but *Ang4* was slightly increased (Figure 6.19). Finally, multiple enterocyte specific genes demonstrated increased expression in EV treated 2-D enteroids than EVdepHES or mock (*Apoa1*, *Apoa4*, *Fabp1*, *Rbp2*) (Figure 6.19).

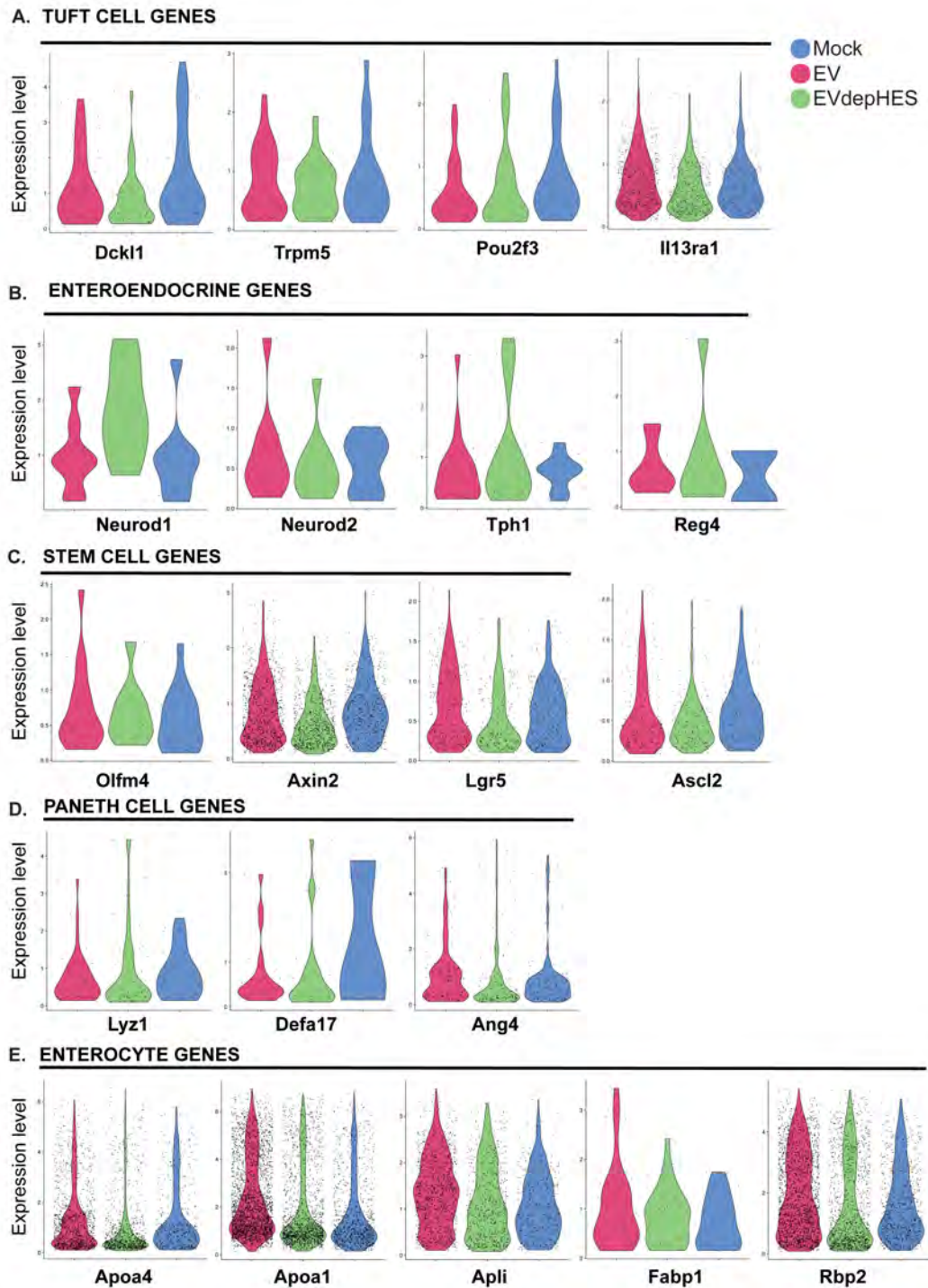


**Figure 6.19 | Qualitative assessment of gene expression in scRNA-seq of 2-D enteroids across treatments.** Violin plot showing expression of genes associated with **A)** tuft cells, **B)** enteroendocrine cells, **C)** stem cells, **D)** Paneth cells or **E)** enterocytes. All genes that express a given gene are plotted by condition, EV (pink), EVdepHES (green), Mock (blue). Expression (logCP10K) in individual cells is indicated by dots, and violin plots visualise the expression distribution for that population of cells.

In order to assess the presence of revSC genes in our scRNA-seq dataset I assessed the expression of revSC specific genes identified by Karo-Atar *et al*, 2022 (Figure 6.20 A). Expression of revSC genes was not highly specific to a single cell cluster but cluster 0, 5 & 7 demonstrated the highest average percentage of reads (Figure 6.20 A). Overall expression of revSC in each condition (Figure 6.20 B) showed a qualitative increase in expression of revSC genes in EV and EVdepHES treated 2-D enteroids compared to mock. Of these revSC associated genes, *Ly6a* which is thought to expressed at the initial stages of revSC conversion, was the most obviously increased after EV and EVdepHES (Karo-Atar *et al.*, 2022; Nusse *et al.*, 2018).

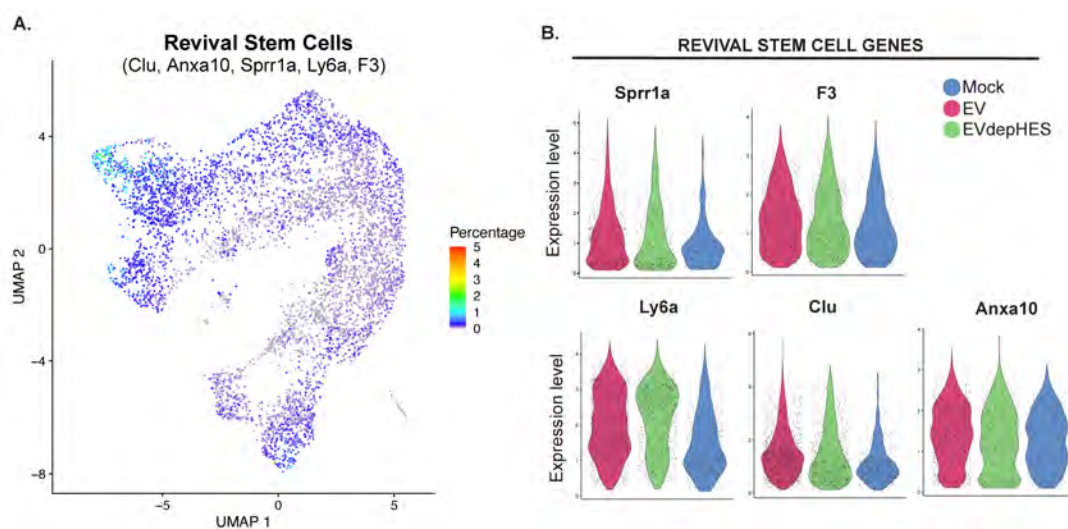


**Figure 6.20 | Expression of revSC genes in scRNA-seq.** **A)** UMAP coloured by average percentage of reads for the genes listed **B)** Violin plot showing expression of revSC specific genes for all cells in each condition EV (pink), EVdepHES (green), Mock (blue). Expression (logCP10K) in individual cells is indicated by dots, and violin plots visualise the expression distribution for that population of cells. revSC = revival stem cells.

Suppression of cell cycle was identified in RNA-seq of both ES treated 2-D enteroids and in co-culture experiments (Section 6.2.1 – 6.2.4). I identified qualitatively lower expression of the cell cycle genes (*Mcm5*, *Mcm6*, *Pcna*) in EV or EVdepHES 2-D enteroids (Figure 6.21). The expression of these genes was restricted to stem and progenitor cells (Figure 6.18, 6.21).

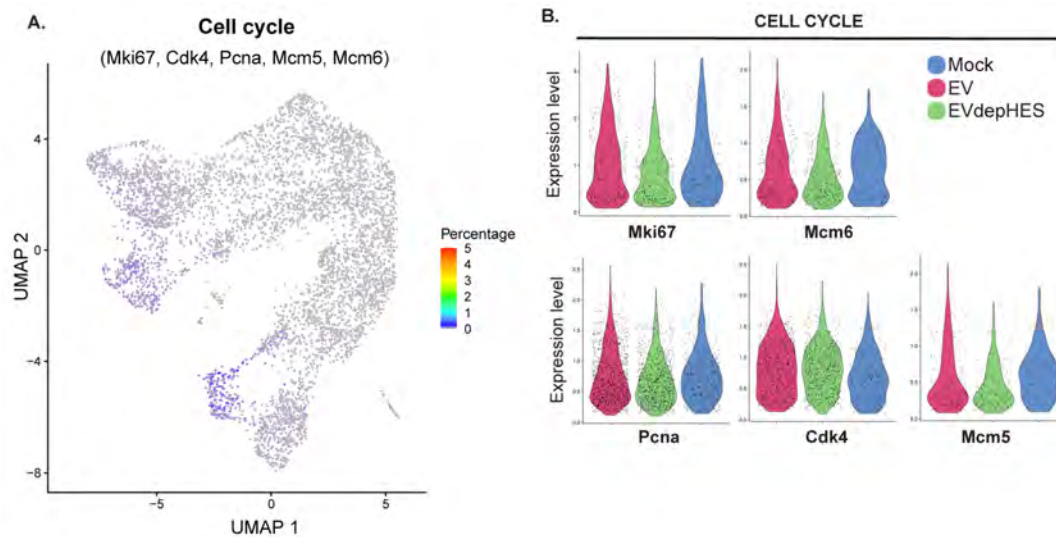


**Figure 6.21 | Expression of cell cycle genes in scRNA-seq. A)** UMAP coloured by average percentage of reads for the genes listed **B)** Violin plot showing expression of cell cycle specific genes for all cells in each condition EV (pink), EVdepHES (green), Mock (blue). Expression (logCP10K) in individual cells is indicated by dots, and violin plots visualise the expression distribution for that population of cells.

### 6.2.6 Bifurcation of UMAP data is driven by cell quality which may or may not be related to treatment

UMAP of our data showed two bifurcated arms that mirrored each other and for some cell types identified multiple clusters of the same cell type one clustered on the upper arm and one on the lower arm (data not shown). This was not consistent with published data from *H. bakeri* infected tissue or organoids, where differences in the proportions of cell in a cluster occurred, but effects that override the cell type identity of a cluster were not seen (Haber et al., 2017; Karo-Atar et al., 2022). To identify whether this bifurcation of our UMAP could be driven by treatment, or by another factor I re-assessed the cell quality in our data. I found that although the majority of our cells were well below the <20% mt gene cut off, the distribution of % mt for cells in each condition was drastically different for our mock control compared to EV or EVdepHES (Figure 6.22 A). The mock condition had a higher average percentage of reads mapping to mt genes than EV or EVdepHES conditions (Figure 6.22 A). This finding suggesting a difference in overall sample quality

between conditions. I then looked to see whether this correlated with the bifurcation of our UMAP and found that expression of mt genes correlates with the lower arm, and the upper arm has relatively low mt genes (Figure 6.22 A). Anoikis is a specific form of cell death that occurs when epithelial cells detach from the surrounding ECM and occurs naturally in the intestinal epithelium as cells move towards the tips of the intestinal villi. During dissociation of cells for scRNA-seq the intestinal epithelial cells are detached from the artificial ECM below, so I assessed the expression of genes related to anoikis in our data set. The percentage of reads mapping to anoikis genes was low and evenly dispersed between the two arms of this data set (Figure 6.22 A). These findings do not rule out that treatment itself to affect the cell quality, however as I performed one replicate per condition, I also cannot prove that treatment is responsible for any effect on cell quality. Previous flow cytometry data of EV treated organoids did not suggest differences in proportions of dead cells (Chapter 5), nor did the sorting data from this experiment. However, cells may have died as a result of, or after sorting, and the processing order (mock were processed first) may explain the difference in quality between conditions.

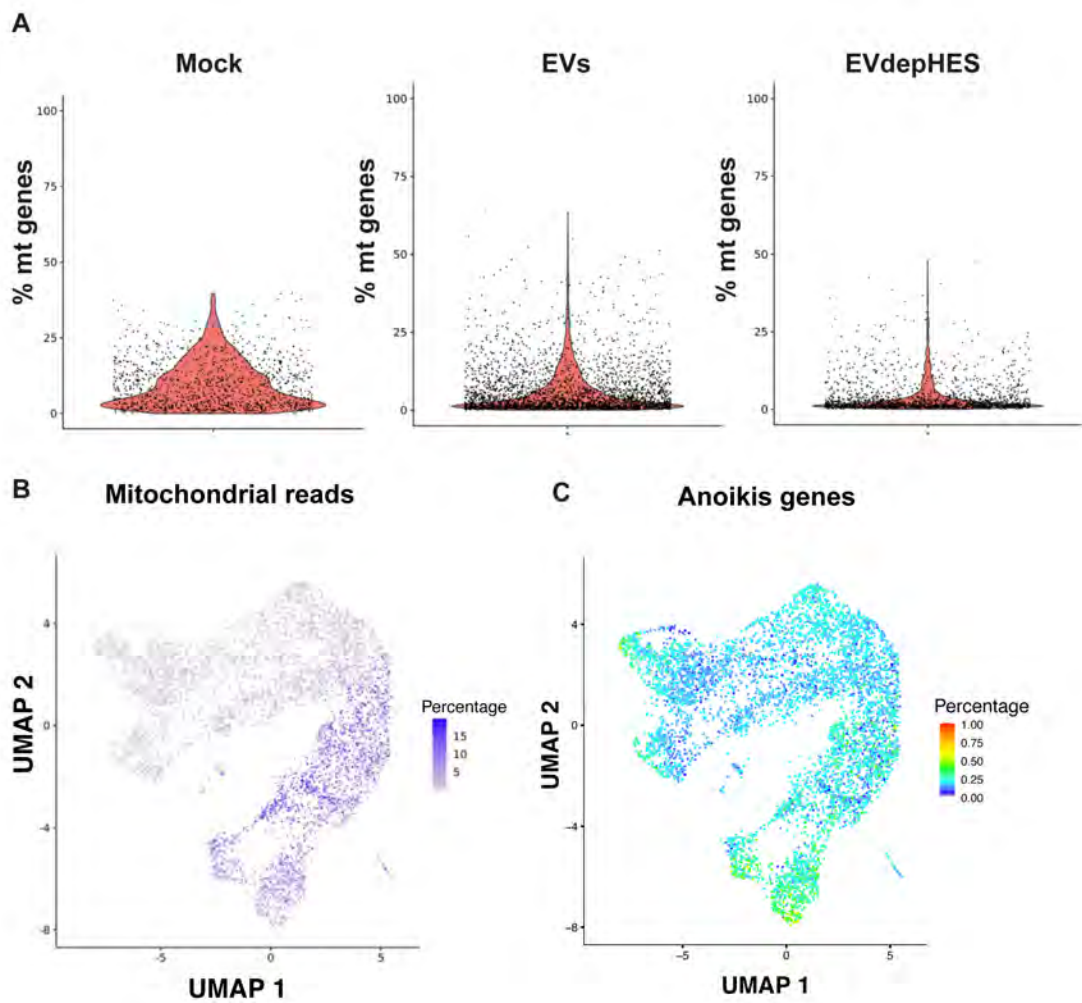


**Figure 6.22 | Bioinformatic quality control of 10x scRNA-seq libraries. A)** Violin plot showing the distribution of percentage of mitochondrial genes in each cell (x-axis) in each condition. Mt = mitochondrial **B)** UMAP coloured by the percentage of mitochondrial genes per cell.

### 6.2.7 Summary of Chapter 6 results

- EVs and EVdepHES induced subtle effect on the transcriptional response in the intestinal epithelium in 2-D enteroids models in the absence of immune cells and cytokines.
- EVs and EVdepHES induce many overlapping functions suggesting there are multiple molecular mechanisms that work synergistically during infection to modify this tissue.
- Some transcriptional changes are more specific to EVs, such as a repression of Paneth cells and antimicrobial peptides.
- EVs showed downregulation of the stem specific gene *Olfm4*, and *Lgr5*, and *Ascl2* which are both critical for ISCs.
- EVs alone do not induce revSCs, but EVdepHES and co-culture with L4's or adult worms strongly induce a revSC signature in 2-D enteroids.
- All ES and live co-culture conditions indicate a strong downregulation of pathways related to cell cycle, and genes specific to TA cells (which rapidly proliferate) suggesting *H. bakeri* interferes with epithelial cell turnover.
- Enteroendocrine cell specific genes and some of their secreted hormones (Ghrelin and Somatostatin) are repressed by all *H. bakeri* ES and co-culture conditions tested.
- The localisation of *H. bakeri* worms to the apical or basal side has an effect on the strength of transcriptional response in 2-D enteroids.
- scRNA-seq confirmed cellular heterogeneity of 2-D enteroids and identified differences between EV and EVdepHES and mock control.
- RevSC associated genes including *Ly6a* showed higher expression after EV and EVdepHES by scRNA-seq. A cluster of cells predominantly comprised of cells from EV and EVdepHES conditions was putatively identified as revSC.

### 6.3 Discussion

In this chapter, I aimed to investigate the host transcriptional response to *H. bakeri* EVs, and EVdepHES in 2-D enteroids in order to discern EV specific responses. The results suggest that *H. bakeri* EVs have subtle suppressive effects on Paneth cells and several of the AMPs produced by these cells, cell cycle, and stem cell specific genes (Figure 6.5, 6.7, 6.8). However, I found the majority of responses to EVs to be concordantly changed by EVdepHES treatment, suggesting EVs and non-vesicular components of HES may act synergistically during infection (Figure 6.4). However, some opposing effects of EVs and EVdepHES were identified. For example, for IFN response genes which were upregulated by EVdepHES, and subtly suppressed by EVs (Figure 6.5). Recent publications identified that *H. bakeri* induces revSCs in the intestinal epithelium during infection, and this phenotype was later reproduced in 3-D enteroids through HES treatment (Karo-Atar et al., 2022; Nusse et al., 2018). revSCs have since been demonstrated to arise in response to damage to ISCs, which would suggest that *H. bakeri* damage of ISCs could drive revSC induction (Ayyaz et al., 2019). Our lab had preliminary data suggesting *H. bakeri* EVs modified genes related to stemness. Indeed, I confirmed our prior findings by identifying in this study subtle changes to key stem cell genes (*Olfm4*, *Ascl2*) in response to both EVs and EVdepHES (Figure 6.5). I then interrogated the presence of revSC signatures in our dataset and found that while EVdepHES induced strong revSC signature this was not the case for EVs when looking at RNA-seq (Figure 6.6). Although, scRNA-seq did show subtly higher expression of revSC associated genes in both EV and EVdepHES treated 2-D enteroids than in the mock condition (Figure 6.20).

In parallel, I investigated the transcriptional response in 2-D enteroids after co-culture with *H. bakeri*. I found stronger effects on gene expression in response to live worms than to purified EVdepHES or EVs (Figure 6.2, 6.3, 6.9, 6.10). In addition, I investigate the effect of parasite localisation by co-culturing either at



the apical epithelium or in the basal compartment. I demonstrated that although overall changes were concordant in both setting, basal co-culture resulted in more differentially expressed genes in 2-D enteroids than apical co-cultures (Figure 6.9, 6.10, 6.11). Finally, I also compared the effects of *H. bakeri* life stages by adding L4 larvae in the basal compartment of 2-D enteroids. Surprisingly, I found this life stage to induce the strongest effects on gene expression of all the live worm co-culture conditions (Figure 6.9, 6.10). All co-culture conditions showed a strong suppression of the stem cell specific genes and cell cycle (Figure 6.12). RevSC signatures were strongly upregulated by all co-culture conditions, but particularly by L4 larvae (Figure 6.13). I identified similar effects on specific cell subpopulations with 2-D enteroids as I saw for EVs and EVdepHES, TA cells, enterocyte progenitors, and Paneth cells were suppressed (Figure 6.13). However, unlike ES conditions these findings coincided with an increase in enterocytes populations (Figure 6.13). Significant suppression of stem cells was only identified for adult basal co-cultures (Figure 6.13).

### 6.3.1 Limitations for RNA-seq

RNA-seq data indicated substantial variability between technical replicates even for the mock condition, which implicated downstream statistics. Variation may be explained by the fact that organoids are heterogeneous in cell type, and differentiation occurs in a stochastic manner, leading to higher variability compared to homogeneous cell lines. Furthermore, compared to *in vivo* tissue, organoids are reductionistic and many factors that tightly control the proportions of cell types within the epithelium may be lost in organoid culture systems. For example: i) the physical architecture of the crypt and villus, and/or ii) additional signals from stromal, immune, and mesenchymal cells that may finely tune differentiation are not present in 2-D models and could result in higher variability.

Findings described in chapter 5 of this thesis indicated that only a proportion of 2-D organoid cells take up EV-AF647, therefore the signal from cells that took up EVs in this dataset is likely to be diluted by cells that were not targeted. One approach to circumvent this issue would be to sort cells that are positive for EV-AF647, this would be a powerful way of identifying direct gene expression changes in response to EV uptake. This strategy could also indicate whether specific sub-populations are targeted by *H. bakeri* EVs for uptake. This approach was performed, however due to low numbers of EV-AF647 positive cells, combined with poor viability, only a very small number of cells could be sorted. Optimisation of the protocols for harvesting and dissociating 2-D organoid cells have since been improved for high viability (80-90% viable cells), and this remains a potential area for future investigation. Alternatively, the concentration of EVs used for this experiment was based on knowledge from MODE-K cells. The experiments detailed in this chapter would have benefited from performing a prior dose response study in my 2-D enteroid model.

We chose to assess the transcriptome 24 hr after treatment based on the understanding of uptake dynamics in MODE-K and 2-D enteroids (Chapter 5 of this thesis), (Coakley et al., 2017). This timepoint is sufficient to see early changes in response to ES products. Interestingly, some genes modified by *H. bakeri* or its ES products are involved in differentiation (*Dll1*, *Atoh1*, *Hes1*, *Sox9*, *Ascl2*) and could impact cellular differentiation within 2-D enteroids. However, the cell cycle time of ISCs is ~ 24 hr, while TA cells undergo faster cell cycling within 12 hr (Ballweg et al., 2018). Therefore, changes within 24 hr will not capture the full impact of treatment on cellular differentiation within 2-D enteroids. Assessing transcriptional changes, or cellular populations by microscopy, over a longer time course would allow better assessment of changes in cellular differentiation after exposure to EVs or EVdepHES. Given the changes I saw in certain cell fate determining factors this could be an area for future investigation. Additionally, during helminth infection parasites are continuously producing, and releasing ES products. Therefore, a more

physiological model for the effect of EVs or EVdepHES on differentiation could also include multiple doses over a longer time course.

Our 2-D enteroid model demonstrated presence all secretory cell lineages (Tuft, Enteroendocrine, Goblet and Paneth cells) (Chapter 4 of this thesis). Despite validation of tuft cell presence in the absence of Th2 cytokines by microscopy, the proportion of these cells is low. I detected the tuft associated genes *Pou2f3* and *Dckl1* in bulk sequencing data, but these were removed due to low CPMs (<1 in > 3 libraries). Therefore, using RNA-seq data I cannot conclude whether EVs play a role in the suppression of these cells by HES (Drurey et al., 2021).

For our live worm co-culture RNA-seq experiment, one concern I had regarding the experimental design was the difference in relative concentrations between the apical and basal compartments. The apical epithelium is cultured in a low media volume (200  $\mu$ l) (Chapter 2 of this thesis), whereas the basal compartment at the stage of co-culture contains 2 ml of media. Therefore, any HES produced by worms during co-culture I anticipated to be more dilute in the basal compartment, than the apical compartment. Differences in concentrations between apical and basal conditions was noted as caveat of this experiment, but I was not able to resolve these due to the transwell design. Additionally, apical worms were in direct contact with 2-D enteroids cells whereas basal worms were physically separated which could also impact our results. Even with these consideration in mind, I saw overall stronger effects on host gene expression during basal co-culture. This was unexpected and suggests that underlying host physiology in the basal vs. apical epithelium may determine the extent of the response. If this were true, then the fact that I chose apical delivery of ES products may also contribute to the subtle gene expression changes I found.

### 6.3.2 Impact of *H. bakeri* and its secreted products of the stem cell niche

Our initial hypothesis was that *H. bakeri* EVs target or modulate stem cells in the intestinal epithelium, based on pilot data 3-D organoids microinjected with *H. bakeri* EVs (Buck, unpublished). Our data demonstrated that both the EV fraction of HES as well as EVdepHES, and co-culture with live *H. bakeri* suppressed critical genes related to stem cell differentiation and maintenance (*Olfm4*, *Lgr5*, *Ascl2*, *Sox9*) (Figure 6.5, 6.12). Although, using CAMERA pathway analysis I only identified a significant negative enrichment of stem cells for the adult worm basal co-culture condition (Figure 6.13).

*H. bakeri* EV repression of the transcription factor *Ascl2* is particularly interesting even though the effect was subtle. *Ascl2* expression is tightly restricted to the base of the crypt in ISCs (Murata et al., 2020), and in combination with the Wnt induced transcription factors  $\beta$ -catenin and TCF4, it controls the expression of stem cell genes including *Lgr5* and *Sox9* (Schuijers et al., 2015). I found *Lgr5* and *Sox9* to also be downregulated by EVs (Figure 6.5). Additionally, forced expression of *Ascl2* within organoid cultures results in increased *Olfm4* expression and the amount of Ki67+ cycling cells (Schuijers et al., 2015). This is interesting as both *Olfm4* and the gene encoding ki67 (*Mki67*) are downregulated by *H. bakeri* EVs, which could represent downstream effects of *Ascl2* downregulation (Figure 6.5). *Ascl2* expression within ISCs is strictly controlled by Wnt signalling (Murata et al., 2020; Schuijers et al., 2015), therefore abrogated Wnt signalling could be an upstream regulator of many of the gene expression changes seen in our dataset. Wnt signalling results in the phosphorylation of  $\beta$ -catenin, leading to translocation of this transcription factor to the nucleus where it performs its function in regulating expression of stemness genes (Fevr et al., 2007; Korinek et al., 1998). Future experiments to assess phosphorylation, and localisation of  $\beta$ -catenin in 2-D enteroids exposed to *H. bakeri* EVs, EVdepHES or during co-culture would elucidate whether these gene expression changes occur as a result of abrogated Wnt signalling, or if they are independent of this pathway.

Findings from other groups have also implicated *H. bakeri* and its ES products in downregulation of stem cell genes, this occurred alongside an induction of a revSC phenotype (Drurey et al., 2021; Karo-Atar et al., 2022; Nusse et al., 2018). revSCs are relatively newly identified cells that are thought to replenish the epithelium after damage. Interestingly, Karo-Atar *et al* found that during infection these cells are capable of replenishing the epithelium, however fewer goblet and tuft cells arose from revSCs than from ISCs. These findings suggest that *H. bakeri* induces revSCs, thereby constricting numbers of goblet and tuft cells (Karo-Atar et al., 2022). revSCs are not helminth specific, and have been shown to be induced in response to various other models of stem cell damage (Ayyaz et al., 2019). While EV treatment had a subtle effect on key stem cell genes summarised above, it did not induce revSC associated genes by RNA-seq (Figure 6.6). Therefore, EVs may modify intestinal stem cells, but are either not involved, or are insufficient, for the conversion to revSC. However, later in this Chapter using scRNA-seq I find that *H. bakeri* EVs may have a subtle effect on the induction of revSC genes namely *Ly6a* (discussed further below).

We observed an induction of a revSC signature in EVdePHES treated 2-D enteroids (Figure 6.6), and to a greater extent in response to co-culture with live worms (Figure 6.13). revSC were initially observed during d 6 of *H. bakeri* infections when L4 larvae are within the host submucosa, and were marked by a transient up-regulation of *Ly6a* (Nusse et al., 2018). Subsequent studies found that at d 14 (when adult worms reside in the lumen) a stronger induction of revSC genes was observed, however *Ly6a* up-regulation was not sustained at this time point (Karo-Atar et al., 2022; Nusse et al., 2018). One interpretation of these results is that the adult parasite is better able to induce these cells. Our data comparing co-culture of adult and L4 worms confirms the finding that L4 stage parasite specifically induces *Ly6a* expression, however at 24 h I see stronger effects with L4 larvae than adult worms (Figure 6.13). These findings,

in context with previous publications, suggest that it is not the parasite life stage that dictates the increased response at d 14 of infection, as I found L4 larvae to induce stronger effects than adult worms. I suggest instead that the sustained delivery of ES products over a longer period of time (14 days rather than 6) results in stronger changes seen *in vivo*. An intriguing question is whether *H. bakeri* ES directly induces the revSCs transcriptional programme, or whether this is an indirect effect of *H. bakeri* ES mediated stem cell damage which then triggers the host to induce these revSCs.

### 6.3.3 Impact of *H. bakeri* and its secreted products on sub-populations within 2-D enteroids

We demonstrated that *H. bakeri* EVs have suppressive effects on Paneth cell specific gene expression within the epithelium (Figure 6.5, 6.8). I saw a consistent effect on Paneth cells with L4 larvae and basal adult co-culture (Figure 6.13). Recent studies also show sequencing data that suggests changes to Paneth cells in HES treated organoids, although neither publications focused on these findings (Drurey et al., 2021; Karo-Atar et al., 2022). Paneth cell hyperplasia has been described during infection with several helminth species, including *H. bakeri*, driven by the Th2 cytokine IL-13 (Forman et al., 2012; Kamal et al., 2002). *H. bakeri* EVs may act to constrain these host responses during infection, in order to limit Paneth cell hyperplasia. The major role of Paneth cells is to secrete antimicrobial peptides (AMPs) which acts to control the intestinal microbiome (Andre J. Ouellette, 2005). Whether AMPs also impact helminth infections is mostly unknown. Although the Paneth cell secreted antimicrobial peptide *Ang4*, which I identify as subtly downregulated in response to *H. bakeri* EVs (Figure 6.5), has been shown to increase in the colon during *T. muris* infection. In these studies *Ang4* negatively correlate with worm burden (Datta et al., 2005; D'Elia et al., 2009; Forman et al., 2012; Kamal et al., 2002). However, it should be noted that in the large intestine, which is void of Paneth cells, the main producer of *Ang4* in this tissue

is goblet cells (Forman et al., 2012). In addition to *Ang4*, a slew of antimicrobial alpha ( $\alpha$ ) defensin genes (*Defa*) were suppressed by *H. bakeri* EVs (Figure 6.5).  $\alpha$ -defensins are known to have broad microbicidal activity, and are effective against protozoa, viruses, some fungi, as well as both gram positive and gram negative bacteria (Andre J. Ouellette, 2005). The role of  $\alpha$ -defensins in helminth infection has not been thoroughly investigated however recently, it was shown that some recombinant  $\alpha$ -defensins can cause cytotoxic damage to *T. muris* worms *in vitro* (Pillai et al., 2019).

Enteroendocrine cells (EECs) are rare terminally differentiated cells of the intestinal epithelium that synthesise and secrete hormones (Worthington et al., 2017). Despite the fact that they are <1% of IECs, the vast number of these cells throughout the intestine make this organ the largest endocrine organ in the body (Worthington et al., 2017). Genes associated with EECs were identified to be suppressed particularly in response to co-culture with *H. bakeri* worms (Figure 6.12), but also in response to EVdepHES (Figure 6.5). Two hormones were consistently downregulated across several conditions, these were Somatostatin (*Sst*) and Ghrelin (*Ghrl*) (Figure 6.5, 6.12). *Ghrl* and *Sst* have been identified as correlating with inflammation in inflammatory bowel disease (IBD) patients suggesting interplay between hormones and the immune system (Worthington et al., 2017). The hormone serotonin also stimulates gut motility by activating enteric nerves. Recently, it was shown that serotonin can be expressed by EECs in response to IL-33 stimulation during *T. muris* infection, enhancing peristalsis and thereby improving worm clearance (Z. Chen et al., 2021). The enzyme tryptophan hydroxylase 1 (*Tph1*) catalyses the production of serotonin and is often used as a readout for serotonin production. I found *Tph1* expression to be suppressed by EVdepHES, L4 larvae, and apical co-culture with adult worms (Figure 6.5, 6.12).

Tuft cells have been recognised as both a key cell type in the recognition of helminth infection (McGinty et al., 2020) that undergo hyperplasia in response to IL-13 during infection (Gerbe et al., 2016; Howitt et al., 2016; Von Moltke et al., 2016). Furthermore tuft cells are repressed by components of HES (Drurey

et al., 2021). Our transcriptomic analysis only captured common tuft cell marker genes at low CPM, therefore I could not confidently assess the effect of treatment with *H. bakeri* ES products or co-culture effected these cells, I did however investigate these further using scRNA-seq (discussed below).

Transit-amplifying (TA) cells are proliferative cells that develop from Lgr5+ ISCs and rapidly proliferative undergoing cell cycle within ~ 12 h. I saw a suppression of TA cells undergoing cell cycle in both G1 and G2 phase (Figure 6.8). In addition, pathway analysis showed negative enrichment in many pathways related to DNA dependant DNA replication, cell cycle, or chromatid segregation, suggestive of a reduction in proliferation in EV and EVdepHES treated 2-D enteroids (Table 6.2, 6.3). This was further supported by scRNA-seq data (Figure 6.21). The protein ki67, encoded by *Mki67*, is well known to be expressed in proliferative cells and I see a down-regulation of this gene under all conditions. In the intestinal epithelium only some cellular populations are capable of undergoing proliferation, these being stem cells, progenitor cells and transit-amplifying cells (Beumer & Clevers, 2020).

#### **6.3.4 Synergistic effects of vesicular and non-vesicular components of HES**

One goal in this work was to determine the unique changes induced by *H. bakeri* EVs. I found that the majority of changes induced by EVs are concordant with changes induced by non-vesicular ES products (Figure 6.4). Suggesting that the vesicular and non-vesicular components act synergistically during *H. bakeri* infection to modify this host tissue. An argument could be made that live co-culture supports this, as I identified stronger effects on 2-D enteroids in these conditions than EVs or EVdepHES. However, one must also consider that in co-culture settings additional factors such as continuous supply of ES products, and physical disruption (in the case of apical co-culture) will also be introduced. Future experimental work could



treat 2-D enteroids with HES spiked with labelled *H. bakeri* EVs at various concentrations, and the assess effects on the epithelium.

### 6.3.5 scRNA-seq analysis of EV and EVdepHES 2-D organoids

A major goal of this thesis was to identify whether *H. bakeri* EVs target specific sub-populations within the intestinal epithelium. scRNA-seq was employed on 2-D enteroids treated with *H. bakeri* EVs or EVdepHES to interrogate host response within each cell type. I identified all cell types of the intestinal epithelium (except M cells) by scRNA-seq (Figure 6.18). Despite the presence of differentiated Paneth, enteroendocrine, goblet and tuft cells in 2-D enteroid cultures (Chapter 4 of this thesis), of these populations only tuft cells were represented by a clear cluster (Figure 6.18). A mixed population of cells (cluster 10) was found to express genes specific to goblet, Paneth and EECs (Figure 6.17 & Figure 6.18). Due to the low numbers of these cell populations, I could not detect significant changes between treatments by differential gene expression analysis (data not shown), but I do identify qualitative differences. Specifically, tuft cell specific genes demonstrate lower expression after treatment with *H. bakeri* EVs or EVdepHES (Figure 6.19). This is interesting as HES has recently been shown to constrain tuft cells in 3-D organoids, and these data may suggest that *H. bakeri* EVs could play a role in this (A. H. Buck et al., 2014; Coakley et al., 2017). I also identified an increase in enterocyte specific gene expression in EV treated 2-D enteroids, and a suppression of cell cycle related genes by EVs and EVdepHES (Figure 6.20 and Figure 6.21). Finally, I see an increase in revSC specific gene expression in cells treated with EVs or EVdepHES compared to mock, most notably in *Ly6a*. *Ly6a* is induced during infection as early as day 2 p.i., prior to the induction of other revSC associated genes, and in 3-D organoids was also found to be induced after 24 h of exposure to HES (Karo-Atar et al., 2022; Nusse et al., 2018). Therefore, it would be interesting to repeat this experiment looking at later time points after treatment, or after multiple doses.

### 6.3.6 Limitations of scRNA-seq

We identified a bifurcation of our scRNA-seq dataset, with multiple clusters identified as the same cell type. These changes could have been driven by treatments, or by cell quality. I found that the two arms of the UMAP plot had differences in the mt percentage between our treatments, and this was also found for the different treatments with mock having a higher percentage of mt reads (Figure 6.22). It should be noted that in publicly available scRNA-seq data from Karo *et al*, 2022 that TA cells have enriched expression of several mt genes. It could be further investigated whether differences in the amount of TA cells between treatments could explain these differences in mt percentages between samples. It is worth remembering that I also saw a suppression of TA cells in our bulk RNA-seq data by EVs and EVdepHES. It is difficult to determine if the differences in cell quality reflects a stochastic difference between samples, or a biologically relevant difference as a result of treatment because I only used one replicate per treatment. Due to the cost of scRNA-seq, having multiple replicates was not affordable and at the time was not mainstream, although in the future with reduced costs it may become more common place.

#### Concluding remarks

Previously, transcriptomics had been performed on epithelium from infected tissue including scRNA-seq analysis (Haber *et al.*, 2017), and more recently on HES treated 3-D organoids (Drurey *et al.*, 2021; Karo-Atar *et al.*, 2021). These publications found HES to modify 3-D organoid cultures. However, no publications had specifically focussed on the role of *H. bakeri* EVs (a component of HES) on organoid cultures. In this chapter I performed RNA-seq to investigate the specific response to *H. bakeri* EVs. Additionally, I

demonstrated the use of our 2-D enteroids for co-culture with live worms for which the use of 3-D cultures have been limited (Ruby White et al., 2022) and characterised the transcriptional response in the epithelium in the absence of other host factors for the first time.

**Chapter 7: General discussion**

The goal of this thesis was to investigate the functional effects of *H. bakeri* EVs on the intestinal epithelium. To achieve this, I first focused on *H. bakeri* EV isolation techniques and characterisation, as well as methodology for EV fluorescent labelling in Chapter 3. I then developed a 2-D enteroid culture system that recapitulated many key features of the intestinal epithelium, detailed in Chapter 4. In chapter 5, I investigated the uptake of *H. bakeri* EVs into intestinal epithelium cells using a range of intestinal epithelial models that increased in complexity from cell lines to *in vivo* tissues. Finally, in Chapter 6 I investigated the functional effects of *H. bakeri* EVs on the intestinal epithelium using RNA sequencing approaches. In parallel, I demonstrate the utility of our 2-D enteroid model for co-culture of live helminth parasites. In this discussion Chapter I discuss my findings within the broader research context, contemplate how my findings contribute to questions in the field and propose future directions for this body of work.

## 7.1 EV uptake and cell type specificity in the intestinal epithelium

Helminth EVs and their immunomodulatory capacities have been the subject of research for just over a decade. While cross-kingdom uptake has been demonstrated previously for several different helminths species to host cells (Coakley et al., 2015; Sánchez-López et al., 2021). *H. bakeri* EVs in particular can enter murine cells as demonstrated by our lab in both bone marrow derived macrophages (BMDMs), and to a lesser degree MODE-K (enterocytes) cells *in vitro* (A. H. Buck et al., 2014). In Chapter 5 I show that *H. bakeri* EVs are capable of entering 2-D enteroids cells, but at lower proportions than in the enterocyte cell line (MODE-K). Several things may explain this (which are not mutually exclusive): i) cell type specificity in these heterogeneous cultures, ii) presence of mucus barrier and cell turnover, or iii) transcytosis of EVs across the epithelium.

One major question I aimed to address was whether *H. bakeri* EVs possess cell type specific targeting for uptake within the intestinal epithelium e.g., do they preferentially enter specific cell types and not others? The fact that only a proportion of cells (<20%) uptake EVs in 2-D enteroids could suggest they target a specific population that is not highly represented. Determining which specific cell population is targeted by *H. bakeri* EVs may give clues towards the mechanism of EV uptake. For example, *S. mansoni* EVs have been shown to interact with the receptor DC-SIGN which mediates uptake, thereby this interaction targets *S. mansoni* EVs to cells that express this receptor e.g., dendritic cells (Kuipers et al., 2020). Identifying a propensity for *H. bakeri* EVs to enter specific cell types could therefore assist in discerning the mechanism of uptake. However, despite multiple attempts to look for cell type specificity in this study this question still remains an open area of research. RNA seq data did suggest that *H. bakeri* EV treatments causes cell type specific effects with changes to genes expressed by Paneth cells, TA cells and possibly stem cells, although this was less clear (discussed further below). Whether *H. bakeri* EVs specifically enter one (or all) or these cells, or if they enter enteroid cells ubiquitously but display stronger functional effects within specific cells is unknown.

Instead of thinking about uptake of *H. bakeri* EVs being 'targeted' to a specific cell types, an alternative perspective could be that uptake is dictated by the capacity of the recipient cell for uptake. For instance, the previously described enhanced uptake of *H. bakeri* EVs by BMDMs compared to MODE-K may be a reflection of the fact that macrophages are specialised phagocytic cells. It is worth considering the uptake capabilities of intestinal epithelial cells, for example enterocytes are not phagocytic, but are capable of endocytosis (including for uptake of bacterial OMVs) and in response to some enteric infections perform micropinocytosis (Amyere et al., 2002; Bittel et al., 2021; Zimmer et al., 2016). Recent reports have also described goblet cells to have endocytic functions, and in response to acetylcholine signals form 'gut associated antigen passages' (GAPS) which allow for the transcytosis of

luminal antigen across the epithelial barrier (Gustafsson et al. 2021). Interestingly, Paneth cells have also recently been described as phagocytes that clear debris from neighbouring dying cells in a process referred to as efferocytosis (Shankman et al., 2021). Based on findings from sequencing data (Chapter 6) I now hypothesise that Paneth cells are functionally modified by *H. bakeri* EVs. Thus, it would be interesting to investigate the phagocytic capacity of these cells in relation to *H. bakeri* EV uptake in the future.

An alternative, but not necessarily mutually exclusive, hypothesis for why I see lower uptake in 2-D enteroids than cell lines is that EVs cross the epithelial barrier. 2-D enteroids, unlike cell line cultures, possess polarised epithelium and a physically separated basal compartment which could allow for transcytosis. Very little is understood about the dissemination of helminth EVs through the host organism. Studies from bacterial outer membrane vesicles (OMVs) may shed some light on what could be possible for helminth derived EVs. For instance, OMVs demonstrate both paracellular (between cells) and transcellular (through cells) mechanisms for crossing the epithelial barrier, and can disseminate to distal sites including the brain (Cuesta et al., 2021; Momma, 2021; Stentz et al., 2018). I did not assess whether *H. bakeri* EVs were found in the basal medium which would indicate transcytosis across the epithelium. A major complication to assessing transcytosis would be the difficulty in differentiating host derived EVs from *H. bakeri* EVs – even if EVs were AF647 labelled due of the low efficiency of this labelling protocol (Chapter 3 of this thesis). Recently other members of our lab have developed single EV immunofluorescence techniques using *H. bakeri* EV specific antibodies, this technique could be used to assess parasite EV transcytosis in the future. Recently, live tracking of EV dissemination in zebrafish has been achieved by genetic modification to produce EV-specific fluorescent reporters, or in *E. coli* Cre-recombinase carrying OMVs have been used to label recipient host cells (explained further below) (Bittel et al., 2021; Verweij et al., 2019). The development of similar approaches for helminth EVs would be a major breakthrough for studying these nanoparticles, however at present genetic

modification is still difficult for helminths (Hagen et al., 2021; Lendner et al., 2008).

A final explanation for the reduced *H. bakeri* EV uptake in 2-D enteroids could be the presence of mucus, which may trap EVs thereby reducing uptake. Anecdotally, when performing microscopy of 2-D caecaloid and enteroid cultures treated with either AF647 labelled *H. bakeri* or *T. muris* EVs I observed fluorescent signal in mucus above the cellular layer. It is worth postulating whether other components of HES may interact with mucus to enable EV uptake *in vivo*. For example, mucus degrading enzymes are produced by other helminths such as *T. muris* parasites (as well as many non-helminthic pathogens) (McGuckin et al. 2011; Duque-Correa et al. 2022). During natural infections, *H. bakeri* EVs secreted as one component of a much larger slew of molecules and enzymes. By fixating on EV isolations being highly pure, I could be missing critical synergistic effects of EVs with other HES molecules that enhance their uptake. It would be interesting to investigate whether *H. bakeri* ES also contains mucus degrading molecules, and if so, whether these enhance EV uptake into epithelial cells.

## **7.2 *H. bakeri* EVs functional response in the host intestinal epithelium**

Our RNA seq analysis of EV treated 2-D enteroids showed large variation between replicates for all conditions including the mock control. Such high variation obviously limits the statistical significance of our findings. Indeed, differential expression analysis of EV treatment vs. mock resulted in 0 significantly differentially regulated genes using standard cut offs (FDR  $P < 0.05$ ). In hindsight this is perhaps somewhat expected as data from chapter 5 suggested only a low (<20%) proportion of cells may take up *H. bakeri* EVs, indicating the effect of EV uptake would be diluted in bulk RNA seq. Even in previously published data from MODE-K cells, where uptake is much higher, only subtle gene expression changes were captured with 128 differentially regulated genes (FDR  $P < 0.05$ ) (Buck et al., 2014).



EV treatment resulted in down regulation of genes that have particular relevance for the biology of the intestinal epithelium or in innate immunity. Pathway analysis yielded significant down regulation of many cell cycle related and antimicrobial pathways. Downregulation of antimicrobial pathways was driven by several genes known to be expressed by Paneth cells namely  $\alpha$ -defensins and Ang4. Furthermore, pathway enrichment analysis using cell type specific genes also identified Paneth cells specific genes as negatively enriched in EVs vs. mock, as well as TA cells undergoing cell cycle and early enterocyte progenitors. Finally, Paneth cells have previously been identified as increasing during infection with several helminths, including *H. bakeri* (Kamal et al., 2002). Therefore *H. bakeri* EVs may play a role in constricting this host response during infection, for example similar to what has recently been documented for HES and tuft cells (Drurey et al., 2021). While the direct effect of Paneth cells on the success of helminth infections has not been thoroughly investigated, it would be intriguing to know whether AMPs can directly impact helminths. Additionally, AMP secretion could impact helminth infection indirectly, through effects on the microbiome given the documented role of AMP on microbial composition (André Joseph Ouellette, 2011). *H. bakeri* has already been shown to alter the microbiome, and interactions between *H. bakeri*, Paneth cells, and the microbiome would be an interesting area of research (Rapin et al., 2020).

It was clear from our sequencing results that many effects of *H. bakeri* EVs and EVdepHES are shared, suggesting that multiple molecules could act synergistically during infection. However, genes that have defined roles as IFN responses genes (ISGs) were differentially regulated by EVs compared to EVdepHES or live worm co-cultures. This is interesting because recent studies found IFN responses genes to be induced by *T. muris* infection of 2-D caecaloids, suggesting they play a role in alerting the immune system, despite being most typically associated with viral infections (Duque-Correa, Goulding, Rodgers, Gillis, et al., 2022). *T. muris* EVs have also been shown to down regulate IFN response genes, and this could reflect an mechanism of constricting host responses (Duque-Correa, Schreiber, et al., 2020).

One factor that is absent in organoid models is the impact of host immune responses. The immune response could be modelled by addition of IL-4 and IL-13 which are the primary cytokines that impact the epithelium during helminth infection, or by additional of primary immune cells to the basal compartment. These factors may be important for understanding the role of *H. bakeri* EVs on infected epithelium and should be explore further in the future.

An obvious alternative approach in the design of sequencing experiments to assess uptake specificity and function of EVs would have been to sort the cells positive for EV-AF647, in order to enrich for cells that take up *H. bakeri* EVs. This approach was trialled, however low labelling efficiency combined with low cell viability (a common challenge when epithelial cells are in single cell suspensions) resulted in very low numbers of cells retrieved and miniscule amounts of RNA (data not shown). Since collection of these datasets, I have made improvements to the collection of 2-D enteroid cells for flow cytometry resulting in high levels of viable cells (80-90%). Furthermore, experimentation with dye:particle ratios during AF647 labelling may improve labelling efficiency. A combination of these two advancements would allow for improvement in our ability to sort live EV-AF647 positive cells for analysis by RT qPCR or RNA seq.

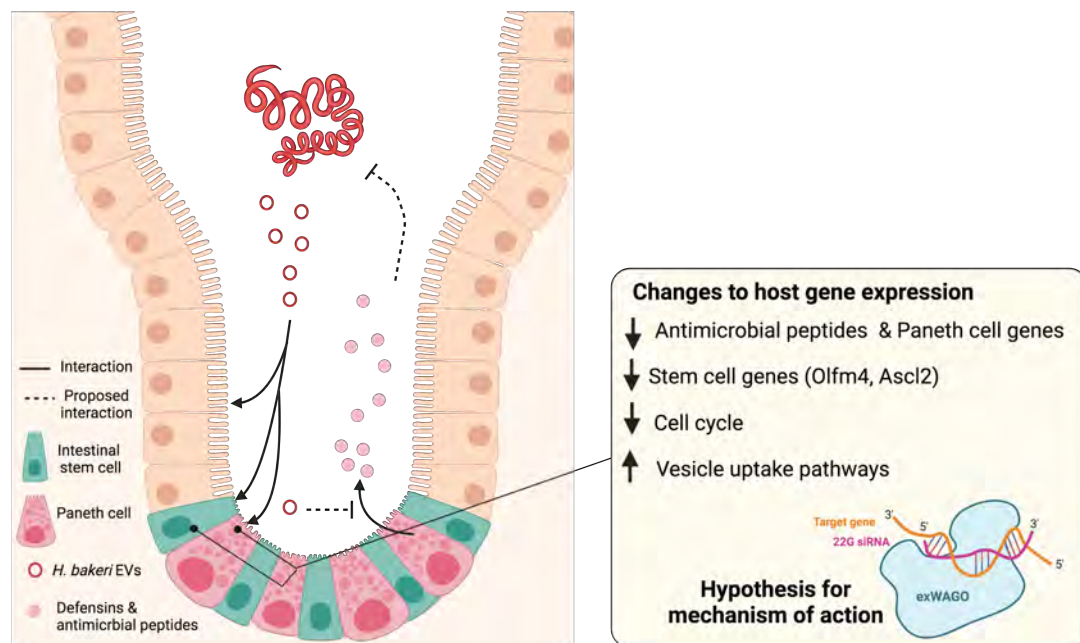


**Figure 7.1 | Summary of thesis findings relating to functional effects of *H. bakeri* EVs in 2-D enteroids.** *H. bakeri* derived EVs enter 2-D enteroid cells, however whether this is targeted to specific cells is an open question. I identified a significant pattern of genes differentially expressed in response to *H. bakeri* EV treatment that are specifically expressed by Paneth cells such as  $\alpha$ -defensins. I hypothesise that *H. bakeri* EVs reduce the secretion of antimicrobial peptides (AMPs) from Paneth cells and possibly Paneth cell differentiation. It is unclear what effect AMPs have on *H. bakeri* infections but I hypothesise they play roles in helminth clearance. I also see suppression of key stem cell genes, TA cells and proliferation which may affect the differentiation and turnover of epithelial cells. Very few responses to *H. bakeri* EVs were upregulated but those that were showed enrichment for vesicle uptake and trafficking pathways. Finally, I propose *H. bakeri* EVs mediate effects via RNA interference, and this is a major focus of the Buck Laboratory. These datasets will be further assessed to identify candidate helminth sRNA interactions with host dysregulated genes. Figure made using BioRender.com.

### 7.3 Organoid models advance the study of host-helminth interactions at the epithelium.

2-D enteroid model development allowed us to investigate *H. bakeri* EV interactions at the intestinal epithelium, however they are also applicable for many other aspects of helminth research. Previous studies have displayed the potential of organoids for co-culture with live helminths using 3-D cultures (Faber et al., 2022; D. Smith et al., 2021), but these have considerable limitations (Ruby White et al., 2022). I showcase the use of 2-D enteroids for helminth investigations by co-culturing with live L4 or adult *H. bakeri* parasites. After 24 h I found many genes to be differentially regulated, surprisingly L4

larvae induced the strongest change in epithelial gene expression. L4 larvae are more difficult to retrieve from infected animals and have far more limited survival in culture. Perhaps for these reasons, most research has focused of HES from cultured adult *H. bakeri*, going forward it will be intriguing to look at the effects of the L4 larvae and their HES products, which may vary from that of adult worms.

Because recent studies have co-cultured HES with 3-D organoids, in which molecules will be in contact with the basal epithelium, I also compared the effect of co-culture on the apical surface to the basal compartment. Basal co-culture of the same number of adult *H. bakeri* worms resulted in stronger effects on gene expression, with more differentially regulated genes than in apical co-culture. This has implications for how I design experiments in order to best replicate host-helminth dynamics.

2-D enteroid models allowed for the first-time the co-culture of live *H. bakeri* adult worms with the epithelium – this will have many downstream implications for the field. Thus far, I have only assessed short term changes (24 h) by RNA seq in response co-culture. However, one could extend these co-cultures for longer periods of time using multiple read outs such as assessment of effects of cell differentiation, mucus and antimicrobial peptide production, epithelial proliferation and barrier integrity.

Something that is a major logistical challenge for helminth research is the reliance of animal hosts for maintaining helminths in the laboratory, and for human infective species, this requires voluntary controlled infections. Very limited progress has been made since the mid-20<sup>th</sup> century with regards to helminth cultivation for most species. It is exciting to consider the possibilities that arise from 2-D organoid cultures for completion of helminth life cycles *in vitro*.

## 7.4 Future directions

In this thesis progress was made in our understanding of *H. bakeri* EV function within the intestinal epithelium. Considerable effort was put into careful testing of methods for isolating and labelling *H. bakeri* EVs and for development of 2-D enteroids. I identified *H. bakeri* EV uptake in a proportion of 2-D enteroid cells. One major question that remains elusive is whether *H. bakeri* EVs target specific cells for uptake. Recent improvements of techniques discussed above will allow for sorting of cells that take up EVs within 2-D enteroids and this will allow for validation of RNA seq and scRNA seq results. Our RNA sequencing analysis revealed *H. bakeri* EVs have subtle effect of on 2-D enteroids (summarised above). However, I have not yet confirmed whether these occur *in vivo*. An alternative viewpoint is that *H. bakeri* EVs might have potent effects on recipient cells, but not within the epithelium. However, if *H. bakeri* EVs target other cell types during infection they must somehow cross this barrier in order to interact with these cells. *H. bakeri* EVs crossing the epithelium without detection, which is could be one interpretation of our findings, is interesting in itself considering that these nanoparticles are abundant with foreign molecules. Studies to determine whether *H. bakeri* EVs cross the epithelium by transcytosis will assist our understanding of their fate *in vivo*.

Pathogen EVs crossing the intestinal epithelium and targeting other organs is not unprecedented. The introduction of Cre recombinase into *E. coli* OMVs has recently allowed researchers to identify which host cells take up OMVs *in vivo* (Bittel et al., 2021). Using the Cre-loxP reporter system, whereby in cells that take up Cre recombinase containing OMVs an excision of loxP flanked stop codon occurs, thus turning on the expression of a tdTomato red reporter protein (Bittel et al., 2021). In this eloquent model, transfer was identified primarily in epithelial villus tips and in crypt cells (stem cells) during infection (Bittel et al., 2021). Interestingly, authors also found rarer events that demonstrated OMV uptake in peripheral organ sites such as in the liver, kidney and brain (Bittel et al., 2021). Unfortunately, similar methods for tracking helminth EVs will be difficult to achieve due the challenges of genetically

modifying these parasites (Lendner et al., 2008). Alternatively, I can search for evidence of their cargo molecules in infected tissues. During my PhD I supervised a student project where I generated small RNA libraries from various organs of infected mice (d 14). Our lab continues to investigate the presence of *H. bakeri* sRNA sequences from this dataset.

One cell type of the intestinal epithelium that is not represented in our 2-D enteroid models are M-cells. M-cells have enhanced endocytic and transcytosis properties compared to enterocytes and play a role in delivering antigen to immune cells in Peyer's patches (Kobayashi et al., 2019; Mabbott et al., 2013). Tissue from intraluminal injections of isolated *H. bakeri* EVs can be further probed to assess whether uptake is seen at Peyer's patches or by M cells. A caveat of our intraluminal injections for looking at *H. bakeri* EV uptake was the limited time (1.5 h) that we could keep animals anesthetised, and previous time course data in MODE-K suggested peak of uptake is 16 – 24 h (Coakley et al., 2017). However, M cells are described to undergo rapid uptake in other contexts (15 min for *Salmonella*) so, the assessment of Peyer's patches from these samples is an immediate research priority going forward (Rey et al., 2020). To assist this, recently our lab has validated additional antibodies against EV specific proteins that could also be used for EV detection in these tissues.

Finally, one hypothesis in our laboratory for how *H. bakeri* EVs mediate their functional effects on recipient cells is through RNA silencing by exWAGO proteins loaded with 22G siRNAs. Bioinformatic approaches can be used to predict which dysregulated host genes could be targets of these parasite derived siRNA sequences utilising both the RNA seq and scRNA seq datasets generated in this thesis. This work is the research focus of other lab members and collaborators namely Jose Roberto Bermudez Barrientos and Yenetzi Villagrana Pacheco.

## 7.5 Concluding remarks

The work presented in this thesis progresses our understanding of interactions between *H. bakeri* EVs and the intestinal epithelium highlighting the utility of 2-D enteroids in the process. I show that *H. bakeri* EVs enter intestinal epithelial cells resulting in subtle gene expression changes in this tissue. Sequencing datasets suggest a suppressive effect on cell cycle, and differential regulation of genes specific to Paneth cells, TA cells and stem cells. This thesis advances our understanding of host modulation at the intestinal epithelium by *H. bakeri* secreted EVs and may have far reaching impacts for the study of helminth infection in the intestinal epithelium.

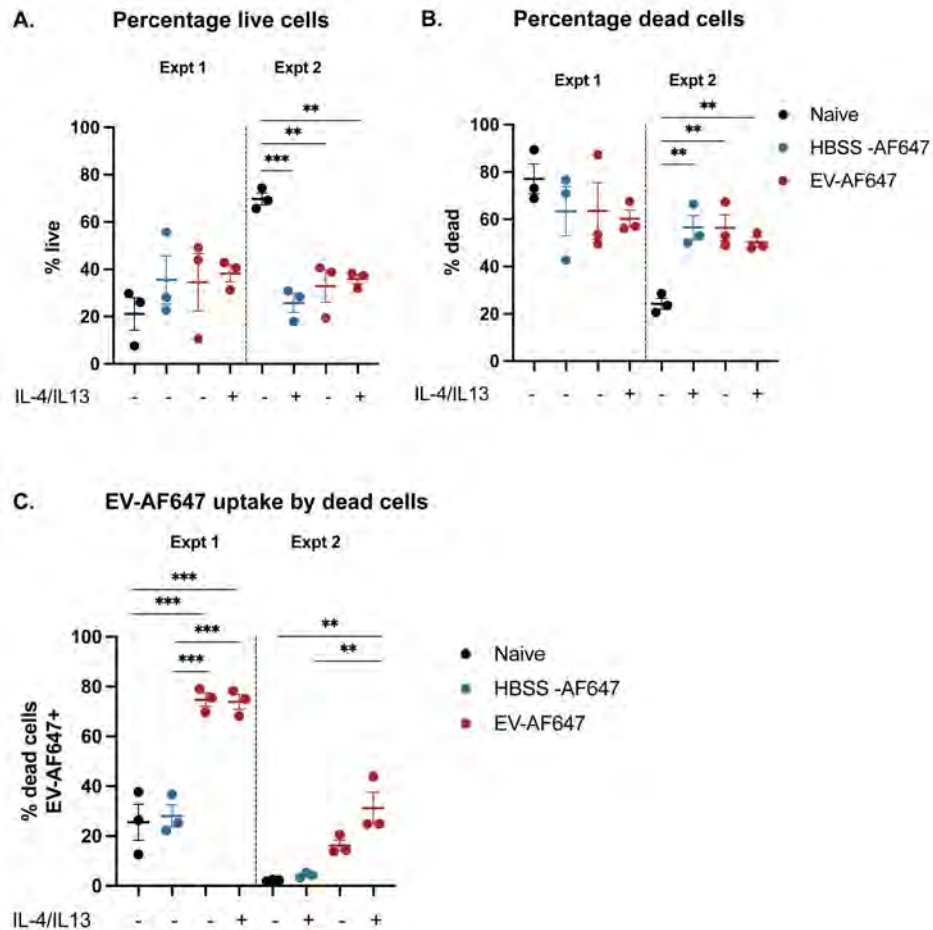
## **Supplement tables and figures**

### **Supplemental Files**

All the Supplemental files are accessible here:

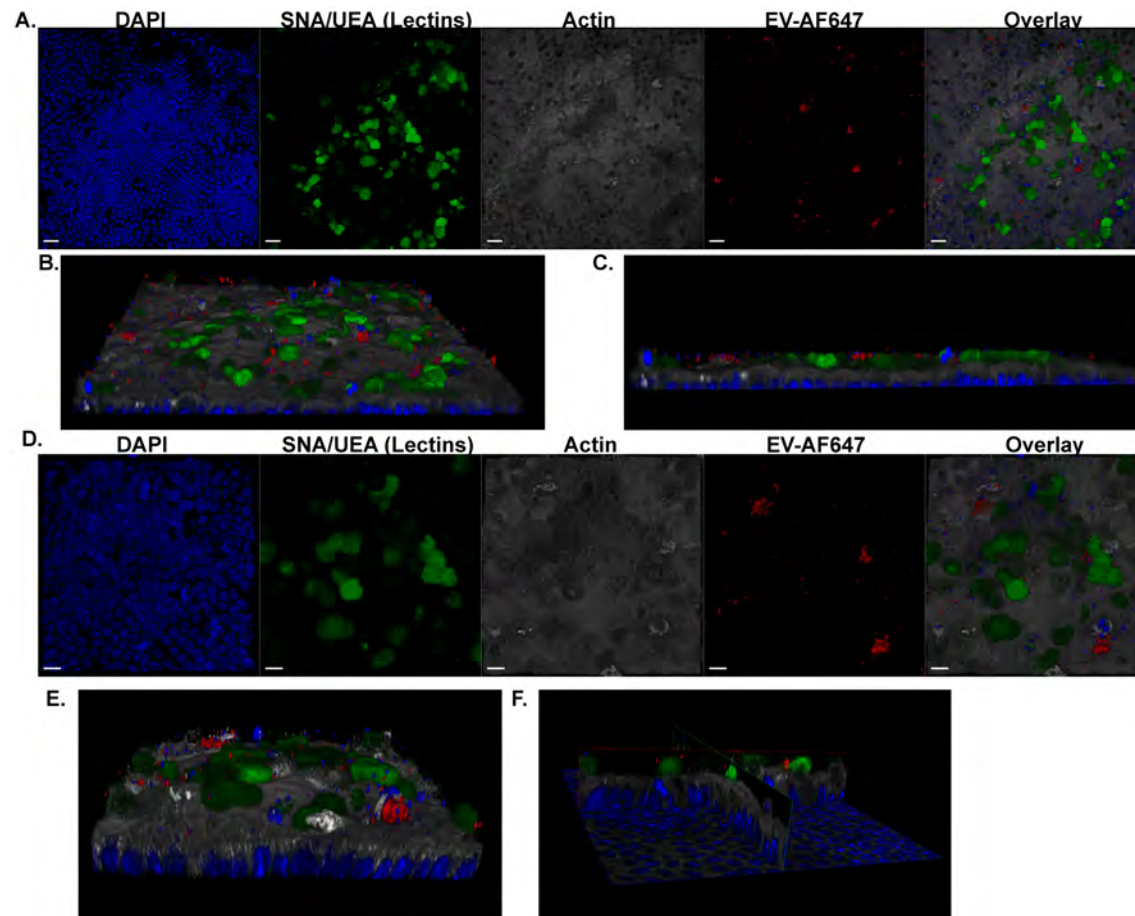
[https://drive.google.com/drive/folders/1dqu7IlwHHKxkmKwJkEZGAexBnb2LW40-?usp=share\\_link](https://drive.google.com/drive/folders/1dqu7IlwHHKxkmKwJkEZGAexBnb2LW40-?usp=share_link)



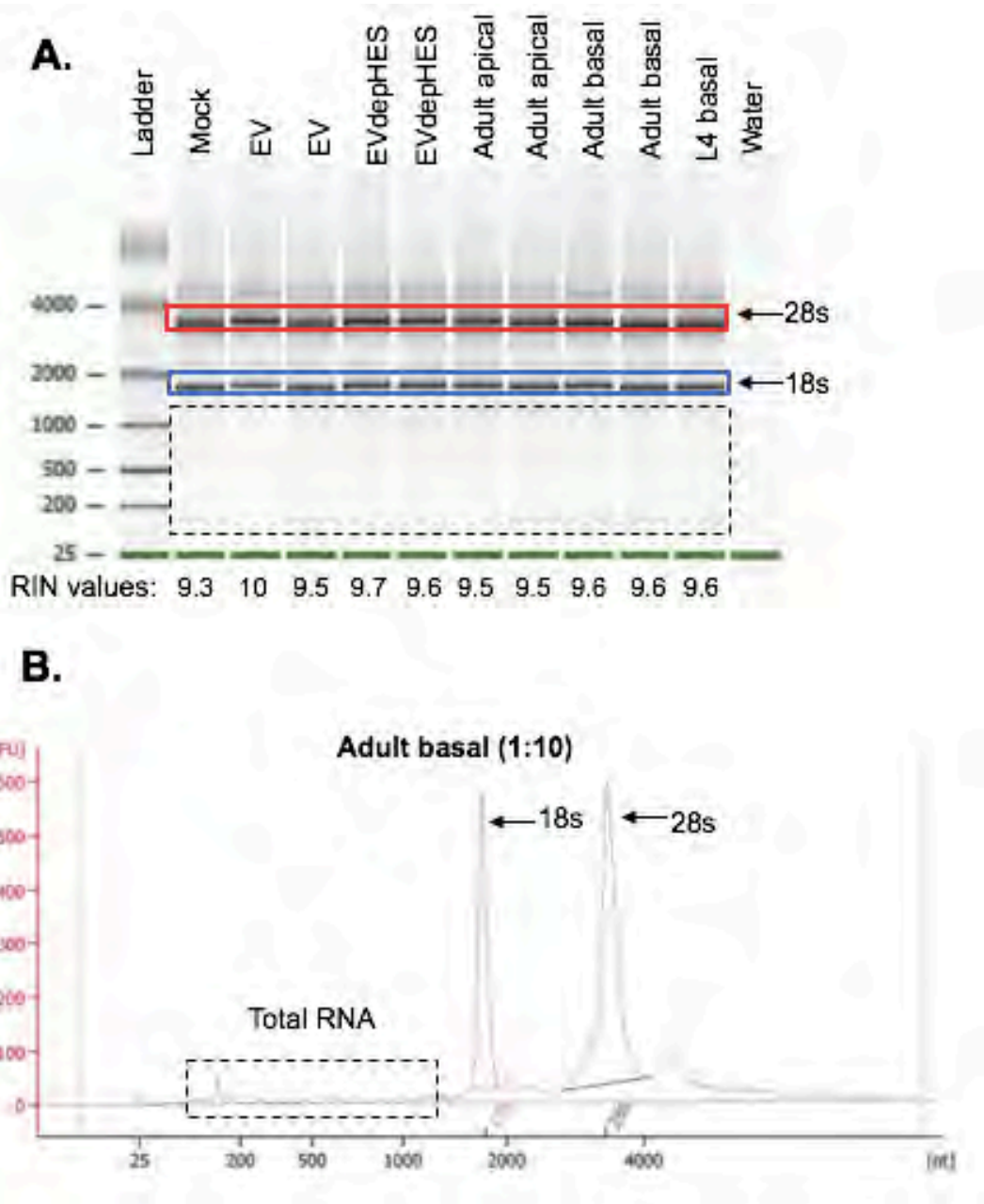
**Supplemental Figures****Supplemental Figure 1**

**Supplemental Figure 1 | Proportions of live and dead cells in EV treated 2-D enteroids** | 2-D enteroids were treated with 20  $\mu\text{g/ml}$  EV-AF647, HBSS-AF647 or untreated for 24 hr cells were then harvested and live cells stained using live/dead fixable blue cell stain kit (Invitrogen) before performing flow cytometry or FACs. Percentage of 2-D enteroid cells that were **A)** alive **B)** dead in two different experiments graphed side-by-side. **C)** Percentage of dead single cells that are EV-AF647 positive. Statistics were performed on each experiment individually. One-way ANOVA was used for analysis of significance. (\* =  $P \leq 0.05$ , \*\* =  $P \leq 0.01$ , \*\*\* =  $P \leq 0.001$ ).

## Supplemental Figure 2



**Supplemental Figure 2 | *T. muris* EVs co-cultured with 2-D caecaloids.** Representative images of 2-D caecaloids co-cultures with *T. muris* EVs for 24 h. nuclei stained with DAPI (blue), SNA/UEA used to identify goblet cells (green), actin stained with Phalloidin (red) and *T. muris* EVs labelled with AF647 (red) **A&D**) Slice image of two representative regions **B&E**) 3-D projection of Z-stack images demonstrating localisation of EVs. **C&F**) Orthogonal views of sections demonstrating EVs were mostly on top of the 2-D monolayer. Images processed



**Supplemental Figure 3: Quality control for RNAseq.** Representative RNA quality analysis performed using Eukaryotic Total RNA Pico chip of RNA diluted 1:10 (prior to ribosomal depletion) **A)** Electropherogram summary results indicating 18s RNA (blue box) and 28s (red box), total RNA ranges from ~100 bp – 1000 bp (black dotted line box), and RIN values. **B)** Example electropherogram of RNA from 2-D enteroids treated for 24 h with adult *H. bakeri* co-cultured in the basal compartment.



## References

- Abdelaal, T., Michielsen, L., Cats, D., Hoogduin, D., Mei, H., Reinders, M. J. T., & Mahfouz, A. (2019). A comparison of automatic cell identification methods for single-cell RNA sequencing data. *Genome Biology*, *20*(1), 194.
- Aguilar, C., Alves da Silva, M., Saraiva, M., Neyazi, M., Olsson, I. A. S., & Bartfeld, S. (2021). Organoids as host models for infection biology – a review of methods. *Experimental & Molecular Medicine*, *53*(10), 1471–1482.
- Ahmad, A. A., Wang, Y., Gracz, A. D., Sims, C. E., Magness, S. T., & Allbritton, N. L. (2014). Optimization of 3-D organotypic primary colonic cultures for organ-on-chip applications. *Journal of Biological Engineering*, *8*, 9.
- Ajendra, J. (2021). Lessons in type 2 immunity: Neutrophils in Helminth infections. *Seminars in Immunology*, *53*, 101531.
- Alabi, A., Hussain, M., Hoogerwerf, M.-A., Mengome, C. N., Egesa, M., Driciru, E., Wammes, L. J., Kruize, Y. C. M., Sartono, E., Adegnika, A. A., Kreamsner, P. G., Yazdanbakhsh, M., & Agnandji, S. T. (2021). Establishing a controlled hookworm human infection (CHHI) model for Africa: A report from the stakeholders meeting held in Lambaréné, Gabon, November 10–11, 2019. *Archives of Public Health*, *79*(1).
- Alcântara-Neves, N. M., Badaró, S. J., dos Santos, M. C. A., Pontes-de-Carvalho, L., & Barreto, M. L. (2010). The presence of serum anti-*Ascaris lumbricoides* IgE antibodies and of *Trichuris trichiura* infection are risk factors for wheezing and/or atopy in preschool-aged Brazilian children. *Respiratory Research*, *11*, 114.
- Allen, J. E., & Wynn, T. A. (2011). Evolution of Th2 immunity: a rapid repair response to tissue destructive pathogens. *PLoS Pathogens*, *7*(5), e1002003.
- Altay, G., Larrañaga, E., Tosi, S., Barriga, F. M., Batlle, E., Fernández-Majada, V., & Martínez, E. (2019). Self-organized intestinal epithelial monolayers in crypt and villus-like domains show effective barrier function. *Scientific Reports*, *9*(1), 8028.
- Amyere, M., Mettlen, M., Van Der Smissen, P., Platek, A., Payrastre, B., Veithen, A., & Courtoy, P. J. (2002). Origin, originality, functions, subversions and molecular signalling of macropinocytosis. *International Journal of Medical Microbiology: IJMM*, *291*(6–7), 487–494.
- An, W. F., Germain, A. R., Bishop, J. A., Nag, P. P., Metkar, S., Ketterman, J., Walk, M., Weiwer, M., Liu, X., Patnaik, D., Zhang, Y.-L., Gale, J., Zhao, W., Kaya, T., Barker, D., Wagner, F. F., Holson, E. B., Dandapani, S., Perez, J., ... Schreiber, S. L. (2012). Discovery of Potent and Highly Selective Inhibitors of GSK3b. In *Probe Reports from the NIH Molecular Libraries Program* (pp. 1–115). National Center for Biotechnology Information (US).
- Andrews, S. (2010). *FastQC: a quality control tool for high throughput sequence data*. Babraham Bioinformatics, Babraham Institute, Cambridge, United Kingdom.
- Anthony, R. M., Rutitzky, L. I., Urban, J. F., Jr, Stadecker, M. J., & Gause, W. C. (2007). Protective immune mechanisms in helminth infection. *Nature Reviews. Immunology*, *7*(12), 975–987.
- Anthony, R. M., Urban, J. F., Alem, F., Hamed, H. A., Roza, C. T., Boucher, J.-L., Van Rooijen, N., & Gause, W. C. (2006). Memory TH2 cells induce alternatively activated macrophages to mediate protection against nematode parasites. *Nature Medicine*, *12*(8), 955–960.

## References

- Arrais, M., Maricoto, T., Nwaru, B. I., Cooper, P. J., Gama, J. M. R., Brito, M., & Taborda-Barata, L. (2022). Helminth infections and allergic diseases: Systematic review and meta-analysis of the global literature. *The Journal of Allergy and Clinical Immunology*, *149*(6), 2139–2152.
- Artis, D., Wang, M. L., Keilbaugh, S. A., He, W., Brenes, M., Swain, G. P., Knight, P. A., Donaldson, D. D., Lazar, M. A., Miller, H. R. P., Schad, G. A., Scott, P., & Wu, G. D. (2004). RELM $\beta$ /FIZZ2 is a goblet cell-specific immune-effector molecule in the gastrointestinal tract. *Proceedings of the National Academy of Sciences*, *101*(37), 13596–13600.
- Ayyaz, A., Kumar, S., Sangiorgi, B., Ghoshal, B., Gosio, J., Ouladan, S., Fink, M., Barutcu, S., Trcka, D., Shen, J., Chan, K., Wrana, J. L., & Gregorieff, A. (2019). Single-cell transcriptomes of the regenerating intestine reveal a revival stem cell. *Nature*, *569*(7754), 121–125.
- Babu, S., Blauvelt, C. P., Kumaraswami, V., & Nutman, T. B. (2006). Regulatory networks induced by live parasites impair both Th1 and Th2 pathways in patent lymphatic filariasis: implications for parasite persistence. *Journal of Immunology*, *176*(5), 3248–3256.
- Bachurski, D., Schuldner, M., Nguyen, P.-H., Malz, A., Reiners, K. S., Grenzi, P. C., Babatz, F., Schauss, A. C., Hansen, H. P., Hallek, M., & Strandmann, E. P. von. (2019). Extracellular vesicle measurements with nanoparticle tracking analysis – An accuracy and repeatability comparison between NanoSight NS300 and ZetaView. *Journal of Extracellular Vesicles*, *8*(1), 1596016.
- Ballweg, R., Lee, S., Han, X., Maini, P. K., Byrne, H., Hong, C. I., & Zhang, T. (2018). Unraveling the Control of Cell Cycle Periods during Intestinal Stem Cell Differentiation. *Biophysical Journal*, *115*(11), 2250–2258.
- Barker, N., Van Es, J. H., Kuipers, J., Kujala, P., Van Den Born, M., Cozijnsen, M., Haegerbarth, A., Korving, J., Begthel, H., Peters, P. J., & Clevers, H. (2007). Identification of stem cells in small intestine and colon by marker gene Lgr5. *Nature*, *449*(7165), 1003–1007.
- Barry, E. R., Morikawa, T., Butler, B. L., Shrestha, K., de la Rosa, R., Yan, K. S., Fuchs, C. S., Magness, S. T., Smits, R., Ogino, S., Kuo, C. J., & Camargo, F. D. (2013). Restriction of intestinal stem cell expansion and the regenerative response by YAP. *Nature*, *493*(7430), 106–110.
- Bartel, D. P. (2004). MicroRNAs: genomics, biogenesis, mechanism, and function. *Cell*, *116*(2), 281–297.
- Bartsch, S. M., Hotez, P. J., Asti, L., Zapf, K. M., Bottazzi, M. E., Diemert, D. J., & Lee, B. Y. (2016). The Global Economic and Health Burden of Human Hookworm Infection. *PLoS Neglected Tropical Diseases*, *10*(9), e0004922.
- Basak, O., van de Born, M., Korving, J., Beumer, J., van der Elst, S., van Es, J. H., & Clevers, H. (2014). Mapping early fate determination in Lgr5+ crypt stem cells using a novel Ki67-RFP allele. *The EMBO Journal*, *33*(18), 2057–2068.
- Baska, P., & Norbury, L. J. (2022). The Role of the Intestinal Epithelium in the “Weep and Sweep” Response during Gastro—Intestinal Helminth Infections. *Animals : An Open Access Journal from MDPI*, *12*(2), 175.
- Basten, A., Boyer, M. H., & Beeson, P. B. (1970). Mechanism of eosinophilia. I. Factors affecting the eosinophil response of rats to *Trichinella spiralis*. *The Journal of Experimental Medicine*, *131*(6), 1271–1287.
- Bastide, P., Darido, C., Pannequin, J., Kist, R., Robine, S., Marty-Double, C., Bibeau, F., Scherer, G., Joubert, D., Hollande, F., Blache, P., & Jay, P. (2007). Sox9 regulates cell proliferation and is required for Paneth cell differentiation in the intestinal epithelium. *The Journal of Cell Biology*, *178*(4), 635–648.
- Beer, K. B., & Wehman, A. M. (2017). Mechanisms and functions of extracellular vesicle release in vivo—What we can learn from flies and worms. *Cell Adhesion*

- & *Migration*, 11(2), 135–150.
- Behnke, J., & Harris, P. D. (2010). *Heligmosomoides bakeri*: a new name for an old worm? *Trends in Parasitology*, 26(11), 524–529.
- Bein, A., Shin, W., Jalili-Firoozinezhad, S., Park, M. H., Sontheimer-Phelps, A., Tovaglieri, A., Chalkiadaki, A., Kim, H. J., & Ingber, D. E. (2018). Microfluidic Organ-on-a-Chip Models of Human Intestine. *Cellular and Molecular Gastroenterology and Hepatology*, 5(4), 659–668.
- Belkaid, Y., & Tarbell, K. (2009). Regulatory T cells in the control of host-microorganism interactions. *Annual Review of Immunology*, 27, 551–589.
- Ben-Smith, A., Lammas, D. A., & Behnke, J. M. (2003). The relative involvement of Th1 and Th2 associated immune responses in the expulsion of a primary infection of *Heligmosomoides polygyrus* in mice of differing response phenotype. *Journal of Helminthology*, 77(2), 133–146.
- Bergstrom, K., & Xia, L. (2022). The barrier and beyond: Roles of intestinal mucus and mucin-type O-glycosylation in resistance and tolerance defense strategies guiding host-microbe symbiosis. *Gut Microbes*, 14(1), 2052699.
- Bermúdez-Barrientos, J. R., Ramírez-Sánchez, O., Chow, F. W.-N., Buck, A. H., & Abreu-Goodger, C. (2020). Disentangling sRNA-Seq data to study RNA communication between species. *Nucleic Acids Research*, 48(4), e21.
- Beumer, J., & Clevers, H. (2020). Cell fate specification and differentiation in the adult mammalian intestine. *Nature Reviews Molecular Cell Biology*, 22(1), 39–53.
- Bevins, C. L., & Salzman, N. H. (2011). Paneth cells, antimicrobial peptides and maintenance of intestinal homeostasis. *Nature Reviews. Microbiology*, 9(5), 356–368.
- Bieren, J. E., Volpe, B., Kulagin, M., Sutherland, D. B., Guet, R., Seitz, A., Marsland, B. J., Verbeek, J. S., & Harris, N. L. (2015). Antibody-Mediated Trapping of Helminth Larvae Requires CD11b and Fcγ Receptor I. *The Journal of Immunology Author Choice*, 194(3), 1154.
- Bishop, D. G., & Work, E. (1965). An extracellular glycolipid produced by *Escherichia coli* grown under lysine-limiting conditions. *The Biochemical Journal*, 96(2), 567–576.
- Bittel, M., Reichert, P., Sarfati, I., Dressel, A., Leikam, S., Uderhardt, S., Stolzer, I., Phu, T. A., Ng, M., Vu, N. K., Tenzer, S., Distler, U., Wirtz, S., Rothhammer, V., Neurath, M. F., Raffai, R. L., Günther, C., & Momma, S. (2021). Visualizing transfer of microbial biomolecules by outer membrane vesicles in microbe-host-communication in vivo. *Journal of Extracellular Vesicles*, 10(12), e12159.
- Bjerknes, M., Khandanpour, C., Möry, T., Fujiyama, T., Hoshino, M., Klisch, T. J., Ding, Q., Gan, L., Wang, J., Martín, M. G., & Cheng, H. (2012). Origin of the brush cell lineage in the mouse intestinal epithelium. *Developmental Biology*, 362(2), 194–218.
- Blache, P., van de Wetering, M., Duluc, I., Domon, C., Berta, P., Freund, J.-N., Clevers, H., & Jay, P. (2004). SOX9 is an intestine crypt transcription factor, is regulated by the Wnt pathway, and represses the CDX2 and MUC2 genes. *The Journal of Cell Biology*, 166(1), 37–47.
- Blackwell, A. D., Tamayo, M. A., Beheim, B., Trumble, B. C., Stieglitz, J., Hooper, P. L., Martin, M., Kaplan, H., & Gurven, M. (2015). Helminth infection, fecundity, and age of first pregnancy in women. *Science*, 350(6263), 970–972.
- Blaxter, M. (1998). *Caenorhabditis elegans* is a nematode. *Science*, 282(5396), 2041–2046.
- Boccellato, F., Woelffling, S., Imai-Matsushima, A., Sanchez, G., Goosmann, C., Schmid, M., Berger, H., Morey, P., Denecke, C., Ordemann, J., & Meyer, T. F. (2019). Polarised epithelial monolayers of the gastric mucosa reveal insights into mucosal homeostasis and defence against infection. *Gut*, 68(3),

- 400–413.
- Böing, A. N., van der Pol, E., Grootemaat, A. E., Coumans, F. A. W., Sturk, A., & Nieuwland, R. (2014). Single-step isolation of extracellular vesicles by size-exclusion chromatography. *Journal of Extracellular Vesicles*, 3(1), 23430.
- Booth, M. (2018). Climate Change and the Neglected Tropical Diseases. In *Advances in Parasitology* (Vol. 100, pp. 39–126). Elsevier.
- Bouchery, T., Kyle, R., Camberis, M., Shepherd, A., Filbey, K., Smith, A., Harvie, M., Painter, G., Johnston, K., Ferguson, P., Jain, R., Roediger, B., Delahunt, B., Weninger, W., Forbes-Blom, E., & Le Gros, G. (2015). ILC2s and T cells cooperate to ensure maintenance of M2 macrophages for lung immunity against hookworms. *Nature Communications*, 6, 6970.
- Bouchery, T., Moyat, M., Sotillo, J., Silverstein, S., Volpe, B., Coakley, G., Tsourouktsoglou, T.-D., Becker, L., Shah, K., Kulagin, M., Guiet, R., Camberis, M., Schmidt, A., Seitz, A., Giacomini, P., Le Gros, G., Papayannopoulos, V., Loukas, A., & Harris, N. L. (2020). Hookworms Evade Host Immunity by Secreting a Deoxyribonuclease to Degrade Neutrophil Extracellular Traps. *Cell Host & Microbe*, 27(2), 277-289.e6.
- Boysen, A. T., Whitehead, B., Stensballe, A., Carnerup, A., Nylander, T., & Nejsum, P. (2020). Fluorescent Labeling of Helminth Extracellular Vesicles Using an In Vivo Whole Organism Approach. *Biomedicines*, 8(7), 213.
- Bray, N. L., Pimentel, H., Melsted, P., & Pachter, L. (2016). Near-optimal probabilistic RNA-seq quantification. *Nature Biotechnology*, 34(5), 525–527.
- Buck, A. H., Coakley, G., Simbari, F., McSorley, H. J., Quintana, J. F., Le Bihan, T., Kumar, S., Abreu-Goodger, C., Lear, M., Harcus, Y., Ceroni, A., Babayan, S. A., Blaxter, M., Ivens, A., & Maizels, R. M. (2014). Exosomes secreted by nematode parasites transfer small RNAs to mammalian cells and modulate innate immunity. *Nature Communications*, 5, 5488.
- Buczacki, S. J. A., Zecchini, H. I., Nicholson, A. M., Russell, R., Vermeulen, L., Kemp, R., & Winton, D. J. (2013). Intestinal label-retaining cells are secretory precursors expressing Lgr5. *Nature*, 495(7439), 65–69.
- Burns, R. C., Fairbanks, T. J., Sala, F., De Langhe, S., Mailleux, A., Thiery, J. P., Dickson, C., Itoh, N., Warburton, D., Anderson, K. D., & Bellusci, S. (2004). Requirement for fibroblast growth factor 10 or fibroblast growth factor receptor 2-IIIb signaling for cecal development in mouse. *Developmental Biology*, 265(1), 61–74.
- Buys, J., Wever, R., & Ruitenberg, E. J. (1984). Myeloperoxidase is more efficient than eosinophil peroxidase in the in vitro killing of newborn larvae of *Trichinella spiralis*. *Immunology*, 51(3), 601–607.
- Cable, J., Harris, P. D., Lewis, J. W., & Behnke, J. M. (2006). Molecular evidence that *Heligmosomoides polygyrus* from laboratory mice and wood mice are separate species. *Parasitology*, 133(Pt 1), 111–122.
- Cai, Jin, Han, Y., Ren, H., Chen, C., He, D., Zhou, L., Eisner, G. M., Asico, L. D., Jose, P. A., & Zeng, C. (2013). Extracellular vesicle-mediated transfer of donor genomic DNA to recipient cells is a novel mechanism for genetic influence between cells. *Journal of Molecular Cell Biology*, 5(4), 227–238.
- Cai, Jing, Zhang, N., Zheng, Y., de Wilde, R. F., Maitra, A., & Pan, D. (2010). The Hippo signaling pathway restricts the oncogenic potential of an intestinal regeneration program. *Genes & Development*, 24(21), 2383–2388.
- Cai, Q., Qiao, L., Wang, M., He, B., Lin, F.-M., Palmquist, J., Huang, S.-D., & Jin, H. (2018). Plants send small RNAs in extracellular vesicles to fungal pathogen to silence virulence genes. *Science*, 360(6393), 1126–1129.
- Camberis, M., Le Gros, G., & Urban, J., Jr. (2003). Animal Model of *Nippostrongylus brasiliensis* and *Heligmosomoides polygyrus*. *Current Protocols in*



- Immunology*, 55(1), 19.12.1-19.12.27.
- Carnell-Morris, P., Tannetta, D., Siupa, A., Hole, P., & Dragovic, R. (2017). Analysis of Extracellular Vesicles Using Fluorescence Nanoparticle Tracking Analysis. In W. P. Kuo & S. Jia (Eds.), *Extracellular Vesicles: Methods and Protocols* (pp. 153–173). Springer New York.
- Cernuda-Cernuda, R., & García-Fernández, J. M. (1996). Structural diversity of the ordinary and specialized lateral line organs. *Microscopy Research and Technique*, 34(4), 302–312.
- Chaiyadet, S., Sotillo, J., Smout, M., Cantacessi, C., Jones, M. K., Johnson, M. S., Turnbull, L., Whitchurch, C. B., Potriquet, J., Laohaviroj, M., Mulvenna, J., Brindley, P. J., Bethony, J. M., Laha, T., Sripa, B., & Loukas, A. (2015). Carcinogenic Liver Fluke Secretes Extracellular Vesicles That Promote Cholangiocytes to Adopt a Tumorigenic Phenotype. *The Journal of Infectious Diseases*, 212(10), 1636–1645.
- Chandra, L., Borchering, D. C., Kingsbury, D., Atherly, T., Ambrosini, Y. M., Bourgois-Mochel, A., Yuan, W., Kimber, M., Qi, Y., Wang, Q., Wannemuehler, M., Ellinwood, N. M., Snella, E., Martin, M., Skala, M., Meyerholz, D., Estes, M., Fernandez-Zapico, M. E., Jergens, A. E., ... Allenspach, K. (2019). Derivation of adult canine intestinal organoids for translational research in gastroenterology. *BMC Biology*, 17(1), 1–21.
- Chapman, P. R., Giacomini, P., Loukas, A., & McCarthy, J. S. (2021). Experimental human hookworm infection: a narrative historical review. *PLoS Neglected Tropical Diseases*, 15(12), e0009908.
- Chen, W., & Ten Dijke, P. (2016). Immunoregulation by members of the TGF $\beta$  superfamily. *Nature Reviews. Immunology*, 16(12), 723–740.
- Chen, Y., Lun, A. T. L., & Smyth, G. K. (2016). From reads to genes to pathways: differential expression analysis of RNA-Seq experiments using Rsubread and the edgeR quasi-likelihood pipeline. *F1000Research*, 5, 1438.
- Chen, Z., Luo, J., Li, J., Kim, G., Stewart, A., Urban, J. F., Huang, Y., Chen, S., Wu, L. G., Chesler, A., Trinchieri, G., Li, W., & Wu, C. (2021). Interleukin-33 Promotes Serotonin Release from Enterochromaffin Cells for Intestinal Homeostasis. *Immunity*, 54(1), 151-163.e6.
- Cheng, H. (1974). Origin, differentiation and renewal of the four main epithelial cell types in the mouse small intestine. II. Mucous cells. *The American Journal of Anatomy*, 141(4), 481–501.
- Cheng, H., & Leblond, C. P. (1974). Origin, differentiation and renewal of the four main epithelial cell types in the mouse small intestine. I. Columnar cell. *The American Journal of Anatomy*, 141(4), 461–479.
- Chow, F. W. N., Koutsovoulos, G., Ovando-Vázquez, C., Neophytou, K., Bermúdez-Barrientos, J. R., Laetsch, D. R., Robertson, E., Kumar, S., Claycomb, J. M., Blaxter, M., Abreu-Goodger, C., & Buck, A. H. (2019). Secretion of an Argonaute protein by a parasitic nematode and the evolution of its siRNA guides. *Nucleic Acids Research*, 47(7), 3594–3606.
- Chuo, S. T.-Y., Chien, J. C.-Y., & Lai, C. P.-K. (2018). Imaging extracellular vesicles: current and emerging methods. *Journal of Biomedical Science*, 25(1), 91.
- Clevers, H. C., & Bevins, C. L. (2013). Paneth cells: maestros of the small intestinal crypts. *Annual Review of Physiology*, 75, 289–311.
- Clevers, H., Loh, K. M., & Nusse, R. (2014). Stem cell signaling. An integral program for tissue renewal and regeneration: Wnt signaling and stem cell control. *Science*, 346(6205), 1248012.
- Cliffe, L. J., Humphreys, N. E., Lane, T. E., Potten, C. S., Booth, C., & Grecis, R. K. (2005). Immunology - Accelerated intestinal epithelial cell turnover: A new mechanism of parasite expulsion. *Science*, 308(5727), 1463–1465.

- Co, J. Y., Margalef-Català, M., Li, X., Mah, A. T., Kuo, C. J., Monack, D. M., & Amieva, M. R. (2019). Controlling Epithelial Polarity: A Human Enteroid Model for Host-Pathogen Interactions. *Cell Reports*, 26(9), 2509-2520.e4.
- Co, J. Y., Margalef-Català, M., Monack, D. M., & Amieva, M. R. (2021). Controlling the polarity of human gastrointestinal organoids to investigate epithelial biology and infectious diseases. *Nature Protocols*, 16(11), 5171–5192.
- Coakley, G. (2017). *Characterisation of secreted exosomes from the intestinal nematode Heligmosomoides polygyrus* (A. Buck, Ed.) [Doctor of Philosophy]. University of Edinburgh.
- Coakley, G., & Harris, N. L. (2020). The Intestinal Epithelium at the Forefront of Host–Helminth Interactions. *Trends in Parasitology*, 36(9), 761–772.
- Coakley, G., Maizels, R. M., & Buck, A. H. (2015). Exosomes and Other Extracellular Vesicles: The New Communicators in Parasite Infections. *Trends in Parasitology*, 31(10), 477–489.
- Coakley, G., McCaskill, J. L., Borger, J. G., Simbari, F., Robertson, E., Millar, M., Harcus, Y., McSorley, H. J., Maizels, R. M., & Buck, A. H. (2017). Extracellular Vesicles from a Helminth Parasite Suppress Macrophage Activation and Constitute an Effective Vaccine for Protective Immunity. *Cell Reports*, 19(8), 1545–1557.
- Codemo, M., Muschiol, S., Iovino, F., Nannapaneni, P., Plant, L., Wai, S. N., & Henriques-Normark, B. (2018). Immunomodulatory Effects of Pneumococcal Extracellular Vesicles on Cellular and Humoral Host Defenses. *MBio*, 9(2), e00559-18.
- Coghlan, A., Tyagi, R., Cotton, J. A., Holroyd, N., Rosa, B. A., Tsai, I. J., Laetsch, D. R., Beech, R. N., Day, T. A., Hallsworth-Pepin, K., Ke, H. M., Kuo, T. H., Lee, T. J., Martin, J., Maizels, R. M., Mutowo, P., Ozersky, P., Parkinson, J., Reid, A. J., ... Berriman, M. (2019). Comparative genomics of the major parasitic worms. *Nature Genetics*, 51(1), 163–174.
- Connor, L. M., Tang, S.-C., Cognard, E., Ochiai, S., Hilligan, K. L., Old, S. I., Pellefigues, C., White, R. F., Patel, D., Smith, A. A. T., Eccles, D. A., Lamiable, O., McConnell, M. J., & Ronchese, F. (2017). Th2 responses are primed by skin dendritic cells with distinct transcriptional profiles. *The Journal of Experimental Medicine*, 214(1), 125–142.
- Corté, A., Sotillo, J., Muñoz-Antolí, C., Molina-Durán, J., Esteban, J. G., & Toledo, R. (2017). Antibody trapping: A novel mechanism of parasite immune evasion by the trematode *Echinostoma caproni*. *Plos Neglected Tropical Disease*, 11(7), e0005773.
- Cuesta, C. M., Guerri, C., Ureña, J., & Pascual, M. (2021). Role of Microbiota-Derived Extracellular Vesicles in Gut-Brain Communication. *International Journal of Molecular Sciences*, 22(8), 4235.
- Danecek, P., Bonfield, J. K., Liddle, J., Marshall, J., Ohan, V., Pollard, M. O., Whitwham, A., Keane, T., McCarthy, S. A., Davies, R. M., & Li, H. (2021). Twelve years of SAMtools and BCFtools. *GigaScience*, 10(2), giab008.
- Datta, R., deSchoolmeester, M. L., Hedeler, C., Paton, N. W., Brass, A. M., & Else, K. J. (2005). Identification of novel genes in intestinal tissue that are regulated after infection with an intestinal nematode parasite. *Infection and Immunity*, 73(7), 4025–4033.
- Davis, C. N., Phillips, H., Tomes, J. J., Swain, M. T., Wilkinson, T. J., Brophy, P. M., & Morphew, R. M. (2019). The importance of extracellular vesicle purification for downstream analysis: A comparison of differential centrifugation and size exclusion chromatography for helminth pathogens. *PLoS Neglected Tropical Diseases*, 13(2), e0007191.
- De Baets, K., Dentzien-Dias, P., Harrison, G. W. M., Littlewood, D. T. J., & Parry, L.

- A. (2021). Fossil Constraints on the Timescale of Parasitic Helminth Evolution. In K. De Baets & J. W. Huntley (Eds.), *The Evolution and Fossil Record of Parasitism: Identification and Macroevolution of Parasites* (pp. 231–271). Springer International Publishing.
- De Clercq, D., Sacko, M., Behnke, J., Gilbert, F., Dorny, P., & Vercruyse, J. (1997). Failure of mebendazole in treatment of human hookworm infections in the southern region of Mali. *The American Journal of Tropical Medicine and Hygiene*, *57*(1), 25–30.
- de Lau, W., Kujala, P., Schneeberger, K., Middendorp, S., Li, V. S. W., Barker, N., Martens, A., Hofhuis, F., DeKoter, R. P., Peters, P. J., Nieuwenhuis, E., & Clevers, H. (2012). Peyer's patch M cells derived from Lgr5(+) stem cells require SpiB and are induced by RankL in cultured "miniguts." *Molecular and Cellular Biology*, *32*(18), 3639–3647.
- de Lau, W., Peng, W. C., Gros, P., & Clevers, H. (2014). The R-spondin/Lgr5/Rnf43 module: regulator of Wnt signal strength. *Genes & Development*, *28*(4), 305–316.
- De, S. N. (1959). Enterotoxicity of bacteria-free culture-filtrate of vibrio cholerae. *Nature*, *183*(4674), 1533–1534.
- de Vlas, S. J., Stolk, W. A., le Rutte, E. A., Hontelez, J. A. C., Bakker, R., Blok, D. J., Cai, R., Houweling, T. A. J., Kulik, M. C., Lenk, E. J., Luyendijk, M., Matthijsse, S. M., Redekop, W. K., Wagenaar, I., Jacobson, J., Nagelkerke, N. J. D., & Richardus, J. H. (2016). Concerted Efforts to Control or Eliminate Neglected Tropical Diseases: How Much Health Will Be Gained? *PLoS Neglected Tropical Diseases*, *10*(2), e0004386.
- Deckx, R. J., Vantrappen, G. R., & Parein, M. M. (1967). Localization of lysozyme activity in a Paneth cell granule fraction. *Biochimica et Biophysica Acta*, *139*(1), 204–207.
- D'Elia, R., DeSchoolmeester, M. L., Zeef, L. A. H., Wright, S. H., Pemberton, A. D., & Else, K. J. (2009). Expulsion of *Trichuris muris* is associated with increased expression of angiogenin 4 in the gut and increased acidity of mucins within the goblet cell. *BMC Genomics*, *10*, 492.
- Demeler, J., Krüger, N., Krücken, J., von der Heyden, V. C., Ramünke, S., Küttler, U., Miltsch, S., López Cepeda, M., Knox, M., Vercruyse, J., Geldhof, P., Harder, A., & von Samson-Himmelstjerna, G. (2013). Phylogenetic characterization of  $\beta$ -tubulins and development of pyrosequencing assays for benzimidazole resistance in cattle nematodes. *PloS One*, *8*(8), e70212.
- Deo, P., Chow, S. H., Hay, I. D., Kleifeld, O., Costin, A., Elgass, K. D., Jiang, J.-H., Ramm, G., Gabriel, K., Dougan, G., Lithgow, T., Heinz, E., & Naderer, T. (2018). Outer membrane vesicles from *Neisseria gonorrhoeae* target PorB to mitochondria and induce apoptosis. *PLoS Pathogens*, *14*(3), e1006945.
- Dobro, M. J., Melanson, L. A., Jensen, G. J., & McDowall, A. W. (2010). Plunge freezing for electron cryomicroscopy. *Methods in Enzymology*, *481*, 63–82.
- Doyle, S. R., & Cotton, J. A. (2019). Genome-wide Approaches to Investigate Anthelmintic Resistance. *Trends in Parasitology*, *35*(4), 289–301.
- Drurey, C., Lindholm, H. T., Coakley, G., Campillo Poveda, M., Löser, S., Doolan, R., Gerbe, F., Jay, P., Harris, N., Oudhoff, M. J., & Maizels, R. M. (2021). Intestinal epithelial tuft cell induction is negated by a murine helminth and its secreted products. *J Exp Med*, *219*(1), e20211140.
- Drurey, C., & Maizels, R. M. (2021). Helminth extracellular vesicles: Interactions with the host immune system. *Molecular Immunology*, *137*, 124–133.
- Duque-Correa, M. A., Goulding, D., Rodgers, F. H., Gillis, J. A., Cormie, C., Rawlinson, K. A., Bancroft, A. J., Bennett, H. M., Lotkowska, M. E., Reid, A. J., Speak, A. O., Scott, P., Redshaw, N., Tolley, C., McCarthy, C., Brandt, C.,

## References

- Sharpe, C., Ridley, C., Moya, J. G., ... Berriman, M. (2022). Defining the early stages of intestinal colonisation by whipworms. *Nature Communications*, 13(1), 1725.
- Duque-Correa, M. A., Maizels, R. M., Grencis, R. K., & Berriman, M. (2020). Organoids - New Models for Host-Helminth Interactions. *Trends in Parasitology*, 36(2), 170–181.
- Duque-Correa, M. A., Schreiber, F., Rodgers, F. H., Goulding, D., Forrest, S., Cormie, C., White, R., Buck, A., Grencis, R. K., & Berriman, M. (2020). Development of caecaloids to study host-pathogens interactions: new insights into immune regulatory functions of *Trichuris muris* extracellular vesicles in the caecum. *International Journal for Parasitology*, 50(9), 707–718.
- Durand, A., Donahue, B., Peignon, G., Letourneur, F., Cagnard, N., Slomianny, C., Perret, C., Shroyer, N. F., & Romagnolo, B. (2012). Functional intestinal stem cells after Paneth cell ablation induced by the loss of transcription factor Math1 (Atoh1). *Proceedings of the National Academy of Sciences of the United States of America*, 109(23), 8965–8970.
- Dutta, D., & Clevers, H. (2017). Organoid culture systems to study host-pathogen interactions. *Current Opinion in Immunology*, 48, 15–22.
- Dutta, D., Heo, I., & Clevers, H. (2017). Disease Modeling in Stem Cell-Derived 3D Organoid Systems. *Trends in Molecular Medicine*, 23(5), 393–410.
- Eichenberger, R. M., Ryan, S., Jones, L., Buitrago, G., Polster, R., de Oca, M. M., Zuvelek, J., Giacomini, P. R., Dent, L. A., Engwerda, C. R., Field, M. A., Sotillo, J., & Loukas, A. (2018). Hookworm secreted extracellular vesicles interact with host cells and prevent inducible colitis in mice. *Frontiers in Immunology*, 9, 850.
- Eichenberger, R. M., Sotillo, J., & Loukas, A. (2018). Immunobiology of parasitic worm extracellular vesicles. *Immunology and Cell Biology*, 96(7), 704–713.
- Eichenberger, R. M., Talukder, M. H., Field, M. A., Wangchuk, P., Giacomini, P., Loukas, A., & Sotillo, J. (2018). Characterization of *Trichuris muris* secreted proteins and extracellular vesicles provides new insights into host–parasite communication. *Journal of Extracellular Vesicles*, 7(1).
- Else, K. J., Keiser, J., Holland, C. V., Grencis, R. K., Sattelle, D. B., Fujiwara, R. T., Bueno, L. L., Asaolu, S. O., Sowemimo, O. A., & Cooper, P. J. (2020). Whipworm and roundworm infections. *Nature Reviews. Disease Primers*, 6(1), 44.
- Emelyanov, A., Shtam, T., Kamyshinsky, R., Garaeva, L., Verlov, N., Miliukhina, I., Kudrevatykh, A., Gavrillov, G., Zabrodskaya, Y., Pchelina, S., & Konevega, A. (2020). Cryo-electron microscopy of extracellular vesicles from cerebrospinal fluid. *PloS One*, 15(1), e0227949.
- Faber, M. N., Smith, D., Price, D. R. G., Steele, P., Hildersley, K. A., Morrison, L. J., Mabbott, N. A., Nisbet, A. J., & McNeilly, T. N. (2022). Development of Bovine Gastric Organoids as a Novel In Vitro Model to Study Host-Parasite Interactions in Gastrointestinal Nematode Infections. *Frontiers in Cellular and Infection Microbiology*, 12, 904606.
- Feary, J., Britton, J., & Leonardi-Bee, J. (2011). Atopy and current intestinal parasite infection: a systematic review and meta-analysis. *Allergy*, 66(4), 569–578.
- Ferguson, S., Yang, K. S., Zelga, P., Liss, A. S., Carlson, J. C. T., Del Castillo, C. F., & Weissleder, R. (2022). Single-EV analysis (sEVA) of mutated proteins allows detection of stage 1 pancreatic cancer. *Science Advances*, 8(16), eabm3453.
- Fevr, T., Robine, S., Louvard, D., & Huelsken, J. (2007). Wnt/beta-catenin is essential for intestinal homeostasis and maintenance of intestinal stem cells. *Molecular and Cellular Biology*, 27(21), 7551–7559.

- Figueiredo, C. A., Barreto, M. L., Rodrigues, L. C., Cooper, P. J., Silva, N. B., Amorim, L. D., & Alcantara-Neves, N. M. (2010). Chronic intestinal helminth infections are associated with immune hyporesponsiveness and induction of a regulatory network. *Infection and Immunity*, *78*(7), 3160–3167.
- Finney, C. A. M., Taylor, M. D., Wilson, M. S., & Maizels, R. M. (2007). Expansion and activation of CD4 CD25 regulatory T cells in *Heligmosomoides polygyrus* infection. *European Journal of Immunology*, *37*(7), 1874–1886.
- Forman, R. A., deSchoolmeester, M. L., Hurst, R. J. M., Wright, S. H., Pemberton, A. D., & Else, K. J. (2012). The goblet cell is the cellular source of the anti-microbial angiogenin 4 in the large intestine post *Trichuris muris* infection. *PloS One*, *7*(9), e42248.
- Franzén, O., Gan, L.-M., & Björkegren, J. L. M. (2019). PanglaoDB: a web server for exploration of mouse and human single-cell RNA sequencing data. *Database: The Journal of Biological Databases and Curation*, *2019*, baz046.
- Fre, S., Huyghe, M., Mourikis, P., Robine, S., Louvard, D., & Artavanis-Tsakonas, S. (2005). Notch signals control the fate of immature progenitor cells in the intestine. *Nature*, *435*(7044), 964–968.
- Fukuda, S., Hase, K., & Ohno, H. (2011). Application of a mouse ligated Peyer's patch intestinal loop assay to evaluate bacterial uptake by M cells. *Journal of Visualized Experiments: JoVE*, *58*, 3225.
- Furness, J. B., Rivera, L. R., Cho, H.-J., Bravo, D. M., & Callaghan, B. (2013). The gut as a sensory organ. *Nature Reviews. Gastroenterology & Hepatology*, *10*(12), 729–740.
- Galioto, A. M., Hess, J. A., Nolan, T. J., Schad, G. A., Lee, J. J., & Abraham, D. (2006). Role of eosinophils and neutrophils in innate and adaptive protective immunity to larval *strongyloides stercoralis* in mice. *Infection and Immunity*, *74*(10), 5730–5738.
- Garcia-Silva, M. R., Cabrera-Cabrera, F., das Neves, R. F. C., Souto-Padrón, T., de Souza, W., & Cayota, A. (2014). Gene expression changes induced by *Trypanosoma cruzi* shed microvesicles in mammalian host cells: relevance of tRNA-derived halves. *BioMed Research International*, *2014*, 305239.
- Gascan, H., Gauchat, J. F., Aversa, G., Van Vlasselaer, P., & de Vries, J. E. (1991). Anti-CD40 monoclonal antibodies or CD4+ T cell clones and IL-4 induce IgG4 and IgE switching in purified human B cells via different signaling pathways. *Journal of Immunology*, *147*(1), 8–13.
- Gaze, S., McSorley, H. J., Daveson, J., Jones, D., Bethony, J. M., Oliveira, L. M., Speare, R., McCarthy, J. S., Engwerda, C. R., Croese, J., & Loukas, A. (2012). Characterising the Mucosal and Systemic Immune Responses to Experimental Human Hookworm Infection. *PLoS Pathogens*, *8*(2), e1002520.
- Gehart, H., & Clevers, H. (2019). Tales from the crypt: new insights into intestinal stem cells. *Nature Reviews. Gastroenterology & Hepatology*, *16*(1), 19–34.
- Gehrmann, U., Qazi, K. R., Johansson, C., Hultenby, K., Karlsson, M., Lundberg, L., Gabrielsson, S., & Scheynius, A. (2011). Nanovesicles from *Malassezia sympodialis* and host exosomes induce cytokine responses--novel mechanisms for host-microbe interactions in atopic eczema. *PloS One*, *6*(7), e21480.
- Gerbe, F., Legraverend, C., & Jay, P. (2012). The intestinal epithelium tuft cells: specification and function. *Cellular and Molecular Life Sciences: CMLS*, *69*(17), 2907–2917.
- Gerbe, F., Sidot, E., Smyth, D. J., Ohmoto, M., Matsumoto, I., Dardalhon, V., Cesses, P., Garnier, L., Pouzolles, M., Brulin, B., Bruschi, M., Harcus, Y., Zimmermann, V. S., Taylor, N., Maizels, R. M., & Jay, P. (2016). Intestinal epithelial tuft cells initiate type 2 mucosal immunity to helminth parasites.

- Nature*, 529(7585), 226–230.
- Gerbe, F., Van Es, J. H., Makrini, L., Brulin, B., Mellitzer, G., Robine, S., Romagnolo, B., Shroyer, N. F., Bourgaux, J. F., Pignodel, C., Clevers, H., & Jay, P. (2011). Distinct ATOH1 and Neurog3 requirements define tuft cells as a new secretory cell type in the intestinal epithelium. *The Journal of Cell Biology*, 192(5), 767–780.
- Ghaleb, A. M., Aggarwal, G., Bialkowska, A. B., Nandan, M. O., & Yang, V. W. (2008). Notch inhibits expression of the Krüppel-like factor 4 tumor suppressor in the intestinal epithelium. *Molecular Cancer Research: MCR*, 6(12), 1920–1927.
- Grainger, J. R., Smith, K. A., Hewitson, J. P., McSorley, H. J., Marcus, Y., Filbey, K. J., Finney, C. A. M., Greenwood, E. J. D., Knox, D. P., Wilson, M. S., Belkaid, Y., Rudensky, A. Y., & Maizels, R. M. (2010). Helminth secretions induce de novo T cell Foxp3 expression and regulatory function through the TGF- $\beta$  pathway. *The Journal of Experimental Medicine*, 207(11), 2331–2341.
- Gregorieff, A., Liu, Y., Inanlou, M. R., Khomchuk, Y., & Wrana, J. L. (2015). Yap-dependent reprogramming of Lgr5+ stem cells drives intestinal regeneration and cancer. *Nature*, 526(7575), 715–718.
- Gregorieff, A., Stange, D. E., Kujala, P., Begthel, H., van den Born, M., Korving, J., Peters, P. J., & Clevers, H. (2009). The ets-domain transcription factor Spdef promotes maturation of goblet and paneth cells in the intestinal epithelium. *Gastroenterology*, 137(4), 1333-45.e1-3.
- Gustafsson, J. K., Davis, J. E., Rappai, T., McDonald, K. G., Kulkarni, D. H., Knoop, K. A., Hogan, S. P., Fitzpatrick, J. A. J., Lencer, W. I., & Newberry, R. D. (2021). Intestinal goblet cells sample and deliver luminal antigens by regulated endocytic uptake and transcytosis. *ELife*, 10, e67292.
- Haber, A. L., Biton, M., Rogel, N., Herbst, R. H., Shekhar, K., Smillie, C., Burgin, G., Delorey, T. M., Howitt, M. R., Katz, Y., Tirosh, I., Beyaz, S., Dionne, D., Zhang, M., Raychowdhury, R., Garrett, W. S., Rozenblatt-Rosen, O., Shi, H. N., Yilmaz, O., ... Regev, A. (2017). A single-cell survey of the small intestinal epithelium. *Nature*, 551(7680), 333–339.
- Hagen, J., Sarkies, P., & Selkirk, M. E. (2021). Lentiviral transduction facilitates RNA interference in the nematode parasite *Nippostrongylus brasiliensis*. *PLoS Pathogens*, 17(1), e1009286.
- Hao, Y., Hao, S., Andersen-Nissen, E., Mauck, W. M., Zheng, S., Butler, A., Lee, M. J., Wilk, A. J., Darby, C., Zager, M., Hoffman, P., Stoeckius, M., Papalexi, E., Mimitou, E. P., Jain, J., Srivastava, A., Stuart, T., Fleming, L. M., Yeung, B., ... Satija, R. (2021). Integrated analysis of multimodal single-cell data. *Cell*, 184(13), 3573-3587.e29.
- Hardwick, J. C. H., Van Den Brink, G. R., Bleuming, S. A., Ballester, I., Van Den Brande, J. M. H., Keller, J. J., Offerhaus, G. J. A., Van Deventer, S. J. H., & Peppelenbosch, M. P. (2004). Bone morphogenetic protein 2 is expressed by, and acts upon, mature epithelial cells in the colon. *Gastroenterology*, 126(1), 111–121.
- Hashimoto, K., Uchikawa, R., Tegoshi, T., Takeda, K., Yamada, M., & Arizono, N. (2009). Depleted intestinal goblet cells and severe pathological changes in SCID mice infected with *Heligmosomoides polygyrus*. *Parasite Immunology*, 31(8), 457–465.
- Hepworth, M. R., Daniłowicz-Luebert, E., Rausch, S., Metz, M., Klotz, C., Maurer, M., & Hartmann, S. (2012). Mast cells orchestrate type 2 immunity to helminths through regulation of tissue-derived cytokines. *Proceedings of the National Academy of Sciences of the United States of America*, 109(17), 6644–6649.
- Herbert, D. R., Douglas, B., & Zullo, K. (2019). Group 2 Innate Lymphoid Cells (ILC2): Type 2 Immunity and Helminth Immunity. *International Journal of Molecular*

- Sciences*, 20(9), 2276.
- Herbert, D. R., Yang, J.-Q., Hogan, S. P., Groschwitz, K., Khodoun, M., Munitz, A., Orekov, T., Perkins, C., Wang, Q., Brombacher, F., Urban, J. F., Jr, Rothenberg, M. E., & Finkelman, F. D. (2009). Intestinal epithelial cell secretion of RELM-beta protects against gastrointestinal worm infection. *The Journal of Experimental Medicine*, 206(13), 2947–2957.
- Hesse, M., Modolell, M., La Flamme, A. C., Schito, M., Fuentes, J. M., Cheever, A. W., Pearce, E. J., & Wynn, T. A. (2001). Differential regulation of nitric oxide synthase-2 and arginase-1 by type 1/type 2 cytokines in vivo: granulomatous pathology is shaped by the pattern of L-arginine metabolism. *The Journal of Immunology*, 167(11), 6533–6544.
- Hewitson, J. P., Filbey, K. J., Bieren, J. E., Camberis, M., Schwartz, C., Murray, J., Reynolds, L. A., Blair, N., Robertson, E., Harcus, Y., Boon, L., Huang, S. C.-C., Yang, L., Tu, Y., Miller, M. J., Voehringer, D., Gros, G. L., Harris, N., & Maizels, R. M. (2015). Concerted Activity of IgG1 Antibodies and IL-4/IL-25-Dependent Effector Cells Trap Helminth Larvae in the Tissues following Vaccination with Defined Secreted Antigens, Providing Sterile Immunity to Challenge Infection. *PLoS Pathogens*, 11(3), e1004676.
- Hewitson, J. P., Filbey, K. J., Grainger, J. R., Dowle, A. A., Pearson, M., Murray, J., Harcus, Y., & Maizels, R. M. (2011). Heligmosomoides polygyrus elicits a dominant non-protective antibody response directed against restricted glycan and peptide epitopes. *Journal of Immunology*, 187(9), 4764.
- Heyneman, D., Beaver, P. C., Jung, R. C., & Cupp, E. W. (1984). Clinical Parasitology. *The Journal of Parasitology*, 70(6), 978.
- Hoepli, R. (1956). The knowledge of parasites and parasitic infections from ancient times to the 17th century. *Experimental Parasitology*, 5(4), 398–419.
- Holz, A., & Streit, A. (2017). Gain and Loss of Small RNA Classes—Characterization of Small RNAs in the Parasitic Nematode Family Strongyloididae. *Genome Biology and Evolution*, 9(10), 2826–2843.
- Hotez, P. J., Bethony, J. M., Diemert, D. J., Pearson, M., & Loukas, A. (2010). Developing vaccines to combat hookworm infection and intestinal schistosomiasis. *Nature Reviews. Microbiology*, 8(11), 814–826.
- Hotez, P. J., Bundy, D. A. P., Beegle, K., Brooker, S., Drake, L., Silva, N. de, Montresor, A., Engels, D., Jukes, M., Chitsulo, L., Chow, J., Laxminarayan, R., Michaud, C., Bethony, J., Correa-Oliveira, R., Shuhua, X., Fenwick, A., & Savioli, L. (2006). *Helminth Infections: Soil-transmitted Helminth Infections and Schistosomiasis* (pp. 468–482). The International Bank for Reconstruction and Development / The World Bank.
- Howitt, M. R., Lavoie, S., Michaud, M., Blum, A. M., Tran, S. V., Weinstock, J. V., Gallini, C. A., Redding, K., Margolskee, R. F., Osborne, L. C., Artis, D., & Garrett, W. S. (2016). Tuft cells, taste-chemosensory cells, orchestrate parasite type 2 immunity in the gut. *Science*, 351(6279), 1329–1333.
- Hung, L.-Y., Lewkowich, I. P., Dawson, L. A., Downey, J., Yang, Y., Smith, D. E., & Herbert, D. R. (2013). IL-33 drives biphasic IL-13 production for noncanonical Type 2 immunity against hookworms. *Proceedings of the National Academy of Sciences of the United States of America*, 110(1), 282–287.
- Hyenne, V., Apaydin, A., Rodriguez, D., Spiegelhalter, C., Hoff-Yoessle, S., Diem, M., Tak, S., Lefebvre, O., Schwab, Y., Goetz, J. G., & Labouesse, M. (2015). RAL-1 controls multivesicular body biogenesis and exosome secretion. *The Journal of Cell Biology*, 211(1), 27–37.
- Ireland, H., Houghton, C., Howard, L., & Winton, D. J. (2005). Cellular inheritance of a Cre-activated reporter gene to determine Paneth cell longevity in the murine small intestine. *Developmental Dynamics: An Official Publication of the*

- American Association of Anatomists*, 233(4), 1332–1336.
- Jadhav, U., Saxena, M., O'Neill, N. K., Saadatpour, A., Yuan, G.-C., Herbert, Z., Murata, K., & Shivdasani, R. A. (2017). Dynamic Reorganization of Chromatin Accessibility Signatures during Dedifferentiation of Secretory Precursors into Lgr5+ Intestinal Stem Cells. *Cell Stem Cell*, 21(1), 65-77.e5.
- Jenny, M., Uhl, C., Roche, C., Duluc, I., Guillermin, V., Guillemot, F., Jensen, J., Kedinger, M., & Gradwohl, G. (2002). Neurogenin3 is differentially required for endocrine cell fate specification in the intestinal and gastric epithelium. *The EMBO Journal*, 21(23), 6338–6347.
- Jensen, W. A. (1965). The composition and ultrastructure of the nucellus in cotton. *Journal of Ultrastructure Research*, 13(1–2), 112–128.
- Johnston, C. J. C., Smyth, D. J., Kodali, R. B., White, M. P. J., Harcus, Y., Filbey, K. J., Hewitson, J. P., Hinck, C. S., Ivens, A., Kemter, A. M., Kildemoes, A. O., Le Bihan, T., Soares, D. C., Anderton, S. M., Brenn, T., Wigmore, S. J., Woodcock, H. V., Chambers, R. C., Hinck, A. P., ... Maizels, R. M. (2017). A structurally distinct TGF- $\beta$  mimic from an intestinal helminth parasite potently induces regulatory T cells. *Nature Communications*, 8(1), 1741.
- Johnstone, R. M., Adam, M., Hammond, J. R., Orr, L., & Turbide, C. (1987). Vesicle formation during reticulocyte maturation. Association of plasma membrane activities with released vesicles (exosomes). *The Journal of Biological Chemistry*, 262(19), 9412–9420.
- Jourdan, P. M., Lambertson, P. H. L., Fenwick, A., & Addiss, D. G. (2018). Soil-transmitted helminth infections. *The Lancet*, 391(10117), 252–265.
- Junttila, I. S. (2018). Tuning the Cytokine Responses: An Update on Interleukin (IL)-4 and IL-13 Receptor Complexes. *Frontiers in Immunology*, 9, 888.
- Kamal, M., Dehlawi, M. S., Brunet, L. R., & Wakelin, D. (2002). Paneth and intermediate cell hyperplasia induced in mice by helminth infections. *Parasitology*, 125(Pt 3), 275–281.
- Kaparakis, M., Turnbull, L., Carneiro, L., Firth, S., Coleman, H. A., Parkington, H. C., Le Bourhis, L., Karrar, A., Viala, J., Mak, J., Hutton, M. L., Davies, J. K., Crack, P. J., Hertzog, P. J., Philpott, D. J., Girardin, S. E., Whitchurch, C. B., & Ferrero, R. L. (2010). Bacterial membrane vesicles deliver peptidoglycan to NOD1 in epithelial cells. *Cellular Microbiology*, 12(3), 372–385.
- Karo-Atar, D., Ouladan, S., Javkar, T., Joumier, L., Matheson, M. K., Merritt, S., Westfall, S., Rochette, A., Gentile, M. E., Fontes, G., Fonseca, G. J., Parisien, M., Diatchenko, L., von Moltke, J., Malleshaiah, M., Gregorieff, A., & King, I. L. (2022). Helminth-induced reprogramming of the stem cell compartment inhibits type 2 immunity. *The Journal of Experimental Medicine*, 219(9).
- Karpowicz, P., Perez, J., & Perrimon, N. (2010). The Hippo tumor suppressor pathway regulates intestinal stem cell regeneration. *Development*, 137(24), 4135–4145.
- Katz, J. P., Perreault, N., Goldstein, B. G., Lee, C. S., Labosky, P. A., Yang, V. W., & Kaestner, K. H. (2002). The zinc-finger transcription factor Klf4 is required for terminal differentiation of goblet cells in the colon. *Development*, 129(11), 2619–2628.
- Kayisoglu, O., Weiss, F., Niklas, C., Pierotti, I., Pompaiah, M., Wallaschek, N., Germer, C.-T., Wiegering, A., & Bartfeld, S. (2021). Location-specific cell identity rather than exposure to GI microbiota defines many innate immune signalling cascades in the gut epithelium. *Gut*, 70(4), 687–697.
- Kazanjian, A., Noah, T., Brown, D., Burkart, J., & Shroyer, N. F. (2010). Atonal homolog 1 is required for growth and differentiation effects of notch/gamma-secretase inhibitors on normal and cancerous intestinal epithelial cells. *Gastroenterology*, 139(3), 918–928, 928.e1-6.



- Khan, W. I., Blennerhasset, P., Ma, C., Matthaei, K. I., & Collins, S. M. (2001). Stat6 dependent goblet cell hyperplasia during intestinal nematode infection. *Parasite Immunology*, 23(1), 39–42.
- Kiela, P. R., & Ghishan, F. K. (2016). Physiology of Intestinal Absorption and Secretion. *Best Practice & Research. Clinical Gastroenterology*, 30(2), 145–159.
- Kim, H. J., Huh, D., Hamilton, G., & Ingber, D. E. (2012). Human gut-on-a-chip inhabited by microbial flora that experiences intestinal peristalsis-like motions and flow. *Lab on a Chip*, 12(12), 2165–2174.
- Kim, R., Attayek, P. J., Wang, Y., Furtado, K. L., Tamayo, R., Sims, C. E., & Allbritton, N. L. (2019). An in vitro intestinal platform with a self-sustaining oxygen gradient to study the human gut/microbiome interface. *Biofabrication*, 12(1), 015006.
- Kim, T.-H., Escudero, S., & Shivdasani, R. A. (2012). Intact function of Lgr5 receptor-expressing intestinal stem cells in the absence of Paneth cells. *Proceedings of the National Academy of Sciences of the United States of America*, 109(10), 3932–3937.
- Kim, T.-H., & Shivdasani, R. A. (2011). Genetic evidence that intestinal Notch functions vary regionally and operate through a common mechanism of Math1 repression. *The Journal of Biological Chemistry*, 286(13), 11427–11433.
- Kimura, S., Yamakami-Kimura, M., Obata, Y., Hase, K., Kitamura, H., Ohno, H., & Iwanaga, T. (2015). Visualization of the entire differentiation process of murine M cells: suppression of their maturation in cecal patches. *Mucosal Immunology*, 8(3), 650–660.
- Kimura, Shunsuke, Kobayashi, N., Nakamura, Y., Kanaya, T., Takahashi, D., Fujiki, R., Mutoh, M., Obata, Y., Iwanaga, T., Nakagawa, T., Kato, N., Sato, S., Kaisho, T., Ohno, H., & Hase, K. (2019). Sox8 is essential for M cell maturation to accelerate IgA response at the early stage after weaning in mice. *The Journal of Experimental Medicine*, 216(4), 831–846.
- King, C. L., Mahanty, S., Kumaraswami, V., Abrams, J. S., Regunathan, J., Jayaraman, K., Ottesen, E. A., & Nutman, T. B. (1993). Cytokine control of parasite-specific anergy in human lymphatic filariasis. Preferential induction of a regulatory T helper type 2 lymphocyte subset. *The Journal of Clinical Investigation*, 92(4), 1667–1673.
- Knoop, K. A., Kumar, N., Butler, B. R., Sakthivel, S. K., Taylor, R. T., Nochi, T., Akiba, H., Yagita, H., Kiyono, H., & Williams, I. R. (2009). RANKL is necessary and sufficient to initiate development of antigen-sampling M cells in the intestinal epithelium. *Journal of Immunology*, 183(9), 5738–5747.
- Knott, M. L., Matthaei, K. I., Giacomini, P. R., Wang, H., Foster, P. S., & Dent, L. A. (2007). Impaired resistance in early secondary *Nippostrongylus brasiliensis* infections in mice with defective eosinophilopoiesis. *International Journal for Parasitology*, 37(12), 1367–1378.
- Kobayashi, N., Takahashi, D., Takano, S., Kimura, S., & Hase, K. (2019). The Roles of Peyer's Patches and Microfold Cells in the Gut Immune System: Relevance to Autoimmune Diseases. *Frontiers in Immunology*, 10, 2345.
- Koeppen, K., Hampton, T. H., Jarek, M., Scharfe, M., Gerber, S. A., Mielcarz, D. W., Demers, E. G., Dolben, E. L., Hammond, J. H., Hogan, D. A., & Stanton, B. A. (2016). A Novel Mechanism of Host-Pathogen Interaction through sRNA in Bacterial Outer Membrane Vesicles. *PLoS Pathogens*, 12(6), e1005672.
- Koga, Y., Yasunaga, M., Moriya, Y., Akasu, T., Fujita, S., Yamamoto, S., & Matsumura, Y. (2011). Exosome can prevent RNase from degrading microRNA in feces. *Journal of Gastrointestinal Oncology*, 2(4), 215–222.
- Kolodny, G. M. (1971). Evidence for transfer of macromolecular RNA between

- mammalian cells in culture. *Experimental Cell Research*, 65(2), 313–324.
- Kolodny, G. M. (1972). Cell to cell transfer of RNA into transformed cells. *Journal of Cellular Physiology*, 79(1), 147–150.
- Korinek, V., Barker, N., Moerer, P., van Donselaar, E., Huls, G., Peters, P. J., & Clevers, H. (1998). Depletion of epithelial stem-cell compartments in the small intestine of mice lacking Tcf-4. *Nature Genetics*, 19(4), 379–383.
- Kosinski, C., Li, V. S. W., Chan, A. S. Y., Zhang, J., Ho, C., Tsui, W. Y., Chan, T. L., Mifflin, R. C., Powell, D. W., Yuen, S. T., Leung, S. Y., & Chen, X. (2007). Gene expression patterns of human colon tops and basal crypts and BMP antagonists as intestinal stem cell niche factors. *Proceedings of the National Academy of Sciences of the United States of America*, 104(39), 15418–15423.
- Kozuka, K., He, Y., Koo-McCoy, S., Kumaraswamy, P., Nie, B., Shaw, K., Chan, P., Leadbetter, M., He, L., Lewis, J. G., Zhong, Z., Charmot, D., Balaa, M., King, A. J., Caldwell, J. S., & Siegel, M. (2017). Development and Characterization of a Human and Mouse Intestinal Epithelial Cell Monolayer Platform. *Stem Cell Reports*, 9(6), 1976–1990.
- Krasteva, G., & Kummer, W. (2012). “Tasting” the airway lining fluid. *Histochemistry and Cell Biology*, 138(3), 365–383.
- Kuipers, M. E., Nolte-t Hoen, E. N. M., van der Ham, A. J., Ozir-Fazalalikhani, A., Nguyen, D. L., de Korne, C. M., Koning, R. I., Tomes, J. J., Hoffmann, K. F., Smits, H. H., & Hokke, C. H. (2020). DC-SIGN mediated internalisation of glycosylated extracellular vesicles from *Schistosoma mansoni* increases activation of monocyte-derived dendritic cells. *Journal of Extracellular Vesicles*, 9(1), 1753420.
- Layrisse, M., Linares, J., Roche, M., Ojeda, A., Carstens, A., & Dugarte, I. (1965). Excess Hemolysis in Subjects with Severe Iron Deficiency Anemia Associated and Nonassociated with Hookworm Infection. *Blood*, 25(1), 73–91.
- Lázaro-Ibáñez, E., Neuvonen, M., Takatalo, M., Thanigai Arasu, U., Capasso, C., Cerullo, V., Rhim, J. S., Rilla, K., Yliperttula, M., & Siljander, P. R.-M. (2017). Metastatic state of parent cells influences the uptake and functionality of prostate cancer cell-derived extracellular vesicles. *Journal of Extracellular Vesicles*, 6(1), 1354645.
- Lebman, D. A., & Coffman, R. L. (1988). Interleukin 4 causes isotype switching to IgE in T cell-stimulated clonal B cell cultures. *The Journal of Experimental Medicine*, 168(3), 853–862.
- Lechner, A., Bohnacker, S., & Esser-von Bieren, J. (2021). Macrophage regulation & function in helminth infection. *Seminars in Immunology*, 53, 101526.
- Lei, W., Ren, W., Ohmoto, M., Urban, J. F., Jr, Matsumoto, I., Margolskee, R. F., & Jiang, P. (2018). Activation of intestinal tuft cell-expressed *Sucnr1* triggers type 2 immunity in the mouse small intestine. *Proceedings of the National Academy of Sciences of the United States of America*, 115(21), 5552–5557.
- Lendner, M., Doligalska, M., Lucius, R., & Hartmann, S. (2008). Attempts to establish RNA interference in the parasitic nematode *Heligmosomoides polygyrus*. *Molecular and Biochemical Parasitology*, 161(1), 21–31.
- Li, H., Handsaker, B., Wysoker, A., Fennell, T., Ruan, J., Homer, N., Marth, G., Abecasis, G., Durbin, R., & 1000 Genome Project Data Processing Subgroup. (2009). The Sequence Alignment/Map format and SAMtools. *Bioinformatics*, 25(16), 2078–2079.
- Liao, Y., Smyth, G. K., & Shi, W. (2014). featureCounts: an efficient general purpose program for assigning sequence reads to genomic features. *Bioinformatics*, 30(7), 923–930.
- Liégeois, S., Benedetto, A., Garnier, J.-M., Schwab, Y., & Labouesse, M. (2006). The V0-ATPase mediates apical secretion of exosomes containing Hedgehog-

- related proteins in *Caenorhabditis elegans*. *The Journal of Cell Biology*, 173(6), 949–961.
- Lindholm, H. T., Parmar, N., Druere, C., Campillo Poveda, M., Vornewald, P. M., Ostrop, J., Díez-Sánchez, A., Maizels, R. M., & Oudhoff, M. J. (2022). BMP signaling in the intestinal epithelium drives a critical feedback loop to restrain IL-13-driven tuft cell hyperplasia. *Science Immunology*, 7(71), eabl6543.
- Liu, H., Tian, Y., Xue, C., Niu, Q., Chen, C., & Yan, X. (2022). Analysis of extracellular vesicle DNA at the single-vesicle level by nano-flow cytometry. *Journal of Extracellular Vesicles*, 11(4), e12206.
- Liu, Q., Kreider, T., Bowdridge, S., Liu, Z., Song, Y., Gaydo, A. G., Urban, J. F., Jr, & Gause, W. C. (2010). B cells have distinct roles in host protection against different nematode parasites. *Journal of Immunology*, 184(9), 5213–5223.
- Liu, Y., Qi, Z., Li, X., Du, Y., & Chen, Y. G. (2018). Monolayer culture of intestinal epithelium sustains Lgr5+ intestinal stem cells. *Cell Discovery*, 4(1), 32.
- Loukas, A., Hotez, P. J., Diemert, D., Yazdanbakhsh, M., McCarthy, J. S., Correa-Oliveira, R., Croese, J., & Bethony, J. M. (2016). Hookworm infection. *Nature Reviews. Disease Primers*, 2, 16088.
- Lun, A. T. L., Riesenfeld, S., Andrews, T., Dao, T. P., Gomes, T., Jamboree, P. in T. 1st H. C. A., & Marioni, J. C. (2019). EmptyDrops: distinguishing cells from empty droplets in droplet-based single-cell RNA sequencing data. *Genome Biology*, 20(1), 63.
- Luo, X.-C., Chen, Z.-H., Xue, J.-B., Zhao, D.-X., Lu, C., Li, Y.-H., Li, S.-M., Du, Y.-W., Liu, Q., Wang, P., Liu, M., & Huang, L. (2019). Infection by the parasitic helminth *Trichinella spiralis* activates a Tas2r-mediated signaling pathway in intestinal tuft cells. *Proceedings of the National Academy of Sciences of the United States of America*, 116(12), 5564–5569.
- Mabaso, M. L. H., Appleton, C. C., Hughes, J. C., & Gouws, E. (2003). The effect of soil type and climate on hookworm (*Necator americanus*) distribution in KwaZulu-Natal, South Africa. *Tropical Medicine & International Health: TM & IH*, 8(8), 722–727.
- Mabbott, N. A., Donaldson, D. S., Ohno, H., Williams, I. R., & Mahajan, A. (2013). Microfold (M) cells: important immunosurveillance posts in the intestinal epithelium. *Mucosal Immunology*, 6(4), 666–677.
- MacDonald, A. S., & Maizels, R. M. (2008). Alarming dendritic cells for Th2 induction [Review of *Alarming dendritic cells for Th2 induction*]. *The Journal of Experimental Medicine*, 205(1), 13–17.
- Macdonald, I. A., & Kuehn, M. J. (2013). Stress-induced outer membrane vesicle production by *Pseudomonas aeruginosa*. *Journal of Bacteriology*, 195(13), 2971–2981.
- Maizels, R. M., Gomez-Escobar, N., Gregory, W. F., Murray, J., & Zang, X. (2001). Immune evasion genes from filarial nematodes. *International Journal for Parasitology*, 31(9), 889–898.
- Maizels, R., Smits, H., & McSorley, H. (2018). Modulation of Host Immunity by Helminths: The Expanding Repertoire of Parasite Effector Molecules. *Immunity*, 49(5), 801–818.
- Maizels, Rick M. (2020). Regulation of immunity and allergy by helminth parasites. *Allergy*, 75(3), 524–534.
- Maizels, Rick M., & Balic, A. (2004). Resistance to helminth infection: the case for interleukin-5-dependent mechanisms [Review of *Resistance to helminth infection: the case for interleukin-5-dependent mechanisms*]. *The Journal of Infectious Diseases*, 190(3), 427–429.
- Maizels, Rick M., & McSorley, H. J. (2016). Regulation of the host immune system by helminth parasites. *The Journal of Allergy and Clinical Immunology*, 138(3),

- 666–675.
- Marillier, R. G., Michels, C., Smith, E. M., Fick, L. C. E., Leeto, M., Dewals, B., Horsnell, W. G. C., & Brombacher, F. (2008). IL-4/IL-13 independent goblet cell hyperplasia in experimental helminth infections. *BMC Immunology*, *9*, 11.
- McCoy, K. D., Stoel, M., Stettler, R., Merky, P., Fink, K., Senn, B. M., Schaer, C., Massacand, J., Odermatt, B., Oettgen, H. C., Zinkernagel, R. M., Bos, N. A., Hengartner, H., Macpherson, A. J., & Harris, N. L. (2008). Polyclonal and Specific Antibodies Mediate Protective Immunity against Enteric Helminth Infection. *Cell Host & Microbe*, *4*(4), 362–373.
- McGinty, J. W., Ting, H.-A., Billipp, T. E., Nadjombati, M. S., Khan, D. M., Barrett, N. A., Liang, H.-E., Matsumoto, I., & von Moltke, J. (2020). Tuft-Cell-Derived Leukotrienes Drive Rapid Anti-helminth Immunity in the Small Intestine but Are Dispensable for Anti-protist Immunity. *Immunity*, *52*(3), 528–541.e7.
- McInnes, L., Healy, J., & Melville, J. (2018). UMAP: Uniform Manifold Approximation and Projection for Dimension Reduction. *ArXiv*, arXiv:1802.03426v3.
- McKenzie, A. J., Hoshino, D., Hong, N. H., Cha, D. J., Franklin, J. L., Coffey, R. J., Patton, J. G., & Weaver, A. M. (2016). KRAS-MEK Signaling Controls Ago2 Sorting into Exosomes. *Cell Reports*, *15*(5), 978–987.
- McSorley, H. J., Blair, N. F., Smith, K. A., McKenzie, A. N. J., & Maizels, R. M. (2014). Blockade of IL-33 release and suppression of type 2 innate lymphoid cell responses by helminth secreted products in airway allergy. *Mucosal Immunology*, *7*(5), 1068–1078.
- McSorley, Henry J., & Maizels, R. M. (2012). Helminth infections and host immune regulation. *Clinical Microbiology Reviews*, *25*(4), 585–608.
- Metchnikoff, E. (1905). *Immunity in infective diseases / by Élie Metchnikoff; translated from the French by Francis G. Binnie*. University Press.
- Metenou, S., Dembele, B., Konate, S., Dolo, H., Coulibaly, S. Y., Coulibaly, Y. I., Diallo, A. A., Soumaoro, L., Coulibaly, M. E., Sanogo, D., Doumbia, S. S., Traoré, S. F., Mahanty, S., Klion, A., & Nutman, T. B. (2010). At Homeostasis Filarial Infections Have Expanded Adaptive T Regulatory but Not Classical Th2 Cells. *The Journal of Immunology*, *184*(9), 5375–5382.
- Milano, J., McKay, J., Dagenais, C., Foster-Brown, L., Pognan, F., Gadiant, R., Jacobs, R. T., Zacco, A., Greenberg, B., & Ciaccio, P. J. (2004). Modulation of notch processing by  $\gamma$ -secretase inhibitors causes intestinal goblet cell metaplasia and induction of genes known to specify gut secretory lineage differentiation. *Toxicological Sciences: An Official Journal of the Society of Toxicology*, *82*(1), 341–358.
- Minutti, C. M., Jackson-Jones, L. H., García-Fojeda, B., Knipper, J. A., Sutherland, T. E., Logan, N., Ringqvist, E., Guillaumat-Prats, R., Ferenbach, D. A., Artigas, A., Stamme, C., Chroneos, Z. C., Zaiss, D. M., Casals, C., & Allen, J. E. (2017). Local amplifiers of IL-4R $\alpha$ -mediated macrophage activation promote repair in lung and liver. *Science*, *356*(6342), 1076–1080.
- Minutti, C. M., Knipper, J. A., Allen, J. E., & Zaiss, D. M. W. (2017). Tissue-specific contribution of macrophages to wound healing. *Seminars in Cell & Developmental Biology*, *61*, 3–11.
- Minutti, C. M., Modak, R. V., Macdonald, F., Li, F., Smyth, D. J., Dorward, D. A., Blair, N., Husovsky, C., Muir, A., Giampazolias, E., Dobie, R., Maizels, R. M., Kendall, T. J., Griggs, D. W., Kopf, M., Henderson, N. C., & Zaiss, D. M. (2019). A Macrophage-Pericyte Axis Directs Tissue Restoration via Amphiregulin-Induced Transforming Growth Factor Beta Activation. *Immunity*, *50*(3), 645–654.e6.
- Mkandawire, T. T., Grecis, R. K., Berriman, M., & Duque-Correa, M. A. (2022). Hatching of parasitic nematode eggs: a crucial step determining infection.

- Trends in Parasitology*, 38(2), 174–187.
- Momma, S. (2021). Extracellular vesicles for remote brain repair. *Current Opinion in Genetics & Development*, 70, 61–65.
- Monguió-Tortajada, M., Gálvez-Montón, C., Bayes-Genis, A., Roura, S., & Borràs, F. E. (2019). Extracellular vesicle isolation methods: rising impact of size-exclusion chromatography. *Cellular and Molecular Life Sciences: CMLS*, 76(12), 2369–2382.
- Montresor, A., Mupfasoni, D., Mikhailov, A., Mwinzi, P., Lucianez, A., Jamsheed, M., Gasimov, E., Warusavithana, S., Yajima, A., Bisoffi, Z., Buonfrate, D., Steinmann, P., Utzinger, J., Levecke, B., Vlamincx, J., Coolsid, P., Vercruyssen, J., Cringoli, G., Rinaldi, L., ... Gyorkos, T. W. (2020). The global progress of soil-transmitted helminthiasis control in 2020 and world health organization targets for 2030. *PLoS Neglected Tropical Diseases*, 14(8), 1–17.
- Moon, C., VanDussen, K. L., Miyoshi, H., & Stappenbeck, T. S. (2014). Development of a primary mouse intestinal epithelial cell monolayer culture system to evaluate factors that modulate IgA transcytosis. *Mucosal Immunology*, 7(4), 818–828.
- Mori-Akiyama, Y., van den Born, M., van Es, J. H., Hamilton, S. R., Adams, H. P., Zhang, J., Clevers, H., & de Crombrughe, B. (2007). SOX9 is required for the differentiation of paneth cells in the intestinal epithelium. *Gastroenterology*, 133(2), 539–546.
- Moro, K., Yamada, T., Tanabe, M., Takeuchi, T., Ikawa, T., Kawamoto, H., Furusawa, J.-I., Ohtani, M., Fujii, H., & Koyasu, S. (2010). Innate production of T(H)2 cytokines by adipose tissue-associated c-Kit(+)/Sca-1(+) lymphoid cells. *Nature*, 463(7280), 540–544.
- Moses, L., & Pachter, L. (n.d.). *BUSpaRse: kallisto | bustools R utilities. R package version 1.13.0.* BUSpaRse. Retrieved 2022, from <https://github.com/BUSTools/BUSpaRse>.
- Mowat, A. M., & Agace, W. W. (2014). Regional specialization within the intestinal immune system. *Nature Reviews. Immunology*, 14(10), 667–685.
- Moya, I. M., & Halder, G. (2019). Hippo-YAP/TAZ signalling in organ regeneration and regenerative medicine. *Nature Reviews. Molecular Cell Biology*, 20(4), 211–226.
- Munhoz da Rocha, I. F., Amatuzzi, R. F., Lucena, A. C. R., Faoro, H., & Alves, L. R. (2020). Cross-Kingdom Extracellular Vesicles EV-RNA Communication as a Mechanism for Host-Pathogen Interaction. *Frontiers in Cellular and Infection Microbiology*, 10, 593160.
- Murata, K., Jadhav, U., Madha, S., van Es, J., Dean, J., Cavazza, A., Wucherpfennig, K., Michor, F., Clevers, H., & Shivdasani, R. A. (2020). Ascl2-Dependent Cell Dedifferentiation Drives Regeneration of Ablated Intestinal Stem Cells. *Cell Stem Cell*, 26(3), 377-390.e6.
- Murray, C. J., & Acharya, A. K. (1997). Understanding DALYs (disability-adjusted life years). *Journal of Health Economics*, 16(6), 703–730.
- Nadsombati, M. S., McGinty, J. W., Lyons-Cohen, M. R., Jaffe, J. B., DiPeso, L., Schneider, C., Miller, C. N., Pollack, J. L., Nagana Gowda, G. A., Fontana, M. F., Erle, D. J., Anderson, M. S., Locksley, R. M., Raftery, D., & von Moltke, J. (2018). Detection of Succinate by Intestinal Tuft Cells Triggers a Type 2 Innate Immune Circuit. *Immunity*, 49(1), 33-41.e7.
- Nair, S. R., Abraham, R., Sundaram, S., & Sreekumar, E. (2017). Interferon regulated gene (IRG) expression-signature in a mouse model of chikungunya virus neurovirulence. *Journal of Neurovirology*, 23(6), 886–902.
- Nausch, N., Midzi, N., Mduluzi, T., Maizels, R. M., & Mutapi, F. (2011). Regulatory

- and activated T cells in human *Schistosoma haematobium* infections. *PLoS One*, 6(2), e16860.
- Neill, D. R., Wong, S. H., Bellosi, A., Flynn, R. J., Daly, M., Langford, T. K. A., Bucks, C., Kane, C. M., Fallon, P. G., Pannell, R., Jolin, H. E., & McKenzie, A. N. J. (2010). Nuocytes represent a new innate effector leukocyte that mediates type-2 immunity. *Nature*, 464(7293), 1367–1370.
- Nikolaev, M., Mitrofanova, O., Broguiere, N., Geraldo, S., Dutta, D., Tabata, Y., Elci, B., Brandenburg, N., Kolotuev, I., Gjorevski, N., Clevers, H., & Lutolf, M. P. (2020). Homeostatic mini-intestines through scaffold-guided organoid morphogenesis. *Nature*, 585(7826), 574–578.
- Noah, T. K., Kazanjian, A., Whitsett, J., & Shroyer, N. F. (2010). SAM pointed domain ETS factor (SPDEF) regulates terminal differentiation and maturation of intestinal goblet cells. *Experimental Cell Research*, 316(3), 452–465.
- Nusse, Y. M., Savage, A. K., Marangoni, P., Rosendahl-Huber, A. K. M., Landman, T. A., De Sauvage, F. J., Locksley, R. M., & Klein, O. D. (2018). Parasitic helminths induce fetal-like reversion in the intestinal stem cell niche. *Nature*, 559(7712), 109–113.
- O'Brien, K., Ughetto, S., Mahjoub, S., Nair, A. V., & Breakefield, X. O. (2022). Uptake, functionality, and re-release of extracellular vesicle-encapsulated cargo. *Cell Reports*, 39(2), 110651.
- Oliphant, C. J., Hwang, Y. Y., Walker, J. A., Salimi, M., Wong, S. H., Brewer, J. M., Englezakis, A., Barlow, J. L., Hams, E., Scanlon, S. T., Ogg, G. S., Fallon, P. G., & McKenzie, A. N. J. (2014). MHCII-mediated dialog between group 2 innate lymphoid cells and CD4(+) T cells potentiates type 2 immunity and promotes parasitic helminth expulsion. *Immunity*, 41(2), 283–295.
- Osbourn, M., Soares, D. C., Vacca, F., Cohen, E. S., Scott, I. C., Gregory, W. F., Smyth, D. J., Toivakka, M., Kemter, A. M., le Bihan, T., Wear, M., Hoving, D., Filbey, K. J., Hewitson, J. P., Henderson, H., González-Ciscar, A., Errington, C., Vermeren, S., Astier, A. L., ... McSorley, H. J. (2017). HpARI Protein Secreted by a Helminth Parasite Suppresses Interleukin-33. *Immunity*, 47(4), 739-751.e5.
- Osorio, D., & Cai, J. J. (2021). Systematic determination of the mitochondrial proportion in human and mice tissues for single-cell RNA-sequencing data quality control. *Bioinformatics*, 37(7), 963–967.
- Ouellette, A. J., Miller, S. I., & Henschen, A. H. (1992). Purification and primary structure of murine cryptdin-1, a Paneth cell defensin. *FEBS Letters*. [https://febs.onlinelibrary.wiley.com/doi/abs/10.1016/0014-5793\(92\)80606-H](https://febs.onlinelibrary.wiley.com/doi/abs/10.1016/0014-5793(92)80606-H)
- Ouellette, Andre J. (2005). Paneth cell alpha-defensins: peptide mediators of innate immunity in the small intestine. *Springer Seminars in Immunopathology*, 27(2), 133–146.
- Ouellette, Andre J., Darmoul, D., Tran, D., Huttner, K. M., Yuan, J., & Selsted, M. E. (1999). Peptide Localization and Gene Structure of Cryptdin 4, a Differentially Expressed Mouse Paneth Cell  $\alpha$ -Defensin. *Infection and Immunity*, 67(12), 6643–6651.
- Ouellette, André Joseph. (2011). Paneth cell  $\alpha$ -defensins in enteric innate immunity. *Cellular and Molecular Life Sciences: CMLS*, 68(13), 2215–2229.
- Pak, J., & Fire, A. (2007). Distinct populations of primary and secondary effectors during RNAi in *C. elegans*. *Science*, 315(5809), 241–244.
- Palviainen, M. I. D., Saraswat, M., Varga, Z., na Kitka, D., Neuvonen, M., Puhka, M., Joenvä, S., Renkonen, R., Nieuwland, R., Takatalo, M., & M Siljander, P. R. (2020). Extracellular vesicles from human plasma and serum are carriers of extravesicular cargo-Implications for biomarker discovery. 15(8), e0236439.
- Paneth, J. (1887). Ueber die secernirenden Zellen des Dünndarm-Epithels. *Archiv*

- Für Mikroskopische Anatomie*, 31(1), 113–191.
- Patel, N., Wu, W., Mishra, P. K., Chen, F., Millman, A., Csóka, B., Koscsó, B., Eltzschig, H. K., Haskó, G., & Gause, W. C. (2014). A2B adenosine receptor induces protective antihelminth type 2 immune responses. *Cell Host & Microbe*, 15(3), 339–350.
- Pelly, V. S., Kannan, Y., Coomes, S. M., Entwistle, L. J., Rückerl, D., Seddon, B., MacDonald, A. S., McKenzie, A., & Wilson, M. S. (2016). IL-4-producing ILC2s are required for the differentiation of TH2 cells following *Heligmosomoides polygyrus* infection. *Mucosal Immunology*, 9(6), 1407–1417.
- Peng, J., Federman, H. G., Hernandez, C. M., & Siracusa, M. C. (2022). Communication is key: Innate immune cells regulate host protection to helminths. *Frontiers in Immunology*, 13, 995432.
- Penttila, I. A., Ey, P. L., & Jenkin, C. R. (1984). Infection of mice with *Nematospiroides dubius*: demonstration of neutrophil-mediated immunity in vivo in the presence of antibodies. *Immunology*, 53(1), 147–154.
- Pesce, J. T., Ramalingam, T. R., Mentink-Kane, M. M., Wilson, M. S., El Kasmi, K. C., Smith, A. M., Thompson, R. W., Cheever, A. W., Murray, P. J., & Wynn, T. A. (2009). Arginase-1-expressing macrophages suppress Th2 cytokine-driven inflammation and fibrosis. *PLoS Pathogens*, 5(4), e1000371.
- Pesce, J. T., Ramalingam, T. R., Wilson, M. S., Mentink-Kane, M. M., Thompson, R. W., Cheever, A. W., Urban, J. F., Jr, & Wynn, T. A. (2009). Retnla (relmalphafizz1) suppresses helminth-induced Th2-type immunity. *PLoS Pathogens*, 5(4), e1000393.
- Pillai, M. R., Mihi, B., Ishiwata, K., Nakamura, K., Sakuragi, N., Finkelstein, D. B., McGargill, M. A., Nakayama, T., Ayabe, T., Coleman, M. L., & Bix, M. (2019). Myc-induced nuclear antigen constrains a latent intestinal epithelial cell-intrinsic anthelmintic pathway. *PloS One*, 14(2), e0211244.
- Potten, C. S., Hume, W. J., Reid, P., & Cairns, J. (1978). The segregation of DNA in epithelial stem cells. *Cell*, 15(3), 899–906.
- Potten, Christopher S. (1998). Stem cells in gastrointestinal epithelium: Numbers, characteristics and death. *Philosophical Transactions of the Royal Society of London. Series B, Biological Sciences*, 353(1370), 821–830.
- Price, A. E., Liang, H.-E., Sullivan, B. M., Reinhardt, R. L., Eisle, C. J., Erle, D. J., & Locksley, R. M. (2010). Systemically dispersed innate IL-13-expressing cells in type 2 immunity. *Proceedings of the National Academy of Sciences*, 107(25), 11489–11494.
- Price, A. E., Shamardani, K., Lugo, K. A., Deguine, J., Roberts, A. W., Lee, B. L., & Barton, G. M. (2018). A Map of Toll-like Receptor Expression in the Intestinal Epithelium Reveals Distinct Spatial, Cell Type-Specific, and Temporal Patterns. *Immunity*, 49(3), 560-575.e6.
- Punnonen, J., Aversa, G., Cocks, B. G., McKenzie, A. N., Menon, S., Zurawski, G., de Waal Malefyt, R., & de Vries, J. E. (1993). Interleukin 13 induces interleukin 4-independent IgG4 and IgE synthesis and CD23 expression by human B cells. *Proceedings of the National Academy of Sciences of the United States of America*, 90(8), 3730–3734.
- Puschhof, J., Pleguezuelos-Manzano, C., & Clevers, H. (2021). Organoids and organs-on-chips: Insights into human gut-microbe interactions. *Cell Host & Microbe*, 29(6), 867–878.
- Pužar Dominkuš, P., Stenovec, M., Sitar, S., Lasič, E., Zorec, R., Plemenitaš, A., Žagar, E., Kreft, M., & Lenassi, M. (2018). PKH26 labeling of extracellular vesicles: Characterization and cellular internalization of contaminating PKH26 nanoparticles. *Biochimica et Biophysica Acta (BBA) - Biomembranes*, 1860(6), 1350–1361.

## References

- Qi, Z., Li, Y., Zhao, B., Xu, C., Liu, Y., Li, H., Zhang, B., Wang, X., Yang, X., Xie, W., Li, B., Han, J.-D. J., & Chen, Y.-G. (2017). BMP restricts stemness of intestinal Lgr5+ stem cells by directly suppressing their signature genes. *Nature Communications*, 8, 13824.
- Qu, X. D., Lloyd, K. C., Walsh, J. H., & Lehrer, R. I. (1996). Secretion of type II phospholipase A2 and cryptdin by rat small intestinal Paneth cells. *Infection and Immunity*, 64(12), 5161–5165.
- Quinnell, R. J., Pritchard, D. I., Raiko, A., Brown, A. P., & Shaw, M.-A. (2004). Immune responses in human necatoriasis: association between interleukin-5 responses and resistance to reinfection. *The Journal of Infectious Diseases*, 190(3), 430–438.
- Rapin, A., Chuat, A., Lebon, L., Zaiss, M. M., Marsland, B. J., & Harris, N. L. (2020). Infection with a small intestinal helminth, *Heligmosomoides polygyrus bakeri*, consistently alters microbial communities throughout the murine small and large intestine. *International Journal for Parasitology*, 50(1), 35–46.
- Raposo, G., Nijman, H. W., Stoorvogel, W., Leijendekker, R., Harding, C. V., Melief, C. J. M., & Geuze, H. J. (1996). B lymphocytes secrete antigen-presenting vesicles. *The Journal of Experimental Medicine*, 183(3), 1161.
- Raposo, G., & Stoorvogel, W. (2013). Extracellular vesicles: exosomes, microvesicles, and friends. *The Journal of Cell Biology*, 200(4), 373–383.
- Rausch, S., Huehn, J., Kirchhoff, D., Rzepecka, J., Schnoeller, C., Pillai, S., Loddenkemper, C., Scheffold, A., Hamann, A., Lucius, R., & Hartmann, S. (2008). Functional analysis of effector and regulatory T cells in a parasitic nematode infection. *Infection and Immunity*, 76(5), 1908–1919.
- Rey, C., Chang, Y.-Y., Latour-Lambert, P., Varet, H., Proux, C., Legendre, R., Coppée, J.-Y., & Enninga, J. (2020). Transcytosis subversion by M cell-to-enterocyte spread promotes *Shigella flexneri* and *Listeria monocytogenes* intracellular bacterial dissemination. *PLoS Pathogens*, 16(4), e1008446.
- Reynolds, L. A., Filbey, K. J., & Maizels, R. M. (2012). Immunity to the model intestinal helminth parasite *Heligmosomoides polygyrus*. *Seminars in Immunopathology*, 34(6), 829–846.
- Ricci, N. D., Fiúza, J. A., Bueno, L. L., Cançado, G. G. L., Gazzinelli-Guimarães, P. H., Martins, V. G., Matoso, L. F., de Miranda, R. R. C., Geiger, S. M., Correa-Oliveira, R., Gazzinelli, A., Bartholomeu, D. C., & Fujiwara, R. T. (2011). Induction of CD4(+)CD25(+)FOXP3(+) regulatory T cells during human hookworm infection modulates antigen-mediated lymphocyte proliferation. *PLoS Neglected Tropical Diseases*, 5(11), e1383.
- Riccio, O., van Gijn, M. E., Bezdek, A. C., Pellegrinet, L., van Es, J. H., Zimmer-Strobl, U., Strobl, L. J., Honjo, T., Clevers, H., & Radtke, F. (2008). Loss of intestinal crypt progenitor cells owing to inactivation of both Notch1 and Notch2 is accompanied by derepression of CDK inhibitors p27Kip1 and p57Kip2. *EMBO Reports*, 9(4), 377–383.
- Rivera, J., Cordero, R. J. B., Nakouzi, A. S., Frases, S., Nicola, A., & Casadevall, A. (2010). *Bacillus anthracis* produces membrane-derived vesicles containing biologically active toxins. *Proceedings of the National Academy of Sciences of the United States of America*, 107(44), 19002–19007.
- Rm, M., Hh, S., & Hj, M. (2018). Modulation of Host Immunity by Helminths: The Expanding Repertoire of Parasite Effector Molecules. *Immunity*, 49(5), 801–818.
- Robinson, M. D., McCarthy, D. J., & Smyth, G. K. (2010). edgeR: a Bioconductor package for differential expression analysis of digital gene expression data. *Bioinformatics*, 26(1), 139–140.
- Ronchese, F., Hausmann, B., & Le Gros, G. (1994). Interferon-gamma- and



- interleukin-4-producing T cells can be primed on dendritic cells in vivo and do not require the presence of B cells. *European Journal of Immunology*, 24(5), 1148–1154.
- Rook, G. A. W. (2012). Hygiene hypothesis and autoimmune diseases. *Clinical Reviews in Allergy & Immunology*, 42(1), 5–15.
- Ross, M., & Pawlina, W. (2011). *Histology: A text and atlas with correlated cell and molecular biology* (6th ed.). Lippincott Williams & Wilkins.
- Ruffner, H., Sprunger, J., Charlat, O., Leighton-Davies, J., Grosshans, B., Salathe, A., Zietzling, S., Beck, V., Therier, M., Isken, A., Xie, Y., Zhang, Y., Hao, H., Shi, X., Liu, D., Song, Q., Clay, I., Hintzen, G., Tchorz, J., ... Cong, F. (2012). R-Spondin potentiates Wnt/ $\beta$ -catenin signaling through orphan receptors LGR4 and LGR5. *PLoS One*, 7(7), e40976.
- Sánchez-López, C. M., Trelis, M., Bernal, D., & Marcilla, A. (2021). Overview of the interaction of helminth extracellular vesicles with the host and their potential functions and biological applications. *Molecular Immunology*, 134, 228–235.
- Sarkies, P., Selkirk, M. E., Jones, J. T., Blok, V., Boothby, T., Goldstein, B., Hanelt, B., Ardila-Garcia, A., Fast, N. M., Schiffer, P. M., Kraus, C., Taylor, M. J., Koutsovoulos, G., Blaxter, M. L., & Miska, E. A. (2015). Ancient and novel small RNA pathways compensate for the loss of piRNAs in multiple independent nematode lineages. *PLoS Biology*, 13(2), e1002061.
- Sasaki, N., Miyamoto, K., Maslowski, K. M., Ohno, H., Kanai, T., & Sato, T. (2020). Development of a Scalable Coculture System for Gut Anaerobes and Human Colon Epithelium. *Gastroenterology*, 159(1), 388-390.e5.
- Satija, R., Farrell, J. A., Gennert, D., Schier, A. F., & Regev, A. (2015). Spatial reconstruction of single-cell gene expression data. *Nature Biotechnology*, 33(5), 495–502.
- Sato, T., & Clevers, H. (2013). Growing self-organizing mini-guts from a single intestinal stem cell: Mechanism and applications. *Science*, 340(6137), 1190–1194.
- Sato, T., van Es, J. H., Snippert, H. J., Stange, D. E., Vries, R. G., van den Born, M., Barker, N., Shroyer, N. F., van de Wetering, M., & Clevers, H. (2011). Paneth cells constitute the niche for Lgr5 stem cells in intestinal crypts. *Nature*, 469(7330), 415–418.
- Sato, T., Vries, R. G., Snippert, H. J., Van De Wetering, M., Barker, N., Stange, D. E., Van Es, J. H., Abo, A., Kujala, P., Peters, P. J., & Clevers, H. (2009). Single Lgr5 stem cells build crypt-villus structures in vitro without a mesenchymal niche. *Nature*, 459(7244), 262–265.
- Satoguina, J., Mempel, M., Larbi, J., Badusche, M., Löliger, C., Adjei, O., Gachelin, G., Fleischer, B., & Hoerauf, A. (2002). Antigen-specific T regulatory-1 cells are associated with immunosuppression in a chronic helminth infection (onchocerciasis). *Microbes and Infection / Institut Pasteur*, 4(13), 1291–1300.
- Satoguina, J. S., Adjobimey, T., Arndts, K., Hoch, J., Oldenburg, J., Layland, L. E., & Hoerauf, A. (2008). Tr1 and naturally occurring regulatory T cells induce IgG4 in B cells through GITR/GITR-L interaction, IL-10 and TGF- $\beta$ . *European Journal of Immunology*, 38(11), 3101–3113.
- Saz, D. K., Bonner, T. P., Karlin, M., & Saz, H. J. (1971). Biochemical observations on adult *Nippostrongylus brasiliensis*. *The Journal of Parasitology*, 57(6), 1159–1162.
- Schepers, A. G., Vries, R., van den Born, M., van de Wetering, M., & Clevers, H. (2011). Lgr5 intestinal stem cells have high telomerase activity and randomly segregate their chromosomes. *The EMBO Journal*, 30(6), 1104–1109.
- Schmitt, M., Schewe, M., Sacchetti, A., Feijtel, D., van de Geer, W. S., Teeuwssen, M., Sleddens, H. F., Joosten, R., van Royen, M. E., van de Werken, H. J. G.,

## References

- van Es, J., Clevers, H., & Fodde, R. (2018). Paneth Cells Respond to Inflammation and Contribute to Tissue Regeneration by Acquiring Stem-like Features through SCF/c-Kit Signaling. *Cell Reports*, *24*(9), 2312-2328.e7.
- Schneider, C., O'Leary, C. E., Moltke, J. von, Liang, H.-E., Ang, Q. Y., Turnbaugh, P. J., Radhakrishnan, S., Pellizzon, M., Ma, A., & Locksley, R. M. (2018). A metabolite-triggered tuft cell-ILC2 circuit drives small intestinal remodeling. *Cell*, *174*(2), 271.
- Schuijers, J., Junker, J. P., Mokry, M., Hatzis, P., Koo, B.-K., Sasselli, V., van der Flier, L. G., Cuppen, E., van Oudenaarden, A., & Clevers, H. (2015). *Ascl2* acts as an R-spondin/Wnt-responsive switch to control stemness in intestinal crypts. *Cell Stem Cell*, *16*(2), 158–170.
- Severinson, E. (2014). Identification of the IgG1 Induction Factor (Interleukin 4). *Frontiers in Immunology*, *5*, 628.
- Shankman, L. S., Fleury, S. T., Evans, W. B., Penberthy, K. K., Arandjelovic, S., Blumberg, R. S., Agaisse, H., & Ravichandran, K. S. (2021). Efferocytosis by Paneth cells within the intestine. *Current Biology: CB*, *31*(11), 2469-2476.e5.
- Sharpe, C., Thornton, D. J., & Grencis, R. K. (2018). A sticky end for gastrointestinal helminths; the role of the mucus barrier. *Parasite Immunology*, *40*(4), e12517.
- Shimokawa, C., Kanaya, T., Hachisuka, M., Ishiwata, K., Hisaeda, H., Kurashima, Y., Kiyono, H., Yoshimoto, T., Kaisho, T., & Ohno, H. (2017). Mast Cells Are Crucial for Induction of Group 2 Innate Lymphoid Cells and Clearance of Helminth Infections. *Immunity*, *46*(5), 863-874.e4.
- Shroyer, N. F., Wallis, D., Venken, K. J. T., Bellen, H. J., & Zoghbi, H. Y. (2005). *Gfi1* functions downstream of *Math1* to control intestinal secretory cell subtype allocation and differentiation. *Genes & Development*, *19*(20), 2412–2417.
- Sihite, I. F., Ali, M., Pasaribu, A. P., Pasaribu, S., & Lubis, C. P. (2014). Efficacy of mebendazole and levamisole, alone or in combination, for soil-transmitted helminthiasis. *Paediatrica Indonesiana*, *54*(1), 9.
- Silverman, J. M., Clos, J., de'Oliveira, C. C., Shirvani, O., Fang, Y., Wang, C., Foster, L. J., & Reiner, N. E. (2010). An exosome-based secretion pathway is responsible for protein export from *Leishmania* and communication with macrophages. *Journal of Cell Science*, *123*(Pt 6), 842–852.
- Silverman, P. H. (1965). In vitro cultivation procedures for parasitic helminths. *Advances in Parasitology*, *3*, 159–222.
- Silverman, P. H., & Hansen, E. L. (1971). In vitro cultivation procedures for parasitic helminths: recent advances. *Advances in Parasitology*, *9*, 227–258.
- Simbari, F., McCaskill, J., Coakley, G., Millar, M., Maizels, R. M., Fabriás, G., Casas, J., & Buck, A. H. (2016). Plasmalogen enrichment in exosomes secreted by a nematode parasite versus those derived from its mouse host: implications for exosome stability and biology. *Journal of Extracellular Vesicles*, *5*, 30741.
- Smith, D., Price, D. R. G., Burrells, A., Faber, M. N., Hildersley, K. A., Chintoan-Uta, C., Chapuis, A. F., Stevens, M., Stevenson, K., Burgess, S. T. G., Innes, E. A., Nisbet, A. J., & McNeilly, T. N. (2021). The Development of Ovine Gastric and Intestinal Organoids for Studying Ruminant Host-Pathogen Interactions. *Frontiers in Cellular and Infection Microbiology*, *11*, 733811.
- Smith, K. A., Harcus, Y., Garbi, N., Hämmerling, G. J., MacDonald, A. S., & Maizels, R. M. (2012). Type 2 innate immunity in helminth infection is induced redundantly and acts autonomously following CD11c(+) cell depletion. *Infection and Immunity*, *80*(10), 3481–3489.
- Smits, H. H., Hartgers, F. C., & Yazdanbakhsh, M. (2005). Helminth infections: protection from atopic disorders. *Current Allergy and Asthma Reports*, *5*(1), 42–50.
- Snoeck, V., Goddeeris, B., & Cox, E. (2005). The role of enterocytes in the intestinal

- barrier function and antigen uptake. *Microbes and Infection / Institut Pasteur*, 7(7–8), 997–1004.
- Sotillo, J., Robinson, M. W., Kimber, M. J., Cucher, M., Ancarola, M. E., Nejsum, P., Marcilla, A., Eichenberger, R. M., & Tritten, L. (2020). The protein and microRNA cargo of extracellular vesicles from parasitic helminths – current status and research priorities. *International Journal for Parasitology*, 50(9), 635–645.
- Soukhathammavong, P. A., Sayasone, S., Phongluxa, K., Xayaseng, V., Utzinger, J., Vounatsou, P., Hatz, C., Akkhavong, K., Keiser, J., & Odermatt, P. (2012). Low Efficacy of Single-Dose Albendazole and Mebendazole against Hookworm and Effect on Concomitant Helminth Infection in Lao PDR. *PLoS Neglected Tropical Diseases*, 6(1), e1417.
- Speich, B., Moser, W., Ali, S. M., Ame, S. M., Albonico, M., Hattendorf, J., & Keiser, J. (2016). Efficacy and reinfection with soil-transmitted helminths 18-weeks post-treatment with albendazole-ivermectin, albendazole-mebendazole, albendazole-oxantel pamoate and mebendazole. *Parasites & Vectors*, 9, 123.
- Stam, J., Bartel, S., Bischoff, R., & Wolters, J. C. (2021). Isolation of extracellular vesicles with combined enrichment methods. *Journal of Chromatography. B, Analytical Technologies in the Biomedical and Life Sciences*, 1169, 122604.
- Stassens, P., Bergum, P. W., Gansemans, Y., Jespers, L., Laroche, Y., Huang, S., Maki, S., Messens, J., Lauwereys, M., Cappello, M., Hotez, P. J., Lasters, I., & Vlasuk, G. P. (1996). Anticoagulant repertoire of the hookworm *Ancylostoma caninum*. *Proceedings of the National Academy of Sciences of the United States of America*, 93(5), 2149–2154.
- Stein, J. M., & Luzio, J. P. (1991). Ectocytosis caused by sublytic autologous complement attack on human neutrophils. The sorting of endogenous plasma-membrane proteins and lipids into shed vesicles. *Biochemical Journal*, 274(2), 381–386.
- Stentz, R., Carvalho, A. L., Jones, E. J., & Carding, S. R. (2018). Fantastic voyage: the journey of intestinal microbiota-derived microvesicles through the body. *Biochemical Society Transactions*, 46(5), 1021–1027.
- Sternini, C., Anselmi, L., & Rozengurt, E. (2008). Enteroendocrine cells: a site of “taste” in gastrointestinal chemosensing. *Current Opinion in Endocrinology, Diabetes, and Obesity*, 15(1), 73–78.
- Strachan, D. P. (1989). Hay fever, hygiene, and household size. *BMJ*, 299(6710), 1259–1260.
- Strunz, E. C., Addiss, D. G., Stocks, M. E., Ogden, S., Utzinger, J., & Freeman, M. C. (2014). Water, Sanitation, Hygiene, and Soil-Transmitted Helminth Infection: A Systematic Review and Meta-Analysis. *PLoS Medicine*, 11(3), e1001620.
- Su, C.-W., Cao, Y., Kaplan, J., Zhang, M., Li, W., Conroy, M., Walker, W. A., & Shi, H. N. (2011). Duodenal helminth infection alters barrier function of the colonic epithelium via adaptive immune activation. *Infection and Immunity*, 79(6), 2285–2294.
- Sulaiman, A. A., Zolnierczyk, K., Japa, O., Owen, J. P., Maddison, B. C., Emes, R. D., Hodgkinson, J. E., Gough, K. C., & Flynn, R. J. (2016). A Trematode Parasite Derived Growth Factor Binds and Exerts Influences on Host Immune Functions via Host Cytokine Receptor Complexes. *PLoS Pathogens*, 12(11), e1005991.
- Svendsen, B., Pedersen, J., Albrechtsen, N. J. W., Hartmann, B., Toräng, S., Rehfeld, J. F., Poulsen, S. S., & Holst, J. J. (2015). An analysis of cosecretion and coexpression of gut hormones from male rat proximal and distal small intestine. *Endocrinology*, 156(3), 847–857.
- Svetić, A., Madden, K. B., Zhou, X. D., Lu, P., Katona, I. M., Finkelman, F. D., Urban, R. J., & Blumberg, P. M. (2017). Helminth-induced gut barrier repair and immune regulation require IL-13. *Cell*, 170(1), 105–117.

- J. F., Jr, & Gause, W. C. (1993). A primary intestinal helminthic infection rapidly induces a gut-associated elevation of Th2-associated cytokines and IL-3. *Journal of Immunology*, *150*(8 Pt 1), 3434–3441.
- Tan, Y., & Cahan, P. (2019). SingleCellNet: A Computational Tool to Classify Single Cell RNA-Seq Data Across Platforms and Across Species. *Cell Systems*, *9*(2), 207-213.e2.
- Teltschik, Z., Wiest, R., Beisner, J., Nuding, S., Hofmann, C., Schoelmerich, J., Bevins, C. L., Stange, E. F., & Wehkamp, J. (2012). Intestinal bacterial translocation in rats with cirrhosis is related to compromised Paneth cell antimicrobial host defense. *Hepatology*, *55*(4), 1154–1163.
- Tetteh, P. W., Basak, O., Farin, H. F., Wiebrands, K., Kretzschmar, K., Begthel, H., van den Born, M., Korving, J., de Sauvage, F., van Es, J. H., van Oudenaarden, A., & Clevers, H. (2016). Replacement of Lost Lgr5-Positive Stem Cells through Plasticity of Their Enterocyte-Lineage Daughters. *Cell Stem Cell*, *18*(2), 203–213.
- Théry, C., Witwer, K. W., Aikawa, E., Alcaraz, M. J., Anderson, J. D., Andriantsitohaina, R., Antoniou, A., Arab, T., Archer, F., Atkin-Smith, G. K., Ayre, D. C., Bach, J.-M., Bachurski, D., Baharvand, H., Balaj, L., Baldacchino, S., Bauer, N. N., Baxter, A. A., Bebawy, M., ... Zuba-Surma, E. K. (2018). Minimal information for studies of extracellular vesicles 2018 (MISEV2018): a position statement of the International Society for Extracellular Vesicles and update of the MISEV2014 guidelines. *Journal of Extracellular Vesicles*, *7*(1), 1535750.
- Thorne, C. A., Chen, I. W., Sanman, L. E., Cobb, M. H., Wu, L. F., & Altschuler, S. J. (2018). Enteroid Monolayers Reveal an Autonomous WNT and BMP Circuit Controlling Intestinal Epithelial Growth and Organization. *Developmental Cell*, *44*(5), 624-633.e4.
- Tominaga, A., Takaki, S., Koyama, N., Katoh, S., Matsumoto, R., Migita, M., Hitoshi, Y., Hosoya, Y., Yamauchi, S., & Kanai, Y. (1991). Transgenic mice expressing a B cell growth and differentiation factor gene (interleukin 5) develop eosinophilia and autoantibody production. *The Journal of Experimental Medicine*, *173*(2), 429–437.
- Tosar, J. P., Witwer, K., & Cayota, A. (2021). Revisiting Extracellular RNA Release, Processing, and Function. *Trends in Biochemical Sciences*, *46*(6), 438–445.
- Tóth, E., Turiák, L., Visnovitz, T., Cserép, C., Mázló, A., Sódar, B. W., Försönits, A. I., Petővári, G., Sebestyén, A., Komlósi, Z., Drahos, L., Kittel, Á., Nagy, G., Bácsi, A., Dénes, Á., Gho, Y. S., Szabó-Taylor, K., & Buzás, E. I. (2021). Formation of a protein corona on the surface of extracellular vesicles in blood plasma. *Journal of Extracellular Vesicles*, *10*(11), e12140.
- Triana, S., Metz-Zumaran, C., Ramirez, C., Kee, C., Doldan, P., Shahraz, M., Schraivogel, D., Gschwind, A. R., Sharma, A. K., Steinmetz, L. M., Herrmann, C., Alexandrov, T., Boulant, S., & Stanifer, M. L. (2021). Single-cell analyses reveal SARS-CoV-2 interference with intrinsic immune response in the human gut. *Molecular Systems Biology*, *17*(4), e10232.
- Turner, J. D., Faulkner, H., Kamgno, J., Cormont, F., Van Snick, J., Else, K. J., Grecis, R. K., Behnke, J. M., Boussinesq, M., & Bradley, J. E. (2003). Th2 cytokines are associated with reduced worm burdens in a human intestinal helminth infection. *The Journal of Infectious Diseases*, *188*(11), 1768–1775.
- Turner, J.-E., Stockinger, B., & Helmbly, H. (2013). IL-22 Mediates Goblet Cell Hyperplasia and Worm Expulsion in Intestinal Helminth Infection. *PLoS Pathogens*, *9*(10), e1003698.
- Udonsi, J. K., Nwosu, A. B. C., & Anya, A. O. (1980). *Necator americanus*: Population structure, distribution, and fluctuations in population densities of infective

- larvae in contaminated farmlands. *Zeitschrift Für Parasitenkunde Parasitology Research*, 63(3), 251–259.
- Urban, J. F., Jr, Katona, I. M., & Finkelman, F. D. (1991). Heligmosomoides polygyrus: CD4+ but not CD8+ T cells regulate the IgE response and protective immunity in mice. *Experimental Parasitology*, 73(4), 500–511.
- Urban, J. F., Jr, Katona, I. M., Paul, W. E., & Finkelman, F. D. (1991). Interleukin 4 is important in protective immunity to a gastrointestinal nematode infection in mice. *Proceedings of the National Academy of Sciences of the United States of America*, 88(13), 5513–5517.
- Urban, J. F., Jr, Maliszewski, C. R., Madden, K. B., Katona, I. M., & Finkelman, F. D. (1995). IL-4 treatment can cure established gastrointestinal nematode infections in immunocompetent and immunodeficient mice. *Journal of Immunology*, 154(9), 4675–4684.
- Vacca, F., Chauché, C., Jamwal, A., Hinchy, E. C., Heieis, G., Webster, H., Ogunkanbi, A., Sekne, Z., Gregory, W. F., Wear, M., Perona-Wright, G., Higgins, M. K., Nys, J. A., Cohen, E. S., & McSorley, H. J. (2020). A helminth-derived suppressor of ST2 blocks allergic responses. *ELife*, 9, e54017.
- Vaishnav, S., Behrendt, C. L., Ismail, A. S., Eckmann, L., & Hooper, L. V. (2008). Paneth cells directly sense gut commensals and maintain homeostasis at the intestinal host-microbial interface. *Proceedings of the National Academy of Sciences of the United States of America*, 105(52), 20858–20863.
- Valadi, H., Ekström, K., Bossios, A., Sjöstrand, M., Lee, J. J., & Lötvall, J. O. (2007). Exosome-mediated transfer of mRNAs and microRNAs is a novel mechanism of genetic exchange between cells. *Nature Cell Biology*, 9(6), 654–659.
- van Es, J. H., Haegebarth, A., Kujala, P., Itzkovitz, S., Koo, B.-K., Boj, S. F., Korving, J., van den Born, M., van Oudenaarden, A., Robine, S., & Clevers, H. (2012). A critical role for the Wnt effector Tcf4 in adult intestinal homeostatic self-renewal. *Molecular and Cellular Biology*, 32(10), 1918–1927.
- van Es, J. H., Sato, T., van de Wetering, M., Lyubimova, A., Nee, A. N. Y., Gregorieff, A., Sasaki, N., Zeinstra, L., van den Born, M., Korving, J., Martens, A. C. M., Barker, N., van Oudenaarden, A., & Clevers, H. (2012). Dll1 secretory progenitor cells revert to stem cells upon crypt damage. *Nature Cell Biology*, 14(10), 1099–1104.
- van Es, J. H., van Gijn, M. E., Riccio, O., van den Born, M., Vooijs, M., Begthel, H., Cozijnsen, M., Robine, S., Winton, D. J., Radtke, F., & Clevers, H. (2005). Notch/gamma-secretase inhibition turns proliferative cells in intestinal crypts and adenomas into goblet cells. *Nature*, 435(7044), 959–963.
- van Niel, G., Carter, D. R. F., Clayton, A., Lambert, D. W., Raposo, G., & Vader, P. (2022). Challenges and directions in studying cell-cell communication by extracellular vesicles. *Nature Reviews. Molecular Cell Biology*, 23(5), 369–382.
- van Niel, G., D'Angelo, G., & Raposo, G. (2018). Shedding light on the cell biology of extracellular vesicles. *Nature Reviews. Molecular Cell Biology*, 19(4), 213–228.
- Vargas, G., Rocha, J. D. B., Oliveira, D. L., Albuquerque, P. C., Frases, S., Santos, S. S., Nosanchuk, J. D., Gomes, A. M. O., Medeiros, L. C. A. S., Miranda, K., Sobreira, T. J. P., Nakayasu, E. S., Arigi, E. A., Casadevall, A., Guimaraes, A. J., Rodrigues, M. L., Freire-de-Lima, C. G., Almeida, I. C., & Nimrichter, L. (2015). Compositional and immunobiological analyses of extracellular vesicles released by *Candida albicans*. *Cellular Microbiology*, 17(3), 389–407.
- Veerman, R. E., Teeuwen, L., Czarnewski, P., Güclüler Akpınar, G., Sandberg, A., Cao, X., Pernemalm, M., Orre, L. M., Gabriëlsson, S., & Eldh, M. (2021). Molecular evaluation of five different isolation methods for extracellular

- vesicles reveals different clinical applicability and subcellular origin. *Journal of Extracellular Vesicles*, 10(9), e12128.
- Verweij, F. J., Balaj, L., Boulanger, C. M., Carter, D. R. F., Compeer, E. B., D'Angelo, G., El Andaloussi, S., Goetz, J. G., Gross, J. C., Hyenne, V., Krämer-Albers, E.-M., Lai, C. P., Loyer, X., Marki, A., Momma, S., Nolte-'t Hoen, E. N. M., Pegtel, D. M., Peinado, H., Raposo, G., ... van Niel, G. (2021). The power of imaging to understand extracellular vesicle biology in vivo. *Nature Methods*, 18(9), 1013–1026.
- Verweij, F. J., Revenu, C., Arras, G., Dingli, F., Loew, D., Pegtel, D. M., Follain, G., Allio, G., Goetz, J. G., Zimmermann, P., Herbomel, P., Del Bene, F., Raposo, G., & van Niel, G. (2019). Live tracking of inter-organ communication by endogenous exosomes in vivo. *Developmental Cell*, 48(4), 573-589.e4.
- Vidal, K., Grosjean, I., Evillard, J. P., Gispach, C., & Kaiserlian, D. (1993). Immortalization of mouse intestinal epithelial cells by the SV40-large T gene. Phenotypic and immune characterization of the MODE-K cell line. *Journal of Immunological Methods*, 166(1), 63–73.
- Villarroya-Beltri, C., Gutiérrez-Vázquez, C., Sánchez-Cabo, F., Pérez-Hernández, D., Vázquez, J., Martín-Cofreces, N., Martínez-Herrera, D. J., Pascual-Montano, A., Mittelbrunn, M., & Sánchez-Madrid, F. (2013). Sumoylated hnRNPA2B1 controls the sorting of miRNAs into exosomes through binding to specific motifs. *Nature Communications*, 4, 2980.
- von Boehmer, H. (2005). Mechanisms of suppression by suppressor T cells. *Nature Immunology*, 6(4), 338–344.
- Von Moltke, J., Ji, M., Liang, H. E., & Locksley, R. M. (2016). Tuft-cell-derived IL-25 regulates an intestinal ILC2–epithelial response circuit. *Nature*, 529(7585), 221.
- Wahid, F. N., & Behnke, J. M. (1993). Immunological relationships during primary infection with *Heligmosomoides polygyrus* (*Nematospiroides dubius*): parasite specific IgG1 antibody responses and primary response phenotype. *Parasite Immunology*, 15(7), 401–413.
- Wahid, F. N., Behnke, J. M., Grecis, R. K., Else, K. J., & Ben-Smith, A. W. (1994). Immunological relationships during primary infection with *Heligmosomoides polygyrus*: Th2 cytokines and primary response phenotype. *Parasitology*, 108 (Pt 4), 461–471.
- Wammes, L. J., Hamid, F., Wiria, A. E., de Gier, B., Sartono, E., Maizels, R. M., Luty, A. J. F., Fillié, Y., Brice, G. T., Supali, T., Smits, H. H., & Yazdanbakhsh, M. (2010). Regulatory T cells in human geohelminth infection suppress immune responses to BCG and *Plasmodium falciparum*. *European Journal of Immunology*, 40(2), 437–442.
- Wammes, L. J., Hamid, F., Wiria, A. E., Wibowo, H., Sartono, E., Maizels, R. M., Smits, H. H., Supali, T., & Yazdanbakhsh, M. (2012). Regulatory T cells in human lymphatic filariasis: stronger functional activity in microfilareemics. *PLoS Neglected Tropical Diseases*, 6(5), e1655.
- Wang, L., Li, Z., Shen, J., Liu, Z., Liang, J., Wu, X., Sun, X., & Wu, Z. (2015). Exosome-like vesicles derived by *Schistosoma japonicum* adult worms mediates M1 type immune- activity of macrophage. *Parasitology Research*, 114(5), 1865–1873.
- Wang, M., Weiberg, A., Lin, F.-M., Thomma, B. P. H. J., Huang, H.-D., & Jin, H. (2016). Bidirectional cross-kingdom RNAi and fungal uptake of external RNAs confer plant protection. *Nature Plants*, 2, 16151.
- Wang, Y., DiSalvo, M., Gunasekara, D. B., Dutton, J., Proctor, A., Lebhar, M. S., Williamson, I. A., Speer, J., Howard, R. L., Smiddy, N. M., Bultman, S. J., Sims, C. E., Magness, S. T., & Allbritton, N. L. (2017). Self-renewing

- Monolayer of Primary Colonic or Rectal Epithelial Cells. *Cellular and Molecular Gastroenterology and Hepatology*, 4(1), 165-182.e7.
- Wang, Y., Gunasekara, D. B., Reed, M. I., DiSalvo, M., Bultman, S. J., Sims, C. E., Magness, S. T., & Allbritton, N. L. (2017). A microengineered collagen scaffold for generating a polarized crypt-villus architecture of human small intestinal epithelium. *Biomaterials*, 128, 44–55.
- Wardell, R., Clements, A. C. A., Lal, A., Summers, D., Llewellyn, S., Campbell, S. J., McCarthy, J., Gray, D. J., & V. Nery, S. (2017). An environmental assessment and risk map of *Ascaris lumbricoides* and *Necator americanus* distributions in Manufahi District, Timor-Leste. *PLoS Neglected Tropical Diseases*, 11(5), e0005565.
- Webb, L. M., Lundie, R. J., Borger, J. G., Brown, S. L., Connor, L. M., Cartwright, A. N. R., Dougall, A. M., Wilbers, R. H. P., Cook, P. C., Jackson-Jones, L. H., Phythian-Adams, A. T., Johansson, C., Davis, D. M., Dewals, B. G., Ronchese, F., & MacDonald, A. S. (2017). Type I interferon is required for T helper (Th) 2 induction by dendritic cells. *The EMBO Journal*, 36(16), 2404.
- Wehman, A. M., Poggioli, C., Schweinsberg, P., Grant, B. D., & Nance, J. (2011). The P4-ATPase TAT-5 inhibits the budding of extracellular vesicles in *C. elegans* embryos. *Current Biology: CB*, 21(23), 1951–1959.
- Wei, H., & Wang, J. Y. (2021). Role of Polymeric Immunoglobulin Receptor in IgA and IgM Transcytosis. *International Journal of Molecular Sciences*, 22(5), 1–20.
- Weiberg, A., Wang, M., Lin, F.-M., Zhao, H., Zhang, Z., Kaloshian, I., Huang, H.-D., & Jin, H. (2013). Fungal small RNAs suppress plant immunity by hijacking host RNA interference pathways. *Science*, 342(6154), 118–123.
- Weisz, O. A., & Rodriguez-Boulan, E. (2009). Apical trafficking in epithelial cells: signals, clusters and motors. *Journal of Cell Science*, 122(23), 4253–4266.
- White, M. P. J., Smyth, D. J., Cook, L., Ziegler, S. F., Levings, M. K., & Maizels, R. M. (2021). The parasite cytokine mimic Hp-TGM potently replicates the regulatory effects of TGF- $\beta$  on murine CD4<sup>+</sup> T cells. *Immunology and Cell Biology*, 99(8), 848–864.
- White, R., Kumar, S., Chow, F. W., Robertson, E., Hayes, K. S., Grecis, R. K., Duque-Correa, M. A., & Buck, A. H. (2020). Extracellular vesicles from *Heligmosomoides bakeri* and *Trichuris muris* contain distinct microRNA families and small RNAs that could underpin different functions in the host. *International Journal for Parasitology*, 50(9), 719–729.
- White, Ruby, Blow, F., Buck, A. H., & Duque-Correa, M. A. (2022). Organoids as tools to investigate gastrointestinal nematode development and host interactions. *Frontiers in Cellular and Infection Microbiology*, 12, 976017.
- Whitlock, M. C. (2015). *The Analysis of Biological Data*. marmamun.gov.np. <https://marmamun.gov.np/sites/marmamun.gov.np/files/webform/pdf-the-analysis-of-biological-data-michael-c-whitlock-dolph-schluter-pdf-download-free-book-8cbddee.pdf>
- WHO. (2012). Accelerating Work to Overcome the Global Impact of Neglected Tropical Diseases: A Roadmap for Implementation. *World Health Organization*, 1–42.
- WHO. (2020). Ending the neglect to attain the Sustainable Development Goals. *WHO (World Health Organization)*, 2.
- Williams, L. M., & Rudensky, A. Y. (2007). Maintenance of the Foxp3-dependent developmental program in mature regulatory T cells requires continued expression of Foxp3. *Nature Immunology*, 8(3), 277–284.
- Wilson, S. S., Mayo, M., Melim, T., Knight, H., Patnaude, L., Wu, X., Phillips, L., Westmoreland, S., Dunstan, R., Fiebiger, E., & Terrillon, S. (2021). Optimized Culture Conditions for Improved Growth and Functional Differentiation of

- Mouse and Human Colon Organoids. *Frontiers in Immunology*, 11. <https://doi.org/10.3389/fimmu.2020.547102>
- Woith, E., Fuhrmann, G., & Melzig, M. F. (2019). Extracellular vesicles—connecting kingdoms. *International Journal of Molecular Sciences*, 20(22), 5695.
- Wojciechowski, W., Harris, D. P., Sprague, F., Mousseau, B., Makris, M., Kusser, K., Honjo, T., Mohrs, K., Mohrs, M., Randall, T., & Lund, F. E. (2009). Cytokine-producing effector B cells regulate type 2 immunity to *H. polygyrus*. *Immunity*, 30(3), 421–433.
- Wolf, P. (1967). The nature and significance of platelet products in human plasma. *British Journal of Haematology*, 13(3), 269–288.
- Worthington, J. J., Reimann, F., & Gribble, F. M. (2017). Enteroendocrine cells—sensory sentinels of the intestinal environment and orchestrators of mucosal immunity. *Mucosal Immunology* 2018 11:1, 11(1), 3–20.
- Wu, D., & Smyth, G. K. (2012). Camera: a competitive gene set test accounting for inter-gene correlation. *Nucleic Acids Research*, 40(17), e133.
- Yang, Q., Bermingham, N. A., Finegold, M. J., & Zoghbi, H. Y. (2001). Requirement of *Math1* for secretory cell lineage commitment in the mouse intestine. *Science*, 294(5549), 2155–2158.
- Yigit, E., Batista, P. J., Bei, Y., Pang, K. M., Chen, C.-C. G., Tolia, N. H., Joshua-Tor, L., Mitani, S., Simard, M. J., & Mello, C. C. (2006). Analysis of the *C. elegans* Argonaute family reveals that distinct Argonautes act sequentially during RNAi. *Cell*, 127(4), 747–757.
- Yin, J., Sunuwar, L., Kasendra, M., Yu, H., Tse, C.-M., Talbot, C. C., Jr, Boronina, T., Cole, R., Karalis, K., & Donowitz, M. (2021). Fluid shear stress enhances differentiation of jejunal human enteroids in Intestine-Chip. *American Journal of Physiology. Gastrointestinal and Liver Physiology*, 320(3), G258–G271.
- Yin, X., Farin, H. F., Van Es, J. H., Clevers, H., Langer, R., & Karp, J. M. (2013). Niche-independent high-purity cultures of *Lgr5+* intestinal stem cells and their progeny. *Nature Methods*, 11(1), 106–112.
- Yu, S., Tong, K., Zhao, Y., Balasubramanian, I., Yap, G. S., Ferraris, R. P., Bonder, E. M., Verzi, M. P., & Gao, N. (2018). Paneth Cell Multipotency Induced by Notch Activation following Injury. *Cell Stem Cell*, 23(1), 46-59.e5.
- Zabeo, D., Cvjetkovic, A., Lässer, C., Schorb, M., Lötvall, J., & Höög, J. L. (2017). Exosomes purified from a single cell type have diverse morphology. *Journal of Extracellular Vesicles*, 6(1), 1329476.
- Zaiss, M. M., Maslowski, K. M., Mosconi, I., Guenat, N., Marsland, B. J., & Harris, N. L. (2013). IL-1 $\beta$  suppresses innate IL-25 and IL-33 production and maintains helminth chronicity. *PLoS Pathogens*, 9(8), e1003531.
- Zhang, X., Lan, Y., Xu, J., Quan, F., Zhao, E., Deng, C., Luo, T., Xu, L., Liao, G., Yan, M., Ping, Y., Li, F., Shi, A., Bai, J., Zhao, T., Li, X., & Xiao, Y. (2019). CellMarker: a manually curated resource of cell markers in human and mouse. *Nucleic Acids Research*, 47(D1), D721–D728.
- Zhao, X., Xu, Z., Xiao, L., Shi, T., Xiao, H., Wang, Y., Li, Y., Xue, F., & Zeng, W. (2021). Review on the Vascularization of Organoids and Organoids-on-a-Chip. *Frontiers in Bioengineering and Biotechnology*, 9, 637048.
- Zimmer, K.-P., de Laffolie, J., Barone, M. V., & Naim, H. Y. (2016). Endocytosis in enterocytes. *Wiener Medizinische Wochenschrift*, 166(7–8), 205–210.
- Zitvogel, L., Regnault, A., Lozier, A., Wolfers, J., Flament, C., Tenza, D., Ricciardi-Castagnoli, P., Raposo, G., & Amigorena, S. (1998). Eradication of established murine tumors using a novel cell-free vaccine: Dendritic cell-derived exosomes. *Nature Medicine*, 4(5), 594–600.
- Zurawski, S. M., Vega, F., Jr, Huyghe, B., & Zurawski, G. (1993). Receptors for interleukin-13 and interleukin-4 are complex and share a novel component



that functions in signal transduction. *The EMBO Journal*, 12(7), 2663–2670.

**Appendices**

**Appendix I**

**Appendix II**

**Appendix III**

**Appendix IV**